CANADIAN THESES ON MICROFICHE

I.S.B.N.

THESES CANADIENNES SUR MICROFICHE

National Library of Canada
Collections Development Branch

Canadian Theses on
Microfiche Service

Ottawa, Canada
K1A 0N4

Bibliothèque nationale du Canada
Direction du développement des collections

Service des thèses canadiennes
sur microfiche

NOTICE

The quality of this microfiche is heavily dependent upon the quality of the original thesis submitted for microfilming. Every effort has been made to ensure the highest quality of reproduction possible.

If pages are missing, contact the university which granted the degree.

Some pages may have indistinct print especially if the original pages were typed with a poor typewriter ribbon or if the university sent us a poor photocopy.

Previously copyrighted materials (journal articles, published tests, etc.) are not filmed.

Reproduction in full or in part of this film is governed by the Canadian Copyright Act, R.S.C. 1970, c. C-30. Please read the authorization forms which accompany this thesis.

AVIS

La qualité de cette microfiche dépend grandement de la qualité de la thèse soumise au microfilmage. Nous avons tout fait pour assurer une qualité supérieure de reproduction.

S'il manque des pages, veuillez communiquer avec l'université qui a conféré le grade.

La qualité d'impression de certaines pages peut laisser à désirer, surtout si les pages originales ont été dactylographiées à l'aide d'un ruban usé ou si l'université nous a fait parvenir une photocopie de mauvaise qualité.

Les documents qui font déjà l'objet d'un droit d'auteur (articles de revue, examens publiés, etc.) ne sont pas microfilmés.

La reproduction, même partielle, de ce microfilm est soumise à la Loi canadienne sur le droit d'auteur, SRC 1970, c. C-30. Veuillez prendre connaissance des formules d'autorisation qui accompagnent cette thèse.

THIS DISSERTATION
HAS BEEN MICROFILMED
EXACTLY AS RECEIVED

LA THÈSE A ÉTÉ
MICROFILMÉE TELLE QUE
NOUS L'AVONS REÇUE

NL-339 (r. 82/08)

Canada

0-315-08932-6

National Library of Canada | Bibliothèque nationale du Canada

43

Canadian Theses Division | Division des thèses canadiennes

Ottawa, Canada
K1A 0N4

56849

PERMISSION TO MICROFILM — AUTORISATION DE MICROFILMER

• Please print or type — Écrire en lettres moulées ou dactylographier

Full Name of Author — Nom complet de l'auteur

~~HUTCHINS~~ DAVID EDWARD HUTCHINSON

Date of Birth — Date de naissance	Country of Birth — Lieu de naissance
27th APRIL 1954	CANADA

Permanent Address — Résidence fixe

SOIL MECHANICS LIMITED, EASTERN ROAD, BRACKNELL, BERKSHIRE, ENGLAND.

Title of Thesis — Titre de la thèse

EFFECTS OF CONSTRUCTION PROCEDURE ON ~~TUNNEL~~ SHAFT AND ~~SHAFT~~ TUNNEL PERFORMANCE

University — Université

UNIVERSITY OF ALBERTA

Degree for which thesis was presented — Grade pour lequel cette thèse fut présentée

MASTER OF SCIENCE

Year this degree conferred — Année d'obtention de ce grade	Name of Supervisor — Nom du directeur de thèse
1982	DR. P. K. KAISER

Permission is hereby granted to the NATIONAL LIBRARY OF CANADA to microfilm this thesis and to lend or sell copies of the film.

The author reserves other publication rights, and neither the thesis nor extensive extracts from it may be printed or otherwise reproduced without the author's written permission.

L'autorisation est, par la présente, accordée à la BIBLIOTHÈQUE NATIONALE DU CANADA de microfilmer cette thèse et de prêter ou de vendre des exemplaires du film.

L'auteur se réserve les autres droits de publication; ni la thèse ni de longs extraits de celle-ci ne doivent être imprimés ou autrement reproduits sans l'autorisation écrite de l'auteur.

Date	Signature
27th April 1982	D. E. Hutchinson

NL-91 (4/77)

THE UNIVERSITY OF ALBERTA

Effects of Construction Procedure on Shaft and Tunnel Performance

by

© David Edward Hutchinson

A THESIS

SUBMITTED TO THE FACULTY OF GRADUATE STUDIES AND RESEARCH

IN PARTIAL FULFILMENT OF THE REQUIREMENTS FOR THE DEGREE

OF M.Sc.

IN

Geotechnical Engineering

Civil Engineering

EDMONTON, ALBERTA

April, 1982

THE UNIVERSITY OF ALBERTA

RELEASE FORM

NAME OF AUTHOR David Edward Hutchinson

TITLE OF THESIS Effects of Construction Procedure on Shaft and Tunnel Performance

DEGREE FOR WHICH THESIS WAS PRESENTED M.Sc.

YEAR THIS DEGREE GRANTED April, 1982

Permission is hereby granted to THE UNIVERSITY OF ALBERTA LIBRARY to reproduce single copies of this thesis and to lend or sell such copies for private, scholarly or scientific research purposes only.

The author reserves other publication rights, and neither the thesis nor extensive extracts from it may be printed or otherwise reproduced without the author's written permission.

(SIGNED) D.E. Hutchinson

PERMANENT ADDRESS:

Soil Mechanics Limited,
Eastern Road, Bracknell,
Berkshire, U.K.

DATED 23rd April 1982

THE UNIVERSITY OF ALBERTA

FACULTY OF GRADUATE STUDIES AND RESEARCH

The undersigned certify that they have read, and recommend to the Faculty of Graduate Studies and Research, for acceptance, a thesis entitled Effects of Construction Procedure on Shaft and Tunnel Performance submitted by David Edward Hutchinson in partial fulfilment of the requirements for the degree of M.Sc. in Geotechnical Engineering.

Dr. P.K. Kaiser ..... supervisor

Dr. N.R. Morgenstern .....

Dr. M.B. Dusseault .....

Date 23rd April 1982

ABSTRACT

A finite element analysis has been developed to study the effects of construction on tunnel and shaft behaviour. Construction was simulated by incremental excavation and support installation, and the ground behaviour was assumed to be linear elastic with infinite strength. The effects of rock damage during construction, and of ground freezing and thawing, were simulated by a change in ground stiffness. The study revealed several important aspects for the numerical modelling of construction procedures, as well as showing various practical implications for the design of supports, the analysis of results from a monitoring programme, and the comparison of numerical analyses to field observations.

ACKNOWLEDGEMENTS

This thesis is a result of the policy of Soil Mechanics Limited to encourage its engineers to undertake post graduate work, and the writer is indebted to them for providing the incentive and the opportunity to study overseas and so broaden his experience.

Financial assistance was provided by a scholarship from E.B.A. Engineering Consultants Limited, by summer vacation employment with Thurber Consultants Limited, and by a teaching assistantship from the Civil Engineering Department of the University of Alberta.

The numerous discussions with fellow graduate students not only provided useful insights to academic topics, but also into a variety of different cultural backgrounds. The writer wishes to express his appreciation to all those concerned, in particular to P. Branco Jr., C. MacKay, and B. Gudmundsdottir.

The interest and support of the University Staff was also appreciated, and the author would like to thank Dr. P.K. Kaiser for the many hours of discussion, and the help in preparing this thesis. Thanks are also extended to J. Sobkowicz for proof reading this work at such short notice.

Most of all the writer would like to express his deepest appreciation to Elizabeth, his wife, for providing both financial and moral support which has made the time spent during this study considerably easier and more enjoyable.

Table of Contents

Chapter — Page

CHAPTER 1
INTRODUCTION 1

CHAPTER 2
NUMERICAL TECHNIQUE 4

2.1 Introduction 4

2.2 CONSTEP2 and SAP4 - Use of the Programs 5

2.3 CONSTEP2 - Nodal Stress Interpolation 9

2.4 CONSTEP2 - Construction Procedures Available ... 14

2.5 Meshes Used in the Analyses 15

2.6 Verification of the Numerical Technique 25

2.6.1 Comparison with Closed Form Solutions . 25

2.6.2 Comparison with Published Numerical Analyses 30

2.6.3 Summary of Comparisons with Other Solutions 37

2.7 Accuracy of the Numerical Model 38

2.7.1 Effect of Element Size on Nodal Stress Interpolation 38

2.7.2 Longitudinal Liner Stresses and Nodal Forces 44

2.7.3 Triangular and Rectangular Elements ... 49

2.7.4 Summary of Inaccuracies in the Technique 51

CHAPTER 3
GROUND BEHAVIOUR 53

3.1 Introduction 53

3.2 Difference Between Weakening and Softening 56

3.3 Simplified Modelling of Ground Behaviour 58

3.4 Rock Damage by Blasting 62

3.5 Numerical Modelling of the Zone of Damaged Ground 65

3.6 Ground Freezing and Thawing 67

CHAPTER 4
EXCAVATION AND SUPPORT CASES STUDIED 71

4.1 Introduction 71

4.2 Tunnels 74

4.3 Shafts 78

CHAPTER 5
GROUND-LINER INTERACTION 82

5.1 Introduction 82

5.2 Ground Convergence Curves 82

5.3 Support Reaction Curves 85

5.4 Bilinear Ground Convergence Curves 87

CHAPTER 6
PRESENTATION OF RESULTS 88

6.1 Introduction 88

6.2 Tunnel Analyses 88

6.2.1 Effect of Mesh Boundary and Initial Construction Effects 88

6.2.2 Radial Displacements; No Ground Damage 89

6.2.3 Radial Displacements; With Damaged Zone 91

6.2.4 Variable Modulus in Damaged Zone, and Excavation in Frozen Ground 93

6.2.5 Liner Stresses; Analyses with Mesh 2 ..93

6.2.6 Application of Nodal Excavation Forces 94

6.2.7 Comparison of Results from Analyses using Meshes 2 & 6 96

6.2.8 Comparison of Results from Analyses

using Meshes 6 & 7 97

6.2.9 Effect of Rock Damage on Liner Stresses 99

6.2.10 Liner Stresses - Frozen Ground Analyses 101

6.2.11 Ground Displacements Around the Opening 102

6.2.12 Ground Stresses Around the Opening ...103

6.3 Shaft Analyses 106

6.3.1 Radial Wall Displacements; Shallow Shafts 106

6.3.2 Liner Stresses; Shallow and Deep Shafts 109

6.3.3 Drilled (Water Supported) Shaft Case .111

CHAPTER 7
PUBLISHED NUMERICAL ANALYSES AND CASE HISTORIES 114

7.1 Introduction 114

7.2 Relative Stiffness Solution 115

7.3 Hanafy and Emery (1980); Numerical Analysis ...119

7.4 Ranken and Ghaboussi (1975); Numerical Analysis 120

7.5 Einstein and Schwartz (1980); Numerical Analysis 123

7.6 Gouch and Conway (1976); Numerical Analysis/Case History 127

7.7 Sharp, Richards and Byrne (1977); Numerical Analysis/Case History 129

7.8 Kielder Experimental Tunnel; Case History 131

7.9 Garrison Dam Tunnel; Case History 134

7.10 Lethbridge Shaft; Case History 135

CHAPTER 8
INTERPRETATION AND DISCUSSION OF RESULTS 138

8.1 Introduction 138

8.2 Effect of Delay in Liner Placement 139
8.3 Effect of Rock Damage 143
8.4 Excavation in Frozen Ground 156
8.5 Radial Wall Displacements at the Face 159
8.6 Variation of Stresses within a Liner 162
8.7 Changes in Ground Stresses 167
8.8 Liner Placement Delay Factor 175
8.9 Shaft Analyses 179

CHAPTER 9
CONCLUSIONS 187

9.1 Introduction 187
9.2 Numerical Technique 187
9.2.1 Introduction 187
9.2.2 Simulation of Excavation 188
9.2.3 Size of Elements 189
9.2.4 Mesh Geometry in the Region of the Excavation 190
9.2.5 Application of Nodal Excavation Forces 191
9.2.6 Additional Effects 192
9.3 Practical Aspects 193
9.3.1 Support Delay and Liner Stresses 193
9.3.2 Effect of Rock Damage 194
9.3.3 Identification of Zones of Softened Ground 195
9.3.4 Effect of Softening on Liner Thrust ..197
9.3.5 Bilinear Ground Convergence Curves and Face Convergence 198
9.3.6 Changes in Ground Stresses 199

9.3.7 Excavation in Frozen Ground, and Drilled Fluid Supported Shaft 200

9.3.8 Shallow Shafts 200

9.4 Further Work 201

REFERENCES 203

APPENDIX 1

GROUND REACTION CURVES AND MODULUS REDUCTION 207

APPENDIX 2

GENERALISED PROCEDURE FOR FINDING NODAL POINT FORCES FROM ELEMENT CENTRE STRESSES 213

APPENDIX 3

CALCULATION OF VALUES FOR A CONVERGENCE CONFINEMENT DIAGRAM AND CORRECTION OF RESULTS 218

APPENDIX 4

VISCO-ELASTIC DEFORMATION OF A THICK WALLED TUBE 222

APPENDIX 5

RESULTS FROM THE ANALYSES - TUNNELS 227

APPENDIX 6

RESULTS FROM THE ANALYSES - SHAFTS 257

List of Tables

Table Page

4.1 Material Properties Used in the Analyses.....72

6.1 Radial Wall Displacements in Shafts.....107

6.2 Liner Stresses in Shafts.....110

8.1 Material Properties used by Einstein and Schwartz (1980).....142

A5.1 Analyses Carried Out - Tunnels.....228

A6.1 Analyses Carried Out - Shafts.....258

List of Figures

Figure Page

2.1 CONSTEP2 and SAP4 Flowchart....6
2.2 Comparison of Different Methods of Calculating Nodal Stresses....11
2.3 Influence of Advancing Face on Radial Displacements. Comparison of Finite Element Simulations - 1....12
2.4 Mesh 1....18
2.5 Mesh 2....18
2.6 Mesh 3....19
2.7 Mesh 3A....19
2.8 Mesh 4....20
2.9 Mesh 5....20
2.10 Mesh 6....21
2.11 Mesh 7....21
2.12 Mesh 8....22
2.13 Boundary Conditions....22
2.14 Influence of Boundary Conditions on Displacements....23
2.15 F.E.M. and Elastic Theory, Lined Tunnel, Radial Displacements Compared....28
2.16 F.E.M. and Elastic Theory, Lined Tunnel, Stresses Compared....28
2.17 Comparison of F. E. Solution and Theory when Ground Modulus is Changing - Displacements....30

2.18 Comparison of F. E. Solution and Theory when Ground Modulus is Changing - Stresses.....30
2.19 Influence of Advancing Face on Radial Displacements, Comparison of Finite Element Simulations - 2.....32
2.20 Influence of Advancing Face on Radial Displacements, Unlined Tunnel Case.....33
2.21 Influence of Advancing Face on Radial Displacements, Lined Tunnel Case 1, Meshes 2 and 6.....35
2.22 Variation of Wall Displacements and Liner Thrusts with Maximum Open Ground and Distance Along the Tunnel.....36
2.23 Influence of Advancing Face on Radial Displacements. Comparison of Finite Element Simulations, Mesh 3.....39
2.24 Error in Interpolating the Stress Distribution.....40
2.25 Influence of Advancing Face on Radial Displacements. Comparison of Finite Element Simulations, Mesh 3A.....42
2.26 Influence of Advancing Face on Radial Displacements. Comparison of Finite Element Simulations, Mesh 2.....44
2.27 Influence of Advancing Face on Radial Displacements. Lined Tunnel Case 1, Mesh 2.....44
2.28 Influence of Advancing Face on Longitudinal Displacements. Lined Tunnel Case 1-(a).....47

2.29 Influence of Advancing Face on Longitudinal Displacements. Lined Tunnel Case 1-(b).....47
2.30 Influence of Advancing Face on Longitudinal Displacements. Lined Tunnel Case 2.....48
2.31 Influence of Advancing Face on Longitudinal Displacements. Lined Tunnel Case 3.....48
2.32 Displacements from Triangular and Rectangular Finite Elements Compared.....50
3.1 Damaged Rock Modulus.....54
3.2 Stress-Strain Behaviour of Rocks.....57
3.3 Simplified Models of Ground Behaviour.....59
3.4 Relationship Between Insitu Deformation Modulus of Rock Masses and Rock Mass Classification, Bieniawski (1978).....63
3.5 Variation in Young's Modulus with Confining Pressure for Both Solid and Broken Specimens, Hobbs (1970).....64
3.6 Relationship between Unconfined Compressive Strength, Young's Modulus and Temperature for Frozen Ground.....69
4.1 Lining Placement and Tunnel Construction Sequences.....73
4.2 Modulus Variation in the Damaged Zone - Simulation of Confining Pressure Effect.....76
4.3 Calculated Hydrostatic Pressure for a Drilled Shaft.....81
5.1 Ground Convergence Curves.....83

7.1 Dimensionless Stiffness Ratios, Einstein and Schwartz (1980).....117
7.2 Relative Stiffness Equations for Liner Thrusts, Moments and Displacements, Einstein and Schwartz (1980).....118
7.3 Finite Element Mesh, Ranken and Ghaboussi (1975).....122
7.4 Finite Element Mesh, Einstein and Schwartz (1980).....122
7.5 Definition of Support Delay, Einstein and Schwartz (1980).....125
7.6 Principal Stresses around an Opening, Gouch and Conway (1976).....128
7.7 Assumed Elastic Load Bearing Profiles for the Drakensberg Trial Excavation, Sharp, Richards, and Byrne (1977).....130
7.8 Support Delay Lengths - Kielder Experimental Tunnel and Garrison Dam Tunnel.....133
7.9 Linearised Ground Convergence Curves from the Kielder Experimental Tunnel in the Four Fathom Mudstone.....134
7.10 Instrumentation Installed in the Lethbridge Shaft, Kaiser et al. (1982).....137
8.1 Support Delay Correction Factor.....141
8.2 Variation of Ultimate Ground Stresses with Distance from Centreline.....144
8.3 Variation of Radial Strain around Openings.....147

8.4 Results of the Analyses Plotted on a Convergence-Confinement Diagram.....152
8.5 Ground Convergence Curves, Frozen and Thawed Ground.....157
8.6 Variation of Displacement with Damage.....160
8.7 Face Convergence with Different Extents of Damage in Front of the Face.....162
8.8 Longitudinal Variation of Radial Displacement and Tangential Thrust in the Liner.....163
8.9 Ground Convergence Curves - Tunnels, Mesh 6.....166
8.10 Longitudinal Variation of Radial and Tangential Stresses Close to the Tunnel Wall, Lined and Unlined Cases, No Rock Damage.....168
8.11 Longitudinal Variation of Radial and Tangential Stresses Close to the Tunnel Wall, Lined Case 6, with Rock Damage.....171
8.12 Comparison of Results of Radial and Tangential Stress Changes with the Lethbridge Shaft, MacKay (1982).....173
8.13 Support Delay Factor.....177
8.14 Ground Convergence Curves - Shafts.....180
8.15 Longitudinal Variation of Radial and Tangential Stresses Close to the Wall, Unlined Shallow Shaft.....185
8.16 Longitudinal Variation of Radial and Tangential Stresses Close to the Wall, Lined Shallow Shaft.....185
A5.1 Influence of Advancing Face on Radial

Displacements. Lined Tunnel Case 1, Mesh 2.....229
A5.2 Influence of Advancing Face on Radial
Displacements, Lined Tunnel Case 2, Mesh 2.....229
A5.3 Influence of Advancing Face on Radial
Displacements, Lined Tunnel Case 3, Mesh 2.....230
A5.4 Influence of Advancing Face on Radial
Displacements, Lined Tunnel Case 4 - a, Mesh 2.....230
A5.5 Influence of Advancing Face on Radial
Displacements, Lined Tunnel Case 4 - b, Mesh 2.....231
A5.6 Influence of Advancing Face on Radial
Displacements, Unlined Tunnel Case.....231
A5.7 Influence of Advancing Face on Radial
Displacements, Lined Tunnel Case 1, Meshes 2 and
6.....232
A5.8 Influence of Advancing Face on Radial
Displacements, Lined Tunnel Case 1, Meshes 6 and
7.....232
A5.9 Influence of Advancing Face on Radial
Displacements, Lined Tunnel Case 2, Mesh 6.....233
A5.10 Influence of Advancing Face on Radial
Displacements, Lined Tunnel Case 5, Mesh 6.....233
A5.11 Influence of Advancing Face on Radial
Displacements, Lined Tunnel Case 6, Meshes 6 and
7.....234
A5.12 Influence of Advancing Face on Radial
Displacements, Line Tunnel Case 7, Mesh 6.....234
A5.13 Influence of Advancing Face on Radial

Displacements, Confining Pressure Effect Simulated.....235
A5.14 Influence of Advancing Face on Radial Displacements, Lined Tunnel Case 1 - Frozen Ground.....235
A5.15 Influence of Advancing Face on Radial Displacements, Lined Tunnel Case 2 - Frozen Ground.....236
A5.16 Influence of Advancing Face and Liner Placement on Liner Radial Stress, Mesh 2.....236
A5.17 Influence of Advancing Face and Liner Placement on Liner Tangential Stress, Mesh 2.....237
A5.18 Influence of Advancing Face and Liner Placement on Liner Longitudinal Stress, Mesh 2.....237
A5.19 Influence of Advancing Face and Liner Placement on Liner Radial Stress, Meshes 2 and 6.....238
A5.20 Influence of Advancing Face and Liner Placement on Liner Tangential Stress, Meshes 2 and 6.....238
A5.21 Influence of Advancing Face and Liner Placement on Liner Longitudinal Stress, Meshes 2 and 6.....239
A5.22 Influence of Advancing Face and Liner Placement on liner Radial Stress, Meshes 6 and 7, Case 1.....239
A5.23 Influence of Advancing Face and Liner

Placement on Liner Tangential Stress, Meshes 6 and 7, Case 1.....240
A5.24 Influence of Advancing Face and Liner Placement on Liner Longitudinal Stress, Meshes 6 and 7, Case 1.....240
A5.25 Influence of Advancing Face and Liner Placement on Liner Radial Stress, Meshes 6 and 7, Case 6.....241
A5.26 Influence of Advancing Face and Liner Placement on Liner Tangential Stress, Meshes 6 and 7, Case 6.....241
A5.27 Influence of Advancing Face and Liner Placement on Liner Longitudinal Stress, Meshes 6 and 7, Case 6.....242
A5.28 Influence of Advancing Face and Liner Placement on Liner Radial Stress, Mesh 6.....242
A5.29 Influence of Advancing Face and Liner Placement on Liner Tangential Stress, Mesh 6.....243
A5.30 Influence of Advancing Face and Liner Placement on Liner Longitudinal Stress, Mesh 6.....243
A5.31 Influence of Advancing Face and Liner Placement on Liner Radial Stress (Confining Pressure Effect Simulated).....244
A5.32 Influence of Advancing Face and Liner Placement on Liner Tangential Stress (Confining Pressure Effect Simulated).....244
A5.33 Influence of Advancing Face and Liner

Placement on Liner Longitudinal Stress (Confining Pressure Effect Simulated).....245
A5.34 Influence of Advancing Face and Liner Placement on Liner Radial Stress (Frozen Ground).....245
A5.35 Influence of Advancing Face and Liner Placement on Liner Tangential Stress (Frozen Ground).....246
A5.36 Influence of Advancing Face and Liner Placement on Liner Longitudinal Stress (Frozen Ground).....246
A5.37 Influence of Advancing Face on Axial Displacements.....247
A5.38 Advancing Face Effect on Radial Displacements, Mesh 2, Case 1.....247
A5.39 Advancing Face Effect on Radial Displacements, Mesh 6, Case 1.....248
A5.40 Advancing Face Effect on Radial Displacements, Mesh 2, Case 2.....248
A5.41 Advancing Face Effect on Radial Displacements, Mesh 2, Case 4.....249
A5.42 Advancing Face Effect on Radial Displacements, Mesh 6, Case 6.....249
A5.43 Stresses Around Advancing Face.....250
A5.44 Variation of Ground Stresses, Unlined Case.....251
A5.45 Variation of Ground Stresses, Case 1.....251
A5.46 Variation of Ground Stresses, Case 6.....252

A5.47 Advancing Face Effect on Principal Stresses, Mesh 2, Case 1.....253
A5.48 Advancing Face Effect on Principal Stresses, Mesh 2, Case 2.....253
A5.49 Advancing Face Effect on Principal Stresses, Mesh 2, Case 4.....254
A5.50 Advancing Face Effect on Principal Stresses, Mesh 6, Case 6.....254
A5.51 Advancing Face Effect on Principal Stress Change, Mesh 2, Case 1.....255
A5.52 Advancing Face Effect on Principal Stress Change, Mesh 6, Case 1.....255
A5.53 Advancing Face Effect on Principal Stress Change, Mesh 2, Case 2.....256
A5.54 Advancing Face Effect on Principal Stress Change, Mesh 2, Case 4.....256
A6.1 Influence of Advancing Face on Radial Displacements - Lined and Unlined Shafts.....259
A6.2 Influence of Advancing Face on Radial Displacements - Unlined Shaft.....259
A6.3 Influence of Advancing Face on Radial Displacements - Lined Shaft Case 1, Ko = 0.5.....260
A6.4 Influence of Advancing Face on Radial Displacements - Lined Shaft Case 1, Ko = 1.0.....260
A6.5 Influence of Advancing Face on Radial Displacements - Lined Shaft Case 1, Ko = 2.0.....261
A6.6 Influence of Advancing Face on Radial

Displacements - Lined Shaft Case 2, Ko = 0.5.....261
A6.7 Influence of Advancing Face on Radial
Displacements - Lined Shaft Case 2, Ko = 1.0.....262
A6.8 Influence of Advancing Face on Radial
Displacements - Lined Shaft Case 2, Ko = 2.0.....262
A6.9 Influence of Advancing Face on Radial
Displacements - Lined Shaft Case 1 (deep).....263
A6.10 Influence of Advancing Face on Radial
Displacements - Lined Shaft Case 2 (deep).....263
A6.11 Influence of Advancing Face and Liner
Placement on Liner Radial Stress (shaft).....264
A6.12 Influence of Advancing Face and Liner
Placement on Liner Tangential Stress (shaft).....264
A6.13 Influence of Advancing Face and Liner
Placement on Liner Longitudinal Stress (shaft).....265
A6.14 Influence of Advancing Face and Liner
Placement on Liner Radial Stress (deep shafts).....265
A6.15 Influence of Advancing Face on Radial
Displacements - Drilled Shaft Case.....266
A6.16 Influence of Advancing Face and Liner
Placement on Liner Radial Stress (Drilled Shaft
Case).....266
A6.17 Influence of Advancing Face and Liner
Placement on Liner Tangential Stress (Drilled
Shaft Case).....267
A6.18 Influence of Advancing Face and Liner
Placement on Liner Longitudinal Stress (Drilled

Shaft Case).....267

Notation

B Radial extent of the zone of damaged ground

E Young's modulus

Ed Damaged ground modulus

Eg Ground modulus

Eu Undamaged ground modulus

G Shear modulus

K Bulk modulus

Ko Coefficient of lateral earth pressure at rest

po Initial field stress

ps Pressure applied to ground by support

p' Equivalent support pressure in softened ground ahead of face before tunnel is excavated

R Radius of tunnel

T Tangential thrust in liner

u Radial displacement of tunnel wall

ue Extra radial displacement at tunnel wall after ground softening ahead of the face

uf Radial displacement of tunnel wall at the face

ui Initial radial displacement at radius R when ground is softened ahead of the tunnel face but before excavation

ul Radial displacement of the liner (outside edge)

uo Ultimate radial wall displacement in undamaged ground

σr Radial stress

σt Tangential stress

ν Poisson's ratio of ground, damaged and undamaged

νg Poisson's ratio of the ground

ν_1 Poisson's ratio of the support

CHAPTER 1

INTRODUCTION

The performance of a tunnel or shaft is greatly influenced by the excavation and support procedure used for its construction, as well as by the initial and long term ground behaviour. A better understanding of these influences and proper consideration of their effect on support design and installation should lead to more efficient and economic tunnel and shaft construction. The objective of this work was to develop a numerical analysis which could be used to study the influence of construction related factors on liner performance and tunnel and shaft behaviour. The numerical technique adopted is not particularly new or innovative but the results are nevertheless relevant to a better understanding of the influence of several different construction procedures and to the design of underground openings and the interpretation of results from monitoring instrumentation.

One dominant factor, namely rock damage during drill and blast excavation, is often neglected when comparing predicted and observed behaviour. This may invalidate many apparently well fitted evaluations of field data because of the significant effects illustrated later. Although there have been many developments in the use of tunnel and shaft boring machines, the drill and blast method of excavation will continue to be used because of its adaptability, especially for short drives and construction in mixed ground

(e.g. Golder Associates and James F. Maclaren Ltd. (1976)).

Another technique used in tunnelling and shaft sinking is excavation within a ring or arch of artificially frozen ground, Jones and Brown (1978), Roesner and Poppen (1978). This technique is used to strengthen soft deposits, prevent saturated cohesionless material from flowing into the excavation and to build up an impermeable barrier around the opening. After support has been installed the ground is allowed to thaw, thereby changing its material properties and altering the equilibrium between the ground and support.

A third technique, which is being used more frequently, is to drill shafts under fluid support, Thyssen (1978). In this method large diameter holes, at present up to about 6 m in diameter, are drilled by rotary methods using drilling fluid to support the sides of the hole. Depths of at least 400 m are generally possible, but a problem is to keep the shaft vertical and true in order that the liner, usually steel, may be installed.

The results presented here are from an initial investigation using a finite element analysis which models construction procedure incrementally and, with simplifying assumptions of the ground behaviour, allows the construction procedures mentioned above to be analysed and compared. An axisymmetric analysis has been used which assumes that the tunnels are deep and unaffected by the ground surface boundary condition. The axisymmetric analysis also enables some three dimensional effects around the tunnel or shaft

face to be studied without having to use more costly three dimensional finite element methods. Shallow shafts have been modelled by including the ground surface as one of the mesh boundaries, whereas deep shafts are similar to deep tunnels. However the axisymmetric condition allows the influence of the coefficient of lateral earth pressure (Ko) on the performance of shafts to be studied.

CHAPTER 2

NUMERICAL TECHNIQUE

2.1 Introduction

The widely available linear elastic finite element program SAP4 (University of California, 1972) was used in this study. Another program called CON(struction)STEP(s)2 was written to manipulate input and output data files to SAP4 and hence control a sequence of excavation and liner installation steps, with SAP4 being used to calculate the increments of stress and displacement arising from each step of construction. CONSTEP2 is discussed in more detail in the following sections and a user manual is being prepared and will be published separately.

Excavation was carried out by reducing the deformation moduli of elements of excavated ground to a very low value, ten orders of magnitude lower than the original ground modulus, and reducing the wall stresses to zero by applying nodal forces calculated by a method similar to that outlined by Kulhawy (1977). The nodal stresses were determined by interpolation from the stresses at the centres of surrounding elements, and the nodal forces, equivalent to the stresses along the sides of the excavated element, were calculated by the theory of virtual work. Appendix 2 presents the method used by CONSTEP2 for calculating the nodal forces for an axisymmetric analysis, modified from

Kulhawy's method for plane strain. A discussion of the inaccuracies in the method, and ways which were adopted to reduce the inaccuracies, is given in Section 2.3.

Where a liner was installed it was assumed to be in direct, non-slip contact with the tunnel or shaft wall. This effectively modelled the case where a liner was cast insitu against the wall. Where a precast (or preformed) liner is installed the bond between the liner and wall will not be as good as assumed here. Indeed, because of irregularities in the wall after excavation (considering mainly excavations in rock) it is unlikely that there will initially be continuous contact between the ground and a precast liner, although the gap between the ground and liner is usually filled at some time during construction.

The sections below briefly describe how CONSTEP2 works and discuss the verification of the method by comparison with closed form solutions and with previously published numerical analyses.

2.2 CONSTEP2 and SAP4 - Use of the Programs

Figure 2.1 shows how the programs CONSTEP2 and SAP4 are used to simulate a sequence of tunnel or shaft excavation and contruction steps. A third program called START, which was written for this study, is also required. The user sets up files containing information on the geometry and boundary conditions of the mesh, the initial stresses in the

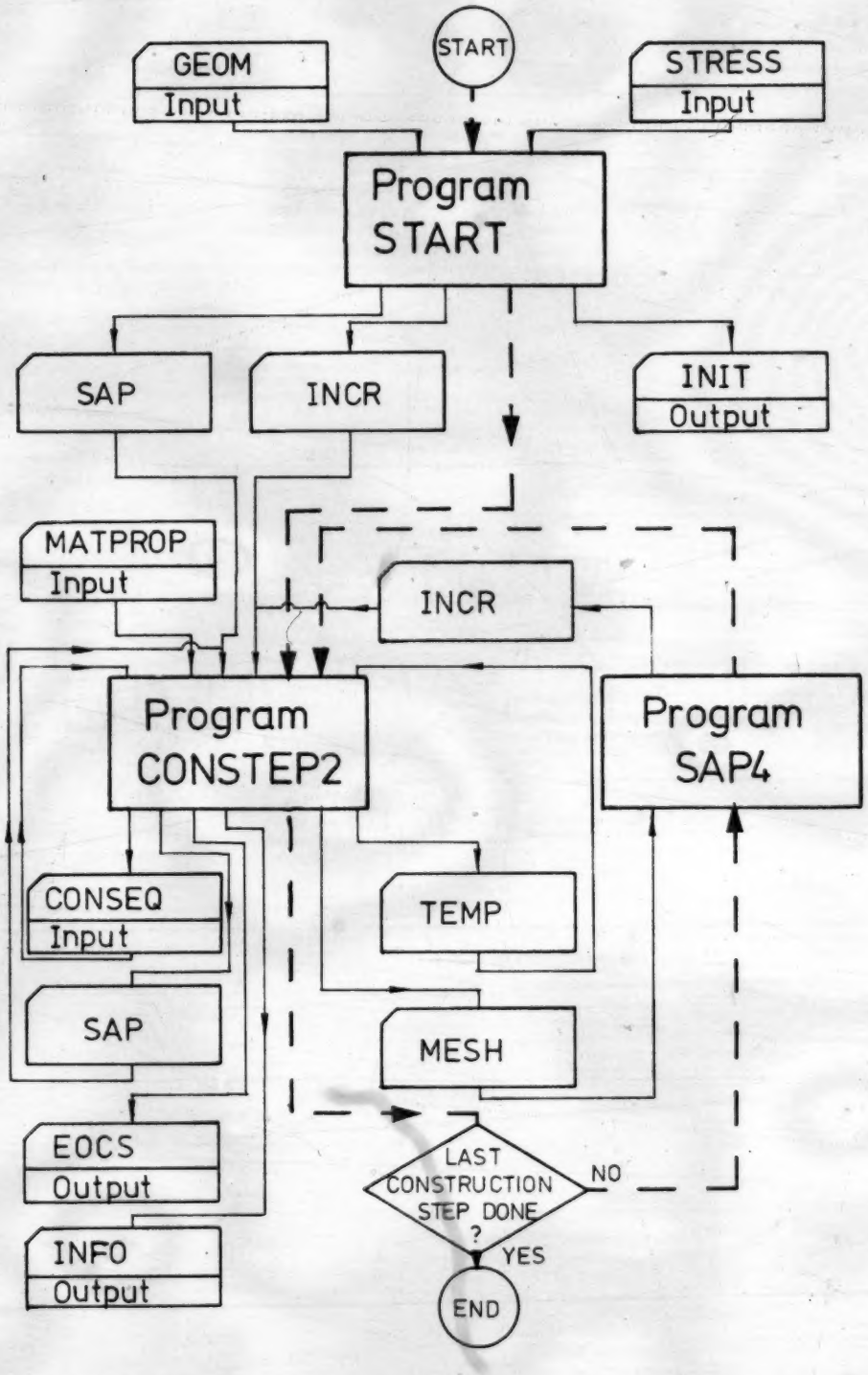

Figure 2.1 CONSTEP2 and SAP4 Flowchart

elements, the material properties which will be used in the analysis, and the commands which specify the construction sequence to be simulated. Communication between the programs is also carried out by using data files for interim storage. The data files input by the user are processed by program START which sets up files containing the initial information in a format which is required by CONSTEP2.

The exact details of the input required, and the output from CONSTEP2, are given in the user manual which also contains more details on how CONSTEP2 works, and its capabilities and limitations. Information on SAP4 is given in Report 72-10, University of California (1972). Many different element types may be used with SAP4, but this analysis only uses linear strain isoparametric axisymmetric elements with nodes at the element corners. The facility for using incompatible displacement modes was not used.

A brief description of each of the files used, and shown in Figure 2.1, is given below. The first four files are input by the user, and the last one contains the results of the analysis.

GEOM - Contains the details of the geometry of the mesh, i.e. node coordinates, node numbers of the nodes at the corners of the elements, the initial material type numbers, and the boundary conditions of the mesh.

STRESS - Contains the values of the initial stresses within each element.

MATPROP - The ground properties, e.g. deformation moduli and Poisson's ratios, for each of the material types used in the analysis are stored in this file.

CONSEQ - This file contains the commands which tell CONSTEP2 the sequence of excavation steps required. It also contains the current excavation step number, which is updated by CONSTEP2.

INIT - This file contains the initial information, output by program START, in a form that enables it to be input to CONSTEP2, but it is not used during the analysis so that comparison between the initial and final states may be made later if required.

SAP - The information in this file is updated by CONSTEP2 with the increments of stress and displacement arising from the previous construction step simulated by SAP4.

INCR - This file is output by SAP4 and contains the increments of stress and displacement arising from the construction step that SAP4 has just analysed.

MESH - CONSTEP2 sets up this file which contains the data SAP4 requires to run a step of excavation.

TEMP - A temporary workfile used by CONSTEP2.

INFO - A file which is output by CONSTEP2 and contains information on the calculation of nodal stresses. It is not normally used, the WRITE statements in the source program are inactivated by turning them into COMMENT statements.

EOCS - A file output by CONSTEP2 containing the updated information on stresses and displacements at the end of the

construction step just carried out.

2.3 CONSTEP2 - Nodal Stress Interpolation

In order to calculate the forces which are applied to nodes of elements being excavated the stresses at those nodes must be obtained. As SAP4 does not output nodal stresses they must be calculated from the element centre stresses. As previously described this may be done by a method similar to that outlined by Kulhawy (1977) which uses the stresses from the centres of the four elements surrounding any particular node. Appendix 2 outlines the procedure used by CONSTEP2 to calculate the stress at a node given the coordinates and stresses at any four points. Kulhawy's calculations have been adapted to the axisymmetric analyses used in this study.

A problem arises when one or more of the elements adjacent to the node being considered have already been excavated, as the stresses in those elements will be zero (or in this numerical analysis, very close to zero) and will adversely affect the calculation of the nodal stresses as described below. Figure 2.2 shows the three different ways used by programs CONSTEP, CONSTEP1 and CONSTEP2 to interpolate the nodal stresses at the wall of a previously excavated tunnel (of radius 5 m) from the stresses calculated by SAP4 at the centres of nearby elements.

It can by seen in Figure 2.2 that if elements of excavated ground are used in the interpolation (CONSTEP) the tangential stresses are grossly underestimated, although the radial stresses are in fact modelled quite closely as they should be zero at the tunnel wall anyway. The calculation of the tangential stress is improved if the stresses of elements of excavated ground surrounding the node are replaced by the average stress of the remaining unexcavated elements which surround that node (CONSTEP1). The calculation is further improved if all four elements used in the interpolation are unexcavated, and so have stresses of similar magnitude to the actual magnitude of stress at the node. CONSTEP2 therefore chooses the four unexcavated elements whose centres are closest to the node where the stresses are to be calculated. These elements are not necessarily attached to that node. Because of the way the program is set up the four elements are actually chosen from the nine elements around, and including, the element currently being excavated. CONSTEP2 ensures that the centres of the four elements chosen for the interpolation do not lie in a straight line as then the calculation becomes indeterminate. All three methods are the same where the four elements adjacent to the node are unexcavated.

Figure 2.2 only presents a two dimensional case rather than the three dimensional situation which will exist around a tunnel face. Figure 2.3 indicates what happens in a three dimensional case, and shows the radial wall displacements

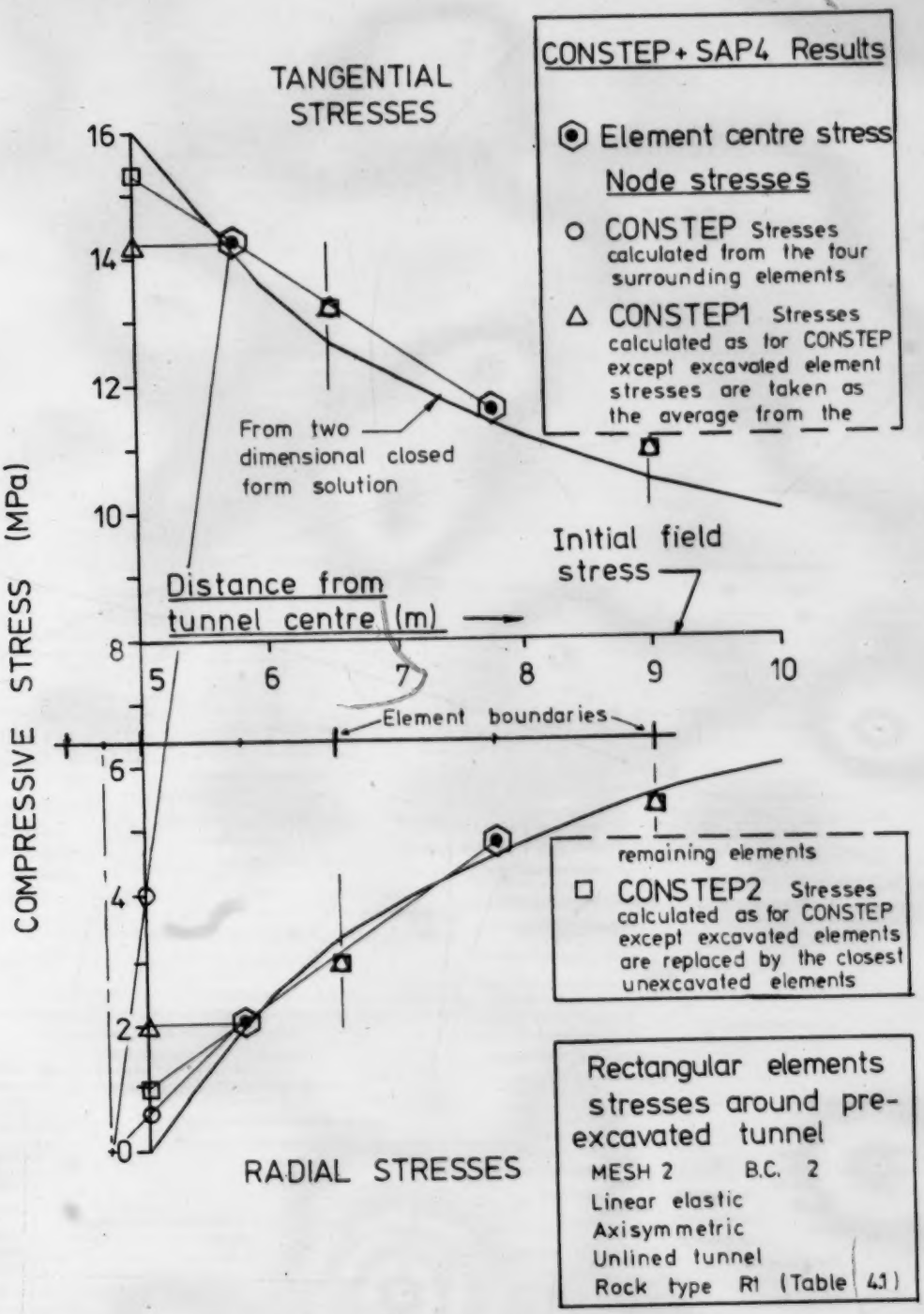
TANGENTIAL STRESSES
CONSTEP + SAP4 Results
Element centre stress
Node stresses
CONSTEP Stresses calculated from the four surrounding elements
CONSTEP1 Stresses calculated as for CONSTEP except excavated element stresses are taken as the average from the remaining elements
CONSTEP2 Stresses calculated as for CONSTEP except excavated elements are replaced by the closest unexcavated elements
From two dimensional closed form solution
Initial field stress
Distance from tunnel centre (m)
Element boundaries
COMPRESSIVE STRESS (MPa)
RADIAL STRESSES
Rectangular elements stresses around pre-excavated tunnel
MESH 2 B.C. 2
Linear elastic
Axisymmetric
Unlined tunnel
Rock type R1 (Table 4.1)

Figure 2.2 Comparison of Different Methods of Calculating Nodal Stresses

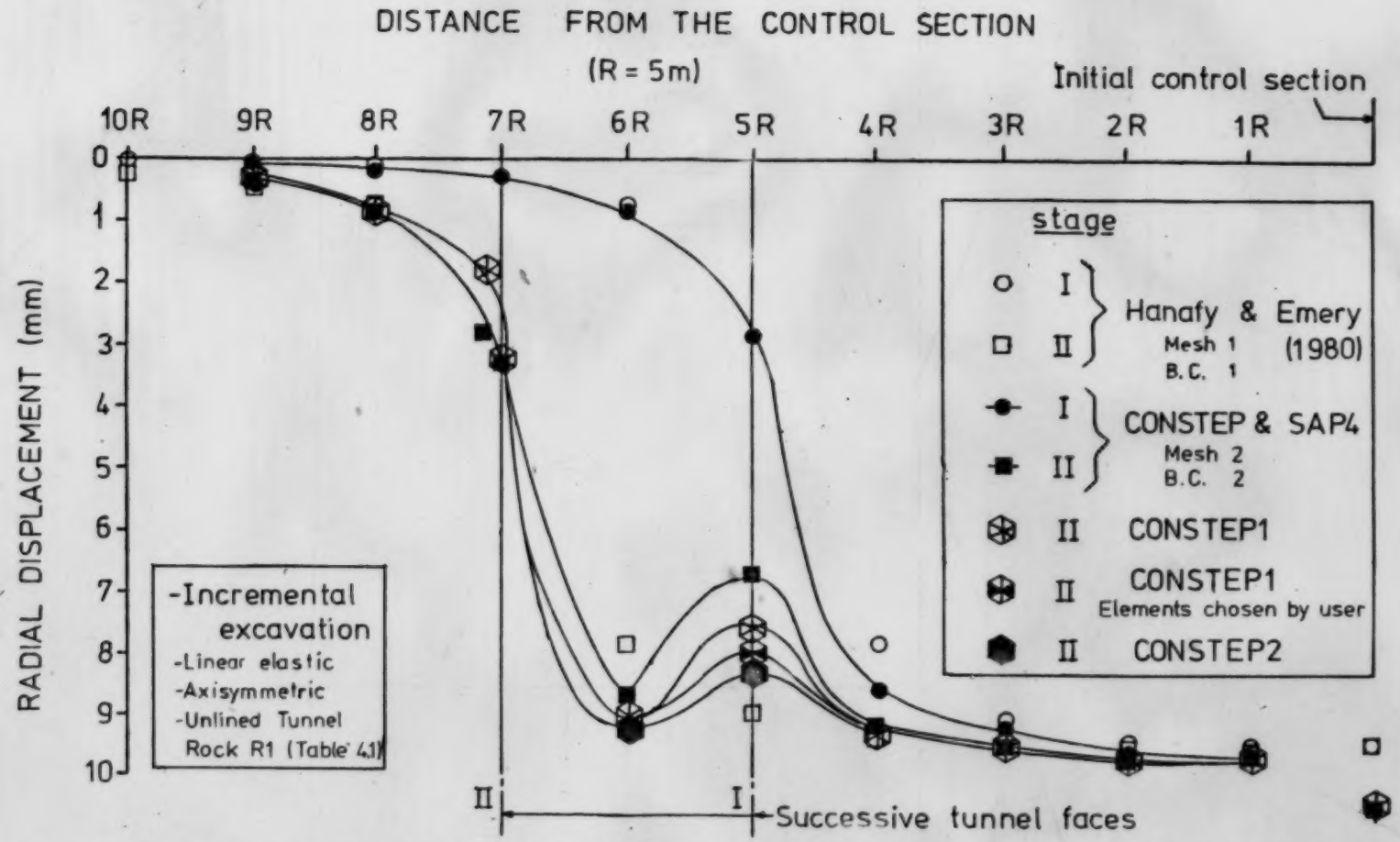

Figure 2.3 Influence of Advancing Face on Radial Displacements. Comparison of Finite Element Simulations - 1

for an unlined tunnel. Details of the analysis by Hanafy and Emery (1980) shown in the figure are given in Section 7.3, and details of the mesh and boundary conditions are given in Section 2.5.

Figure 2.3 compares five methods of calculating the nodal stresses by showing their effect on radial wall displacements. The analyses are for two steps of tunnel excavation, the first being five tunnel radii in length, Stage I, followed by a further excavation of length two tunnel radii, Stage II. All the Stage I excavations carried out by CONSTEP, CONSTEP1 and CONSTEP2 show the same radial displacements, but in Stage II they show "kinks" of various sizes in the distribution of displacements.

The reason for these "kinks" is the inaccuracy in calculating the values of the nodal stresses at the nodes next to elements that have been previously excavated. There also appears to have been an overcompensation at the nodes further away from the old face, and this is explained later.

As might be expected CONSTEP gives the largest "kink" and CONSTEP2 the smallest. CONSTEP1 was also used in a modified form whereby the user could specify from which elements the nodal stresses could be interpolated. The elements were not the same as those chosen by CONSTEP2 and gave slightly worse results. Hanafy and Emery's (1980) results are even better and show no sign of a kink. Their analysis uses a mesh (Mesh 1, Section 2.5) which has twice the number of elements as that used by the CONSTEP programs,

which will improve the accuracy as described in Section 2.7, and also it is not clear exactly how they calculated the equivalent nodal forces. It will be shown later that a regular curve will be obtained by excavating only the length of one element at a time, in this case one R, and this may have been done by Hanafy and Emery as they later describe excavations in one R steps. The effect of the element sizes and positions in the mesh, and the number of elements excavated at one step are discussed in Section 2.7. For the same size and position of elements CONSTEP2 gives the best results, and it is this program that has been used in the analyses, except where comparisons with other CONSTEP programs have been carried out.

2.4 CONSTEP2 - Construction Procedures Available

The following commands were written into CONSTEP2 to enable the user to choose a sequence of excavation and construction steps to simulate the construction of a tunnel or shaft. A brief description of each command is given to show what sort of construction procedures can be modelled by using CONSTEP2. Each command when used applies to a specified element, and the commands will contain other parameters, such as the number of a new material type for that element. Any number of commands, similar or different, may be used at each construction step.

EXC - Excavate an element in the manner described previously, i.e. by reducing the deformation modulus of the element to a very low value, and by applying forces to the nodes which are equivalent to the stresses along the element boundaries. The stresses in the element are reduced to zero.
NMT - Change the material of the element specified to a new material which has a lower deformation modulus. The element stresses are reduced by the ratio of the new to the old moduli. The nodal forces are calculated as for EXC, but are also reduced, by one minus the ratio of the new to old moduli, and are applied to the nodes to simulate this "partial excavation". Reduction of deformation moduli is more fully described in Chapter 3 on ground behaviour.
MTP - Change the material of the element specified to the material specified, but no other changes are made.
LNG - Place an element of liner. The material properties of the element are changed to those of the liner specified, and the stresses in the element reduced to zero.
CHV - Change the unstressed volume of the element specified by using the SAP facility of temperature contraction or expansion. See the CONSTEP2 User Manual for more details.

2.5 Meshes Used in the Analyses

The following meshes, presented in Figures 2.4 to 2.12, have been used in this study, and a brief description of the use of each mesh is given below.

Mesh 1 - This mesh was used by Hanafy and Emery (1980) in their analyses and has 168 triangular elements with 104 nodes at the corners of the triangles. Meshes 2, 3, 3A, 6 and 7 are based on this mesh.

Mesh 2 - This mesh has the same geometry as Mesh 1 but with 84 rectangular elements instead of 168 triangular elements. It also has 104 nodes, at the corners of the elements. Many of the initial analyses were run using this mesh.

Mesh 3 - Similar to Mesh 2, but with extra elements placed in front of three successive face positions in order to explore ways of reducing the errors which arise from the interpolation of nodal stresses from element stresses. This mesh has 98 elements and 120 nodes.

Mesh 3A - A further modification of Mesh 2, having the same number of elements and nodes as Mesh 3, but with a more regular increase in element size in front of the face position at 5 tunnel radii from the control section. It was used to explore ways of reducing stress interpolation errors.

Mesh 4 - This mesh was used in a two dimensional plane strain analysis to verify CONSTEP's ability to model a change of material deformation modulus. The 80 elements used were concentrated in the liner and in a region of stiff frozen ground which was subsequently thawed and softened. There are 102 nodes.

Mesh 5 - The 55 elements in this mesh are mainly concentrated in the zone closest to the tunnel wall. This

mesh was not actually used in the analyses.

Mesh 6 - One of the three meshes used most often in this study. It has a similar geometry to Mesh 2 but in the main part of the mesh the elements are one quarter of a tunnel radius in length along the tunnel axis rather than one tunnel radius. It has 264 elements and 306 nodes.

Mesh 7 - This is another of the meshes most frequently used in this study. In the main part of the mesh the length of the elements in the direction of the tunnel axis is one half of a tunnel radius. The mesh has 273 elements and 308 nodes. There is a concentration of elements in the liner and in the zone near the tunnel wall.

Mesh 8 - This mesh was used to study the variation of stresses within a liner (not installed in the ground) under certain simple applied loads. It has 120 elements and 147 nodes. The analyses have not been presented in this thesis.

Four different combinations of boundary conditions were considered in this study and they are shown in Figure 2.13. With Boundary Condition 1 no displacements are allowed across the axis of symmetry (i.e. a rollered boundary), and there is a fixed corner on the axis of symmetry ahead of the advancing face. Boundary Condition 2 is similar, but in addition no displacements are allowed across the side of the mesh perpendicular to the axis and ahead of the advancing face. Boundary Condition 3 has rollered boundaries on all its sides except the outer side of the mesh parallel to the tunnel centreline, and in Boundary Condition 4 this side is

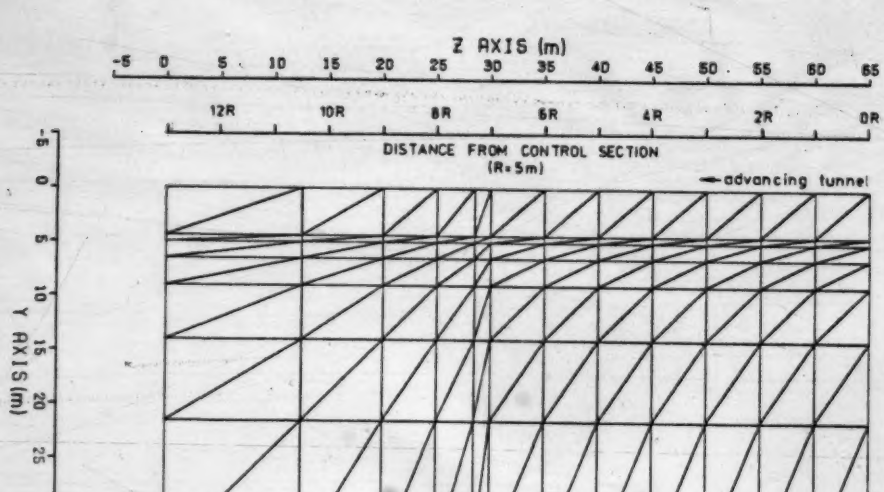
Z AXIS (m)
-5 0 5 10 15 20 25 30 35 40 45 50 55 60 65
12R 10R 8R 6R 4R 2R 0R
DISTANCE FROM CONTROL SECTION
(R=5m)
advancing tunnel
Y AXIS (m)
-5 0 5 10 15 20 25 30

Figure 2.4 Mesh 1

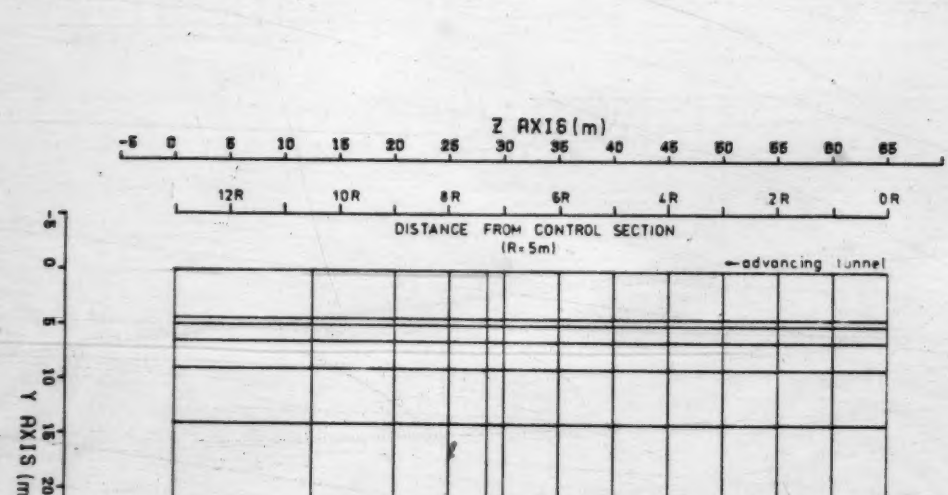
Z AXIS (m)
-5 0 5 10 15 20 25 30 35 40 45 50 55 60 65
12R 10R 8R 6R 4R 2R 0R
DISTANCE FROM CONTROL SECTION
(R=5m)
advancing tunnel
Y AXIS (m)
-5 0 5 10 15 20 25 30

Figure 2.5 Mesh 2

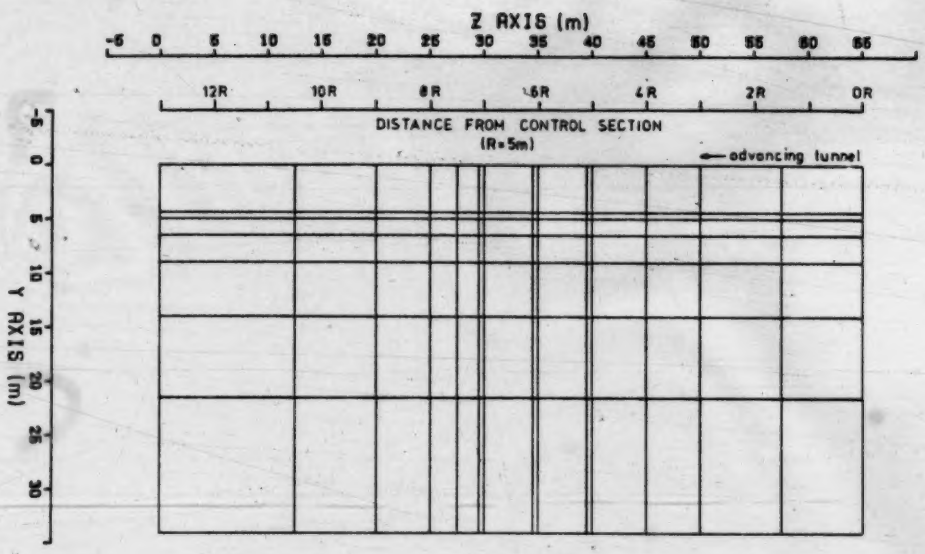
Z AXIS (m)
-5 0 5 10 15 20 25 30 35 40 45 50 55 60 65
12R 10R 8R 6R 4R 2R 0R
DISTANCE FROM CONTROL SECTION
(R=5m)
advancing tunnel
Y AXIS (m)
-5 0 5 10 15 20 25 30

Figure 2.6 Mesh 3

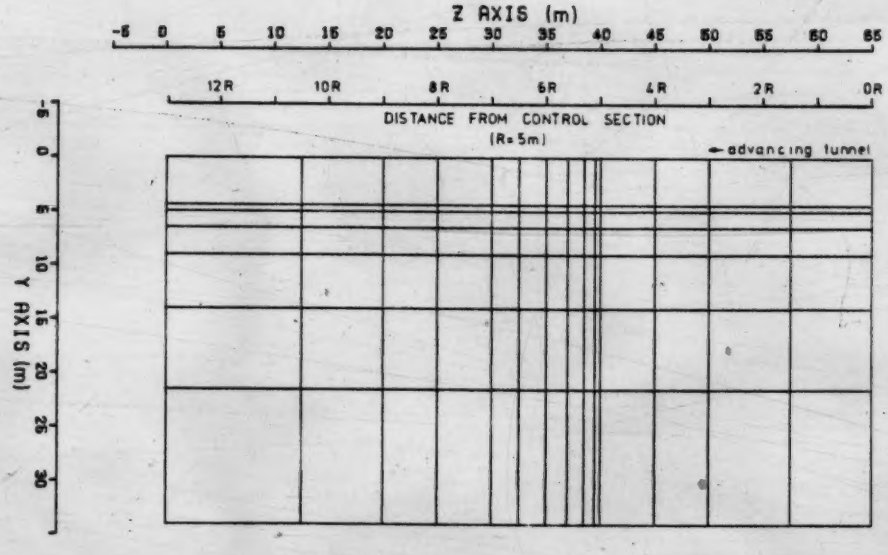
Z AXIS (m)
-5 0 5 10 15 20 25 30 35 40 45 50 55 60 65
12R 10R 8R 6R 4R 2R 0R
DISTANCE FROM CONTROL SECTION
(R=5m)
advancing tunnel
Y AXIS (m)
-5 0 5 10 15 20 25 30

Figure 2.7 Mesh 3A

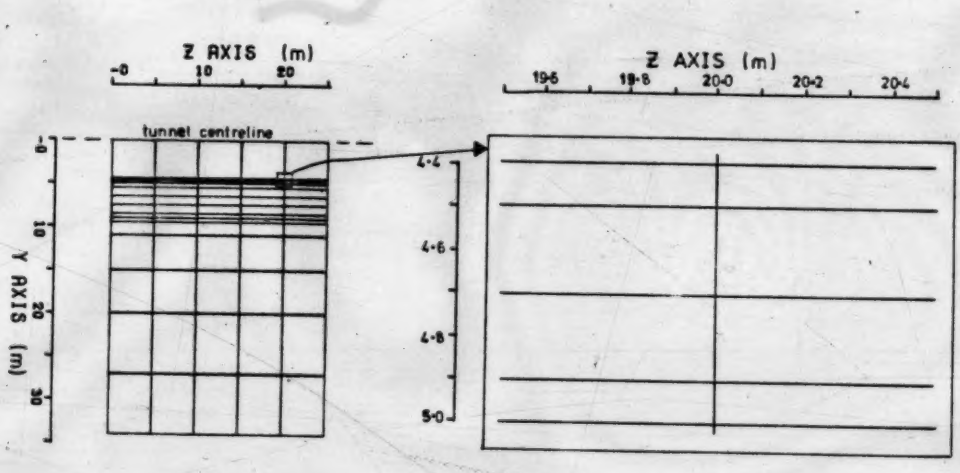

Figure 2.8 Mesh 4

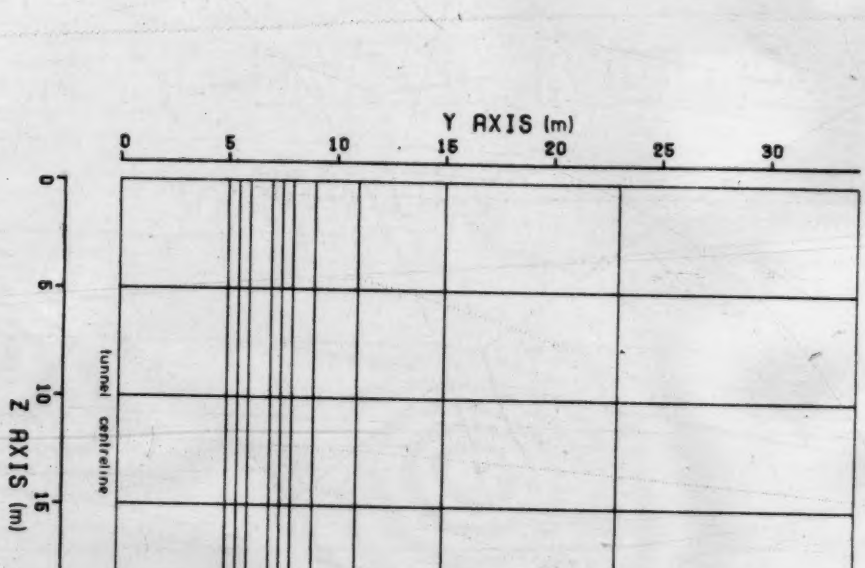

Figure 2.9 Mesh 5

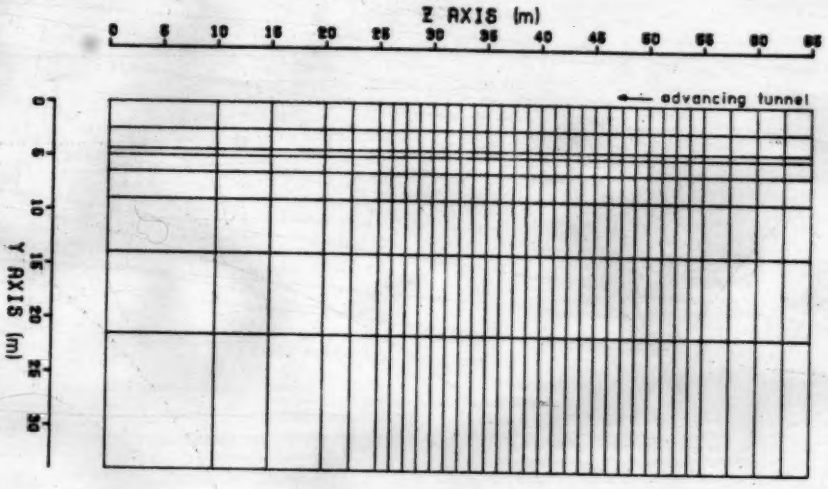

Figure 2.10 Mesh 6

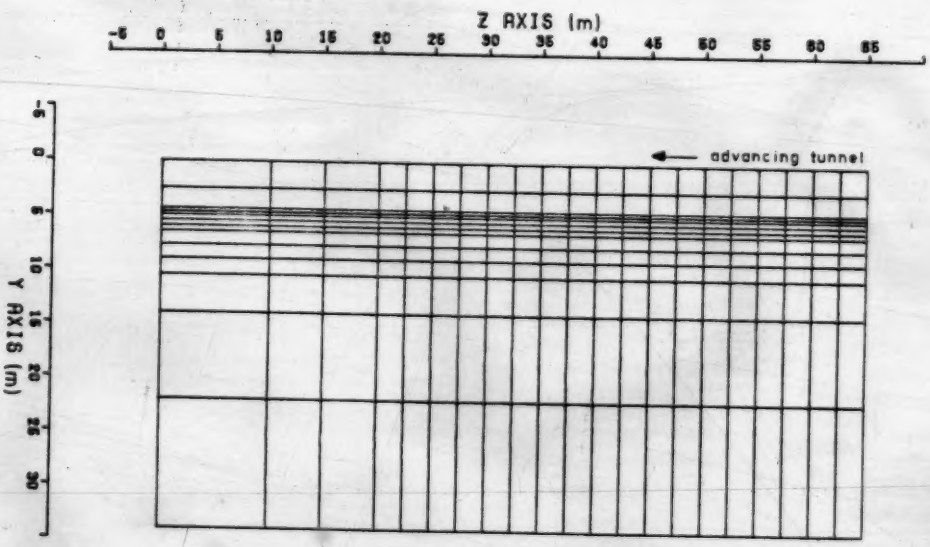

Figure 2.11 Mesh 7

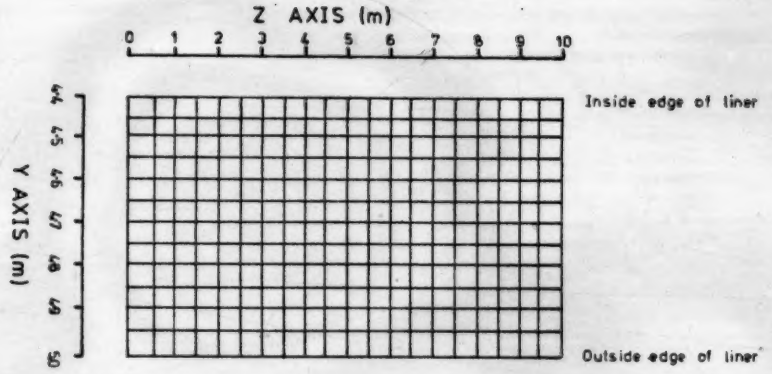

Figure 2.12 Mesh 8

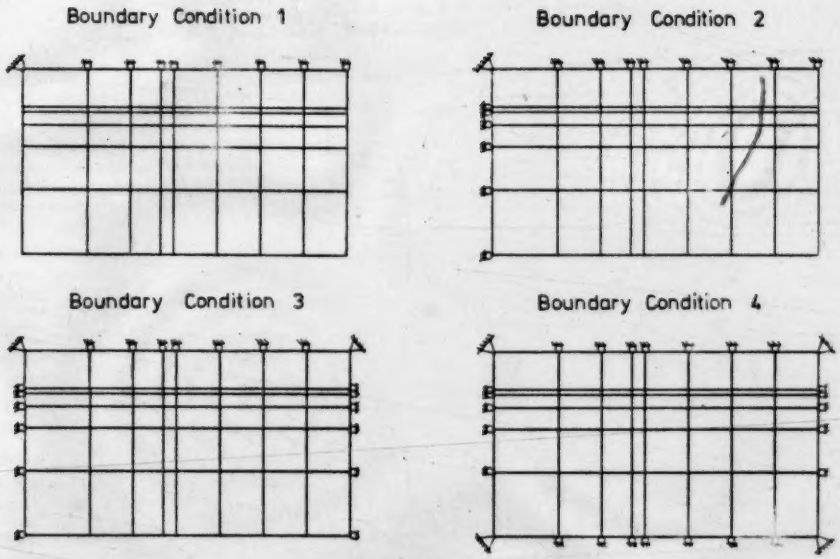

Figure 2.13 Boundary Conditions

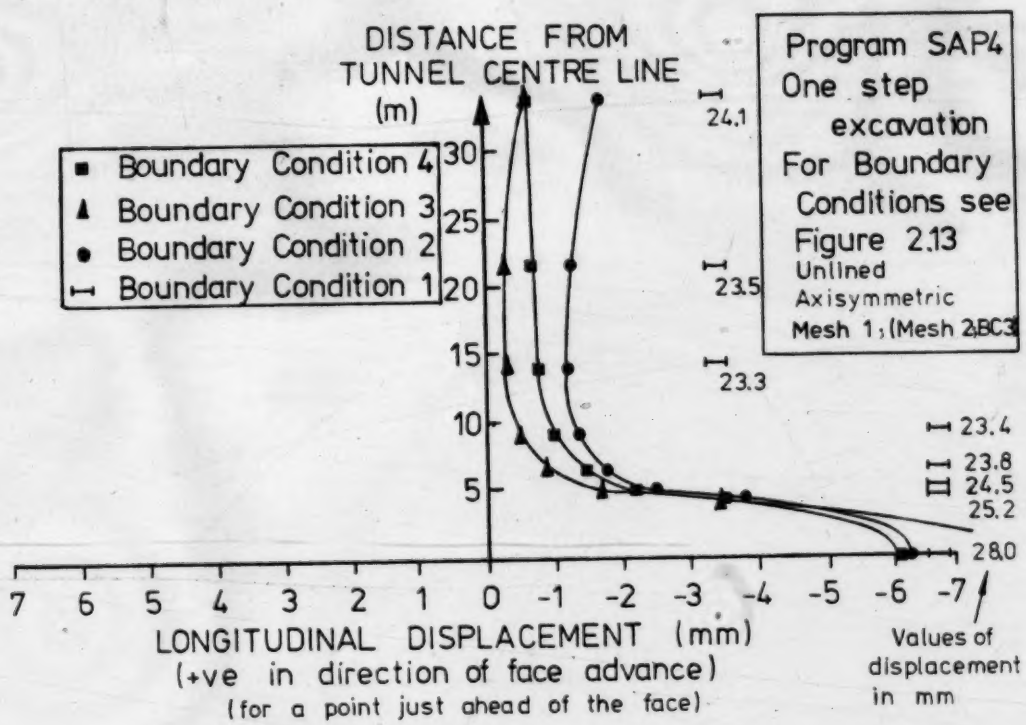

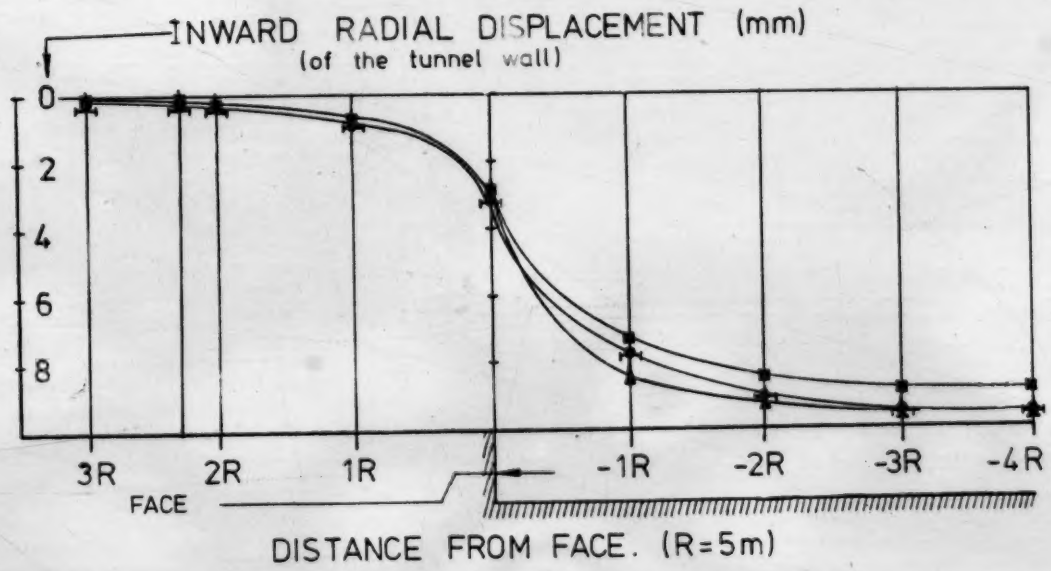

Figure 2.14 Influence of Boundary Conditions on Displacements

also rollered. Boundary Condition 1 was used by Hanafy and Emery (1980) in their analyses; Boundary Condition 2 was the one used for most of the analyses in this study and was also used in the analyses by Einstein and Schwartz (1980).

Figure 2.14 shows the results from a one step excavation of an unlined tunnel using the four different boundary conditions. It can be seen that in the case where Boundary Condition 1 was used the longitudinal displacements for a point just ahead of the face are considerably greater than with the other boundary conditions. It was decided that Boundary Condition 1 would not give reasonable displacements and so was not used in this study. The displacements where Boundary Conditions 2,3, and 4 have been used are all very similar, although Mesh 2 was used with Condition 3, and Mesh 1 with Conditions 2 and 4.

Boundary Condition 2 was chosen for use in this study because it did not restrict the longitudinal displacements at the boundary where tunnel excavation was commenced (although ideally there should not have been complete freedom of longitudinal displacements either). It was also chosen because the results it gave appeared to be reasonable, and the other axisymmetric analyses with which this study is compared, (i.e. Ranken and Ghaboussi (1975) (initially) and Einstein and Schwartz (1980), also used that boundary condition. They did not however explain why they used the boundary conditions they did. It is possible to apply stiff springs to the boundaries of the mesh to

simulate the partially restrained behaviour, but for these analyses it was decided to excavate further into the mesh instead. No case histories were encountered which gave measurements of longitudinal movements with which to compare these results.

Other two dimensional analyses also tend to use Boundary Condition 2, with pressures applied to the free boundaries, for example Gouch and Conway (1976). However in the two dimensional analyses both the boundaries where there are restrictions on the degrees of freedom are also planes of symmetry, whereas in the axisymmetric analysis only the boundary along the tunnel liner is an axis of symmetry.

2.6 Verification of the Numerical Technique

In order to check that the numerical technique gave reasonable results, comparisons with various closed form solutions and other published numerical analyses were made. These comparisons are described below.

2.6.1 Comparison with Closed Form Solutions

The results from the unlined analyses were compared to the results from calculations using the formulae for a thick walled hollow cylinder of infinite length under internal and external pressure. The formulae are presented in Appendix 3 which is referred to below, and in Appendix 1 where bi-linear ground convergence curves are calculated for the

discussion in Chapter 5. The formulae can be found in many standard textbooks, for example, Timoshenko (1941). The situation analysed in order to obtain these formulae is one where the pressure within the hollow cylinder is reduced to zero under a state of plane strain. The cylinder is made of a homogeneous isotropic elastic material and is acted upon by a uniform pressure on its outside face. The displacements are taken as those which occur after the cylinder has been stressed to its initial state, and occur only as a result of changes from the initial state.

Kulhawy (1977) states that the number of excavation steps taken should not influence the stresses and displacements in a homogeneous isotropic body. Thus in the unlined tunnels studied here there should be no difference between those cases where excavation is carried out in several stages and the case where excavation is carried out in one step. Unlined analyses have been compared in Figure 2.20, but are discussed later in more detail in Section 2.6.2.

The elastic hollow cylinder analysis may be extended to include the effect of liner installation on the wall displacements and the ground and liner stresses. The liner is assumed to be another hollow cylinder, concentric and in contact with the first (which represents the ground), having a different elastic deformation modulus and being inserted before the internal pressure is reduced. Continuity of displacement and radial stress is maintained across the

boundary between the liner and ground when the internal pressure is reduced.

Figures 2.15 and 2.16 show the results of a single step excavation using SAP4 compared to the results from a hollow cylinder calculation as outlined above. It can be seen that there is very little discrepancy between the two analyses.

In a large part of this study it has been assumed that with certain construction methods the elastic modulus of deformation was altered, either becoming stiffer or softer. The physical processes by which the modulus may be altered is discussed in Chapter 3 on ground behaviour. In order to check that CONSTEP2 could properly model modulus reduction a situation was analysed where a tunnel was excavated through a cylinder of stiff "frozen" ground surrounded by softer (i.e. lower deformation modulus, see Section 3.2) unfrozen ground. After tunnel construction the frozen ground was thawed so that it had the same deformation modulus as the unfrozen ground.

A two dimensional closed form plane strain visco-elastic analysis was used to check the numerical simulation of a reduction in ground modulus. Only the stresses and displacements at time t = 0 and t = infinity were considered, which correspond to the initial and final states before and after softening. The situation used for the comparison was the excavation of lined and unlined tunnels with a radius of 5 m through a cylinder of frozen ground of radius 9 m, which was thawed (softened) after

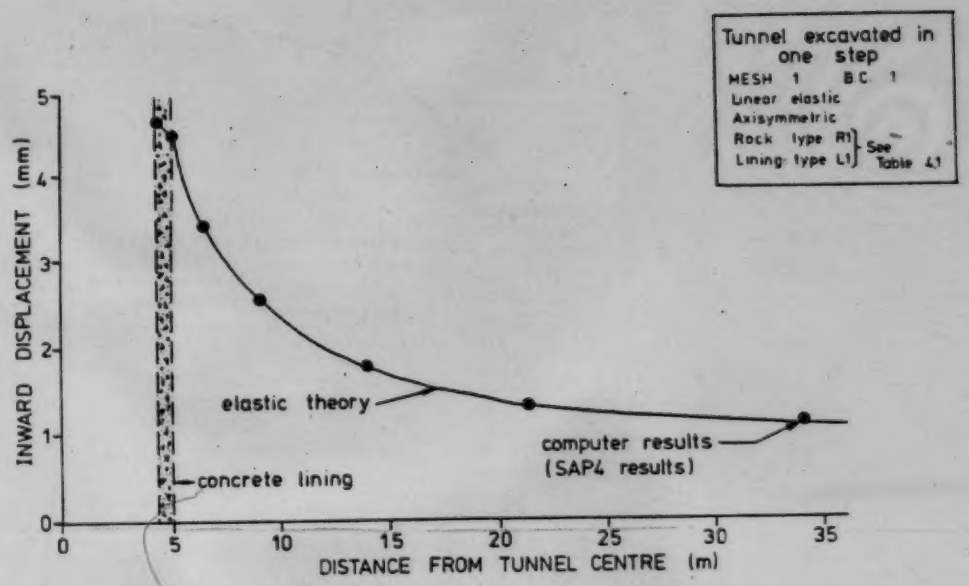

Figure 2.15 FEM and Elastic Theory, Lined Tunnel, Radial Displacements Compared

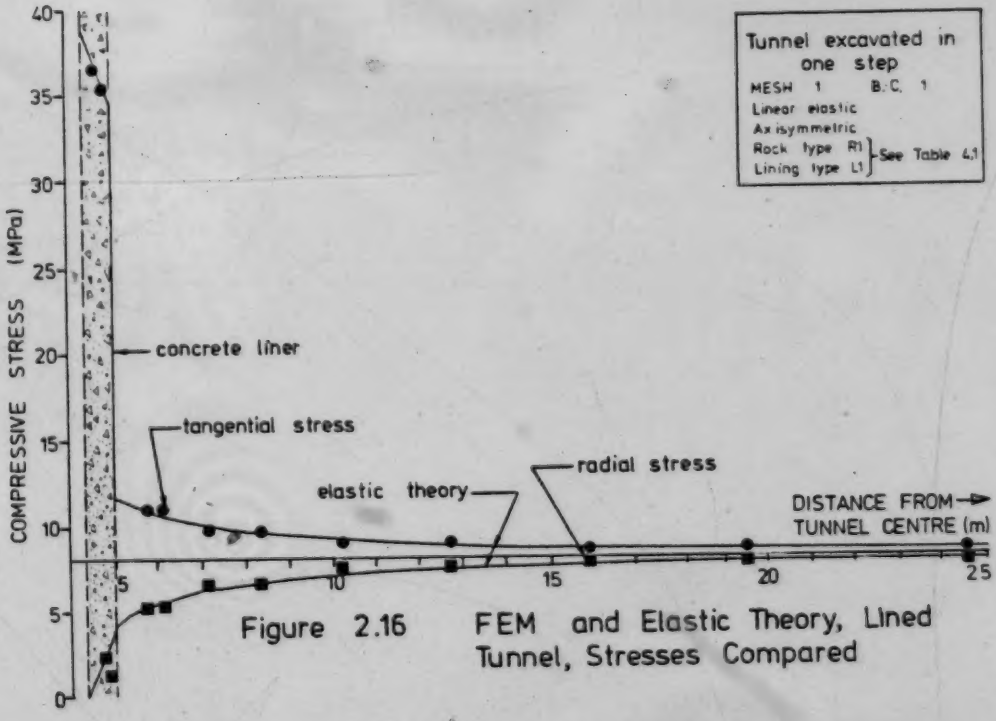

Figure 2.16 FEM and Elastic Theory, Lined Tunnel, Stresses Compared

tunnel construction. The frozen ground modulus was three times greater than the unfrozen and thawed ground moduli. The calculations followed a method outlined by Flügge (1975) and are presented in Appendix 4. A comparison between the results from the calculations and from the analyses using CONSTEP2 are shown in Figures 2.17 and 2.18. It can be seen that the results from CONSTEP2 obtained by using Mesh 4 are very close to those calculated, and confirm that CONSTEP2 can model a change in deformation modulus. The results obtained by using Mesh 2 are not so good (only radial displacements are shown) because of the lower number of elements which are used in the most critical areas, i.e. near the boundaries between different material types.

2.6.2 Comparison with Published Numerical Analyses

Three axisymmetric finite element analyses which modelled the effects around an advancing tunnel face were selected for comparison with the results from the present study. The studies chosen were by Ranken and Ghaboussi (1975), Hanafy and Emery (1980) and Einstein and Schwartz (1980). These analyses are discussed more fully in Chapter 7 where details of the construction and analytical procedures, the material properties and the meshes used are presented. All three analyses studied tunnel excavation in a homogeneous isotropic linear elastic material (as well as some elasto-plastic materials which are not considered here), with and without liner placement at various distances

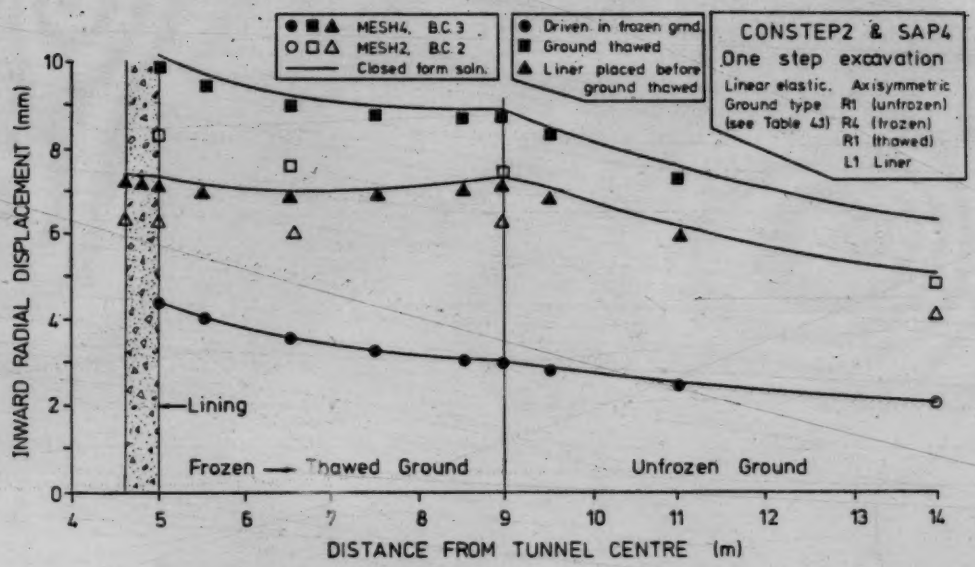

Figure 2.17 Comparison of F.E. Solution and Theory when Ground Modulus is Changing - Displacements

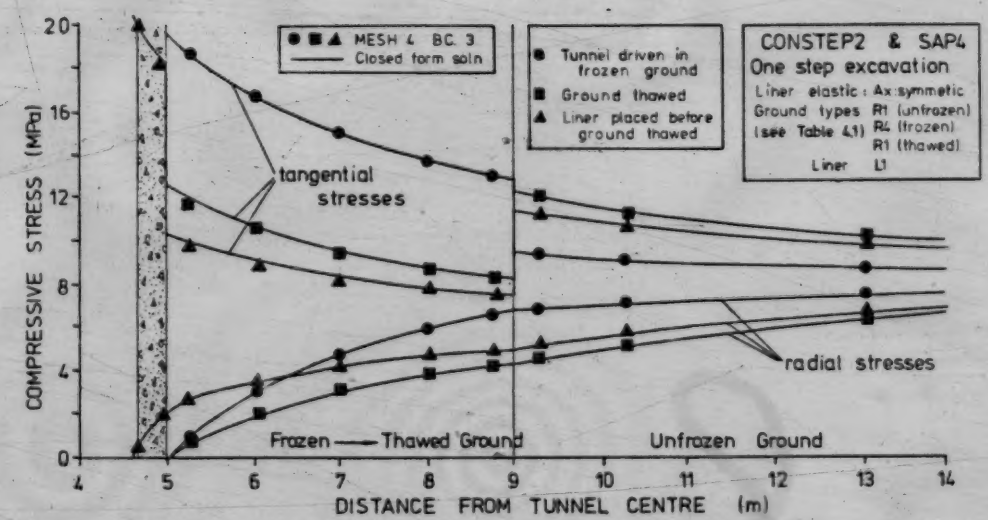

Figure 2.18 Comparison of F.E. Solution and Theory when Ground Modulus is Changing - Stresses

behind the face.

Figure 2.19 compares Hanafy and Emery's (1980) analysis with excavations of length 5R and 7R carried out in one step using SAP4. Agreement between the analyses is quite reasonable. (The applied pressure facility of SAP4 mentioned in the figure refers to a feature which enables a pressure along one boundary of an element to be specified, and thus eliminates the need to calculate nodal forces equivalent to this pressure.) Figure 2.3, discussed previously, compares Hanafy and Emery's results with analyses using CONSTEP, CONSTEP1 and CONSTEP2. Even with CONSTEP2 there is a 'kink' as discussed earlier, but the figure does show that the results are similar, but might be better if more elements were used.

Meshes 6 and 7 were set up with a greater number of elements so that more refined analyses could be undertaken, and they are similar to those meshes used by Ranken and Ghaboussi (1975) and Einstein and Schwartz (1980). Figure 2.20 compares the results from analyses of unlined tunnels using CONSTEP2 and Meshes 2,6 and 7, with the analysis carried out by Ranken and Ghaboussi. The value of u/uo for the unlined two dimensional plane strain case is equal to 1.0. uo is the ultimate radial displacement for an unlined opening in a homogeneous material, calculated from plane strain two dimensional closed form solutions. The "initial construction effects" arise in the analyses using Meshes 6 and 7 because the first construction step is 3R in length,

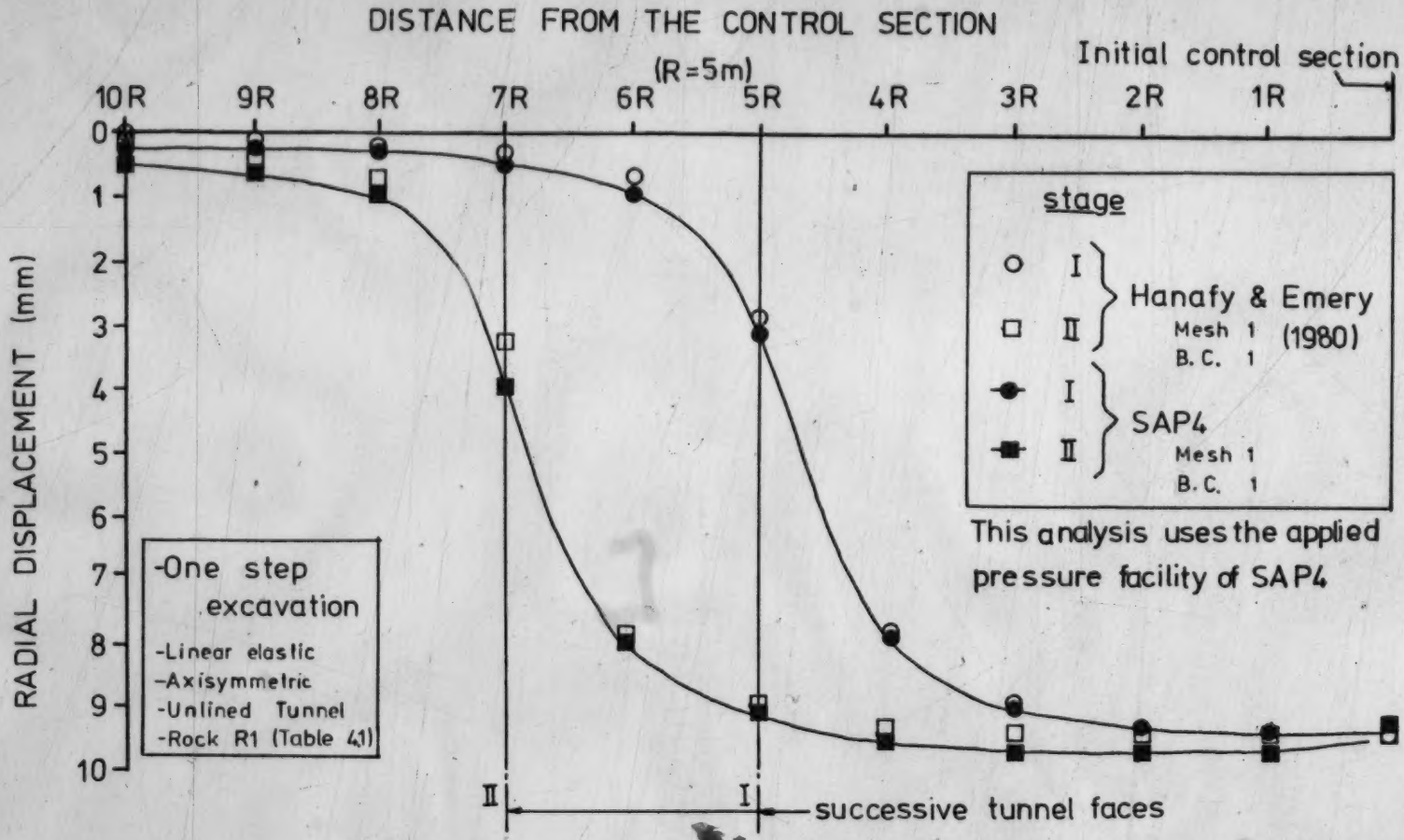

Figure 2.19 Influence of Advancing Face on Radial Displacements, Comparison of Finite Element Simulations - 2

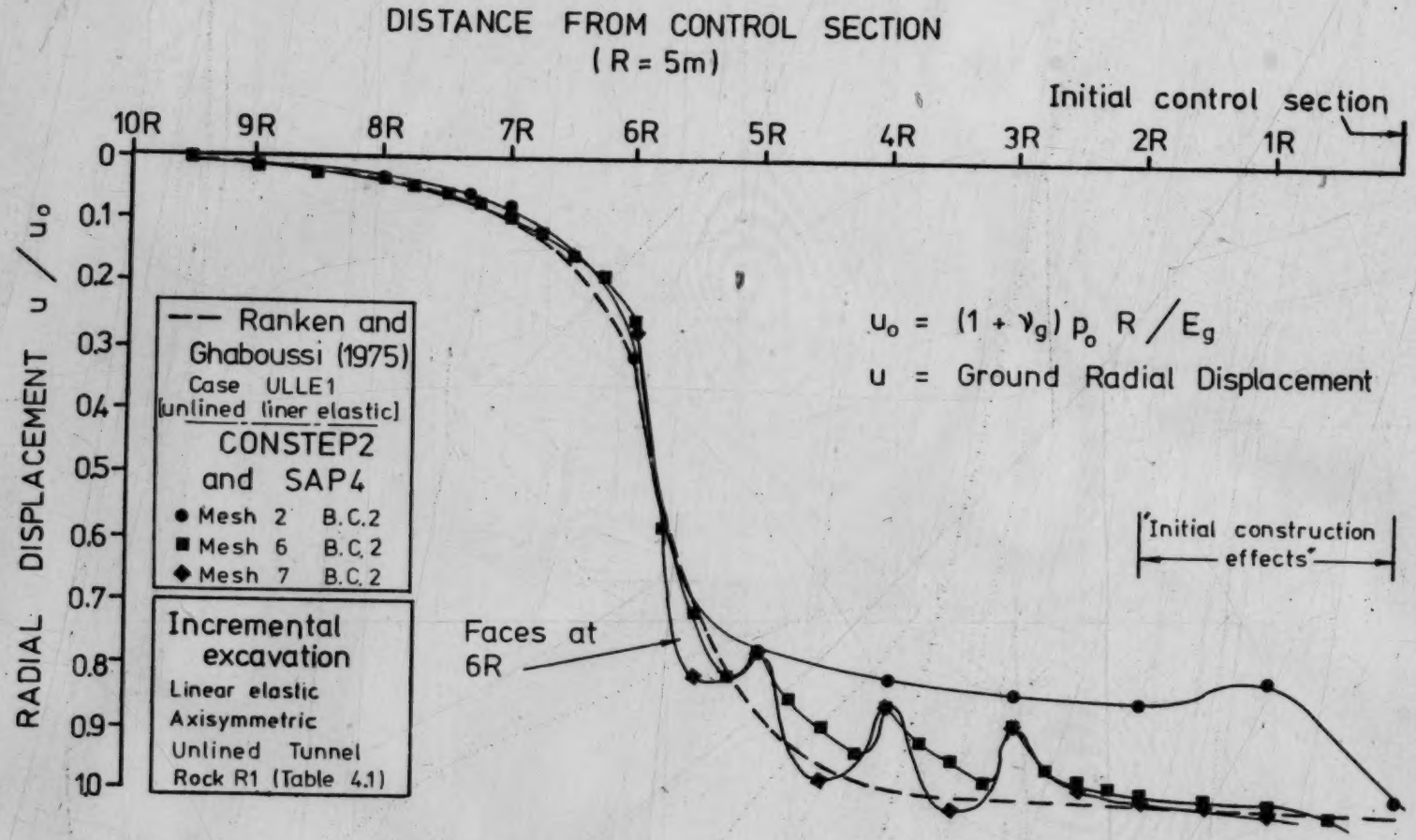

Figure 2.20 Influence of Advancing Face on Radial Displacements, Unlined Tunnel Case

rather than 1R. It can be seen in the figure that there is still a "kink" where excavation steps are longer (along the tunnel axis) than one element. However the analyses using Meshes 6 and 7 approach the "correct" analysis by Ranken and Ghaboussi, and as long as corrections are applied to eliminate the "kink", the analyses can be used to simulate the construction of a tunnel.

The radial displacements at the tunnel wall for one of Hanafy and Emery's (1980) lined tunnel cases is compared to a similar analysis from this study in Figure 2.21. The liner placement is shown in Figure 4.1 - Case 1. The comment about nodal excavation forces made on the figure is discussed in Section 2.7.2 below. The results from this study using Mesh 2 lie below Hanafy and Emery's results, but those from using Mesh 6 generally lie above. As the results for the unlined tunnel using Mesh 6 (Figure 2.20) would appear, if anything, to underpredict tunnel wall radial displacements, it is considered that they would not overpredict displacements in the lined tunnel case, and as Mesh 6 has more elements than that used by Hanafy and Emery (Mesh 1) it should give more accurate results. The fact that a smoother radial displacement distribution is obtained using Mesh 1, but it is not considered to be the most accurate, is discussed in Section 2.7.1.

Further confirmation of the accuracy of the lined tunnel analyses, this time using Mesh 7, is given in Figure 2.22 where the analyses from this study are compared to

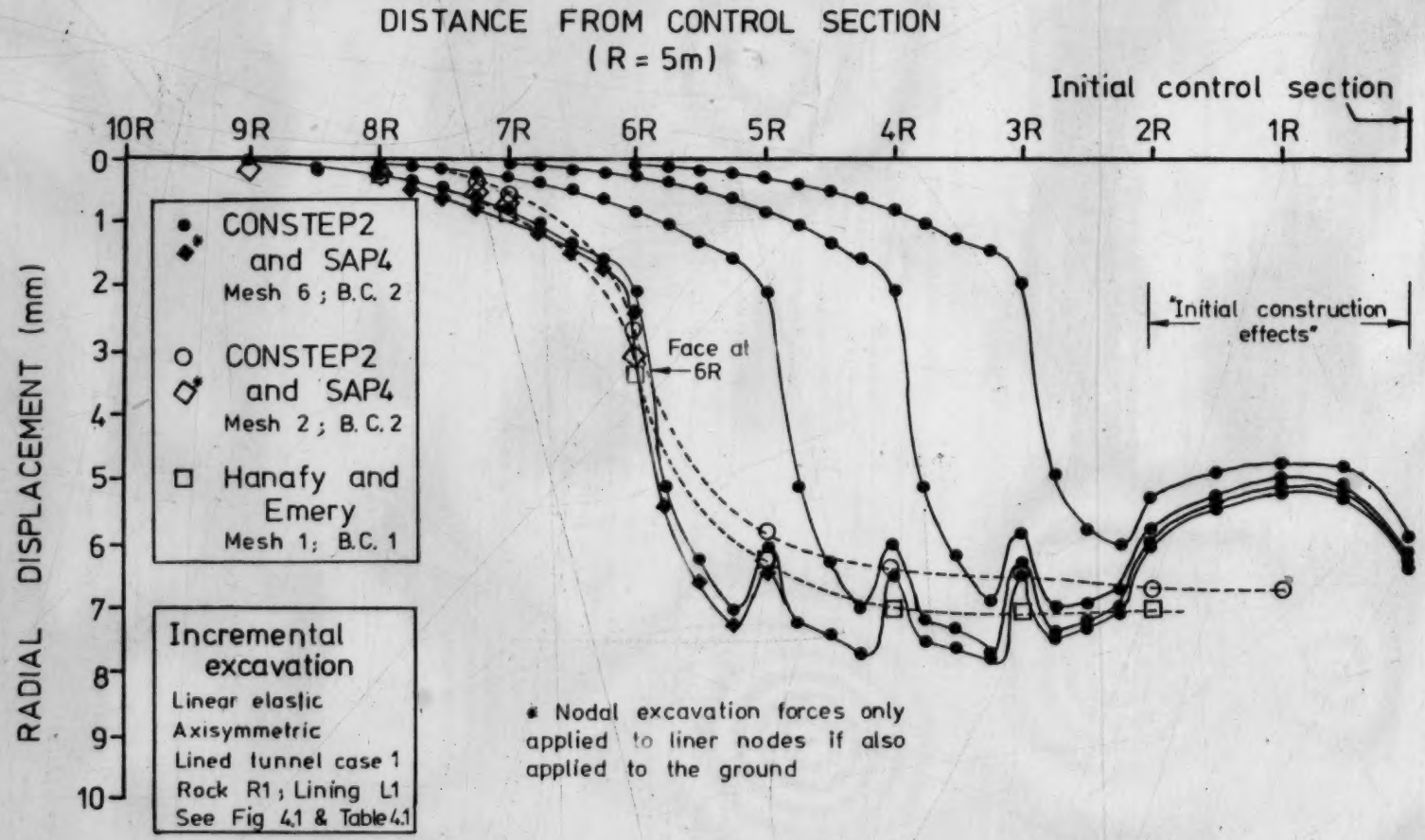

Figure 2.21 Influence of Advancing Face on Radial Displacements, Lined Tunnel Case 1, Meshes 2 and 6

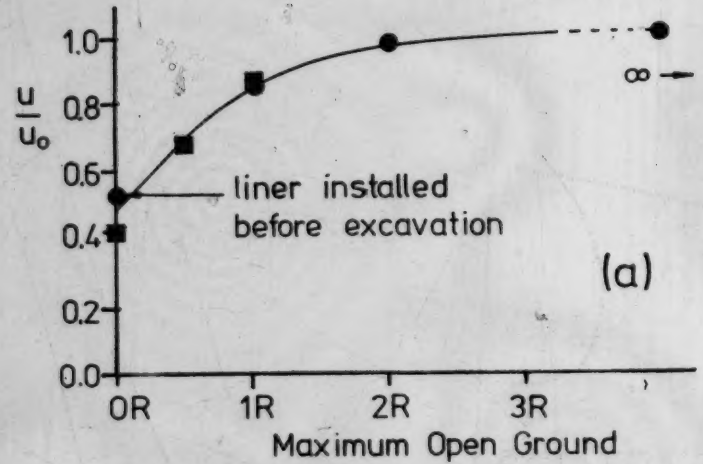

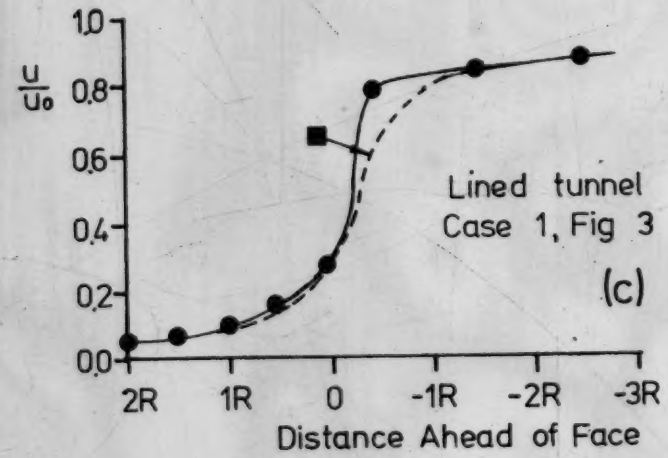

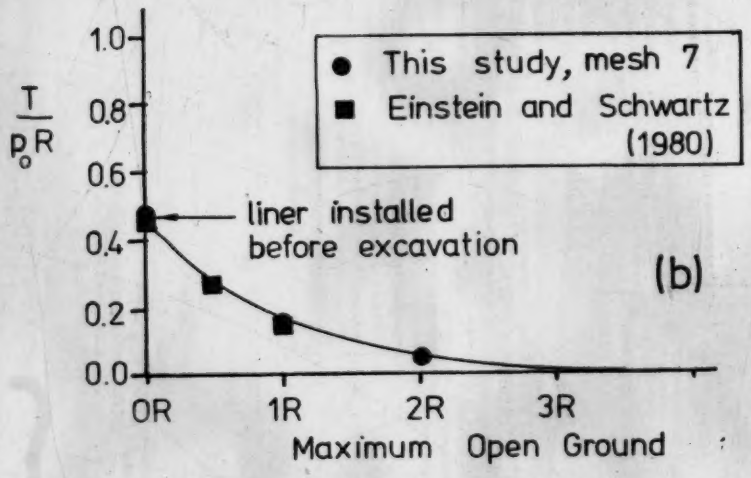

Figure 2.22 Variation of Wall Displacements and Liner Thrusts with Maximum Open Ground and Distance Along the Tunnel

similar analyses by Einstein and Schwartz (1980). Figures 2.22a and 2.22b show the non-dimensionalised ultimate radial displacement and non-dimensionalised liner thrust plotted against the maximum unlined (unsupported) distance, called the open ground, during tunnel construction. Figure 2.22c shows the radial wall displacement against distance from the face. The analyses appear to agree reasonably well.

2.6.3 Summary of Comparisons with Other Solutions

This section shows that as long as a mesh with sufficient elements is used, CONSTEP2 can produce results comparable to other closed form and finite element solutions. There are still discrepancies very close to the face or close to areas of changing material properties, but by comparison with other solutions, particularly the unlined case, it should be possible to calculate correction factors to eliminate them. This is discussed later and the method used to correct the results from these analyses is shown in Appendix 3. Numerical solutions using meshes similar to Meshes 1 and 2 (and similar steps of excavation) are not always accurate enough, and where excavation of length (along the tunnel axis) equal to only one element width is used a "kink", which indicates the extent of the inaccuracy, does not appear. The next section discusses the accuracy of the analyses in more detail.

2.7 Accuracy of the Numerical Model

There are several factors which have an influence on the results obtained from the analyses. Two of these, namely the method used to interpolate nodal stresses from element stresses, and the influence of the mesh boundary conditions, have already been discussed in Sections 2.3 and 2.5 respectively. Other factors are discussed below.

2.7.1 Effect of Element Size on Nodal Stress Interpolation

An attempt was made to reduce the "kink" in the relationship between radial wall displacement and distance along the tunnel axis by using meshes with different sized elements.

The first attempt used Mesh 3 (Figure 2.6) and the results are presented in Figure 2.23. Mesh 3 contains some small elements placed just in front of three successive face positions in order to help improve the interpolation of nodal stresses by reducing the size of the elements close to the face and in the region of high stress gradients. The results show that the radial displacements at Stages IA and II have been overestimated. It will be seen later that the radial stresses in the ground near the tunnel face do not significantly drop below the initial insitu stress po and are generally above po.

Figure 2.24 illustrates how the stress distribution ahead of the face will be calculated, in a two dimensional case for simplicity, and how it overestimates the actual

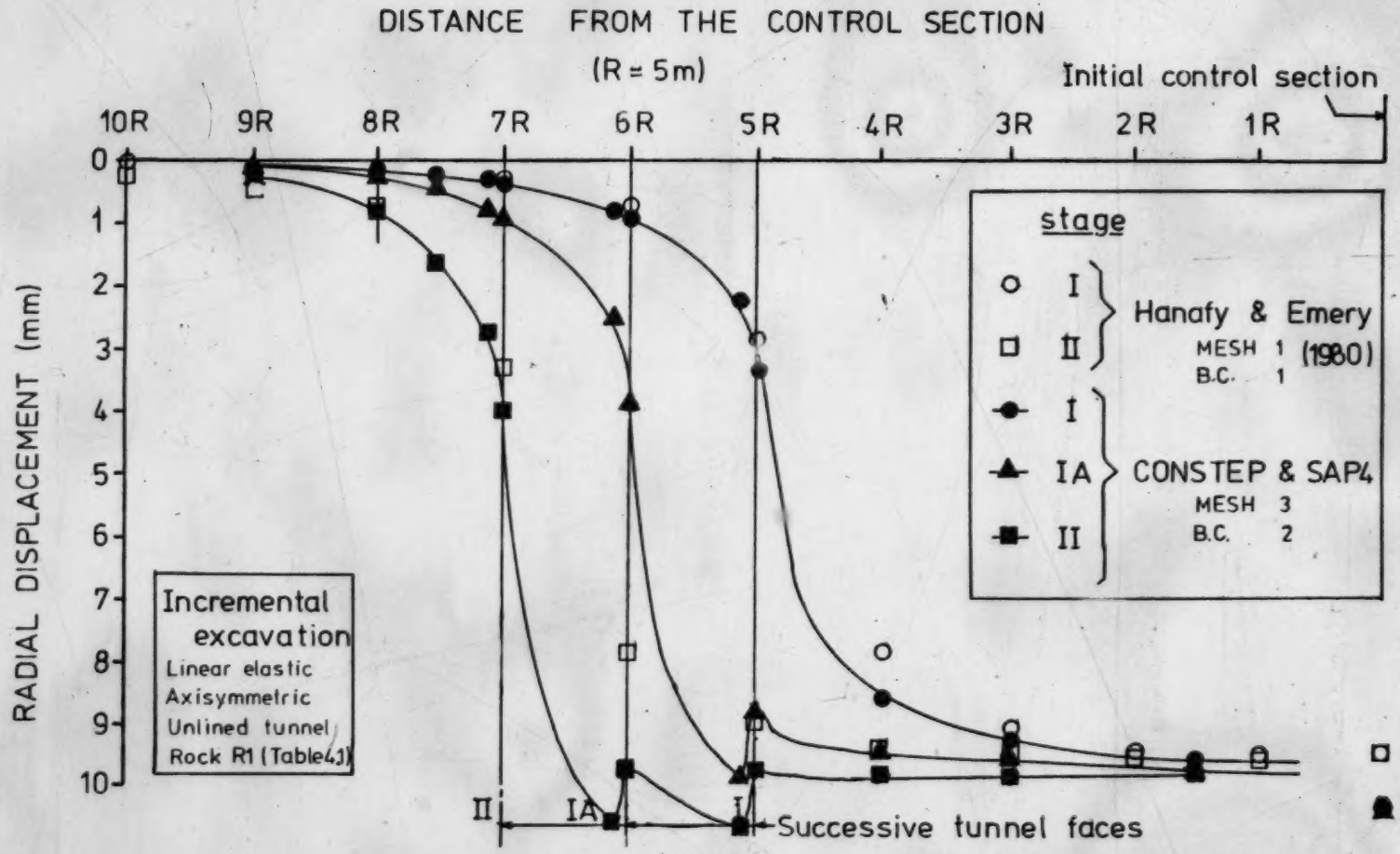

Figure 2.23 Influence of Advancing Face on Radial Displacements. Comparison of Finite Element Simulations, Mesh 3

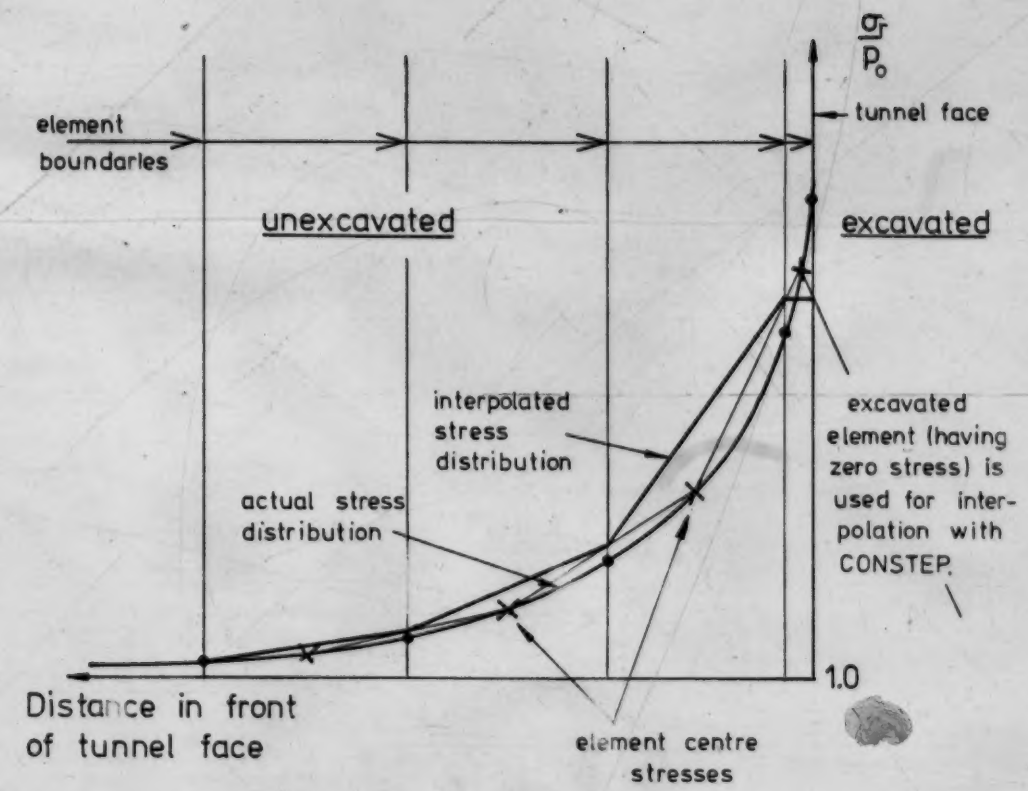

Figure 2.24 Error In Interpolating the Radial Stress Distribution

stress distribution within the ground beyond the immediate vicinity of the face. The use of a small element immediately in front of the face aids the interpolation of stresses near the face, particularly in the method used by CONSTEP, and the effect of any discrepancies are reduced because the forces applied to the nodes will be small as the area of the element boundary next to the (future) wall is also small (see Appendix 2). However, within the unexcavated ground, and where the actual stress distribution is increasing as shown, the interpolation of nodal stresses will produce values larger than the actual values, and when a linear stress distribution is assumed between nodes for the calculation of nodal forces, the actual stress distribution is further overestimated. Hence as the applied nodal forces within the ground being excavated are greater than they ought to be they will produce larger radial displacements than should occur, as shown in Figure 2.23.

A better method is to use more elements within the zone of ground being excavated, and Mesh 3A (Figure 2.7) was designed with the elements increasing in length (along the tunnel axis) away from the face. Only two steps of incremental excavation were carried out using this mesh, and the results are shown in Figure 2.25. There is still a "kink" next to the face in Stage IA, which will always be the case when program CONSTEP is being used, as here. However the distribution of displacements is more reasonable than in the previous case, indicating that with a careful

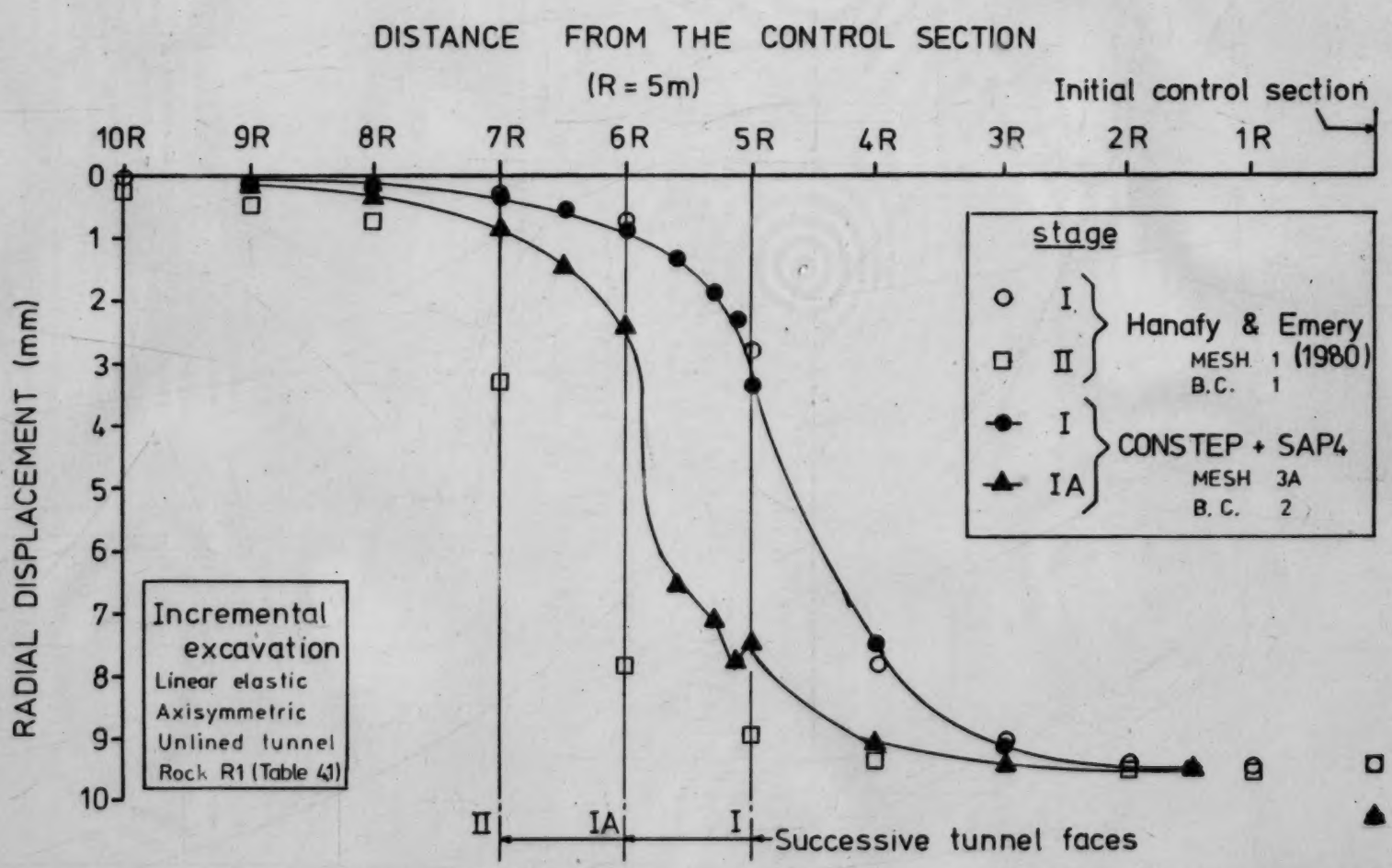

Figure 2.25 Influence of Advancing Face on Radial Displacements. Comparison of Finite Element Simulations, Mesh 3A

choice of elements the results can be improved.

As the excavation of an opening was going to be simulated by a stepwise excavation of successive elements, the effect of excavating through different numbers of elements at each step was considered, and the results are shown in Figures 2.26 and 2.27. These two figures show that as long as the element geometry (i.e. the pattern of elements in the mesh) of the part of ground excavated at each step is kept the same, the radial wall displacement distribution will be the same from one step to the next. When there is a change in the element geometry, as at Stage IIA in Figure 2.26, and when the face is at 8R as in Figure 2.27, the radial wall displacement distribution changes as shown in the figures. In fact a change in element geometry in front of the face, rather than within the zone of excavated ground, can also have some effect on the wall displacements as shown in Figure 2.27 when the face is at 7R.

2.7.2 Longitudinal Liner Stresses and Nodal Forces

In these analyses the material has been assumed to have infinite compressive and tensile strengths. In addition adjacent elements remain in contact with each other and are not allowed to become disconnected. Thus no tensile fracture within the material, or between different materials, e.g. between the ground and the liner, is possible. This becomes important when the liner is placed right up to the face,

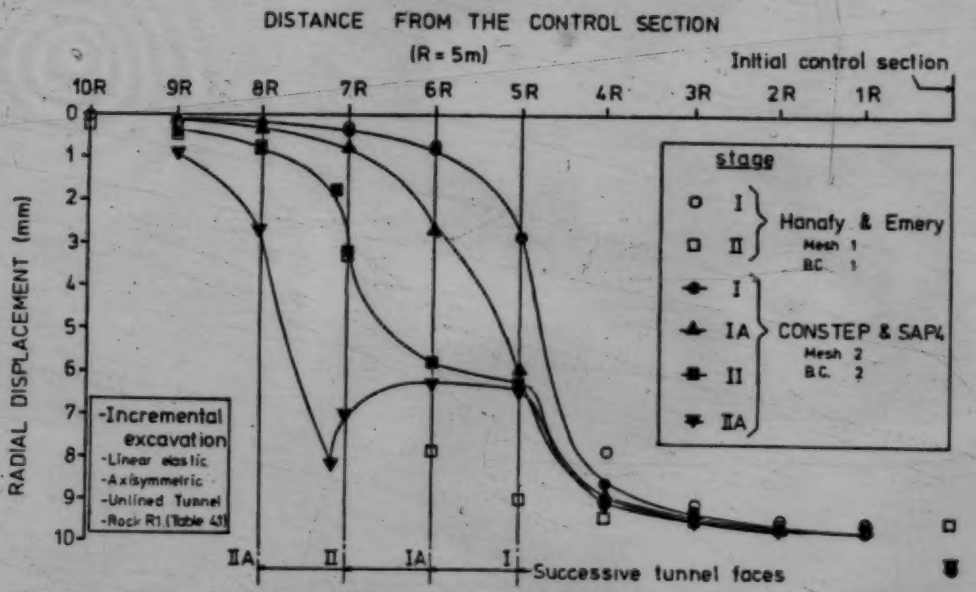

Figure 2.26 Influence of Advancing Face on Radial Displacements. Comparison of Finite Element Simulations. (mesh 2)

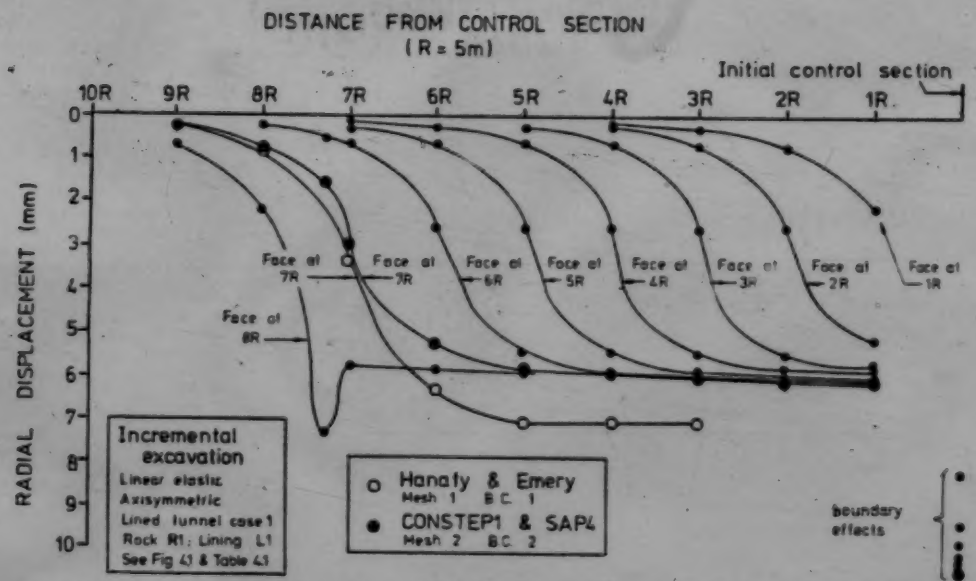

Figure 2.27 Influence of Advancing Face on Radial Displacements Lined Tunnel Case 1, Mesh 2

with its leading element in direct contact with the ground elements at the face. The numerical analysis thereafter assumes that the liner and the face are inseparable, whereas in reality the bond between them, if any, is likely to be small. Because of the various inaccuracies in calculating the nodal stresses and excavation forces, inappropriate forces may be applied to the leading edge of the liner which cause additional, unrealistic, stresses and displacements. For the first few analyses in this study excavation forces were applied to all those nodes which were not completely surrounded by excavated ground after excavation in that step. Thus the forces could be applied to nodes, which after excavation, were only attached to elements of the liner. This method is referred to as *method A* and tended to cause large longitudinal liner stresses and longitudinal ground movements. Thereafter the excavation forces were only applied to those nodes which after that excavation step were still nodes of at least one element of ground (referred to as *method B*).

Although the face is unstressed in a direction normal to it the procedure used for the stress interpolation tends to give a compressive stress normal to the face. Thus using method A the corresponding nodal forces which are subsequently calculated will be applied not only to the nodes attached to elements of the ground and liner, but incorrectly to nodes attached only to elements of liner after excavation has taken place. These incorrect forces

will be applied in the same direction as the tunnel advance increasing the longitudinal tensile stress in the liner. This effect will accummulate during the incremental excavation and inappropriately large tensile liner stresses in the longitudinal direction, and longitudinal liner displacements in the direction of the tunnel advance, will result.

Figures 2.28 to 2.31 illustrate the longitudinal movements within the ground for various cases using method A and method B to apply the nodal excavation forces. The tunnel construction cases are shown in Figure 4.1 and are described in detail in Chapter 4, but for this comparison it is sufficient to know that in Cases 1 and 3 the liner is placed right up to the face, but in Case 2 the liner is not. In Case 3 the ground in front of the face is softened, and thus its stresses reduced, during excavation of the ground adjacent to it. The nodal forces at the face were applied according to method A in all the figures, except Figure 2.29 where method B was used. Because in Case 2 (Figure 2.30) the liner is not placed right up to the face the nodal forces are effectively applied according to method B. The results show quite clearly that where nodal forces are not applied to the liner only (Figures 2.29 and 2.30, method B) the longitudinal displacements are all away from the direction of face advance. Where the nodal forces are applied to the liner only (Figures 2.28 and 2.31, method A) relatively large displacements occur in the direction of the tunnel

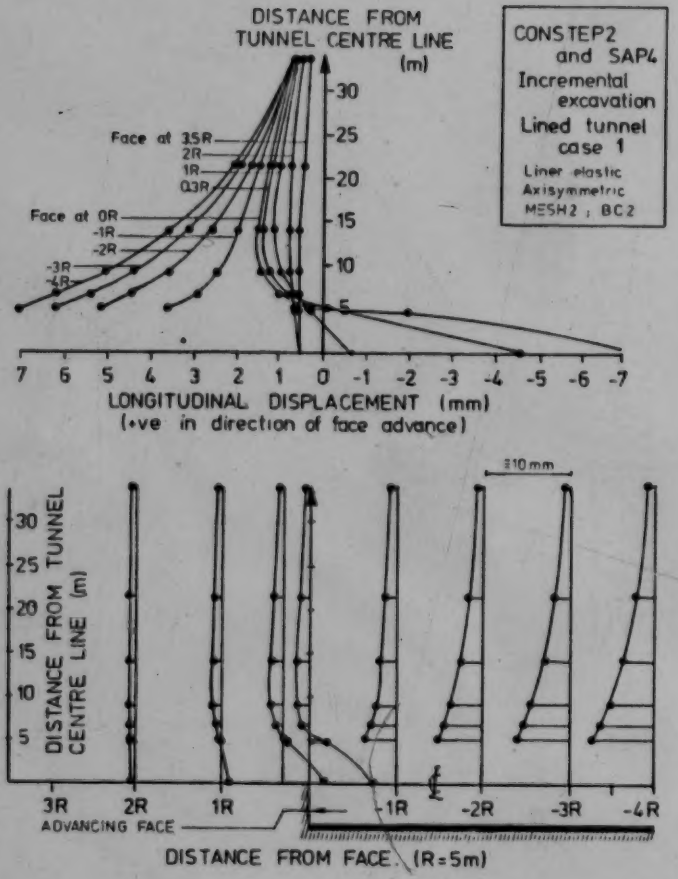

Figure 2.28 Influence of Advancing Face on Longitudinal Displacements. Lined Tunnel Case 1 - (a)

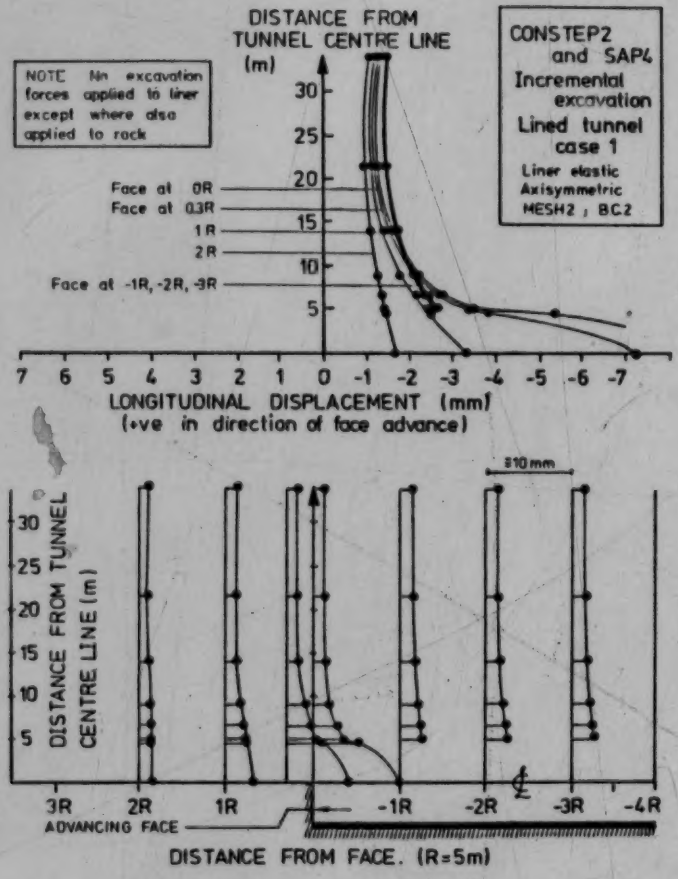

Figure 2.29 Influence of Advancing Face on Longitudinal Displacements. Lined Tunnel Case 1 - (b)

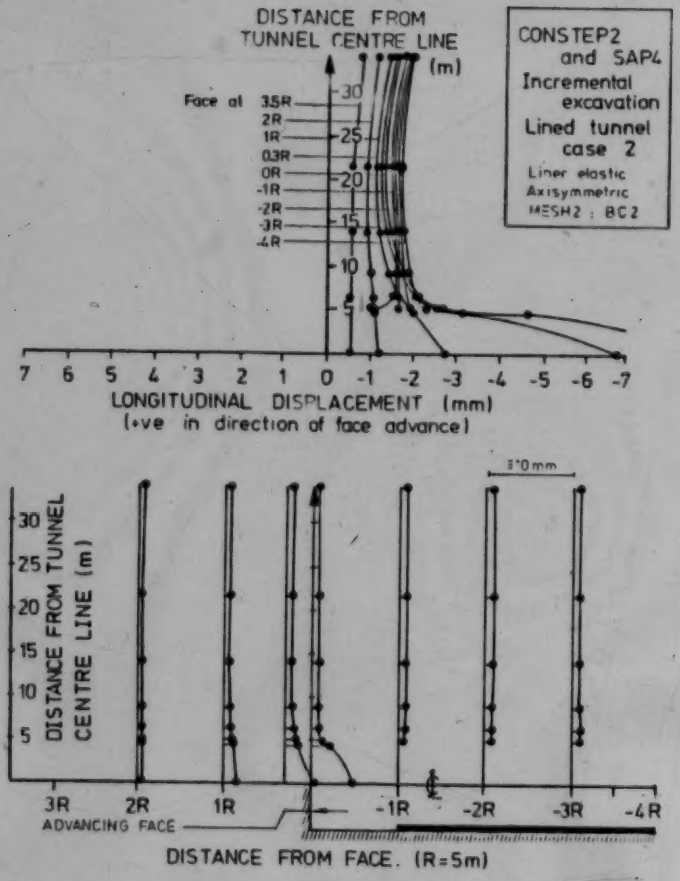

Figure 2.30 Influence of Advancing Face on Longitudinal Displacements. Lined Tunnel Case 2

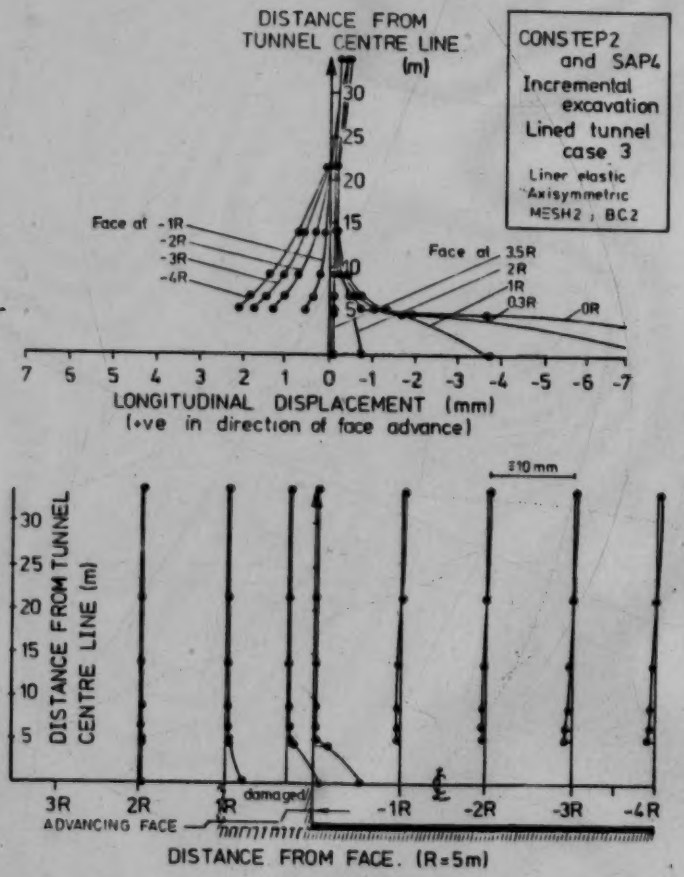

Figure 2.31 Influence of Advancing Face on Longitudinal Displacements. Lined Tunnel Case 3

advance, although the displacements are less in Case 3 because the face is less stressed before it is excavated.

In most of the analyses method B has been used for the application of the nodal excavation forces. However the adverse effects of using method A were not discovered until after the initial analyses were done and so it should be assumed that all the analyses carried out using Meshes 1,2,3 and 3A do *not* follow this procedure unless otherwise stated.

2.7.3 Triangular and Rectangular Elements

As CONSTEP, CONSTEP1 and CONSTEP2 were programmed to handle only rectangular elements, and not triangular elements, a comparison between an analysis using triangular elements and a similar one using rectangular elements was carried out with SAP4. The results are shown in Figure 2.32 where a stress of 8 MPa is applied to the inner face of a ring of material, the z axis being the axis of rotation. Because the triangular elements are not symmetrical about an axis in the plane of the ring, non-symmetrical deformations were produced, whereas with the rectangular elements symmetrical deformations were produced. It was therefore considered that as reasonable results could be obtained with rectangular elements alone it was not necessary for the initial versions of CONSTEP to have the ability to handle triangular elements, which would have added some complexity to the programming.

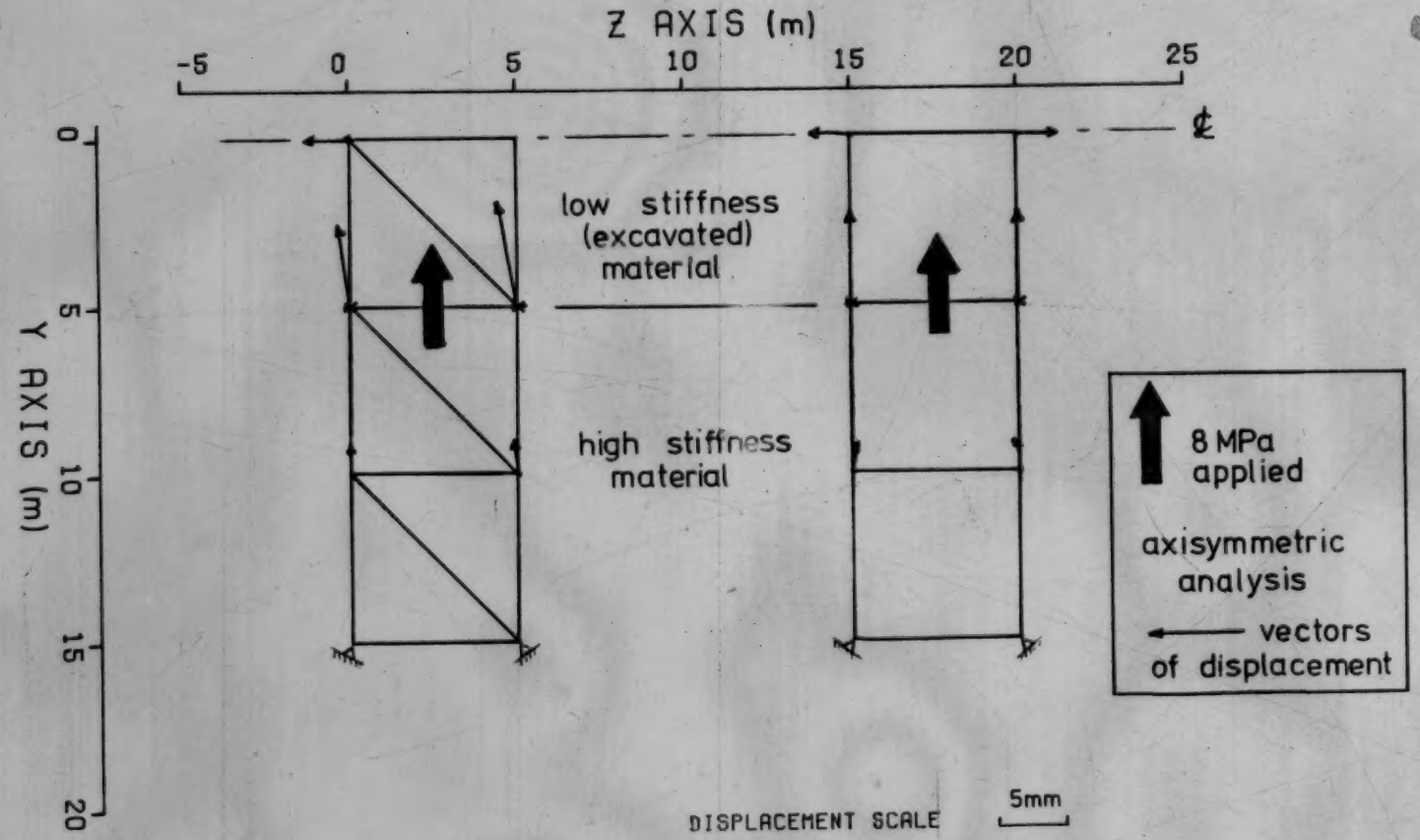

Figure 2.32 Displacements from Triangular and Rectangular Finite Elements Compared

2.7.4 Summary of Inaccuracies in the Technique

The accurate interpolation of nodal stresses becomes very difficult in regions of high stress gradients. Where these gradients occur at a boundary between the excavated and unexcavated ground CONSTEP2 uses a technique whereby it selects only unexcavated elements for the stress interpolation. This reduces errors at the walls of the opening. High stress gradients also occur within the ground and linear interpolation, with the assumption of linear stress distribution at the element boundaries, does not accurately model the actual stress distribution unless the elements are small. Element sizes should be chosen so that they are small in areas which will at some time during the excavation have high stress gradients.

The boundary conditions chosen along the edges of the mesh will affect the results. In the area of interest, around the tunnel face, the situation is neither plane stress nor plane strain, and so a compromise is reached by using roller supported boundaries at the axis of rotation, and at the edge of the mesh perpendicular to the axis of rotation and which does not have the opening passing through it.

Care has to be taken with the application of nodal forces to simulate excavation, especially where these may not be accurately calculated. In most of the analyses in this study excavation forces were only applied to those nodes which were at corners of at least one element of

ground which remained unexcavated at the end of that step of construction. However it should be noted that this procedure was not carried out with analyses using Meshes 1,2,3 and 3A unless otherwise stated.

The shape of the element has an effect on the results, and rectangular elements were used here because it was shown that triangular elements can produce discrepancies, and also the programming was greatly simplified if only rectangular elements were used. This produces its own problems as without triangular elements it becomes difficult to design a mesh having large elements in all the regions of low stress gradients and small elements in all the regions of high stress gradients. The compromise between accuracy and computing time then becomes more difficult to achieve.

CHAPTER 3

GROUND BEHAVIOUR

3.1 Introduction

In this investigation the ground was assumed to be homogeneous, linear elastic, time independent and to have infinite strength. The stiffness or deformation modulus of the ground close to the opening was varied to simulate the effects of various construction methods on the ground. These assumptions obviously oversimplify the behaviour of ground masses, which will be dependent on the intact ground properties, the mass structure, the nature of the infilling in discontinuities and many other factors. Ground strength and stiffness will also depend on factors such as loading rate, confining pressure and time.

During a round of blasting it has been assumed that the rock to be excavated has been highly disintegrated and no longer provides any substantial support to the surrounding ground mass. The blasting process also fractures some of the surrounding rock which still maintains its ability to support itself and provides confinement to the remaining ground. An idealised picture of blast damage is shown in Figure 3.1a, taken from Hoek and Brown (1980), where the pulverised zone is equivalent to the disintegrated rock, and the cracked zone to the damaged or fractured rock. The crack pattern developed during blasting will depend upon the type

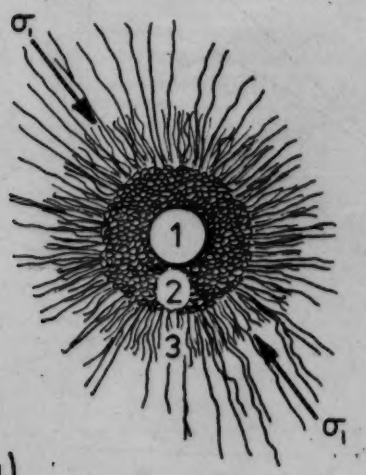

(a)

Idealised picture of fracturing induced by detonation of an explosive in a borehole. (Hoek & Brown, 1980)

1. Borehole
2. Pulverised zone
3. Radial cracks with preferential growth parallel to σ_1, the major principle stress

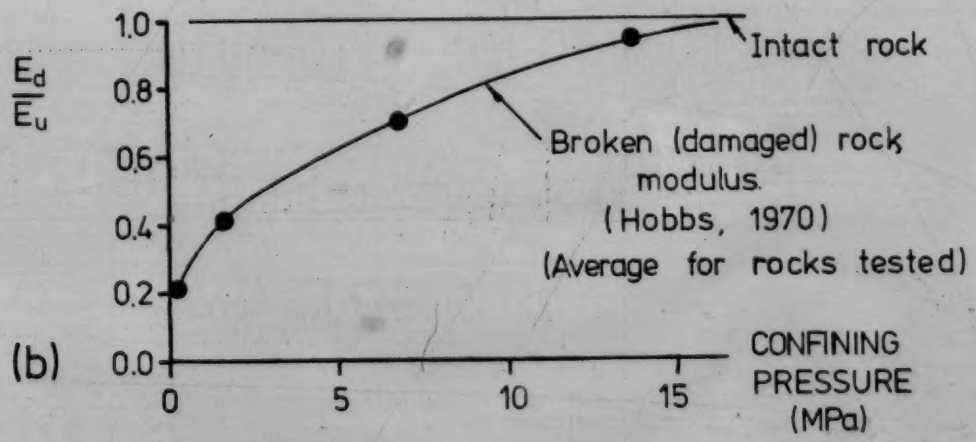

(b)

Figure 3.1 Damaged Rock Modulus

of rock, its anisotropy, pre-existing fissures, the initial state of stress and the proximity of the free boundary. The extent of the cracking will also be influenced by the shot hole diameter and the size of charge. Gustafsson (1976) states that a fully charged 40mm diameter hole in relatively homogeneous rock of the gneiss-granite type may be expected to give a 2 m deep cracked zone. Section 3.4 below discusses how blast damaged rock was modelled and how it relates to observed ground behaviour.

The technique of supporting an opening by ground freezing has been often used, and its main functions are to help support the excavation and to prevent water seepage into the opening. It is only effective in ground which contains pore water or water in the fissures (for rock) and where the ground water flow rates are sufficiently low to enable a complete ring of ground to freeze. In this study the frozen ground is, like the unfrozen ground, assumed to be homogeneous, linear elastic, time independent and have infinite strength. However frozen soil in reality behaves visco-plastically, i.e. creeps under stress, and is strongly dependent on time, temperature and stress level. In addition to ground movements caused by stress relief during excavation, there will be movements caused by frost heave and thaw consolidation. A general review of these effects is given by Andersland and Anderson (1978), but the behaviour of ground during freezing and thawing is too complex to be accurately modelled by the simplified method of analysis

used here. Section 3.3 discusses the way in which frozen ground behaviour has been modelled and Section 3.6 relates it to actual construction methods and field observations.

3.2 Difference Between Weakening and Softening

Rock exhibits both weakening and softening behaviour under stress, but as this study only considers softening, the difference between them is illustrated in this section.

A material becomes weaker if the maximum stress which it can sustain is reduced, whereas it becomes softer if it undergoes more deformation for the same change in applied stress. Figure 3.2 illustrates the difference between weakening and softening for different conditions of confining pressure and strain rate shown by the results from laboratory tests on several different rock types. The Westerley Granite exhibits a decrease in material strength for a decrease in confining pressure, although its stiffness is not significantly altered under different confining stresses, particularly at low values of stress difference. The stress-strain curves for the Tuff show that it becomes weaker with a reduction in strain rate, but does not become softer. The sandstone behaves in a different manner, its stiffness reduces, i.e. the material becomes softer, with decreasing strain rate, but the peak strength is only slightly reduced.

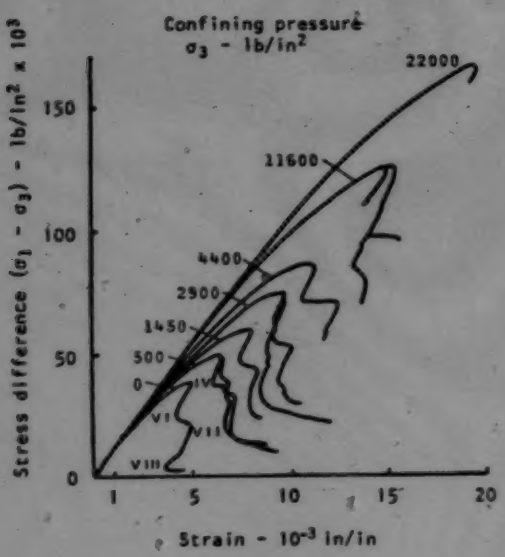

a) Complete stress-strain curves for Westerley granite tested by Wawersik and Brace (1971)

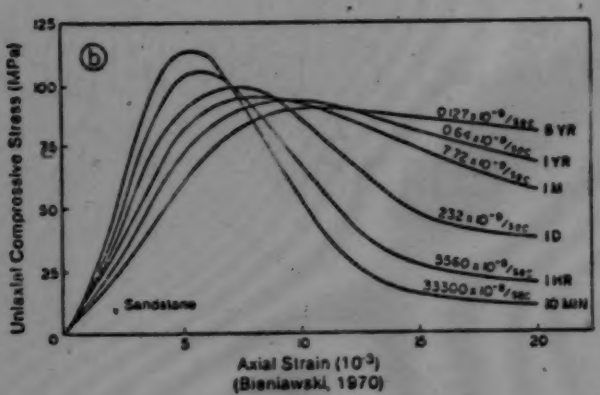

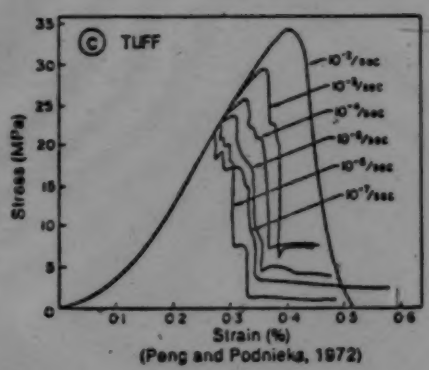

Stress strain diagrams from uniaxial compressive tests reported by (b) Bieniawski (1970) and (c) Peng and Podnieks (1972).

Figure 3.2 Stress-Strain Behaviour of Rocks

In this investigation the strengths of the materials are not altered, but the deformation moduli are changed during the course of construction. In the field both the strength and the stiffness of the ground will be affected to a varying extent by the construction procedure. However, even with ground of infinite strength a change in its stiffness can cause a substantial stress redistribution within the ground.

3.3 Simplified Modelling of Ground Behaviour

As described previously the ground in this study was assumed to behave linear elastically. However using the ability of CONSTEP2 to model a change of deformation modulus, and to do so in several different ways, it is possible to simulate in a simplified manner the change of ground behaviour in response to the construction procedure.

Figure 3.3 shows four different models of ground behaviour. The first, Figure 3.3a, is the material which behaves according to Hooke's Law, with a unique Young's modulus, or modulus of deformation, E. In Figure 3.3b the behaviour of a bilinear elastic material is shown, which has a certain stiffness E1 up to some defined point and thereafter a reduced stiffness E2. The change point has to be defined by some criterion based on the factors described above which affect material behaviour. This model can be used to approximate non-linear elastic behaviour. If E2 is

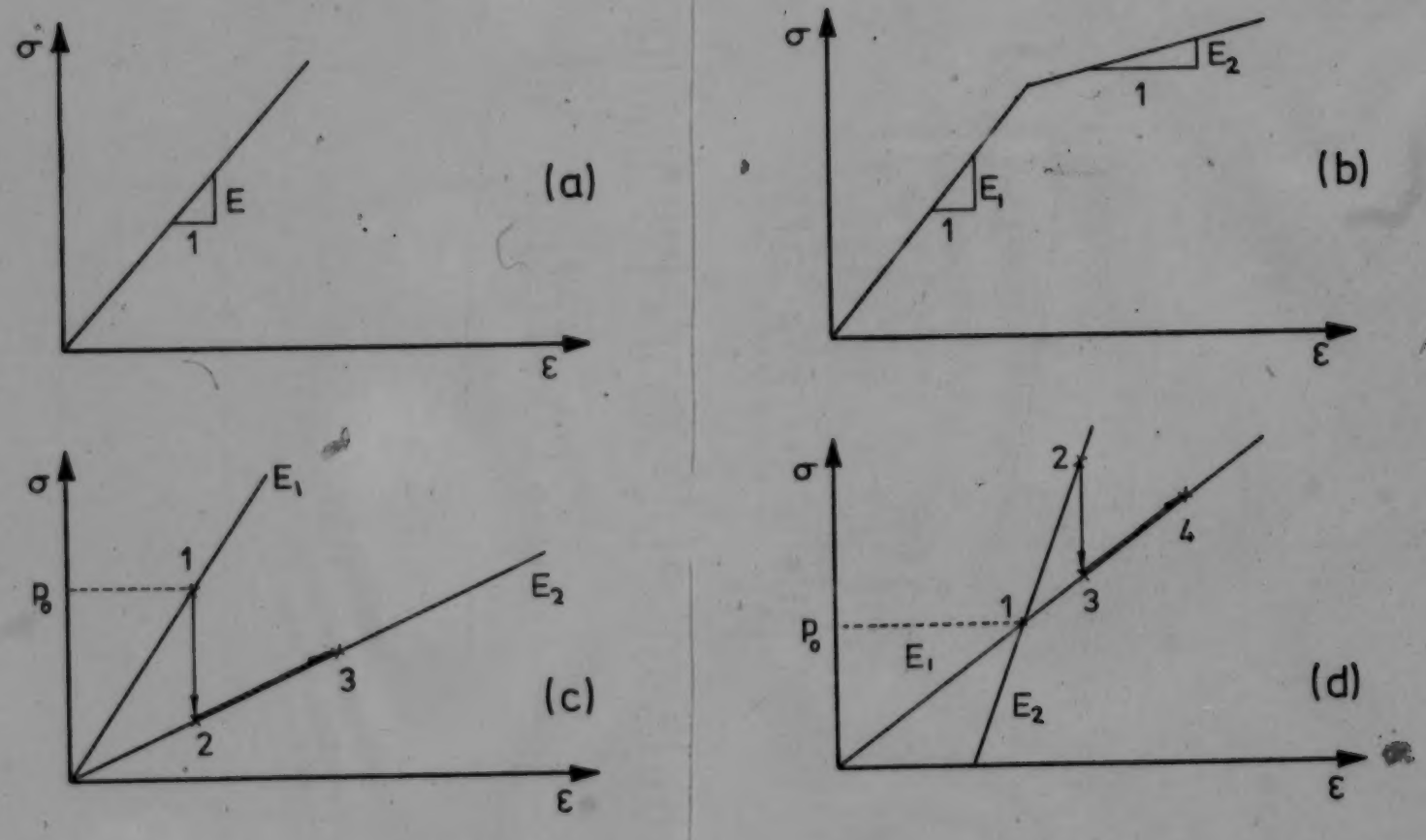

Figure 3.3 Simplified Models of Ground Behaviour

very small a pseudo elastic-perfectly plastic material may be modelled where the volume changes associated with plastic yielding are handled through the selection of an appropriate Poisson's ratio. However, if the changes of stress at any point are not always of the same sign during construction, and the unloading modulus is not the same as the loading modulus, complications in the programming occur.

In Figure 3.3c the mechanism of softening is shown. In the initial state, point 1, the ground is under an initial insitu stress po. If it becomes softened, but is not allowed to deform, it can only sustain a lower stress, and move to point 2, the balance of the remaining stress having been taken up by stresses applied to the system. If these balancing stresses are removed the stresses within the system are redistributed, displacements occur, and the softened ground moves to point 3. The softened ground has in effect shed some of its stress to the surrounding ground.

A simple method of simulating freezing and thawing is shown in Figure 3.3d. The model assumes that no volume change occurs in the material solely as a result of processes of freezing and thawing, i.e. there is no frost heave or thaw consolidation. The stiffness of the thawed ground has been assumed to be the same as that for the unfrozen ground, but this need not be the case, and the frozen ground is assumed to be stiffer than the unfrozen ground. The ground is initially unfrozen, with a modulus E1, and under an initial insitu stress po. It is then frozen and

has a new stiffness E2, but as there are no changes in volume during freezing, and since the new stiffness only applies to subsequent stress changes, the material stays at point 1. To verify that in this case a stiffness increase does not produce stress changes, consider the ground to be a saturated sand. The initial effective stress is taken by the soil skeleton, which on freezing at no volume increase, or other changes to the soil fabric, still retains the initial effective stress. The frozen water in the pores remains stressed only with the hydrostatic pressure, which has been ignored in these analyses. On excavation there are ground movements and stress changes, and the frozen ground mass, now behaving with a stiffness E2, moves to point 2. When the ground is thawed the process is similar to that described for a stiffness reduction, but in this case the origins of the two stress-strain relationships will be different. This must be the case, for if the ground were frozen and then unfrozen without any excavation there would be no resultant change in the system, the soil skeleton would still be carrying the initial effective stress, and not "know" that the water in the pores had been frozen and thawed. The way in which these assumptions about ground freezing and thawing relate to actual practice is discussed in Section 3.6.

3.4 Rock Damage by Blasting

As described above blasting will not only loosen and pulverise the rock to such a degree that it can be considered excavated, but will also fracture and damage surrounding rock and hence change its material properties.

Bieniawski (1978) has presented a relationship which shows the rock mass deformation modulus decreasing with decreasing rock mass quality, Figure 3.4. The fracture spacing is one of the dominant parameters which affects the deformation modulus, particularly for rock masses of fair to good quality (NGI classification). In rock of poor quality other factors, such as the nature of the infilling in discontinuities, become more important and exert a greater influence on the ground behaviour. The pattern and extent of the fractures caused by blasting can have a considerable effect on the stiffness of the material in the damaged zone.

Hobbs (1970) has tested intact and broken specimens of English Coal Measure rocks under various confining pressures, and average values of his results have been presented in Figure 3.1. The actual results of modulus against confining pressure for solid specimens, and for specimens which were broken at different confining pressures but with similar fracture patterns, are shown in Figure 3.5. The modulus of the intact specimens was virtually unaffected, but as the confining pressure was reduced below about 15 MPa the modulus of the damaged rock specimens reduced rapidly from an initial value comparable to the

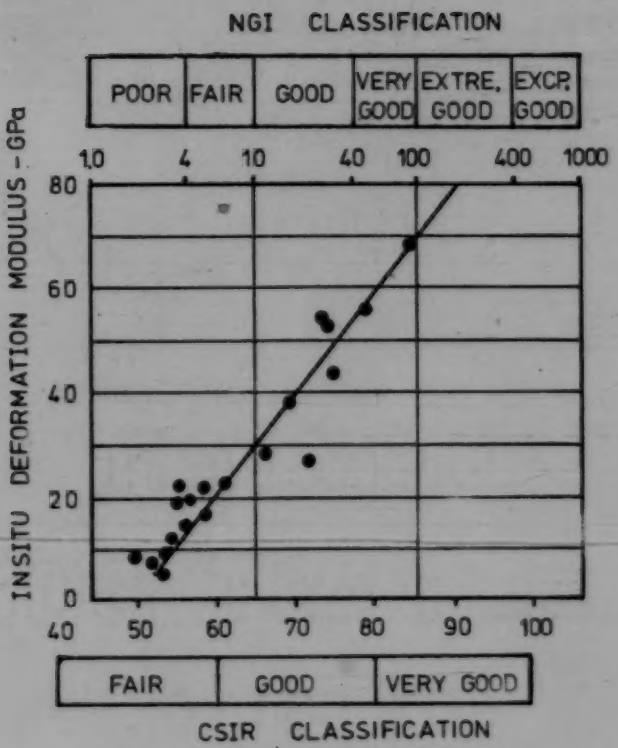

Figure 3.4 Relationship Between Insitu Deformation Modulus of Rock Masses and Rock Mass Classification, Bieniawski (1978)

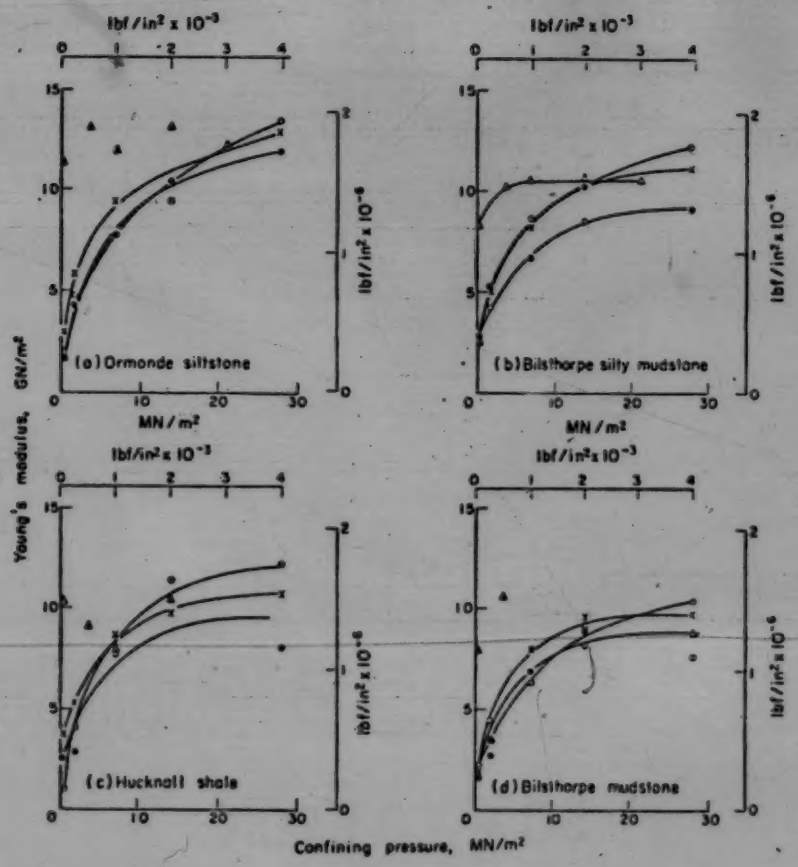

Confining pressure at which solid specimens were broken before testing	MPa	lb/in²
●	0	0
×	3.4	500
o	13.8	2000
△	Solid (unbroken) specimens	

Figure 3.5 Variation in Young's Modulus with Confining Pressure for Both Solid and Broken Specimens, Hobbs (1970)

undamaged rock modulus. Near an excavation the local confining pressure will be dependent on the three dimensional state of stress, which will itself be influenced by the variation and severity of the damage around the opening. It is therefore difficult to define a reasonable confining pressure for the determination of the damaged rock modulus and so the simplified approach described in the next section and in Chapter 4 has been adopted.

3.5 Numerical Modelling of the Zone of Damaged Ground

Many published analyses of the behaviour of underground openings have assumed that a zone of rock around the opening has been damaged by the construction process, and various different assumptions on how this damage should be modelled have been made. Details of some of the published analyses are presented below, and and further information is presented in Chapter 7.

Gouch and Conway (1976) have carried out a two dimensional finite element analysis of closure in a rectangular shaft sunk in the Coeur d'Alene mining district of northern Idaho. Observations made by the U.S. Bureau of Mines in the same region showed that the inner 0.5 m or so of rock was fractured and could be considered a "no tensile strength material". Gouch and Conway therefore assumed the material around the opening to be considerably weakened, i.e. reduced in strength, but to have the same deformation

modulus as the surrounding undamaged rock.

Another way in which the zone of damaged ground may be considered is to assume that it is not able to carry any load. Field observations at the trial excavation for the Drakensberg Pumped Storage Scheme, Sharp et al. (1978), showed that the rock at the surface of the excavation was considerably loosened. In finite element analyses carried out to model the excavation an inner zone of rock was ignored. The thickness of this zone was chosen to be greater in the areas where the stresses around the trial excavation would be concentrated, and the analyses considered only the stresses and displacements in the undamaged rock beyond.

A third way in which the damaged zone can be considered, which was used here, is to assume that the damaged ground is softened rather than weakened. Kaiser (1981) reanalysed the data presented by Ward (1978) and Ward et al. (1976) from the Kielder Experimental Tunnel and found that a zone of softened material around the opening may be more appropriate than a strain weakening plastic zone which was used by Hoek and Brown (1980) in their evaluation of the performance of the tunnel.

In this study it was assumed that the damaged rock, like the undamaged rock, is homogeneous, isotropic, and behaves like a linear elastic material with infinite strength and a deformation modulus reduced from that of the undamaged rock. Simulation of this modulus reduction has been described previously, but it may be thought of as a

partial excavation. Dilation of the rock during the process of damaging has been ignored in this study.

3.6 Ground Freezing and Thawing

The first reported use of the technique of ground freezing was during the sinking of a mine shaft in Swansea, Wales, in 1862 (Jones and Brown, 1978). Since then the technique has been widely used to provide temporary ground stabilization during the construction of tunnels, shafts, drifts and other underground excavations. Its main functions are to strengthen and stiffen ground that would not otherwise be able to support itself around an excavation, for example, in soft cohesive soil where other methods of reducing ground movements due to tunnelling (e.g. grouting) may not be posible, and also to prevent seepage of water into the excavation, for example from a saturated cohesionless deposit or from rock aquifers. It can take several months to form the required thickness of ring or arch of frozen ground, which means that if ground freezing is to be used it has to be started some time before the excavation is begun.

It is usual practice when ground freezing is being used to aid shaft sinking to provide a relief well or wells within the ring of freeze pipes to which the excess water is allowed to flow (Walli, 1964). In tunnel construction, freezing is usually carried out from the ground surface, and

an arch rather than a ring of ground may be frozen and the excess water can be dissipated. It is not unusual for the excavation to be mainly carried out in a soft core of unfrozen ground, which will be significantly easier to excavate than frozen material, although in this study a solid cylinder of ground was assumed to be frozen. It was therefore considered that the assumption of no volume changes during freezing and thawing, due to the freezing and thawing processes themselves, was not too inconsistent with normal practice, particularly for free draining granular deposits. To completely model the ground freezing and thawing processes was beyond the scope of this simple analysis.

When soil is frozen it not only becomes impermeable, (although discontinuities in the frozen ground can be a major source of construction difficulties), but its strength and stiffness are usually greatly increased. Figure 3.6 from Andersland and Anderson (1978) shows how the strength and the stiffness of soils increase with decreasing temperature. In this study it was not only assumed that the frozen ground was, like the unfrozen ground, homogeneous, isotropic linear elastic, and had infinite strength, but that it was temperature and strain rate independent, with a deformation modulus three times greater than for the unfrozen ground. This value of E was chosen so that reasonable comparisons could be made with the other analyses, rather than being the modulus for any particular type of frozen material. It was

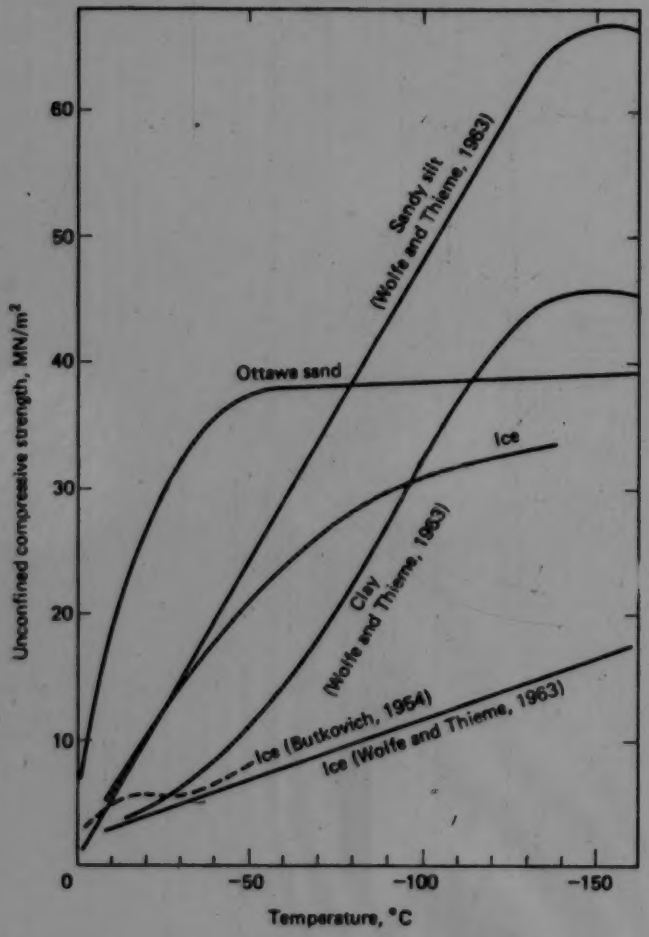

(Sayles, 1966)

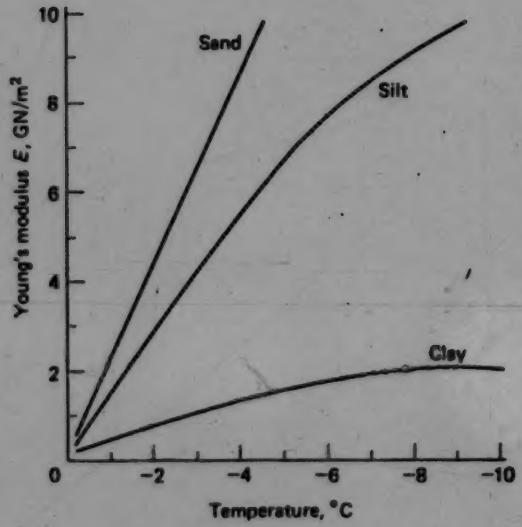

(Tsytovich, 1975)

Diagrams from Andersland and Anderson, (1978)

Figure 3.6 Relationship between Unconfined Compressive Strength, Young's Modulus and Temperature for Frozen Ground

also assumed that the ground was a free draining material such as a clean sand, so that on freezing water would be expelled, and frost heave would not occur. For thawing it was assumed that there were no massive ice lenses within the ground that would cause a change of volume of the ground mass.

CHAPTER 4

EXCAVATION AND SUPPORT CASES STUDIED

4.1 Introduction

A situation similar to the one analysed by Hanafy and Emery (1980) was used in this study, i.e. construction of an opening of radius R = 5 m, with excavation rounds of length R. The initial insitu stress was 8 MPa, except in the case of the shallow shafts, and the initial ground and liner deformation moduli were 5 GPa and 30 GPa respectively. The rock modulus is that which might be expected for a good quality clay shale, and the liner modulus is in the expected range for precast concrete liners. Both the liner and the ground, whether damaged or undamaged, had assumed Poisson's ratios of 0.2, which were the values used by Hanafy and Emery, and are representative of the values for rock and concrete. The thickness of the liner was 600 mm, and it was placed in lengths of one R. The properties of the different types of ground and liner used are presented in Table 4.1.

Most of the construction procedures used in this study are shown in Figure 4.1. The diagrams show the liner positions just before excavation and rock damage takes place, and the extent of the excavation and damage which will occur at the next step is shown by the dashed lines. Several construction sequences are not shown, such as combinations of cases, for example, damage as Case 6 but

Table 4.1
Material Properties used in the Analyses

Material Number	Material Type	E GPa	ν	G GPa	Density KN/m^3
R1	Ground*	5	0.2	2.083	0+
R2	Excav-ated Ground	1×10^{-10}	0.2	$.417\times10^{-10}$	0
R4	Frozen Ground	15	0.2	6.25	0
R5	Damaged Ground	2.5	0.2	1.042	0
R7	Damaged Ground	0.5	0.2	0.2083	0
R8	Damaged Ground	3.75	0.2	1.563	0
R9	Water	3.6×10^{-6}	0.4999997	1.0×10^{-6}	10
R10	Water (Weight -less)	3.6×10^{-6}	0.4999997	1.0×10^{-6}	0
R11	Damaged Ground	1.25	0.2	0.521	0
L1	Liner	30	0.2	12.5	0×

*Ground in initial state and in thawed state.
+Weight density equals 20KN/m^3 for shaft cases.
×Weight density equals 25KN/m^3 for shaft cases.

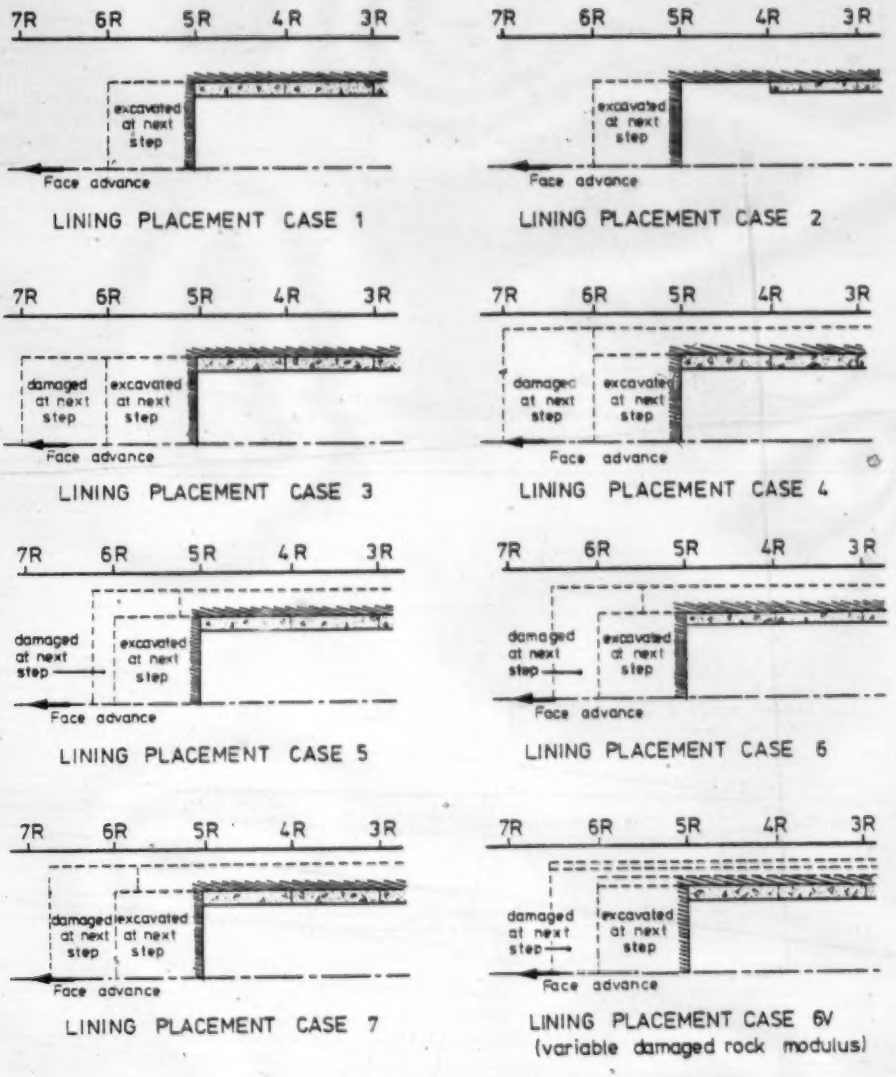

Figure 4.1 Lining Placement and Tunnel Construction Sequences

liner placement as Case 2. Also not shown is Case 0, which is the unlined, undamaged case. Other construction procedures not shown in Figure 4.1 are described in the following sections.

4.2 Tunnels

A table summarising the analyses carried out is given at the beginning of Appendix 5. The table gives information on the ground types used, mesh numbers, excavation procedures and also in which figures data for each analysis may be found.

Unlined and lined tunnels with no rock damage were studied first and then the effect of rock damage on tunnel performance arising from the drill and blast method of construction was considered. The main factors studied were:

1) the degree of damage, i.e. by how much the stiffness is reduced;
2) the position of the damaged ground, i.e. in front of the face (e.g. Case 3), and radially around the tunnel (ahead of the face) (e.g. Case 4); and
3) the depth of damage in front of the face.

The radius of the zone of damage (B) was kept constant at 6.5 m (B/R = 1.3) and the length of the damaged zone in front of the face was varied between R/4 and R (Cases 4 to 7). Different moduli for the damaged rock were chosen which,

except in one set of analyses, were kept constant over the whole region of damaged rock. Where a varying damaged rock modulus was assumed (e.g. Case 6V) it was increased linearly in increments from zero at the tunnel wall to a maximum equal to the undamaged modulus at the contact between the damaged and undamaged rock. The distribution of the modulus of the damaged ground is shown in Figure 4.2.

Two analyses were carried out in which lined tunnels were constructed within frozen ground which was subsequently thawed. The sequence of tunnel construction was exactly the same as Cases 1 and 2, except that they were carried out within a concentric cylinder of frozen ground of radius 6.5m. Construction was halted part way through the mesh (as in the previous analyses) and the ground then thawed.

The properties assumed for the frozen and thawed ground are presented in Table 4.1. In order to model the simplified frozen and thawing ground behaviour explained in Section 3.3 and shown in Figure 3.3d, a slightly different and unusual sequence of using the SAP4 and CONSTEP2 programs was required. The reason for this is that in Figure 3.3d the ratio of the stresses at points 2 and 3 is not $\sigma 3 / \sigma 2 = E1 / E2$ which would be calculated by the command NMT (Section 2.4), but is given by $(\sigma 3 - \sigma 1) = (\sigma 2 - \sigma 1) \times (E1 / E2)$. In other words the original insitu stresses (at point 1) have to be substracted from the stresses at point 2 before the command NMT is used, and then added again afterwards to give the

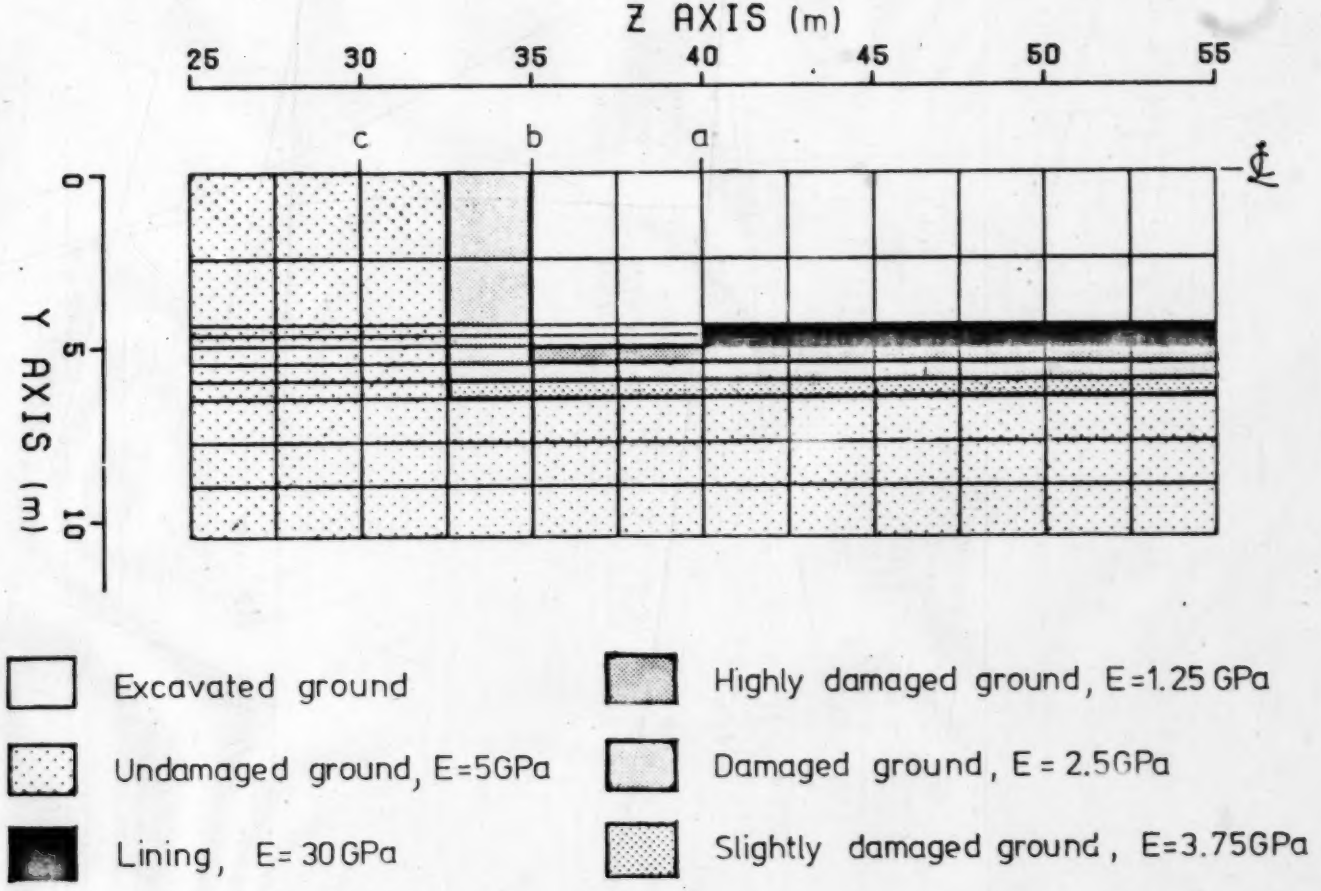

Figure 4.2 Modulus Variation in the Damaged Zone – Simulation of Confining Pressure Effect

stresses at point 3. This was achieved by the method described below.

Two files of data similar to file INCR, described in Section 2.2, were stored in files called INITNEG and INITPOS. In these files the increments of nodal displacements were zero and the increments of element stresses were set equal to the initial insitu stresses, but in file INITNEG the initial insitu stresses were all multiplied by minus one. When the last step of excavation had been carried out in the frozen ground INITNEG was added to file SAP (which contained the up to date stresses and displacements) to give values equivalent to ($\sigma 1 - \sigma 2$) above. For programming reasons INITNEG was added to SAP before file INCR (Section 2.2), which contained the incremental stresses and displacements for the last construction step in the frozen ground. This addition of file INITNEG was carried out using CONSTEP2 in the usual manner as if INITNEG had been file INCR. The frozen ground was then thawed (softened) by using the command NMT in the usual way. The initial insitu stresses, stored in INITPOS, were then added back into file SAP using CONSTEP2. Again for programming reasons INITPOS was added to file SAP before file INCR, now containing the increments of stresses and displacements from the thawing.

4.3 Shafts

A table summarising the analyses carried out on shaft construction is given at the beginning of Appendix 6. The table presents information on the ground types used, the meshes used (which in all cases except the drilled shaft case is Mesh 2), the excavation procedures, values of Ko the coefficient of lateral earth ressure at rest (the horizontal insitu stress in the ground being Ko times the vertical insitu stress), and also in which figures data for each analysis may be found.

Unlined and lined shafts with no rock damage were studied, with the different values of Ko used being 0.5, 1.0 and 2.0. Shallow shafts were considered initially, and were excavated to a depth of seven tunnel radii from the ground surface, which was modelled by an unrestrained mesh boundary. The initial insitu vertical stress was increased linearly from zero at ground level at a rate of 20 KN/m^2 per metre depth, which corresponds to the ground having a bulk density similar to that of a saturated glacial till. The horizontal initial insitu stress was determined by the value of Ko used for each analysis, with the initial principal stresses being in the horizontal and vertical directions.

The liner was at first considered to have a weight density of 25 KN/m^3, but in one of the analyses, indicated on the figures, it was considered to be weightless. This assumption was not found to alter the results very much and, partly because of the coarseness of Mesh 2, not investigated

further, with subsequent analyses assuming the liner had weight.

Deep shafts were also considered. These were basically the same as the tunnel analyses, but because the longitudinal axis was vertical the axisymmetric finite elements used no longer restricted Ko to unity.

Lastly a completely different form of shaft construction was considered, namely drilled shafts constructed under fluid support. In this simplified study the fluid was assumed to be water with a weight density of 10 KN/m^3. Water is generally considered to be an incompressible material with no shear strength. Franks (1972) gives the isothermal compressibility of water as 10^5 bar^{-1}. This gives a K (bulk deformation modulus) approximately equal to 2 GPa. For the shear modulus (G) to be zero, the Young's modulus must also be zero, but then K is zero as well unless Poisson's ratio is equal to 0.5, which SAP4 cannot handle. Therefore Poisson's ratio was chosen to be 0.4999997 so that with E = 3.6 kPa, K was equal to 2 GPa. G should have been approximately 1.2 kPa, but actually 1.0 kPa was used in the analyses.

It was found that with water modelled in this way it was difficult to get the correct hydrostatic stresses within the elements of water in an incremental sequence of excavation and construction. A procedure was eventually adopted such that at each stage of ground excavation all the water was excavated as well, and then immediately replaced

again, including the elements from which the ground had just been excavated, the water material having its weight density of 10 kN/m^3. (It should be noted that any material having weight should only have this weight considered once in the sequence of construction. At the step after the material is "placed" within the mesh it should be "replaced" with a similar, but weightless material so that SAP4 does not consider the weight a second time). Figure 4.3 shows the range of hydrostatic pressures calculated in such an incremental unlined drilled shaft analysis and the range of values is shown to be reasonably small, particularly if only the element centre stresses are considered.

In the drilled shaft case studied here the liner was to be inserted after the whole shaft had been excavated, and so it was considered that all the ground could be excavated and replaced with water at one step. Replacing the ground with water is very similar to replacing it with air, except there is effectively a residual applied internal pressure on the walls of the shaft. The next and last stage was to place the liner and remove the water, which was done in the usual manner. The liner was of similar dimensions to the one used throughout the study, and was open ended at the base of the shaft, although in practice it would be more usual to install a closed ended steel liner.

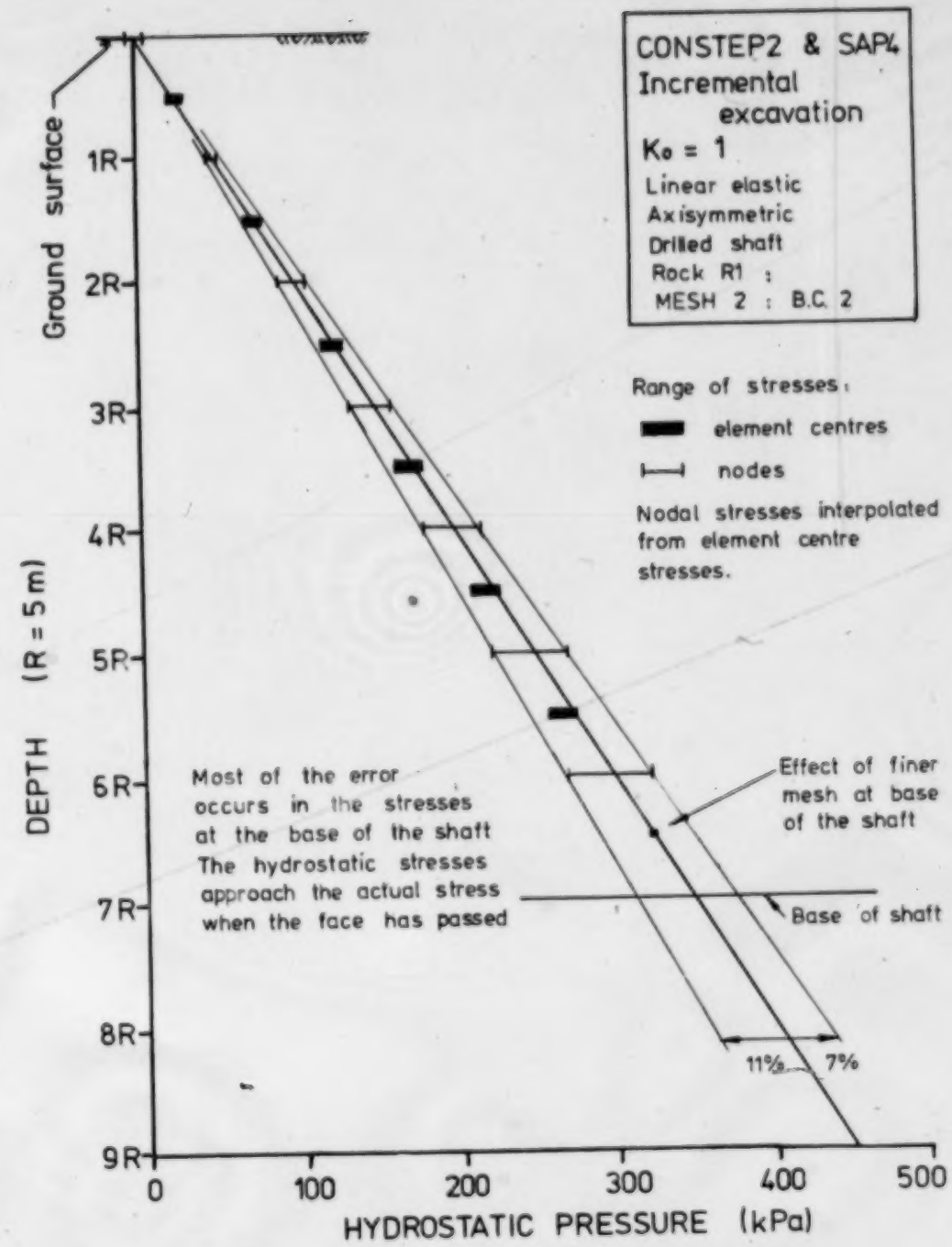

Figure 4.3 Calculated Hydrostatic Pressure for a Drilled Shaft.

CHAPTER 5

GROUND-LINER INTERACTION

5.1 Introduction

Ground convergence curves (GCC) and support reaction curves (SRC) are used here to aid the interpretation of tunnel and support behaviour and the interaction between them. Such characteristic curves were frequently used in engineering at the turn of the century, and have since been reintroduced for use in tunnelling by various authors, for example Lombardi (1973). A brief description of GCCs and SRCs follows which shows how they can assist in the interaction between the ground and the liner during excavation of a core of ground, and the insertion of a liner of different compressibility and initial size in the remaining cavity, which has since contracted.

5.2 Ground Convergence Curves

A typical ground convergence curve is shown in Figure 5.1a, in a diagram of radial wall displacement u plotted against the equivalent support pressure ps, for the opening as shown in the figure, under two dimensional plane strain deformation. As ps is reduced the ground behaviour is assumed to be initially linear elastic, but on further reduction the ground may yield or deform in a non-linear elastic manner and the GCC deviates from a straight line as

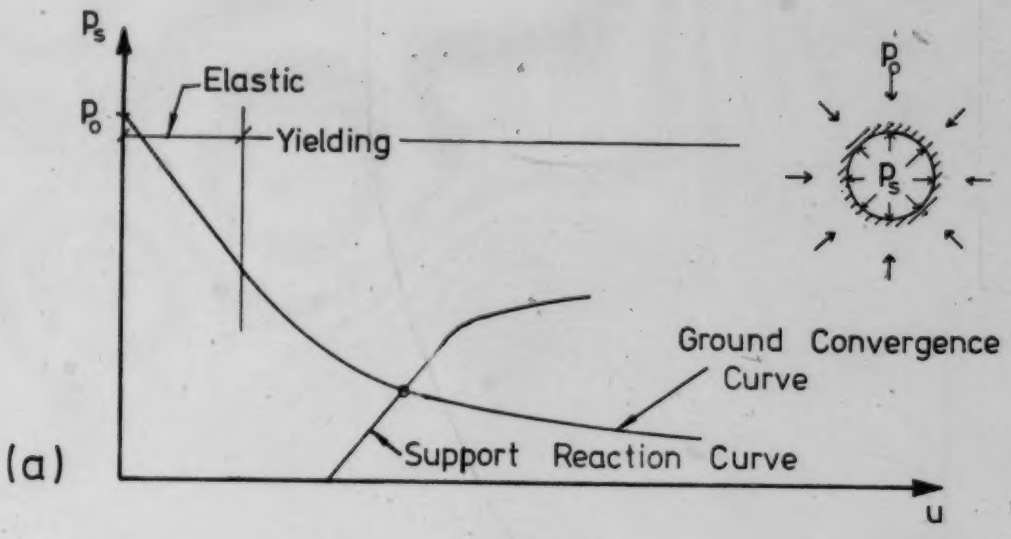

$$u_i = \frac{(1+\nu)(1-2\nu)R\,p_o\,(1-E_d/E_u)}{E_d + E_u(1-2\nu)}$$

$$u_e = \frac{(1+\nu)R}{E_d}\underbrace{\left[\frac{p_o E_d\,2(1-\nu)}{E_d+E_u(1-2\nu)}\right]}_{p'}\frac{R^2(1-2\nu)(E_d/E_u-1)+B^2(1-2\nu+E_d/E_u)}{R^2(1-E_d/E_u)+B^2(1-2\nu+E_d/E_u)}$$

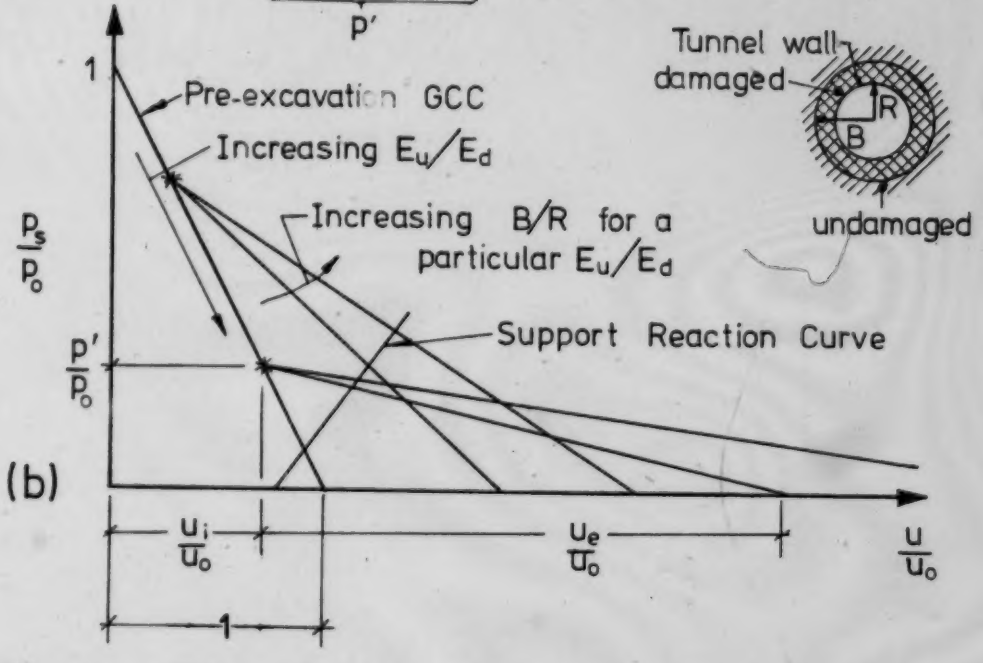

Figure 5.1 Ground Convergence Curves

shown.

The equivalent support pressure should not be confused with the radial stress in the rock at the wall of the cavity, although these two are equal in a two dimensional case. For example consider a three dimensional unsupported tunnel. The radial movements in the vicinity of the face will be less than the ultimate value of radial displacement because of the support from the core of unexcavated ground at the face (which will be removed in the next round of excavation). The actual radial stress in the core of ground at a radius of R is likely to be in excess of po because it is giving support to more rock than it did before excavation of the rock adjacent to it took place. Just behind the face, where the ground has already been excavated, the radial stress at the wall will be zero, although the radial displacements will not have reached their ultimate value, and the equivalent support pressure will not yet have become zero because of the supporting effect of the core of ground at the face.

For any particular opening the GCC is not usually unique. In a three dimensional supported cavity there can be many GCCs, and different parts of the wall may be on different parts of the same GCC. In two dimensions gravity and the value of Ko will produce several different GCCs for different points of the same opening. Consider first the case with gravity and Ko = 1. At the roof, or crown, of the tunnel the weight of the ground will cause additional inward

movements and the GCC for the crown will be above the average curve shown in Figure 5.1a. At the invert, or floor, of the tunnel the weight of the ground will reduce inward (upward) radial movements, and the GCC for the invert will lie below the average curve shown in the figure. At the tunnel springline gravity should have little effect in a homogeneous material, and the GCC will be close to the average curve. If blocks of material in the roof become loosened they may fall out of the roof and the GCC curve trends upwards, and does not intersect the ps = 0 axis, even for very large values of displacement, u.

With no gravity, but Ko ≠ 1, the ultimate radial displacements around the walls of the cavity will not be uniform, and so there will be a different GCC for each point along the opening wall.

5.3 Support Reaction Curves

The SRC can be plotted on the same graph as the GCC, and this is also shown on Figure 5.1a. The support is only activated after it comes into contact with the rock and so will start from some point at ps = 0 and u > 0, which will depend upon the ground convergence before the support is installed, and the size of any initial gap left between the ground and the support. The intersection of the GCC and SRC is the equilibrium position giving the final wall displacement and support pressure. However this point may

change with time. The ground or support may creep, or other factors may cause them to soften or weaken, in which case the GCC and/or the SRC will change position with a resulting change in the equilibrium point.

The minimum radial displacement at which support can be installed is equal to the wall displacement at the tunnel face or shaft base and a major problem in tunnel and shaft design, based on the use of GCCs and SRCs, is to find its value, uf. For unlined tunnels in homogeneous ground uf can be estimated from closed form solutions, for example by assuming the face to be hemispherical. This is done by using equilibrium equations similar to those used for the analysis of a pressurised hollow cylinder except that the corresponding equations for a spherical cavity are used. In this way the radial displacements for a spherical cavity with no support can be calculated for various different ground behaviour, and these are taken to be uf.

In situations where the opening is supported uf becomes more difficult to predict because of the interaction between the ground and support. Even where tunnel convergence in the field is recorded uf is often not known unless measurements are taken from a nearby opening or from the ground surface, and begun before the advancing tunnel causes any ground movements. An innovative approach to determine uf from stress changes measured ahead of the face has been illustrated by Kaiser et al. (1982).

5.4 Bilinear Ground Convergence Curves

Kaiser (1981) has calculated the GCC for a prestressed body where a ring of softer material exists around the opening. He assumed for the derivation of the closed form solution a circular tunnel under hydrostatic pressure, linear elastic materials, plane strain conditions and radial stress and displacement continuity at the interface between materials of different stiffnesses. Furthermore he assumed that a core of radius B was first softened and that an opening of radius R, less than B was subsequently excavated by reducing the support pressure.

The resulting GCC's for a similar analysis carried out here are presented in Figure 5.1b. In this figure the two points marked with a star (*) correspond to the states immediately after a core of radius B is softened, but before the tunnel is excavated, and are independent of B/R but depend upon Ed/Eu, the ratio of the modulus of softened material to the modulus of unsoftened material. The behaviour during subsequent tunnel excavation depends on both the B/R and Ed/Eu ratios. The equations of the lines are given above the figure, and their derivation is presented in Appendix 1.

CHAPTER 6

PRESENTATION OF RESULTS

6.1 Introduction

In this section the information presented on the plots of raw data given in Appendices 5 and 6 is discussed and explained. The objectives here are to bring out details in the figures which are not considered elsewhere, and to introduce those more important figures which are used in Chapter 8 to discuss the practical implications of the results from this study. The figures are presented in the appendices and are discussed in approximately the order in which they appear. As this section will be mainly used for reference the figure numbers, when mentioned, are printed in bold characters so that they can be more easily located within the text.

6.2 Tunnel Analyses

6.2.1 Effect of Mesh Boundary and Initial Construction Effects

In the analyses which used Mesh 2 the first round of construction was usually only 1R deep into the mesh and took place at the unrestrained side of the mesh where longitudinal movements could occur. The node at the wall of the tunnel and at the edge of the mesh was thus free to move

into the tunnel and also in the direction of the tunnel advance. **Figure A5.1** shows that this lack of restraint causes the radial displacement at the edge of the mesh to be much greater than it should be, and where this has been observed and plotted in the figures it has been ignored in the consideration of radial displacements.

In most of the analyses using Meshes 6 and 7 the first round of excavation is 3R into the mesh. Where required the liner is also placed in this first step, and because the moduli are changed before the nodal forces are applied within the same construction step, the liner is, in effect, installed before the ground is excavated. This causes the ultimate values of radial displacement and liner stresses within that region to be different from the ultimate values obtained later in the same analysis because the sequence of construction is not the same. This region of different ultimate values is marked "initial construction effects" on the figures, and can be seen for example on **Figure A5.7**.

6.2.2 Radial Displacements; No Ground Damage

The radial displacements ahead of the face for analyses of the same construction case, but using different meshes, are very similar as can be seen for example in **Figures A5.6, A5.7** and **A5.8**, and therefore they are considered to be reasonably accurate.

Figures A5.6, A5.7 and **A5.8** also show that for analyses of the same excavation case, but using different meshes, all

those nodes at the tunnel wall, which had been at the face at some moment during the excavation, have similar ultimate radial displacements which are *lower* than those of the surrounding nodes. In an unlined excavation in homogeneous linear elastic ground there should be no variation along the tunnel in the distribution of ultimate displacements, as the displacements (and stresses) should be independant of the number of the excavation steps (Kulhawy, 1977). The reason for this "kink" in the displacement distribution is therefore unclear, but as Meshes 6, 7 and even Mesh 2 give very similar values of displacement it may be that the stress gradient is very large at the corner of the tunnel cavity, and can only be accurately modelled if very small elements are used in that area. However, in the lined case, particularly Case 1 (Figure 4.1), the reduced value of radial displacement at nodes in the tunnel wall which were once at the face will also be due in part to the supporting effects from the face and the liner. A node in such a position in the mesh will initially be at the face and will be supported by the "core" of unexcavated rock at the face. Its radial displacement up to that moment will therefore be small. The liner is then installed, up to the face in Case 1, and excavation takes place. Because of the supporting effect from the leading edge of the liner the additional displacement is also small. The radial displacements at the rest of the nodes along the unsupported span of wall will vary. They will be least near the supporting "core" of

unexcavated ground at the face and at the leading edge of the liner, and will be greatest somewhere between these two points. The radial stress distribution will also vary in a manner similar to the wavy radial displacement distribution observed.

6.2.3 Radial Displacements; With Damaged Zone

The radial tunnel wall displacements for three cases having different lengths of damage ahead of the face (Cases 5,6, and 7) are shown in **Figures A5.10, A5.11** and **A5.12.**

In each of the three cases the node at the interface between the damaged and undamaged ground ahead of the face has a lower radial displacement than the nodes around it. An inspection of **Figures A5.39** and **A5.42** shows that at the tunnel face the displacements are longitudinal, and have almost no radial component except near the wall. Similarly **Figure A5.42** shows that the displacements at the plane of contact, perpendicular to the tunnel axis, between the undamaged and damaged ground ahead of the face are also mainly longitudinal. This implies that when the modulus is reduced by a factor of 10 (the analysis was carried out with Eu/Ed = 10) the plane of contact between the damaged and undamaged zones behaves like a tunnel face. Because the radius of the zone of damage, B, is greater than R in Cases 5, 6 and 7, the influence of the "wall" of undamaged ground on the longitudinal displacements at the interface is insignificant at a radius of R, and points at this radius

will tend to move longitudinally rather than radially. Other points not at the interface and so not acted upon by "nodal partial excavation forces", will generally move towards the open face, with both radial and longitudinal components of displacement.

Figures A5.10 to A5.12 also show that there is a unique pattern of ultimate radial wall displacements for each of the three excavation cases (Cases 5, 6, and 7). Each pattern repeats itself, and has a "wavelength" equal to the length of a round of excavation. The ultimate radial wall displacements are very much alike at nodes in different excavation cases which are in similar positions with respect to the zones of damaged and undamaged ground. For example the nodes in the tunnel wall which were adjacent to one or more elements of damaged ground when ahead of the face (except nodes which were at the face) all have similar ultimate radial displacements. Those nodes that were once at the tunnel face also have similar ultimate radial displacements, as do those which were completely within undamaged rock while ahead of the face. The maximum radial displacement in each of the patterns is always at those positions (on the wall) which were once at the interface between the damaged and undamaged ground.

6.2.4 Variable Modulus in Damaged Zone, and Excavation in Frozen Ground

The distribution of radial displacements for cases where the modulus in the damaged zone is varied to simulate the effect of a variable confining pressure on the modulus is shown in **Figure A5.13**. The curves show similar results to those from the other cases with rock damage, and are discussed further in Section 8.2.

The distribution of radial displacements for cases where excavation was carried out within a ring of frozen ground are shown in **Figures A5.14** and **A5.15** along with the displacements which exist after the frozen ring has been thawed. Again these show similar results to those described previously. The pattern of displacements after thawing is the same as the pattern before, but in those areas where a liner has not been placed (eg. near the face in Case 2) displacements are greater because of the lack of support. Excavation in frozen ground is discussed further in Chapter 8.

6.2.5 Liner Stresses; Analyses with Mesh 2

Figures A5.16, A5.17 and **A5.18** show the radial, tangential and longitudinal liner stresses respectively for those analyses carried out using Mesh 2. Only the liner stresses at the end of the seventh step of excavation are shown, except in one case where those at the end of the sixth step of excavation are also shown (marked "face at

6R"). The effect of a change in element geometry ahead of the face can therefore be seen by comparing the liner stresses from the sixth and seventh steps (see Mesh 2, Figure 2.5). The effect of the mesh boundary is also evident, and extends about 3R into the mesh, as shown by the increase in radial and tangential stresses and the decrease in longitudinal stress.

The liner stresses in these figures have been calculated from analyses where the nodal excavation forces are applied even to those nodes, which after the ground has been excavated in that construction step, are only attached to liner elements. Different ways of applying the calculated nodal excavation forces have been discussed in Section 2.7.2 and are also discussed further in Section 6.2.6 below with reference to the figures in Appendix 5. In the method used for the analyses presented in these three figures (method A, Section 2.7.2) unrealistically large tensile longitudinal liner stresses can be developed, as shown in some of the cases plotted in **Figure A5.18**, particularly Cases 1 and 4.

The analyses are discussed in more detail in Section 8.3, where the results are also plotted on ground convergence curves.

6.2.6 Application of Nodal Excavation Forces

The influence of different methods of applying nodal excavation forces to the mesh has been discussed in Section 2.7.2, in particular with respect to the longitudinal

displacements. In this section the effects of the different methods are discussed with reference to **Figures** A5.19, A5.20 and A5.21 where data from analyses carried out using Meshes 2 and 6 are presented. These figures are also discussed further in the next section.

Figure A5.20 shows that there is only a small difference between the tangential liner stresses calculated from analyses using methods A and B (Section 2.7.2) to apply the nodal excavation forces (Case 1). There is also not much difference in the radial stress distribution (**Figure** A5.19) except in the part of each liner segment closest to the face when it was installed, where the ultimate radial stresses differ by a factor of about 6. This difference arises from the reduction in compressive radial liner stress at its leading edge caused by the application of nodal excavation forces, to the inside leading edge of the liner, which will generally be in the direction of tunnel advance. The liner becomes slightly thinner and so the pressure of the surrounding ground on it becomes less. Without these forces applied to the inside leading edge of the liner the radial stress there is highly compressive, as would be expected from the transfer of load from the rock core at the face to the liner.

The biggest difference between the two methods of applying nodal excavation forces is in the longitudinal liner stresses, as shown in **Figure** A5.21. When excavation forces are only applied by method B the longitudinal liner

stresses are greatly reduced, and even in Case 1 (Mesh 6) become slightly compressive at the trailing edge of each liner segment. In Case 2, where the liner never comes into contact with any ground which will later be excavated, the longitudinal stresses (along the middle of the liner) are always compressive. The tensile longitudinal stresses at the leading edge of the liner in Case 1 will be caused by ground movement towards the new face. Further away, the ground will be contracting around the liner and causing it to try and expand longitudinally which will produce compressive stresses in the liner.

6.2.7 Comparison of Results from Analyses using Meshes 2 & 6

Figures A5.19, A5.20 and A5.21 compare liner radial, tangential and longitudinal stresses respectively for analyses using Meshes 2 and 6. Because Mesh 6 has four elements for each segment of liner (where a segment is 1R in length) rather than just one as with Mesh 2, it allows the variation of stresses along the liner to be studied. As found for the radial displacement distribution, there is a pattern of stresses which is repeated for every 1R segment.

The figures show that generally the radial, tangential and longitudinal stresses are greatest at the leading edge of the liner and reduce towards the trailing edge of each segment (tangential and radial stresses being compressive and longitudinal stresses being tensile). The radial stress distribution however shows a "kink" in its curve, whereas

the others steadily decrease. The distribution of stresses within liners is discussed in detail in Section 8.6.

It can be seen from the figures that the stress in a liner element in Mesh 2 is always greater than the average stress in the four elements of a liner segment in Mesh 6. (Greater in compressive radial and tangential stress and greater in tensile longitudinal stress). The reason for this is likely to be that with Mesh 2 the liner segments have only one element, which is not capable of fully modelling the bending in the liner, and so does not give accurate values of stress.

6.2.8 Comparison of Results from Analyses using Meshes 6 & 7

Figures A5.22 to A5.27 show liner radial, tangential and longitudinal stresses from analyses of Cases 1 and 6 using Meshes 6 and 7. The results shown in Figures A5.25, A5.26 and A5.27 are from analyses of Case 6, but as the results are of a similar form to those shown in the first three figures, which show results from an analysis of Case 1 and are discussed below, they are not considered further, except to mention that the degree of rock damage (i.e. size of the modulus reduction) is different for the analyses using Meshes 6 and 7.

The main difference between the analyses using Meshes 6 and 7 is that Mesh 6, having four elements along the length of a 1R long liner segment, gives the longitudinal variation of liner stresses down the centre of the liner, whereas Mesh

7, having four elements placed with a common apex, gives an indication of the variation of stresses radially across the thickness (t) of the liner as well as longitudinally. In general the three figures show that the stresses at the centre of the liner (Mesh 6) lie between those at points 1/4 t and 3/4 t from the outer edge (Mesh 7).

Figure A.5.22 shows that the radial stresses vary across the thickness of the liner much more at the leading edge of the liner than at the trailing edge. However **Figure A.5.23** shows that the tangential stresses do not vary much across the liner thickness, which is to be expected for a very thick liner under no bending. There is only a small change in the difference across the liner with distance longitudinally along it. The longitudinal stresses, shown in **Figure A.5.24**, do though vary greatly longitudinally as well as radially across the liner, with the radial variation reducing by 2/3 over the middle half of the liner segment length. Another point to note is that although at the trailing edge of each liner segment the longitudinal stress at the centre of the liner is almost zero, there is still a variation radially, with the longitudinal stress at a point 1/4 t from the inside of the liner twice as compressive (about 0.2 po) as the stress at a point 1/4 t from the outer edge of the liner is tensile (about 0.1 po).

6.2.9 Effect of Rock Damage on Liner Stresses

Liner stresses from analyses of Cases 1,2,5,6 and 7 using Mesh 6 are presented in **Figures A5.28, A5.29** and **A5.30**, which show radial, tangential and longitudinal stresses respectively. The open symbols show results from analyses using method B (see Section 2.7.2) for the application of nodal excavation forces, whereas the solid symbols are for analyses using method A. The results show the variations of liner stresses to be of a similar form to those described previously. Different extents of damage ahead of the face (Cases 5,6, and 7) do not appear to have much influence on the liner stresses, although all the stresses are below the ones of the undamaged case (Case 1). This would indicate that the difference between the results from Case 1 and from Cases 5, 6 and 7 is due to the damage around the tunnel and not from damage in front of it.

An interesting result appears in **Figure A5.30** where the longitudinal stresses are plotted. Case 1, when using method B for the application of nodal forces, shows greatly reduced tensile longitudinal stresses as previously described. However there is not as much reduction in tensile stress from that given with method A when method B is used for excavation Case 5. Indeed with method B the longitudinal tensile stresses in the liner in Case 5 are greater than those in Case 1 for nearly the whole of the liner segment. This may be explained by the fact that there is a ring of softened (damaged) material around the liner to which the

excavation forces are applied, but as the liner is so much stiffer than the damaged ground it "attracts" the longitudinal stresses and builds up a large longitudinal tensile stress within itself. Applying a nodal force to the inside leading edge of the liner is therefore not too significant in Case 5 in comparison to the reaction to the "correctly" applied nodal force at the outside leading edge which is mostly given by the liner and not significantly shared between the liner and surrounding ground. However in Case 1 the reaction to the "correctly" applied force is shared and the incorrect application of another force becomes more significant. **Figure A5.30** shows the longitudinal tensile stress to be more uniformly distributed along the length of each segment in Case 5 than in Case 1. This is because of the rock damage at the face effectively "delays" the liner installation which produces a more uniform distribution as dicussed in Section 8.6, and because the soft damaged ground around the liner spreads the longitudinal stress applied to it along more of its length.

The stress distributions in a liner placed where there is a ring of damaged rock with a varying modulus are shown in **Figures A5.31, A5.32** and **A5.33**. The stress distributions are very similar to those shown in the previous figures for corresponding cases of liner placement and rock damage.

6.2.10 Liner Stresses - Frozen Ground Analyses

The distributions of liner radial, tangential and longitudinal stresses are shown in **Figures A5.34, A5.35** and **A5.36** respectively, and generally have similar forms to those discussed previously, but some comments on the differences are made below.

The most obvious point to note is that thawing causes all the stresses to become more compressive, but with very little change in the shape of the stress distributions within the liner segments. Before thawing, in other words for excavation within the stiff frozen ground, the stresses are, not surprisingly, less than for excavation in the softer materials (comparing excavation Case 1 in the unfrozen and frozen ground). The inner element radial stresses in the frozen ground are uniform along the length of the liner, whereas in the unfrozen ground they are greater at the leading edge of the liner. The longitudinal liner stresses for excavation in frozen ground are nearly all compressive, whereas they are tensile for excavation in unfrozen ground, the difference being that the frozen ground is stiffer and more able to restrain the longitudinal movements towards the face during excavation, and thus less stress is applied to the liner. After thawing all the stresses become more compressive but they do not vary as much along each segment as they do for excavation within unfrozen ground

6.2.11 Ground Displacements Around the Opening

The first of the figures showing ground displacements is **Figure A5.37** which presents the longitudinal displacements along the tunnel centreline. It shows that at a point about 3 R ahead of the face the ground movement towards the face is about 10% of its (final) value when the face reaches the point. This final value is very close to the value (9.6 mm) of ultimate radial wall convergence in an unlined tunnel. The similarity of these two values is not too surprising as it has already been shown that when the liner is placed at 2R from the face there is only a slight reduction in ultimate radial movements from those in an unlined tunnel, and at the face we have a similar unsupported distance across the opening diameter.

Figures A5.38 to **A5.42** show, in cross section, vectors of ground movements around the opening. In all cases, except Case 2, the longitudinal movements are too great in the direction of the face advance because of the method (method A) that was used in applying the nodal excavation forces (see Sections 2.7.2 and 6.2.6). However in the cases where rock damage occurs ahead of the face (**Figures A5.41** and **A5.42**) the longitudinal movements are less affected.

The main points brought out by these figures are that the liner tends to "freeze" the displacements after it has been placed (as was observed by Ranken and Ghaboussi, 1975) and that, as noted earlier in Section 6.2.3, displacements at the contact between damaged and undamaged ground at the

face tend to be in a more longitudinal direction than displacements at points in the immediate vicinity.

6.2.12 Ground Stresses Around the Opening

Figure A5.43 shows the radial, tangential and longitudinal ground stresses along a radius at 0.15 R in front of the face (calculated using program CONSTEP, see Section 2.3). The stress in the z, or longitudinal, direction is close to zero near the centreline of the tunnel, because of the proximity of the face and the fact that the minor principal stress lies in a longitudinal direction near the tunnel centreline (see later figures). It rises quickly up to the initial insitu stress at a radius of just slightly greater than R. The stress in the x, or tangential, direction remains close to, but above, the initial insitu stress over the whole length of the radius in front of the face. The stress in the y, or radial direction, varies the most rapidly starting close to the initial insitu stress, but rising to about 1.5 times po at a radial distance of R, and thereafter falling sharply to a value just below po.

The next three figures, **A5.44**, **A5.45** and **A5.46**, show similar ground stress variations, but within planes perpendicular to the tunnel axis at a range of distances ahead of and behind the face. Program CONSTEP2 was used for these analyses and so the stresses calculated will be more accurate than those in **Figure A5.43**. One difference is that

the tangential, or x direction stress, reaches a greater value just in front of the face than shown in the previous figure.

The variation of ground stresses around an unlined tunnel is shown in **Figure A5.44**. The radial stress distribution has essentially reached its ultimate form in a plane at 0.75 R behind the face, whereas it is not until 1.75 R that the tangential stresses are essentially at their ultimate values. This important fact will be more fully discussed in Section 8.7.

A similar effect can be observed in **Figure A5.45** for a lined tunnel with no rock damage. The radial stresses still reach their minimum values in a plane at 0.75 R from the face, but thereafter they rise again as the liner begins to provide support, and are at their final values at 1.75 R behind the face. The tangential stresses rise steadily up to their ultimate values, reached when the plane they are in is at a distance of 1.75 R from the face.

The stresses in Case 6, lined with rock damage, are shown in **Figure A5.46**. The variations of stresses are similar to the previous figures, except that in the damaged zone the stresses, particularly the tangential stresses, are lower. In the undamaged zone the radial stresses are lower, and the tangential stresses higher, than for the equivalent lined but undamaged case, showing that some stress has been transferred from the damaged to the undamaged zone.

Figures A5.47 to **A5.50** show the principal stresses in a plane through the tunnel axis for various cases. Except for Case 2, the liner stresses are more tensile in a longitudinal direction than they should be, on account of the method (method A) of applying nodal excavation forces as explained in Section 2.7.2. This has the effect of slightly reducing the longitudinal compressive stresses in the ground behind the face, but because of the lower relative stiffness of the ground it is not affected as much as the liner. The figures show that large compressive principal stresses are built up across the corner at the face of the tunnel, with a smaller principal stress in the perpendicular direction, giving a large shear stress. Within the damaged ground stresses are greatly reduced, as shown in **Figure A5.50**. A similar reduction of stresses in the damaged zone was obtained in the analyses by Gouch and Conway (1976), and is shown in Figure 7.6. However in their analyses the ground strength rather than the modulus was reduced. This leads to the possibility that as the effects of weakening and softening may produce similar ground behaviour, they may often be confused when interpreting data from a programme of monitoring. The figures also show that the ground outside the tunnel experiences a rotation of principal stresses as the tunnel passes. A more detailed analysis of this last point is beyond the scope of this study, but obviously merits further investigation.

Figures A5.51 to A5.54 present results similar to the preceding figures, but the stresses shown are the changes of principal stresses from the initial insitu stresses.

6.3 Shaft Analyses

6.3.1 Radial Wall Displacements; Shallow Shafts

Figures A6.1 to A6.10 show the radial wall displacements for shallow shafts, mined up to 7R from ground level, and deep shafts, both lined and unlined, for various values of Ko. Figure A6.1 presents a summary of the results for the shallow shafts and shows that the radial displacement increase with depth is greater in the unlined cases and is greater for larger values of Ko.

Table 6.1 is a summary of the ultimate radial wall displacements uo, (at a depth of 4 R for the shallow shafts) and the radial wall displacements at the shaft bottom, uf, for both shallow and deep shafts. Numbers in brackets along the rows show the factors between adjacent values. It should be remembered when considering the table that the analyses are not accurate because of the coarseness of the mesh and the other factors described in previous sections. However it is possible to compare results in the table, and the following observations have been made.

As Ko is increased by a factor of two the values of uf and uo for any particular excavation case increase by a

Table 6.1
Radial Wall Displacements in Shafts

Shallow Shafts.

u_f (mm) (face at 7R depth)

Case \ K_o	0 5		1.0		2.0
Unlined	0.125	(x2.28 =)	0.285	(x2.00=)	0.570
2	0.125	(x2.24 =)	0.280	(x2.04=)	0.565
1	0.105	(x2.48=)	0.260	(x2.15=)	0.560

u_o (mm) (at 4R depth)

Unlined	0.195	(x2.05=)	0.400	(x2.04=)	0.815
2	0.180	(x2.06=)	0.375	(x2.08=)	0.780
1	0.145	(x2.17=)	0.315	(x2.02=)	0.635

Deep Shafts.

u_f (mm)

Case \ K_o	0.5		1.0		2.0
2	1.6	(x2.13=)	3.4	(x2.06=)	7.0
1	1.2	(x2.58=)	3.1	(x2.16=)	6.7

u_o (mm)

2	3.8	(x2.16=)	8.1	(x1.93=)	15.6
1	3.0	(x2.17=)	6.5	(x2.00=)	13.0

factor of between 1.93 and 2.58. The factors are generally at the larger end of this range for an increase in Ko from 0.5 to 1.0. For the same increase in Ko (i.e. from 0.5 to 1.0 or from 0.5 to 2.0) the factors between values of uf are the same in Case 2 as they are in the unlined case (for shallow shafts); similarly for the factors between values of uo. The factors between Case 1, Ko = 0.5, and Case 1, Ko = 1.0 generally give the highest values by far within any particular box of results shown in the table.

A factor of greater than 2.0 in the table indicates that in a two dimensional plane strain analysis the inward radial displacement with the lower value of Ko is relatively less than would be expected in comparison to that calculated with a higher Ko. If it is assumed that with an accurate analysis the factors would be 2.00 in the unlined case (and for deep shafts assume Case 2 is similar enough to the unlined case to be considered as such) the values of these factors could be corrected, in a consistent manner throughout each box, such that the factors in the unlined case are 2.00. If this is done it is found that the only cases which give factors significantly different from (and in fact greater than) 2.00 are Case 1 for Ko = 0.5 to Ko = 1.0 for both shallow and deep shafts and for uf and uo. This appears to show that when the liner is placed close to the shaft bottom before excavating the next round the radial wall displacements are dependent on Ko. If Ko is less than 1.0 then, because the factors are greater than 2.0, the

radial displacements are relatively more restricted than if Ko is greater than 1.0. In other words with a lower value of Ko the ground behaves as if the liner were placed closer to the bottom of the shaft.

All the analyses were carried out using a liner with a weight density of 25 KN/m^3, except one which was assumed to be weightless and is shown in **Figure A6.3**. It can be seen that at a depth greater than 1R there is very little difference between the cases where the liner had weight and where it was weightless, and so this was not considered further as it was unlikely that Mesh 2 was sufficiently fine enough to study this factor properly.

6.3.2 Liner Stresses; Shallow and Deep Shafts

Figures A6.11 to **A6.14** show the radial, tangential and longitudinal liner stresses for shallow shafts and radial liner stresses for deep shafts, respectively. The results have been summarised on Table 6.2, the values for the shallow shafts being at a distance of 3.5 R from the shaft base. The numbers in brackets along each row are the factors between adjacent values.

The values of the factors for the radial stresses (shallow and deep shafts) and the tangential stresses are not too dissimilar from those already discussed for the corresponding cases in the boxes of radial displacement results. The factor for Case 1, between Ko = 0.5 and Ko = 1.0, being the largest in each box. This is consistent with

Table 6.2
Liner Stresses in Shafts

Shallow Shafts. (values at 3.5R from shaft base)

σ_r (kPa)

Case \ K_o	0.5		1.0		2.0
2	5	(x2.00=)	10	(x1.90=)	19
1	22	(x2.14=)	47	(x2.04=)	96

σ_t (kPa)

2	80	(x2.00=)	160	(x1.94=)	310
1	280	(x2.21=)	620	(x2.11=)	1310

σ_l (kPa) (-ve compression)

2	45	(x2.56=)	115	(x2.57=)	295
1	-610	(÷1.15=)	-530	(÷1.60=)	-350

Deep Shafts.

σ_r (kPa)

Case \ K	0 5		1.0		2.0
2	90	(x1.89=)	170	(x1.76=)	300
1	340	(x2.35=)	800	(x2.15=)	1720

the discussion in the previous section, because if the inward radial displacements are relatively less one would expect the radial and tangential stress also to be relatively less.

The longitudinal liner stresses do not follow the same pattern as the radial and tangential stresses. Instead of the stresses becoming more compressive with increasing Ko and reducing distance of liner placement from the face, they become more tensile with increasing Ko and increasing distance from the face. (Although the values of longitudinal tensile stress in Case 1 are overestimated because of the method used in applying nodal excavation forces as described in previous sections.) The factors show that with Case 1 the lower the value of Ko, the lower is the relative value of tensile longitudinal stress, however the stresses do not appear to have reached their ultimate values (**Figure A6.13**) and so the shaft would have to be excavated deeper for the results to be meaningfully analysed.

6.3.3 Drilled (Water Supported) Shaft Case

Figure A6.15 presents the radial displacements for a drilled shaft, and **Figures A6.16** to **A6.18** present the liner radial, tangential and longitudinal stresses respectively.

The results in **Figure A6.15** are compared to the theoretical unlined case, the theoretical lined two-dimensional case using the relative stiffness solution, see Section 7.2, and the results from an analysis of Case 1

using Mesh 2, corrected by using the method described in Appendix 3. It can be seen that the radial displacements with excavation under fluid support are very close to the relative stiffness solution before the liner is inserted and the water removed, but are a lot less than if it were excavated without fluid support. The final displacements are less than with Case 1 which has the same liner but placed in stages during the excavation (and has no fluid support).

The values of liner stresses at the base of the shaft are not shown in **Figures A6.16** to **A6.18** because of an error in the final step of the construction procedure. However the following comments can still be made.

The radial stresses with Case 1 are between the stresses of the inner and outer elements of liner in the drilled shaft case. If excavation were carried out deeper then the radial stress distribution for Case 1 would not increase as rapidly with depth as with the drilled shaft case because the liner in Case 1 applies less support pressure to the surrounding ground. This is more obvious in **Figure A6.17** which compares the tangential stresses. The longitudinal stresses, shown in **Figure A6.18**, are completely different as they are compressive in the drilled shaft case, but at the centre of the liner, segment are tensile in Case 1. The longitudinal stresses do not vary across the thickness of the liner in the drilled shaft case as they do with the other excavation cases studied. Another point is that all the stresses and displacements in the drilled shaft

case vary uniformly rather than periodically, as with Case 1, because the liner is placed at one step, rather than in many steps, during the excavation.

CHAPTER 7

PUBLISHED NUMERICAL ANALYSES AND CASE HISTORIES

7.1 Introduction

Published results from other numerical analyses and case histories have been compared with the results from the numerical model developed for this thesis. The numerical analyses by Hanafy and Emery (1980), Ranken and Ghaboussi (1975) and Einstein and Schwartz (1980) simulated the tunnel excavation sequence using axisymmetric finite element models and could therefore be directly compared to some of the results presented here. Other finite element analyses did not model the same situation, but the results, or the methods that were used, have a bearing on this study. Such analyses were carried out by Gouch and Conway (1976) and Sharp et al. (1977). Three case histories were compared to the results from this study, and these are the Kielder Experimental Tunnel, the Garrison Dam Tunnels, and the Lethbridge Shaft. The details of these numerical analyses and case histories are presented in the sections below.

To assess the similarity between this study and the other numerical analyses and case histories the values of the compressibility ratio, C, were calculated and compared. C is a dimensionless number which depends on the relative stiffness between the ground and the support, and is defined in the next section.

7.2 Relative Stiffness Solution

The original analysis of the deformation and thrust in a tunnel liner was presented by Burns and Richard (1964) for buried culverts subjected to one dimensional overloads. Peck et al. (1972) have presented another analysis in which they considered a plane strain situation with the tunnel and liner inserted into the ground before the initial insitu stresses were applied to the boundary of the ground considered. Two dimensionless ratios were defined which are measures of the relative stiffness of the ground and the liner under different loading conditions. The compressibility ratio is obtained by a comparing the extensional stiffnesses of the liner and the ground under a uniform compression, and the flexibility ratio, F, is obtained from a comparison of the flexural stiffnesses under a pure shear loading. The extensional and flexural stiffnesses of the ground are calculated for its unperforated (unexcavated) state.

Einstein and Schwartz (1979) and (1980) present another method of calculating the compressibility and flexibility ratios. They assumed the ground to be in plane strain and applied the field stresses to the outside of the ground considered *before* the tunnel is constructed. The stiffnesses of the liner and the ground in its perforated state are then compared and the *changes* in displacements and stresses from those existing before tunnel excavation are calculated.

The two methods give different definitions of the compressibility ratio, the difference being a factor which is a function of the Poisson's ratio of the ground. For the case considered in this study where there is no slip between the liner and the ground, Ko = 1.0, and the liner is relatively inflexible the two methods also give different values for the liner thrusts and displacements which are different by a factor which is a function of the Poisson's ratio of the ground. In this report the definitions of compressibility ratio and flexibility ratio given by Einstein and Schwartz (1980) have been used and are presented in Figure 7.1. The equations they have developed for liner thrusts, moments and displacements are given in Figure 7.2. The greater the value of C the softer the liner is with respect to the ground, and it will generally be above 1.0 for supports in rock and less than 1.0 in soil. A larger F implies that the liner is more flexible relative to the ground. It is a difficult parameter to determine accurately as it depends heavily on construction details, such as the tightness of the bolts joining segments of a precast concrete liner.

The values of the compressibility and flexibility ratios have been calculated for the more important of the numerical analyses and case histories presented, and are given below in the relevant sections. The compressibility ratio calculated for the situation studied here is 1.389 and the flexibitity ratio is 1157.4.

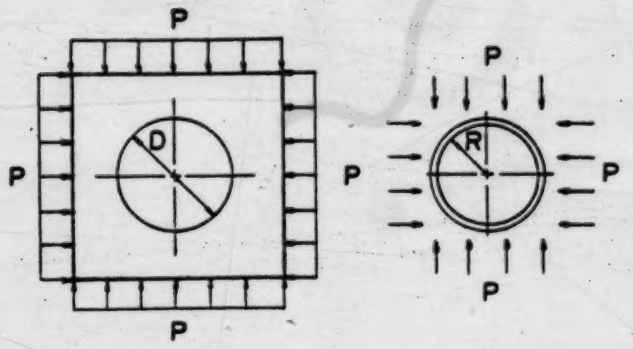

E, E_s = Elastic moduli for ground and support

ν, ν_s = Poisson's ratios for ground and support

A_s = Cross-sectional area of support per unit length of tunnel

$$\frac{P}{\Delta D/D} \propto \frac{E}{(1-\nu^2)} \qquad \frac{P}{\Delta D/D} = \frac{E_s A_s}{(1-\nu_s^2)R}$$

$$C = \text{Compressibility Ratio} = \frac{ER(1-\nu_s^2)}{E_s A_s (1-\nu^2)}$$

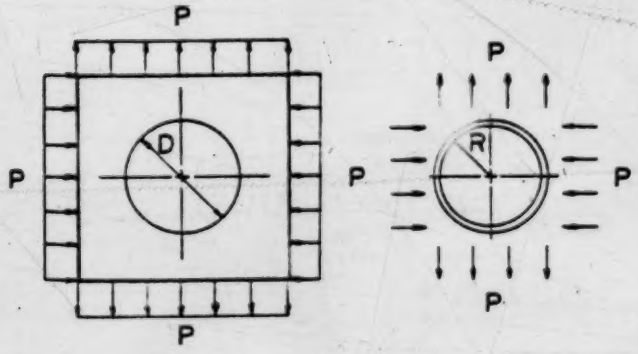

I_s = Moment of inertia of support per unit length of tunnel

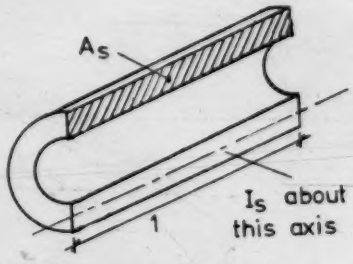

$$\frac{P}{\Delta D/D} \propto \frac{E}{(1-\nu^2)} \qquad \frac{P}{\Delta D/D} \propto \frac{E_s I_s}{(1-\nu_s^2)R^3}$$

$$F = \text{Flexibility Ratio} = \frac{ER^3(1-\nu_s^2)}{E_s I_s (1-\nu^2)}$$

Figure 7.1 Dimensionless Stiffness Ratios, Einstein and Schwartz (1980)

For the no-slip case:

$$\frac{T}{PR} = \frac{1}{2}(1+K)(1-a_0^*) + \frac{1}{2}(1-K)(1+2a_2^*)\cos 2\theta$$

$$\frac{M}{PR^2} = \frac{1}{4}(1-K)(1-2a_2^*+2b_2^*)\cos 2\theta$$

$$\frac{u_s E}{PR(1+\nu)} = \frac{1}{2}(1+K)a_0^* + \frac{1}{2}(1-K)[4(1-\nu)b_2^* - 2a_2^*]\cos 2\theta$$

$$\frac{v_s E}{PR(1+\nu)} = -(1-K)[a_2^* + (1-2\nu)b_2^*]\sin 2\theta$$

in which:

$$a_0^* = \frac{C\,F\,(1-\nu)}{C + F + C\,F\,(1-\nu)} \qquad a_2^* = \hat{b}b_2^*$$

$$b_2^* = \frac{C\,(1-\nu)}{2[C\,(1-\nu) + 4\nu - 6\hat{b} - 3\hat{b}C\,(1-\nu)]}$$

$$\hat{b} = \frac{(6+F)C\,(1-\nu) + 2F\,\nu}{3F + 3C + 2C\,F\,(1-\nu)}$$

C and F given in Figure 7.1

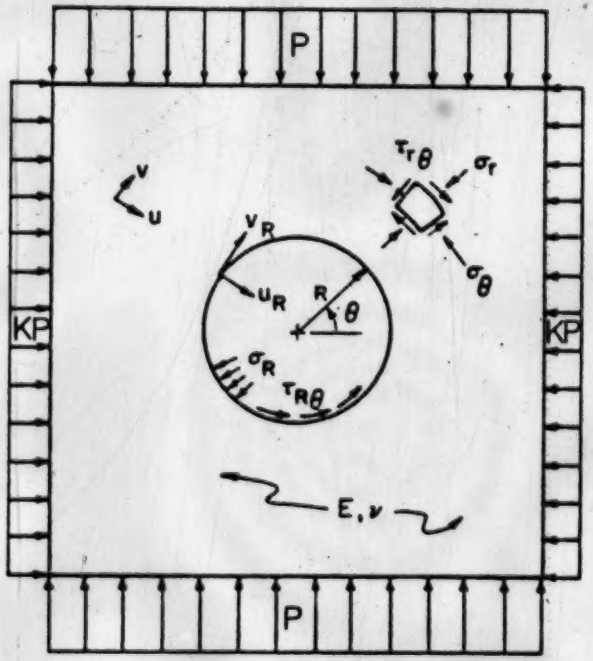

Notation used in calculating the equations

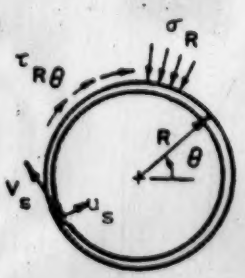

Figure 7.2 Relative Stiffness Equations for Liner Thrusts, Moments and Displacements, Einstein and Schwartz (1980)

7.3 Hanafy and Emery (1980): Numerical Analysis

In their study they considered unlined and lined tunnels in ground having elastic and elastic-plastic-creep properties by using axisymmetric finite element analyses. Only the unlined and lined linear elastic analyses were used for comparison. The ground properties and the tunnel geometry used in this study are generally the same as those in Hanafy and Emery's work. Their analyses used Mesh 1, shown in Figure 2.4, with nodes at each element apex, Boundary Condition 1 shown in Figure 2.13, and the parameters listed below:

Tunnel radius, R = 5 m
Liner thickness, t = 600 mm
Ground modulus, Eu = 5 GPa
Ground Poisson's ratio, νg = 0.2
Liner modulus, El = 30 GPa
Liner Poisson's ratio, νl = 0.2
Compressibility ratio, C = 1.389
Flexibility ratio, F = 1157.4
Initial insitu stress, po = 8 MPa
Mesh length, 13 R
Mesh width, 6.8 R
Length of excavation round, 1 R
Distance of edge of liner from face before next excavation, 0 R, 1 R.

The tunnel excavation and liner installation sequence consisted of "deactivating" the elements of ground being excavated by reducing the modulus to Eu x 10^{-6} and applying equivalent nodal forces in the same manner as in this study. Liner placement involved reactivation of the corresponding elements and reducing the stresses and strains within these

elements, and the nodal displacements, to zero. The liner placement cases studied were the same as Cases 0, 1 and 2 studied here (see Chapter 4).

The results of the analyses, in terms of radial displacement plots, have already been shown, e.g. Figure 2.19. The tangential liner stresses are also shown in Hanafy and Emery's paper, but appear to be 100 times too large because a linear elastic two dimensional closed form analysis gave the tangential stress at the liner centre as about 37 MPa, whereas Hanafy and Emery had a value of about 3800 MPa. However it is possible to compare percentages of the tangential stresses obtained for Cases 1 and 2. They report the maximum liner stress as 46% and 18% of the two dimensional case whereas this study gives 24% and 7% respectively for the stress at the centre of the liner. The difference in the results is probably due to their reporting the ultimate stress in the triangular element closest to the leading edge of a liner segment, where the stresses will be greater than the ultimate stress at the centre of the liner segment, but this could not be confirmed.

7.4 Ranken and Ghaboussi (1975): Numerical Analysis

Ranken and Ghaboussi studied lined and unlined tunnels in linear elastic and elastic-perfectly plastic ground. They used the finite element program GEOSYS, which is a modified form of a program written for the U.S. Bureau of Mines by

Agbabian Associates. Only the linear elastic analyses have been used for comparison with the present work, and it should be noted that the material properties listed below are more representative of soft ground tunnelling conditions than of rock tunnelling conditions.

The finite element mesh that was used is shown in Figure 7.3 , with nodes at the corners of the quadrilateral elements. Boundary Condition 2 (Figure 2.13) was used initially when boundary stresses were applied to achieve a uniform hydrostatic stress state throughout the mesh, before the start of construction. Thereafter Boundary Condition 3 was used during tunnel excavation. The mesh consisted of quadrilateral, isoparametric, axisymmetric finite elements. The main parameters used in their analyses are listed below:

Tunnel radius, R = 3.05 m
Liner thickness, t = 305 mm
Ground modulus, Eu = 34.5 MPa
Ground Poisson's Ratio, ν_g = 0.4
Liner modulus, El = 13.8 GPa
Liner Poisson's Ratio, ν_l = 0.15
Compressibility ratio, C = 0.0291
Flexibility ratio, F = 349.2
Initial insitu stress, po = 0.575 MPa
Mesh length, 14 R
Mesh width, 6 R
Length of excavation round, R/2, R/4
Distance of edge of liner from face before next excavation, 0 R, R.

The tunnel excavation and liner installation sequence consisted of a series of analyses in which the elements within the mesh were activated or deactivated according to

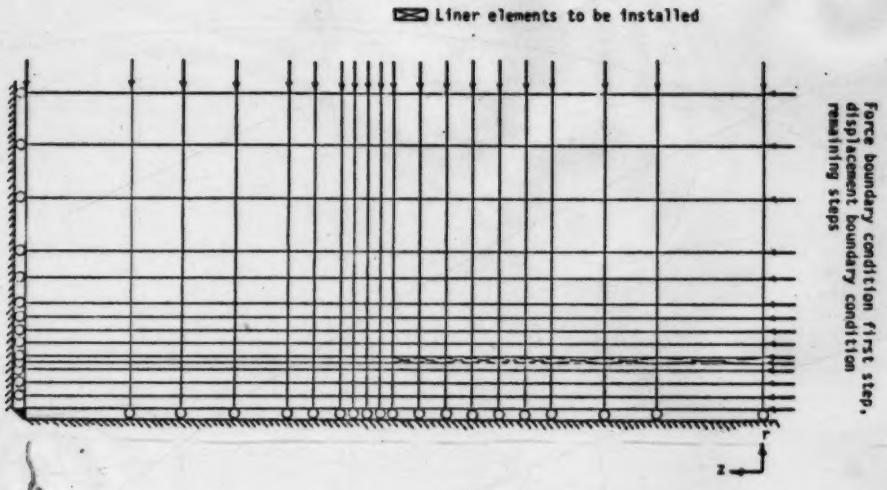

Figure 7.3 Finite Element Mesh, Ranken and Ghaboussi (1975)

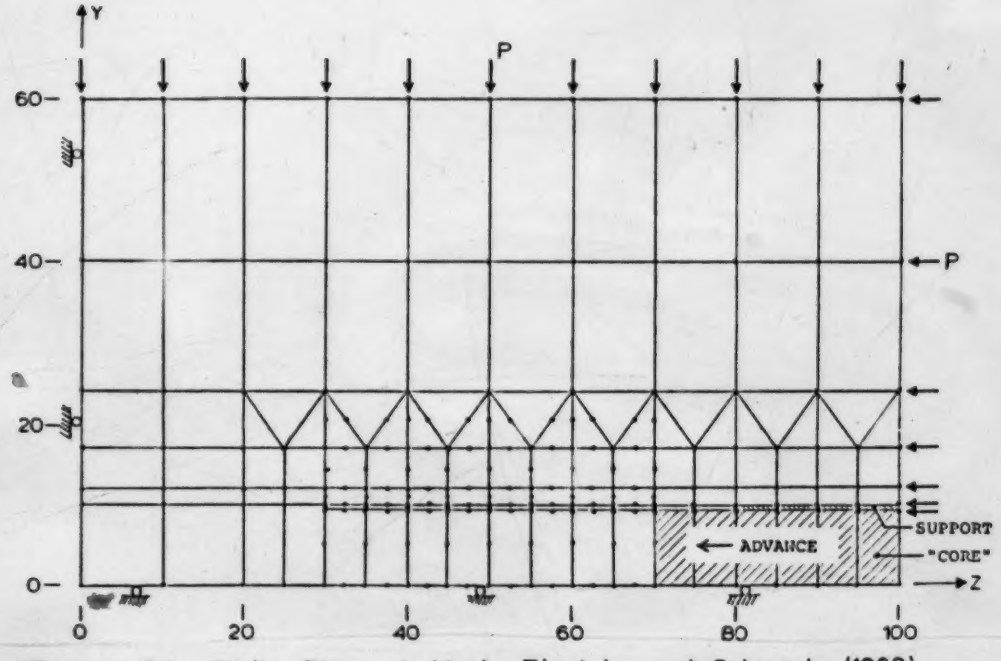

Figure 7.4 Finite Element Mesh, Einstein and Schwartz (1980)

whether they were being excavated or a liner was being installed. When elements were deactivated they did not contribute to the global stiffness of the finite element system.

There were two lined cases studied, one with the liner placed right up to the face throughout the excavation, and one where the liner was always one R behind the face. However only the unlined case has been presented (see Figure 2.20) as comparisons between the lined cases and the present study are difficult because of the great difference in compressibility ratios. It is interesting to note though that Ranken and Ghaboussi mention that "minor distortions of the data due to boundary and other procedural effects have been removed in order to isolate and clarify the information related solely to the behaviour of an advancing tunnel". It is unfortunate that these distortions, and how they arose, were not discussed as a comparison with the inaccuracies in this study would have been of interest.

7.5 Einstein and Schwartz (1980); Numerical Analysis

Einstein and Schwartz studied lined tunnels in linear elastic and elastic plastic ground by using an incremental axisymmetric finite element analysis. They used a general purpose finite element program called ADINA which was developed at MIT as a further development of the SAP4 and NONSAP programs.

The finite element mesh used by Einstein and Schwartz is shown in Figure 7.4 which, in the area of interest, has nodes at the midpoints of the sides of the quadrilateral elements as well as at the corners. The Boundary Condition used is type 2, Figure 2.13, with the isotropic insitu ground stresses applied as nodal loads at the boundaries of the mesh before any excavation took place. The analysis which had parameters similar to those of the present study was chosen for the comparison, and they are listed below:

Tunnel radius, R = 3.05 m
Liner thickness, t = 175 mm
Ground modulus, Eu = 1.03 GPa
Ground Poisson's ratio, νg = 0.15
Liner modulus, El = 20.7 GPa
Liner Poisson's ratio, νl = 0.15
Compressibility ratio, C = 1.0
Flexibility ratio, F = 4800
Initial insitu stress, po (not given)
Mesh length, 10 R
Mesh width, 6 R
Length of excavation round, R/2
Distance of edge of liner from face before next excavation, 0 R, R/2, R. (see comments below)

The sequential excavation of ground elements and installation of support elements was simulated by using the "birth/death" option in ADINA. Einstein and Schwartz compared the actual and simulated tunnelling sequences in a diagram reproduced here as Figure 7.5. In the diagram it can be seen that one round of actual tunnel construction consists of a stage of excavation followed by a stage of support installation. Their diagram shows that in a finite

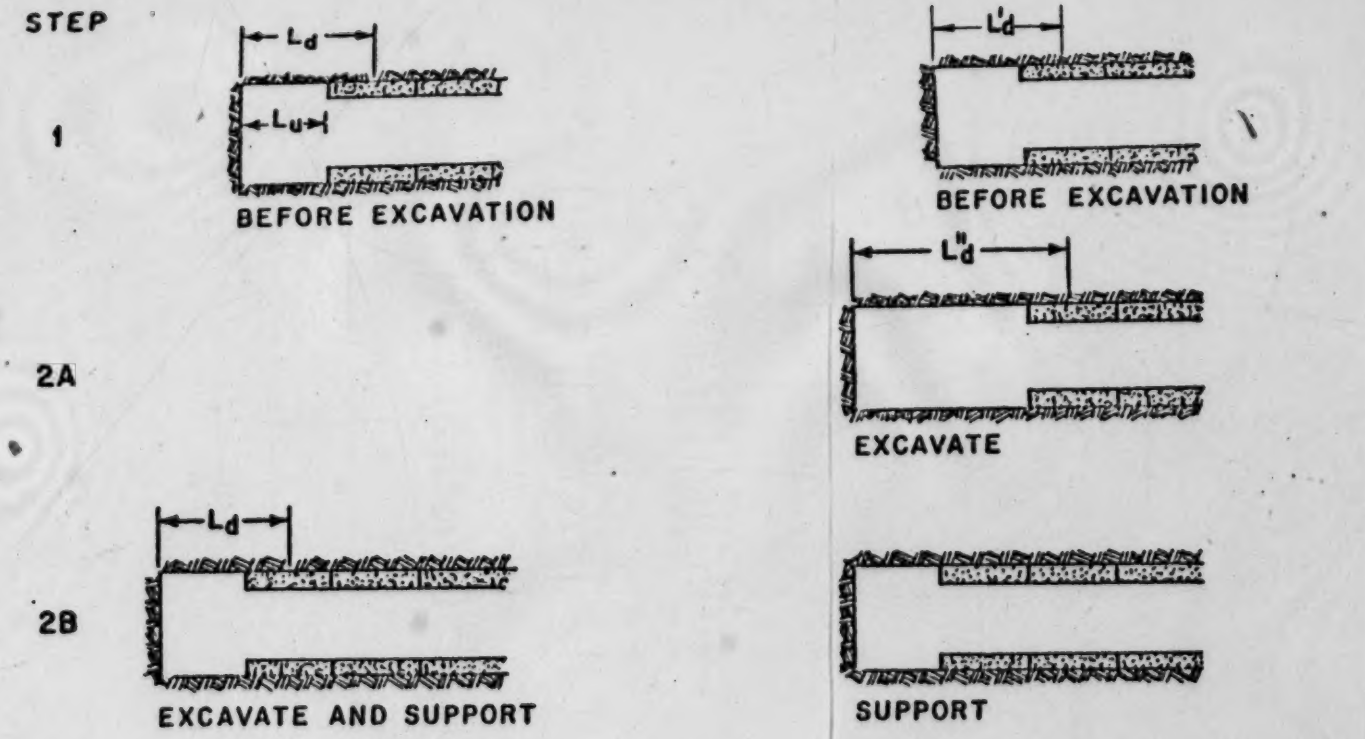

Figure 7.5 Definition of Support Delay, Einstein and Schwartz (1980)

element analysis excavation and support occur at one calculation step, equivalent to one round of tunnel construction. However they do not point out that the computer program does not necessarily carry out the two operations simultaneously. For instance with program CONSTEP2 the ground may be excavated and the liner installed at the same step, but the nodal excavation forces do not have an effect on the system until program SAP4 is used, i.e. until after the material property numbers have been changed, and thus after the liner has been installed. The liner segment is therefore installed *before* excavation in the same construction step occurs.

Einstein and Schwartz go on to say that the value of Ld", shown Figure 7.5, for actual tunnelling sequences is the parameter which corresponds to the value of Ld in the finite element sequence. This is true if in the finite element sequence the liner is installed before excavation, because then Ld is equal to the distance from the new face after excavation to the centre of the closest liner segment, which is the same as the definition of Ld" shown in the figure. If the results of this study are compared to Einstein and Schwartz's results on the basis of the length Ld" they do not agree. The difference is discussed in Section 8.2 where it will be shown that there is better agreement between the results if they are compared on the basis of Ld', the distance from the old face before excavation to the centre of the closest liner segment.

7.6 Gouch and Conway (1976): Numerical Analysis/Case History

Gouch and Conway undertook a series of elastic-plastic two dimensional finite element analyses of the Lucky Friday Mine in the Coeur d'Alene mining district of northern Idaho. The actual situation studied is not the same as the present case, but several points are noteworthy and are discussed below.

Excavation was simulated by applying the insitu stresses in ten increments to the nodes along two perpendicular, free, mesh boundaries. Both the stiffness and the strength of the ground were varied, and in particular the inner two feet of rock around the opening was considered to be a weaker material with no tensile strength. This was done to model the zones of fractured rock observed in similar situations and in the same rock stratum. Rock bolts were simulated by using three model bolts with adjusted properies to represent a larger number of bolts.

Figure 7.6 presents the distribution of principal stresses around the opening after excavation, showing the stresses in the assumed zone of fractured weaker rock to be significantly lower than in the surrounding stronger rock. This is compared in Section 8.3 to the results from the present study.

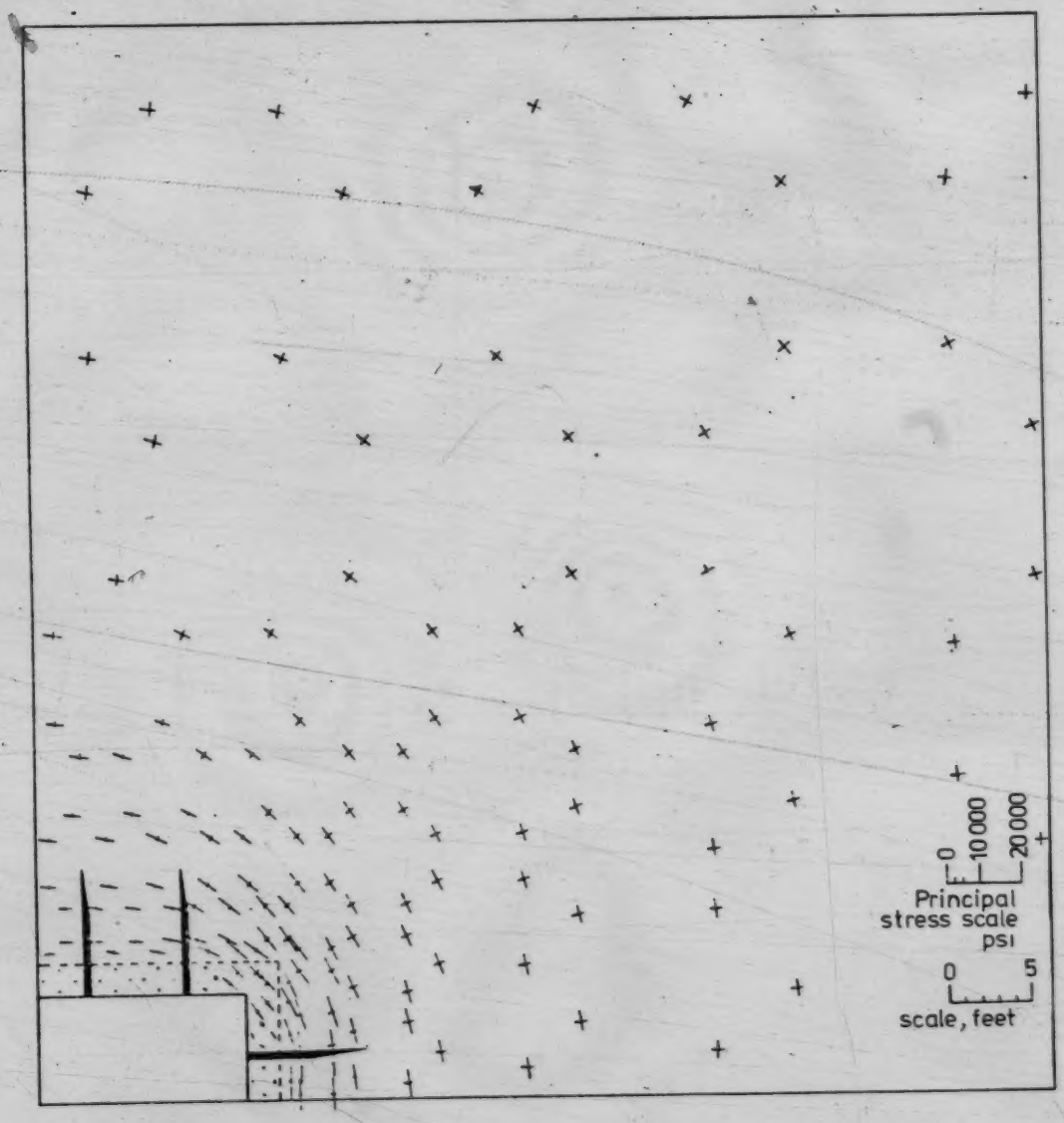

Figure 7.6 Principal Stresses around an Opening, Gouch and Conway (1976)

7.7 Sharp, Richards and Byrne (1977): Numerical Analysis/Case History

Sharp et al. compare the results from a monitoring programme in a trial excavation for the Drakensberg Pumped Storage Scheme with elastic, presumably two dimensional finite element, analyses. Data from the monitoring indicated that the near surface zone of the rock, a sedimentary sequence of sandstones and siltstones, was considerably loosened. Figure 7.7 shows the different stages of the trial excavation modelled, and in particular the three assumed effective load bearing profiles that were analysed (number one being the actual excavation profile). The rock between the wall of the opening and the load bearing profile was assumed to carry no load and the results from these analyses compared to those from the field measurements. In this way they were able to simulate the elastic response of the competent rock and to identify the extent of the loosened rock at any stage. They did not discuss whether the reduction in the load bearing capacity of the rock they were modelling was a result of softening or weakening, though they did show that relating field measurements to even a simple numerical model can improve the predictions of the performance of the final excavated opening.

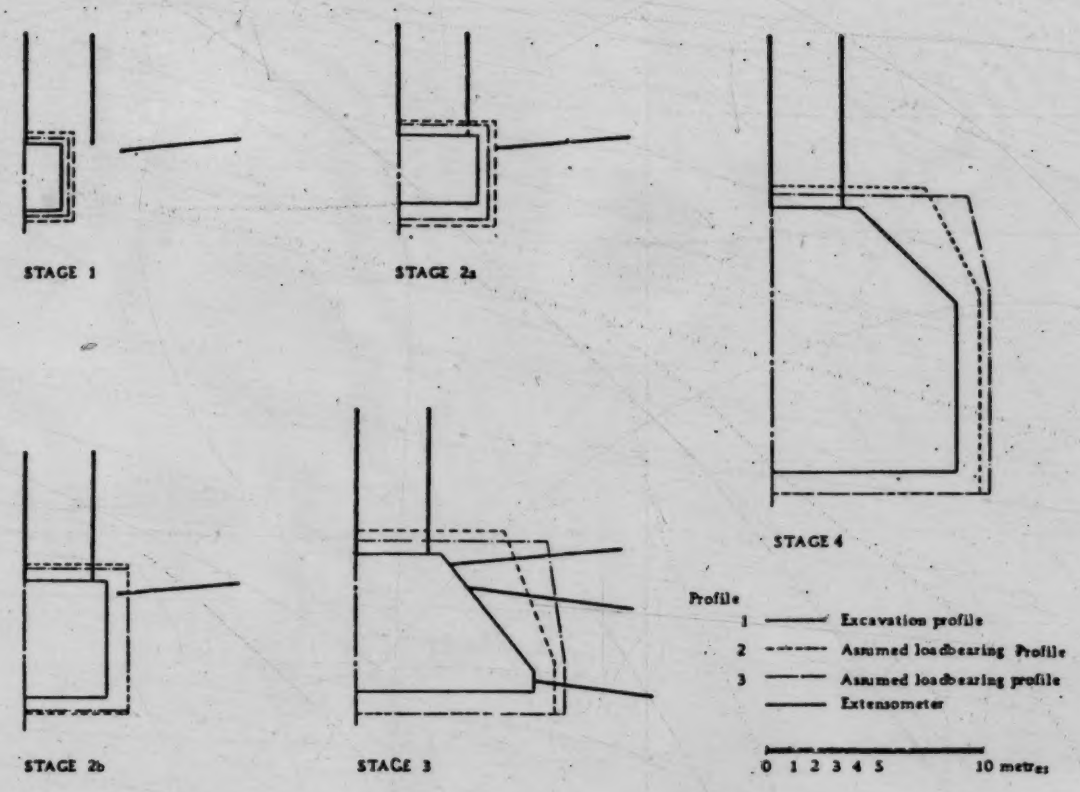

Figure 7.7 Assumed Load Bearing Profiles for the Drakensberg Trial Excavation, Sharp, Richards and Byrne (1977)

7.8 Kielder Experimental Tunnel: Case History

This 3.3 m diameter experimental tunnel was constructed as part of the Northumbrian Water Authority's Kielder Water Scheme in Northern England. Several tunnels were actually constructed in different strata, although it is the main investigation, in the Four Fathom Mudstone, which is considered here. The objective was to measure and compare the performance of different support systems and excavation methods. Details of the project have been presented in numerous papers, but the information presented here and used in this study has been taken from Ward et al. (1976) and Ward (1978). The first 50 m of the tunnel in the relatively soft and weak mudstone were excavated by drilling and blasting, and four different types of support were installed in this section. These were rockbolts with sprayed concrete, sprayed concrete arch, rockbolts only and blocked steel ribs. The rest of the tunnel was then excavated by a Dosco roadheader down to about 1 m above the invert and by hand to the final level. The four types of support used in this section were a steel liner, rockbolts and sprayed concrete, sprayed concrete ring, and no support.

The following information on the machine excavated portion with a steel liner for support is presented for comparison with the finite element analyses.

Tunnel radius, R = 1.65 m
Liner thickness, t = 12.7 mm
Ground modulus, Eu = 5 GPa
Ground Poisson's ratio, ν_g = 0.25

Liner modulus, El = 207 GPa
Liner Poisson's ratio, ν_l = 0.3
Compressibility ratio, C = 0.3046
Flexibility ratio, F = $0.62 \times 10^{+6}$
Initial insitu stress, po = 2.56 MPa
Length of excavation round, 2.1 m (1.273 R)
Distance of edge of liner from face before next excavation, 0.3 m, 1.0 m, 1.7 m.

The sequence of excavation and liner placement is shown in Figure 7.8 and the thrusts after ten days in each of the three liner segments were 1050 kN, 550 kN and 400 kN, the highest value was for the segment closest to the face, and the lowest value for the segment furthest from the face.

Kaiser (1981) has reanalysed the data presented by Ward et al.(1976), and plotted it on a convergence-confinement diagram. The same data is presented in Figure 7.9 but with a different interpretation of the ground convergence curves. This figure is discussed in Section 8.3.

7.9 Garrison Dam Tunnel: Case History

Eight outlet tunnels for the Garrison Dam in North Dakota were constructed in the heavily overconsolidated Fort Union Clay Shale Formation. Several of the tunnels were instrumented, and the information from one section (4A) of tunnel 4 is presented here. The information has been taken from Einstein and Schwartz (1980) who have summarised the relevant data published by various authors. Section 4A was chosen because it has a compressibility ratio similar to

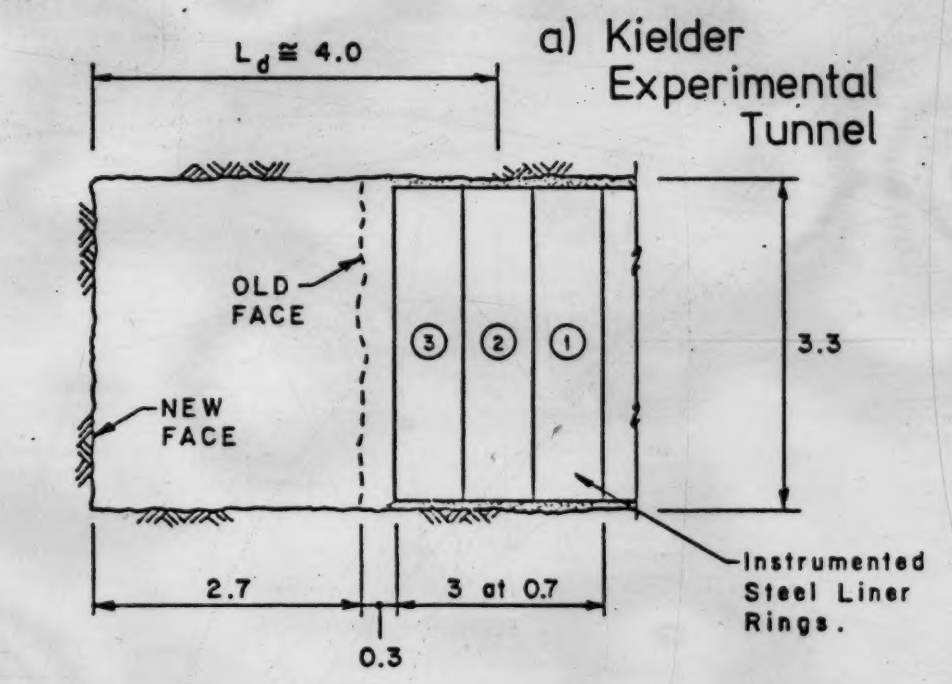

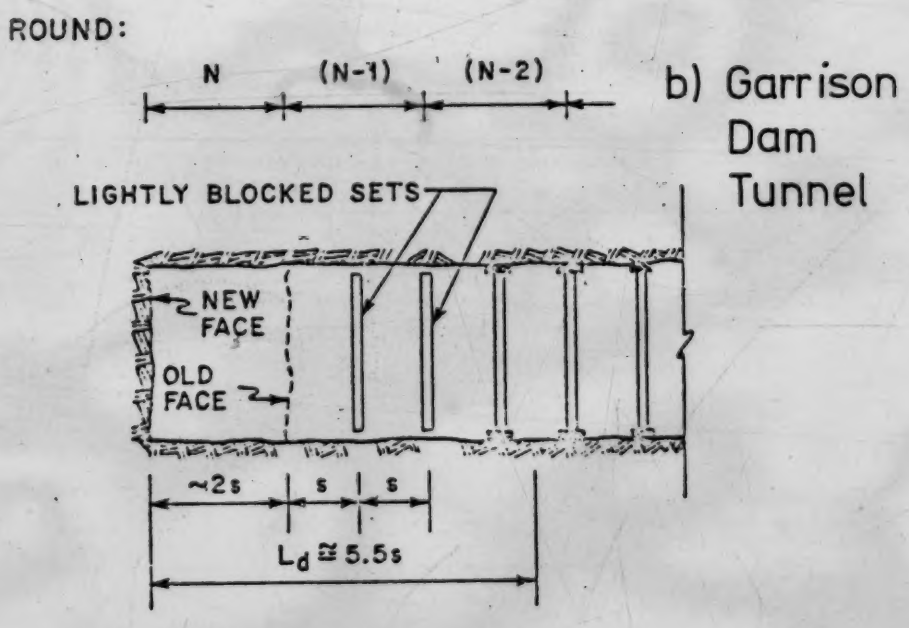

Figure 7.8 Support Delay Lengths - Kielder Experimental Tunnel and Garrison Dam Tunnel

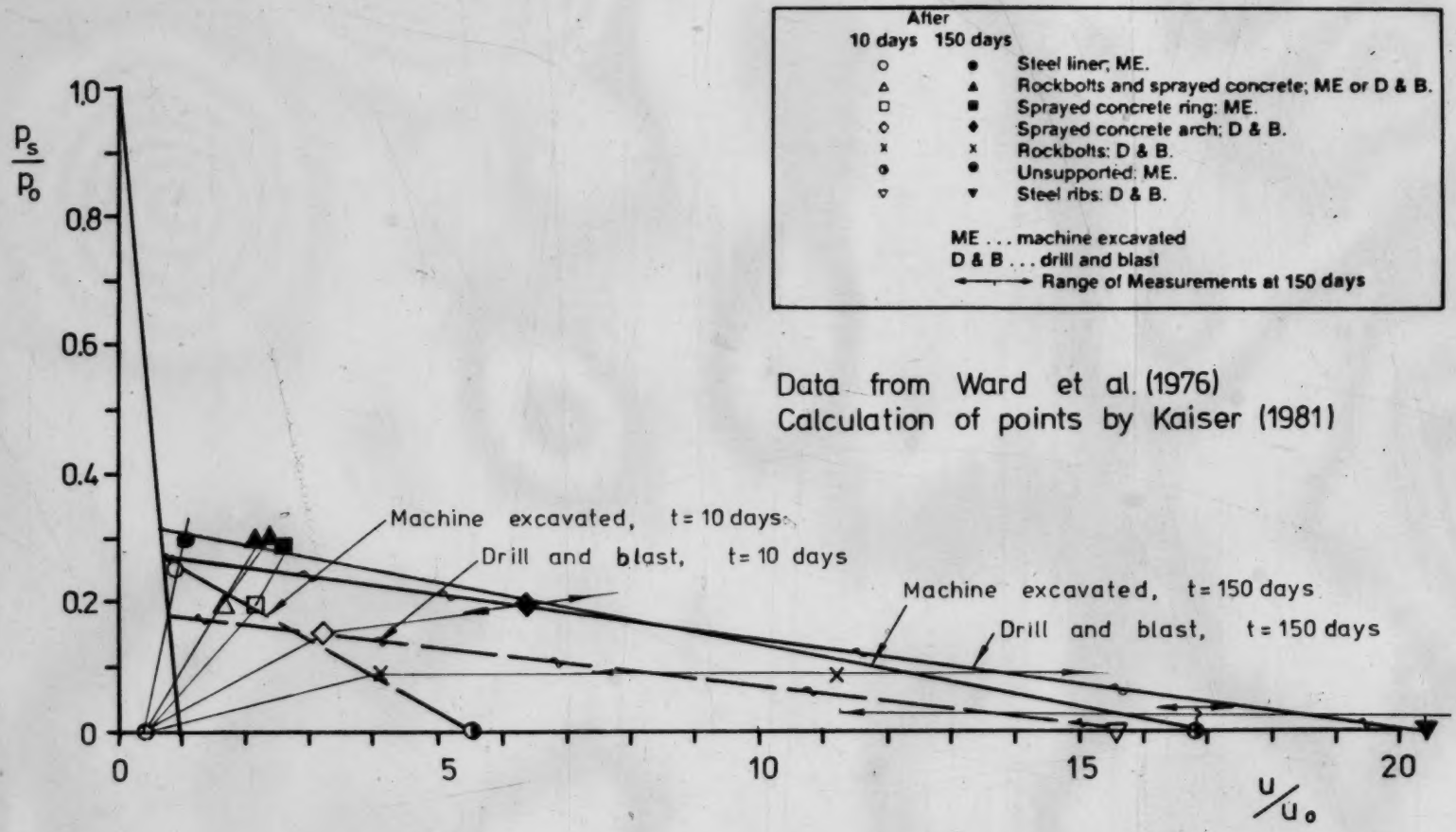

Figure 7.9 Linearised Ground Convergence Curves from the Kielder Experimental Tunnel in the Four Fathom Mudstone

that of the analyses in this study. The various important parameters are listed below:

Tunnel radius, R = 5.5 m
Liner thickness, t = 4.1 mm (calculated equivalent, Einstein and Schwartz, 1980)
Ground modulus, Eu = 192 MPa
Ground Poisson's ratio, ν_g = 0.5
Liner modulus, El = 200 GPa
Liner Poisson's ratio, ν_l = 0
Compressibility ratio, C = 1.69
Flexibility ratio, F = 549
Initial insitu stress, po = 7.24 kPa
Length of excavation round, 1.82 m (0.331 R)
Distance of edge of support from face before next excavation, 4.55 m (0.827 R).

The sequence of excavation and support is shown in Figure 7.8. The drill and blast method of excavation was used, with a temporary support of blocked steel sets and lagging, followed much later by a cast in place concrete liner. The measured value of T/po.R for section 4A was 0.132, with a value of T/po.R = 0.410 given by the two dimensional relative stiffness solution presented in Section 7.2. This thrust is compared with the thrusts calculated by numerical analyses in Section 8.2 and 8.8.

7.10 Lethbridge Shaft; Case History

A 235 m deep circular shaft with a finished diameter of 4.3 m was excavated at Kipp, near Lethbridge, Alberta. A monitoring programme was carried out by the University of Alberta, and the results have been presented by MacKay

(1982). The findings from the programme were summarised by Kaiser et al. (1982), from which the information below has been taken.

The shaft was sunk through sediments of Upper Cretaceous Age. At the levels in the shaft where the instruments were installed the rock consisted of alternating beds of sandy and shaley mudstones of the Bearpaw Formation. Only limited initial insitu stress measurements were possible, but in conjunction with a review of the literature they determined that the vertical stress was close to the overburden pressure, about 4.2 MPa at the 180 m depth. The value of Ko was considered to be between 0.8 and 1.3 and the resulting horizontal stress ratio, N, to be greater than or equal to 0.62. The maximum principal stress was considered to be in the NE-SW direction.

Instruments were installed at 111 m, 152 m and 180 m depths. The results considered later in Chapter 8 are from the mechanical multipoint extensometers at 180 m, and the tangential and radial vibrating wire borehole stress change gauges at 152 m. The layout of these installations are shown in Figure 7.10.

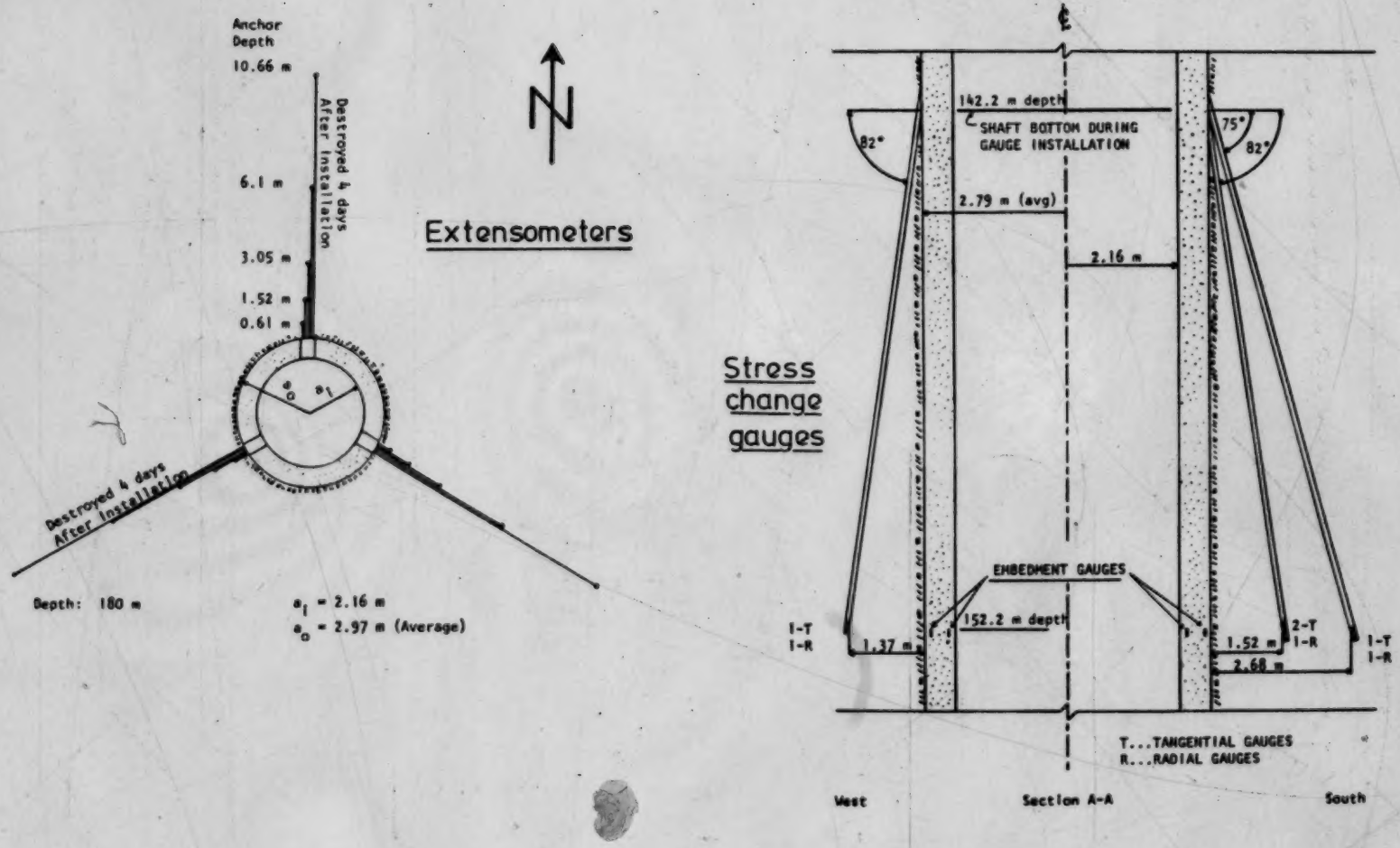

Figure 7.10 Instrumentation Installed in the Lethbridge Shaft, Kaiser et al. (1982)

CHAPTER 8

INTERPRETATION AND DISCUSSION OF RESULTS

8.1 Introduction

This section discusses the main effects of construction procedures, illustrated by the present study on the behaviour of tunnels and shafts. It is shown how these factors affect the analysis of results from a monitoring programme of the behaviour during construction and the comparison of the results with other numerical analyses. The implications for the design of excavation and support procedures are also discussed.

The main topics considered are: 1) the effect of delaying the installation of support on the ultimate radial wall convergence and on the stresses within the support; 2) the effect of rock damage caused by the construction process (i.e. by drill and blast excavation, simulated by ground softening rather than by weakening) on wall convergence, support stresses and on the stress distribution in the ground surrounding the opening; 3)the effects of construction within frozen ground, and subsequent thawing; 4) the variation of the radial wall convergence at the face; 5) the variation of radial and tangential stresses within the ground as the tunnel passes; 6) the variation of stresses within the liner for various cases of excavation and liner placement; and 7) how the tangential thrusts

within a liner might be evaluated for various delays in liner placement and for various extents and degrees of rock damage around the excavation.

Shallow and deep shafts were studied and the influence of Ko considered. A shaft constructed by drilling under fluid support, with the liner installed after excavation but before removal of the fluid, was analysed by a simple method. The effects on the liner with this method of construction were compared to the effects with the common method of shaft construction, by drill and blast excavation.

8.2 Effect of Delay in Liner Placement

Figure 2.22 presents some of the effects of varying the length of the delay in placing the liner behind the face. (The maximum open ground is the greatest distance between the face and the leading edge of the liner during a round of excavation.) The figure shows the wall convergence and liner thrust forces in a tunnel constructed without any surrounding ground damage, and shows that there is little increase in the ultimate radial displacements at the tunnel wall, and liner thrusts become very small, if the open ground exceeds two radii (Figures 2.22a and 2.22b). Even if it were possible to install this particular liner before excavation, the figures show that about 50% of the convergence in the unlined case would still occur, and the liner thrusts would not be greater than about 50% of the

original field stress.

The results from these analyses and from those by Einstein and Schwartz (1980) are compared in Figure 8.1 for different definitions of Ld, the liner support delay (Section 7.5). In the figure Einstein and Schwartz's results (solid and open circles) are from analyses of the cases shown in Table 8.1. The points in the diagram are non-dimensional liner thrusts (T/po.R), normalised by the value of non-dimensional thrust given by the relative stiffness solution, plotted against different definitions of support delay. The solid circles correspond to the delay defined as Ld", the distance from the new face after excavation to the centre of the closest liner segment, and the open circles correspond to the delay defined as Ld', the distance from the old face before excavation to the centre of the closest liner segment (see Figure 7.5). It has been assumed that within the same construction step in Einstein and Schwartz's (1980) finite element analyses the liner is placed before excavation.

The results from the analyses in this study, and from two case histories, are also plotted on Figure 8.1. Again the open symbols are for a support delay defined as Ld' and the solid symbols for Ld". It can be seen, apart from Case 2, that all the results agree very well if they are plotted against Ld'. Case 2 would not be expected to follow the linear relationship shown by the other results because in an elastic analysis some thrust would be obtained even at

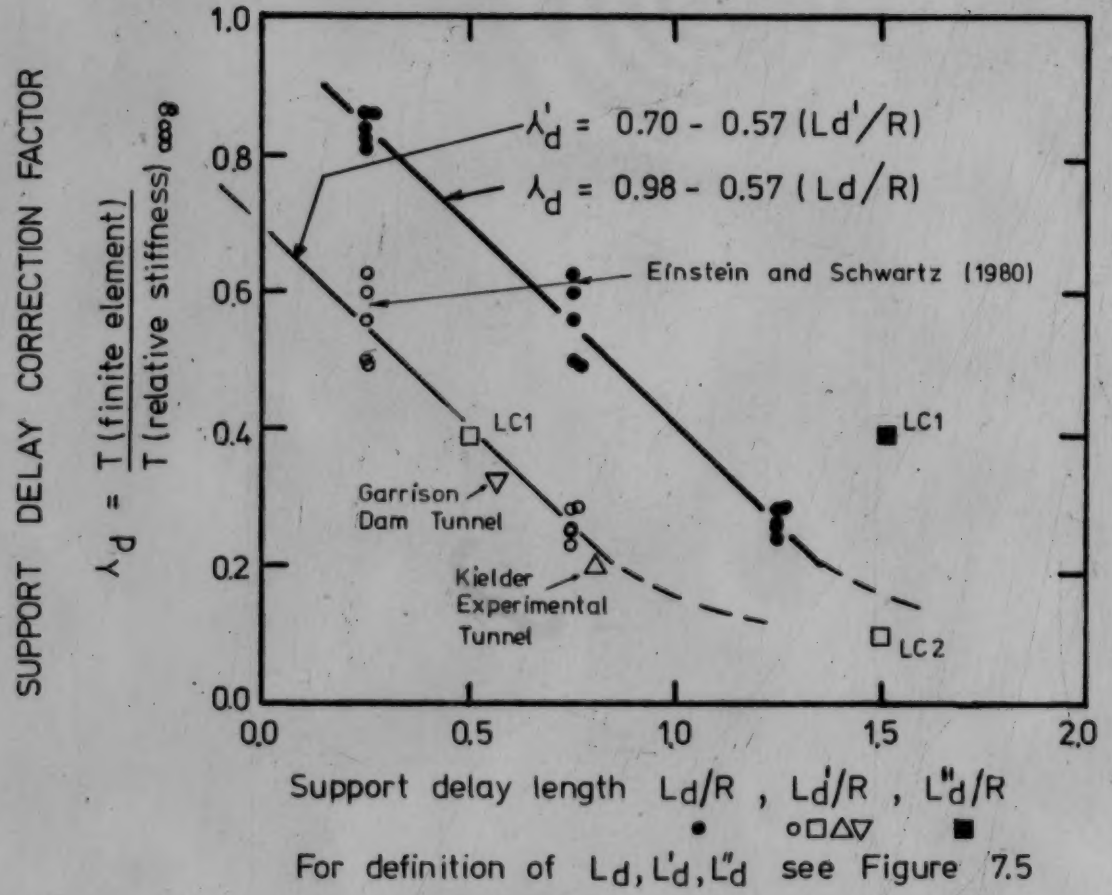

Figure 8.1 Support Delay Correction Factor

Table 8.1

Material Properties used by Einstein and Schwartz (1980)

Case	Radius (m)	Ground Properties		Support Properties			C	F
		E (GPa)	ν	E_s (GPa)	ν_s	t (mm)		
1	3.0	0.103	0.30	13.376	0.30	175	0.134	484.0
2A	3.0	0.034	0.48	13.376	0.30	175	0.0528	191.0
2B	3.0	0.034	0.30	13.376	0.30	175	0.0447	161.0
3	3.0	1.034	0.15	20.685	0.15	175	1.0	4800.0
4	3.0	10.343	0.15	20.685	0.15	175	10.0	48000.0
This Study	5.0	5.0	0.2	30.0	0.2	600	1.389	1157.4

large values of support delay, and the relationship becomes asymptotic to the $\lambda d = 0$ axis. This indicates that Ld' is a better parameter than Ld" for describing the support delay, and the equation of the best fit line through the points is shown on the figure. This line is not applicable for values of Ld' greater than about 0.8. Ld' has been used in Section 8.8 where a non-linear relationship for λd, valid over a larger range of values of Ld' than shown in Figure 8.1, is discussed. It can be appreciated that whichever parameter is taken to measure the support delay, it is an important factor which dominates support thrusts (and ground movements). The complete geometry of the sequence of excavation, and the exact locations of the instruments relative to the face are seldom adequately considered in the analysis of field measurements, and are often not reported in the published literature, even where a comprehensive monitoring programme has been carried out (e.g. Kaiser et al. 1982). Sections 8.6 and 8.8 discuss how the stresses vary within a liner and the importance of knowing the location of the instruments, both within the liner and relative to the face.

8.3 Effect of Rock Damage

Several observations of practical significance can be made from Figure 8.2 where the ultimate stresses in the ground around a tunnel can be seen. The four cases shown

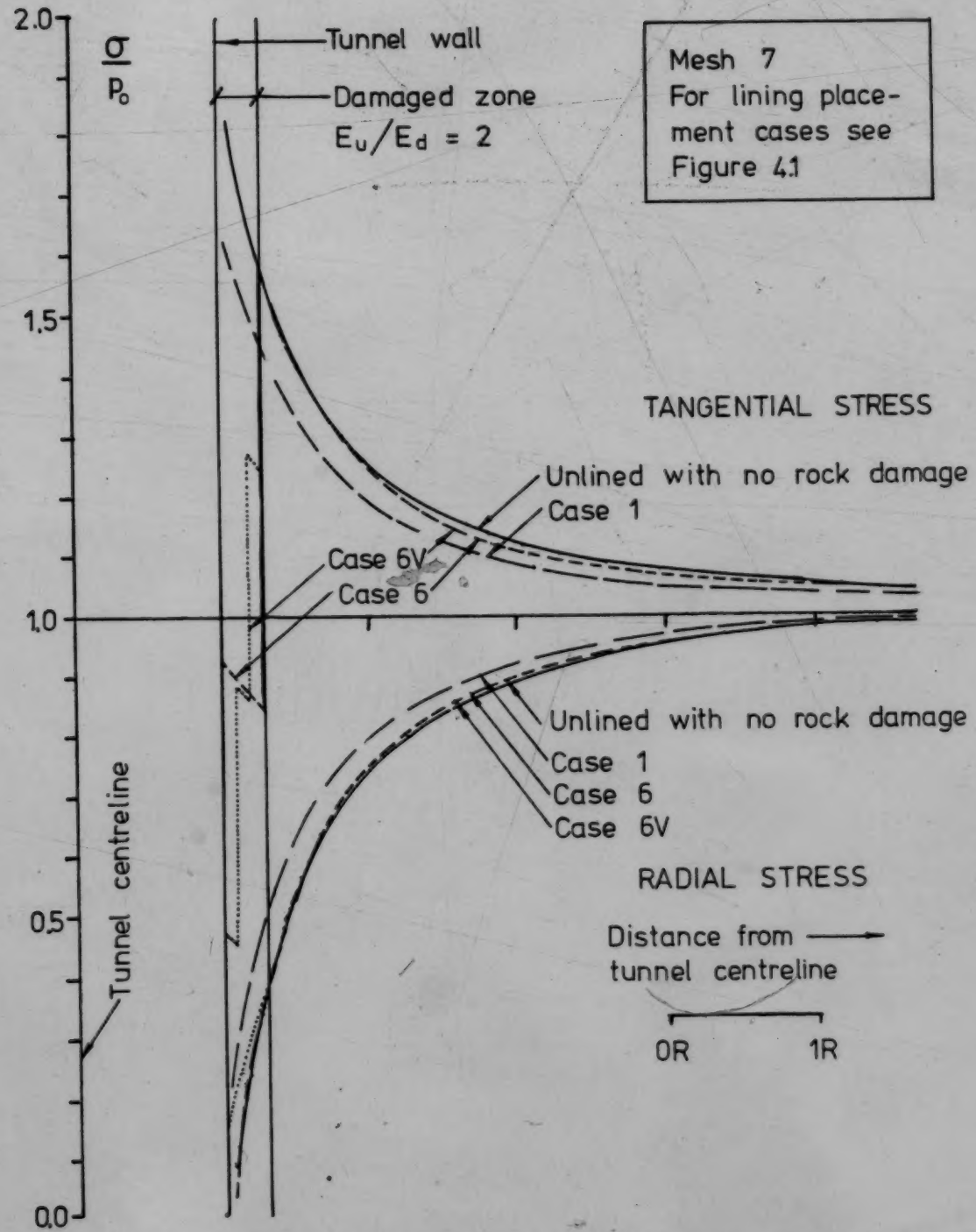

Figure 8.2 Variation of Ultimate Ground Stresses with Distance from Centreline

are: Unlined, Case 1 - lined, Case 6 - lined with rock damage, and Case 6V - lined with the damaged rock having a variable modulus.

A comparison between Cases 1 and 6 shows that the tangential stresses in the ring of damaged ground are lower than the stresses in the equivalent ring of undisturbed ground. The principal stress difference in Case 1 is greatest at the tunnel wall, whereas in Case 6 the maximum occurs at the interface between the damaged and undamaged zones (where higher confining stresses exist) and is lower than in Case 1. The stress distribution beyond the radius of damage, B, is almost identical to the distribution beyond a radius of B in an unlined tunnel with no rock damage. A zone of sightly softened rock, i.e. with a modulus reduced by a factor of 0.5 (as in the case shown), may cause significant stress redistribution which influences the behaviour of tunnels in two ways.

First, it transfers stresses to areas where the capacity of the ground is higher due to greater confinement by the radial stress. Consequently high stress concentrations near the opening wall, which may cause ground yielding, are reduced and the opening may be more stable, particularly where brittle failure modes such as spalling are likely to occur. Some yielding may occur in the damaged zone where the rock mass may have been weakened as well as softened, however the progressive strain-weakening failure process may be prevented or confined to the immediate near

surface area. Kaiser (1981) has indicated that in the case of the Kielder Experimental Tunnel (Ward, 1978 and Ward et al., 1976), the plastic zone in a strain-weakening rock (for example see the stress-strain curves shown in Figure 3.2) would have to be unreasonably large to fit the observed field data. The actual displacement measurements inside the rock mass indicate that the assumption of a softened zone around the tunnel may be more applicable. Furthermore the time dependent deformations can be more easily explained by the propagation of a softened zone rather than by a zone of broken, weakened, material.

Second, the stress transfer from the damaged to the undamaged zone is associated with additional deformations in the rock mass outside the damaged zone. The overall rock mass therefore appears to behave as a softer material, or alternatively, the tunnel behaves like an equivalent opening of larger size in undamaged rock. This increase in convergence must be considered during tunnel design and when comparing measurements with results from numerical models.

The identification of zones of softened rock around an opening should be attempted from field measurements taken. As rock stress measurements are rarely made and radial displacements observations are more common, it would be desirable to use the pattern of radial displacement, or strain, to identify zones of softened rock. The variations of ultimate radial strain around the lined tunnels, with and without rock damage, analysed here are presented in

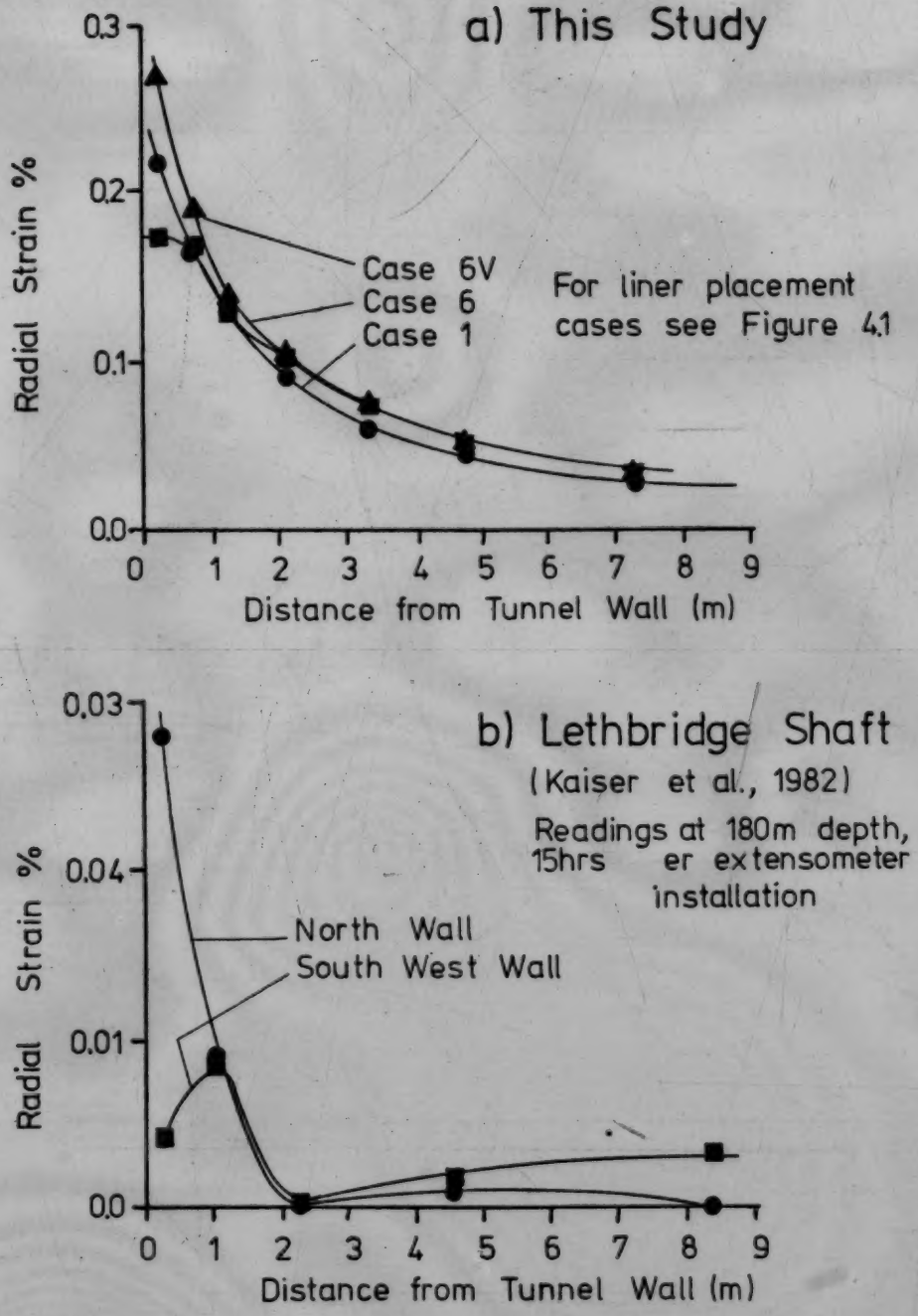

Figure 8.3 Variation of Radial Strain around Openings

Figure 8.3a. In Case 6V the modulus of the damaged rock (Ed) increases linearly from the opening wall to the interface between the damaged and undamaged zones (Figure 4.2), whereas in Case 6 Ed is constant. Case 1 is the undamaged case. The figure shows that if the rock is softened so that its modulus is uniform throughout the damaged zone the radial strain will level off to a constant value near the wall, and a zone of softening can be identified. If, as is more likely around an actual opening, the damage is such that the modulus in the damaged zone decreases towards the wall, the strains will correspondingly increase, and can almost not be differentiated from the case where there is no rock damage. In these analayses the number of elements in and near the damaged zone was rather small, and so only a few points were available from which to draw the strain distribution in the critical area at the damaged/undamaged rock interface. This made it difficult to reach any conclusions and further study using a finer mesh is required. However in practice extensometers will be installed with a relatively wide spacing between anchoring points and interpretation of the information obtained from them is likely to be equally inconclusive.

Figure 8.3b shows the radial strains calculated from extensometer readings taken in a shaft at Lethbridge, Alberta (Kaiser et al. (1982), see Section 7.10). The extensometers were placed at a depth of 180 m and the readings were taken 15 hours after installation. It would

appear that there could be up to a 2 m thick zone of damaged rock at the south west wall as the strains vary in a manner not too dissimilar from Case 6, Figure 8.3a. It is more difficult to ascertain whether there is a damaged zone at the north wall, and the large strains observed may be due to rock loosening or dilation which could have masked the effect of softening. In fact the north wall has higher tangential stresses than the south west wall and hence loosening and yielding is more likely to occur there. As the extensometers were installed above the base of the shaft the readings do not reflect the full rock straining, and will also have been affected by rock and initial insitu stress anistropy.

This difficulty in assessing the zone of damaged ground from measurements of radial ground movements has implications for the monitoring of the behaviour of a tunnel or shaft during construction. It has already been shown that significant stress reductions occur within zones of softened rock (see for example Figures 8.2 and A5.50), particularly for the tangential stresses. The amount of this stress change will depend upon the Eu/Ed ratio and the radial extent of the damage as well as other factors. Given the same number of measuring points it will be easier to detect a drop near the wall in the tangential stress distribution than a difference in the strain distribution from the distribution in the undamaged case (which is unlikely to have been measured anyway), or to detect a change in the

rate of increase in the slope of the strain distribution. Only if Ed is constant within the damaged zone, for example when the ground is deforming perfectly plastically without dilation, will the strain distribution give an indication of the damaged area. However other factors will have a bearing on the choice of monitoring method. Sharp et al. (1977) discuss different types of instrumentation for monitoring underground openings and point out that rock stress measurements are made only at a point in the rock, and because the stresses will be very sensitive to the ground conditions in the immediate vicinity of that point the stress measurements are usually erratic. Measurements of ground movements made by borehole extensometers are usually less erratic because they give the overall rock mass response rather than the local behaviour.

It has already been noted, in Section 6.2.12, that there is a reduction of stress in a zone of weakened ground, as shown in the results presented by Gouch and Conway (1976), Figure 7.6. This stress reduction is similar to that observed in these analyses in a zone of softened ground. It may be difficult therefore to differentiate between the effects of softening and weakening in any particular case based on only the results of monitoring, and so accurate tests should be performed to measure the insitu rock mass strength and deformation properties, and the effects and extent of rock damage due to construction procedures considered. Although it may be difficult to differentiate

between the two processes of softening and weakening it should not be assumed that both processes are equally valid for modelling any particular situation. If ground parameters are adjusted to fit the observed behaviour using only one of these processes the correct stress and strain fields may be predicted, but extrapolations to other cases for stability evaluation may not be justified. For example where a ductile rock is modelled by a strain weakening behaviour unrealistically large zones of weakened rock could be predicted for situations other than that from which the model was derived.

The results from Gouch and Conway (1976), Figure 7.6, and the results shown in Figures A5.49 and A5.50, indicate that both with weakened and softened zones there is a high stress concentration at the corners of the opening. If the ground is assumed to have very low strength, as in the analyses by Sharp et al. (1977) (Section 7.7), the stress that would be taken by the damaged ground will be transfered further outwards, possibly creating or increasing a zone of weakening.

The effect of rock damage on the liner stresses and tunnel wall displacements is illustrated in Figure 8.4 where all the relevant results from the analyses have been plotted on a convergence-confinement diagram. The ground convergence curves for these analyses, calculated from the two dimensional analysis according to Kaiser (1981), and recalculated in Appendix 1, are also plotted on this figure.

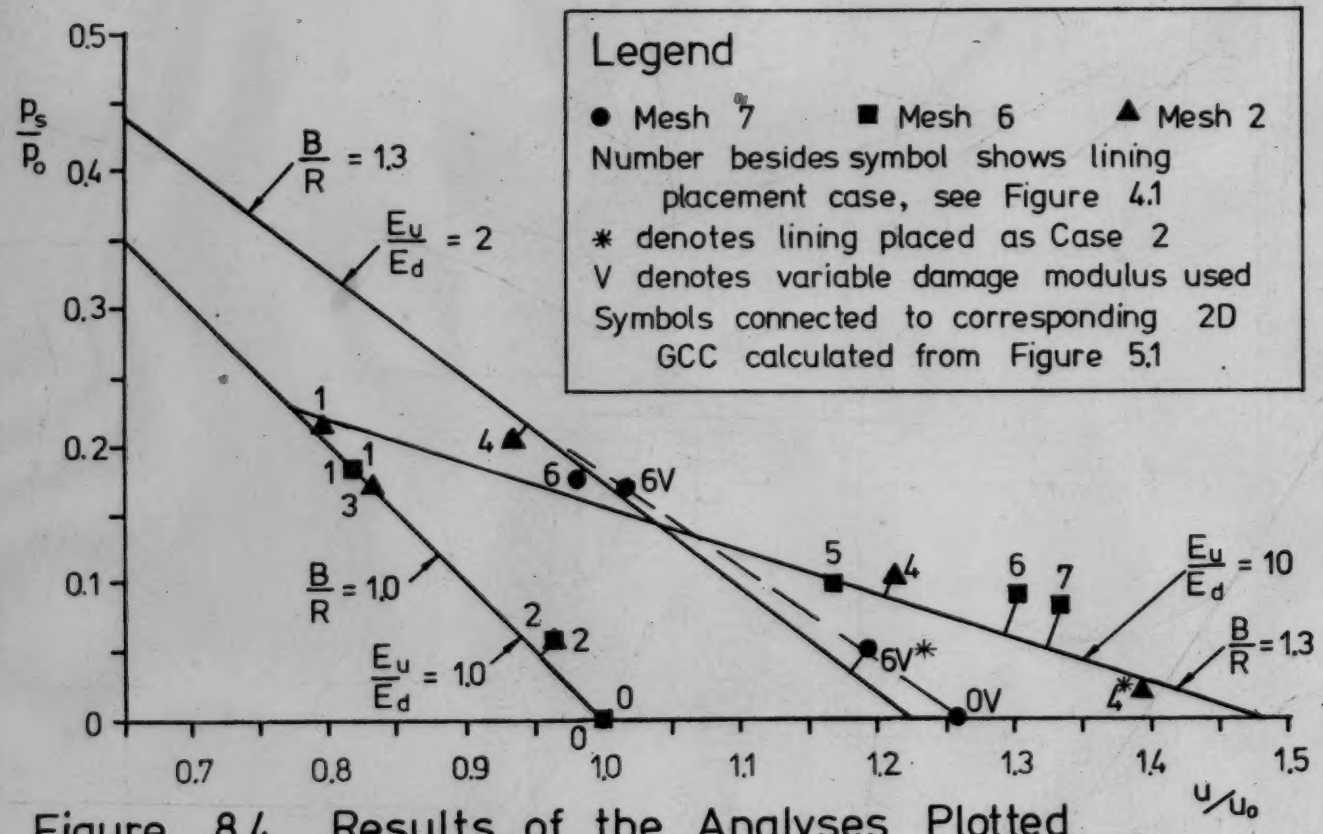

Figure 8.4 Results of the Analyses Plotted on a Convergence - Confinement Diagram

Values of support pressure and wall displacements have been averaged over the length of a round of excavation. They have been adjusted to reduce the inaccuracies arising from the stress interpolation by comparing the results from unlined numerical analyses with those from similar unlined cases calculated from two dimensional closed form solutions. In other words, the correction factor, that has to be applied to the numerical analysis of the unlined case in order to make it agree with the closed form two dimensional solution, is applied to the other excavation and liner placement cases. Appendix 3 shows how these correction factors are obtained, and presents examples of the calculation of the adjusted results.

The results of the analyses shown in Figure 8.4 lie close to the bilinear ground convergence curves calculated from the two dimensional plane strain equations. The scatter of the results is largely related to the coarseness of the meshes, particularly where Mesh 2 is used for the Eu/Ed = 10 analyses. For the various cases analysed the final wall displacements vary between 0.79 and 1.39 times the ultimate (unlined) elastic convergence, uo. Accordingly the support pressure varies between 0.22 and 0.0 times the field stress po. This shows that alteration of the ground properties during construction affects the tunnel and liner performance drastically. For example, damage ahead of the tunnel face causes a reduction in support pressure by about 20% (considering Cases 1 and 3) and softening of the tunnel

walls causes an additional 32% reduction in support pressure (Case 4, Eu/Ed = 10). A delay in liner installation by one extra radius in the latter case reduces the support pressure (Case 4) to less than 10% of Case 1.

The effect of confining pressure variation can be evaluated by comparing Cases 6 and 6V. In Case 6 the damaged ground modulus is constant within the softened zone, whereas in Case 6V it is varied in an attempt to simulate the influence of a changing confining pressure. Figure 8.4 shows that there is slightly greater convergence in Case 6V, but little change in support pressure. A comparison between the GCC calculated for Eu/Ed = 2, and that drawn in Figure 8.4 as a dashed line for the cases with a varying damaged rock modulus, shows that the equivalent constant modulus ratio, Eu/Ed, for the variable modulus cases would be slightly greater than the average value of 2. The stresses in the rock mass in Case 6V are almost identical to those in Case 6, as shown in Figure 8.2, except that the tangential stress increases, stepwise, through the damaged rock zone.

The actual variation of the deformation modulus in a zone of damaged ground in the field will depend upon the variation of the degree of damage caused by the blasting and the final distribution of the confining pressures in the ground. The initial stress field po will also have some influence. If po is greater than the confining pressure (say pc) at which the damaged and undamaged rock moduli are the same, Figure 3.1b, the region of significantly reduced

modulus in the damaged rock zone will be smaller than if po were much lower than pc. For example, assume that the radial stress is the main factor in determining the confining pressure at any point, and that around an opening it takes the form shown in Figure 8.2. Also, only consider rock softening, and not rock weakening. With a small po, below pc, even a small amount of damage will cause a large modulus reduction which will occur throughout the whole damaged zone (from the more highly damaged area close to the opening to the slightly fractured rock at the furthest extent of the zone of damage) because the confining stress is always lower than pc. With a po above pc, only in the region where the confining pressure drops below pc will there be a significant reduction in modulus below the undamaged value. Of course the final stress field is difficult to determine because it depends upon the relative stiffnesses of the different areas of rock, which in the damaged zone in particular will depend on the confining pressure, which in turn is a function of the stress field. Further analysis and field measurements are required to provide a more accurate basis for the selection of the modulus distribution function.

Convergence-confinement data calculated by Kaiser (1981) from the published results of the Kielder Experimental Tunnel (Section 7.9) is shown in Figure 7.9. Although the results for each support type lie over a considerable range in most cases, and several assumptions

have been made in assessing the data, it appears that the information could be represented by bilinear ground convergence curves. Different curves are drawn for the machine excavated and drill and blasted sections, and also for measurements at 10 days and at 150 days after excavation. Considering only the measurements at 10 days, in the machine excavated case the ground ahead of the face behaves as if Eu/Ed = 8.9 (comparing the curves with those shown in Figure 5.1), and in the drill and blasted case as if Eu/Ed = 14.7. Behind the face the processes of dilation and additional softening due to reduced confinement have increased the convergence so that the equations in Figure 5.1 may no longer apply. However, if Eu/Ed is assumed to equal 100 then B = 1.26 R in the machine excavated case, and B = 23.3 R in the drill and blasted case. This latter result would indicate that a significant amount of dilation or additional softening has occured, because it is very unlikely that damage would occur to such an extent. Further work is required to study these effects.

8.4 Excavation in Frozen Ground

Figure 8.5 shows the corrected results from the analyses carried out on tunnel construction within a ring of frozen ground which was subsequently thawed. The results lie close to the calculated linear ground convergence curves for a two dimensional plane strain case for an opening in a ring

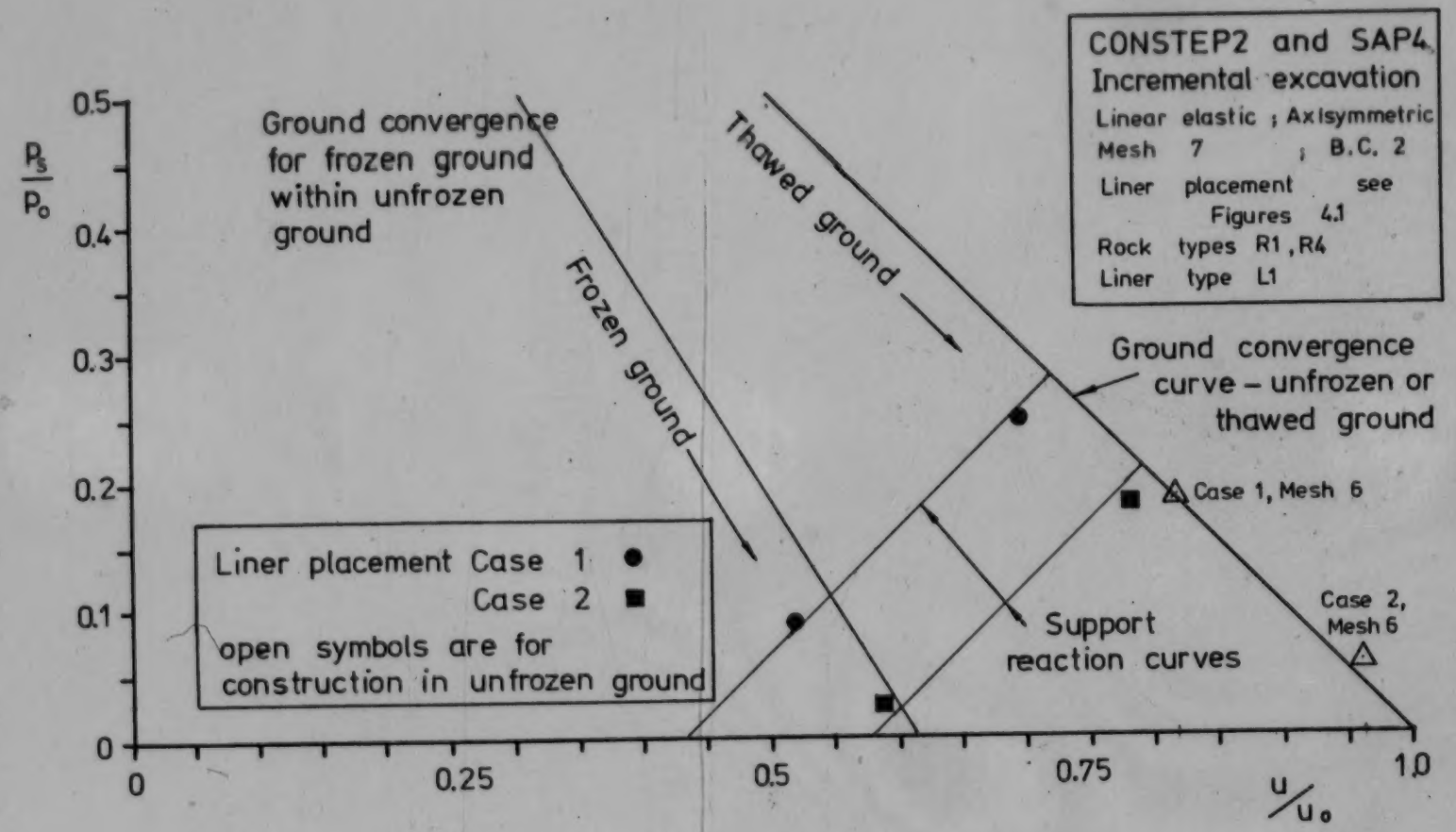

Figure 8.5 Ground Convergence Curves, Frozen and Thawed Ground

of frozen ground surrounded by unfrozen ground and for an opening in unfrozen ground. In each of the two cases of liner placement studied (Cases 1 and 2) the points move during thawing along the support reaction curves shown, and end up with greatly increased liner support pressures.

The results for construction within unfrozen ground are also shown in Figure 8.5 for comparison. It can be seen that the support pressures are considerably lower than for construction within stiff frozen ground with subsequent thawing. There is a minimum value of support pressure for this liner, no matter how large the support delay, as long as it is installed before thawing and in contact with the wall. This minimum value happens to be similar to the value of support pressure for Case 1 in unfrozen ground. However freezing is used where the ground displacements for the same opening, but unsupported, are too large because yielding causes the unfrozen ground convergence curve to deviate to the right of the straight line shown. As ground freezing steepens (and linearises) the GCC it effectively enables the support to be installed earlier than with most other construction methods, i.e. at lower values of u/uo. Thus the large ground movements can be reduced, but larger liner loads have to accepted instead.

8.5 Radial Wall Displacements at the Face

The magnitude of the radial displacement of the tunnel or shaft wall at the face of the opening is a parameter required for the design of supports installed close to the face using convergence-confinement curves. This value is the minimum value of radial wall displacement at which a support can be installed, but because of the interaction between the support and the ground ahead, and the response of the ground to the excavation process, it is a difficult parameter to predict.

Figure 8.6 presents the ultimate radial displacements of the tunnel wall, and the radial displacements at the tunnel face, plotted against the ratio of the damaged to undamaged rock modulus. It can be seen from this figure that the location of support installation has little effect on the *face* displacement when the open ground immediately before the liner is placed reaches one radius or more in length. The normalised face displacement increases almost linearly with decreasing ratio of damaged to undamaged rock modulus (plotted for Case 6), but this relationship will depend on other factors such as the size of the damaged zone. This is in contrast to the ultimate radial displacement which varies non-linearly and is affected by the liner placement sequence. For open ground of less than one radius in length a similar non-linear variation might be expected in face displacements. These observations are of practical importance because they illustrate how sensitive

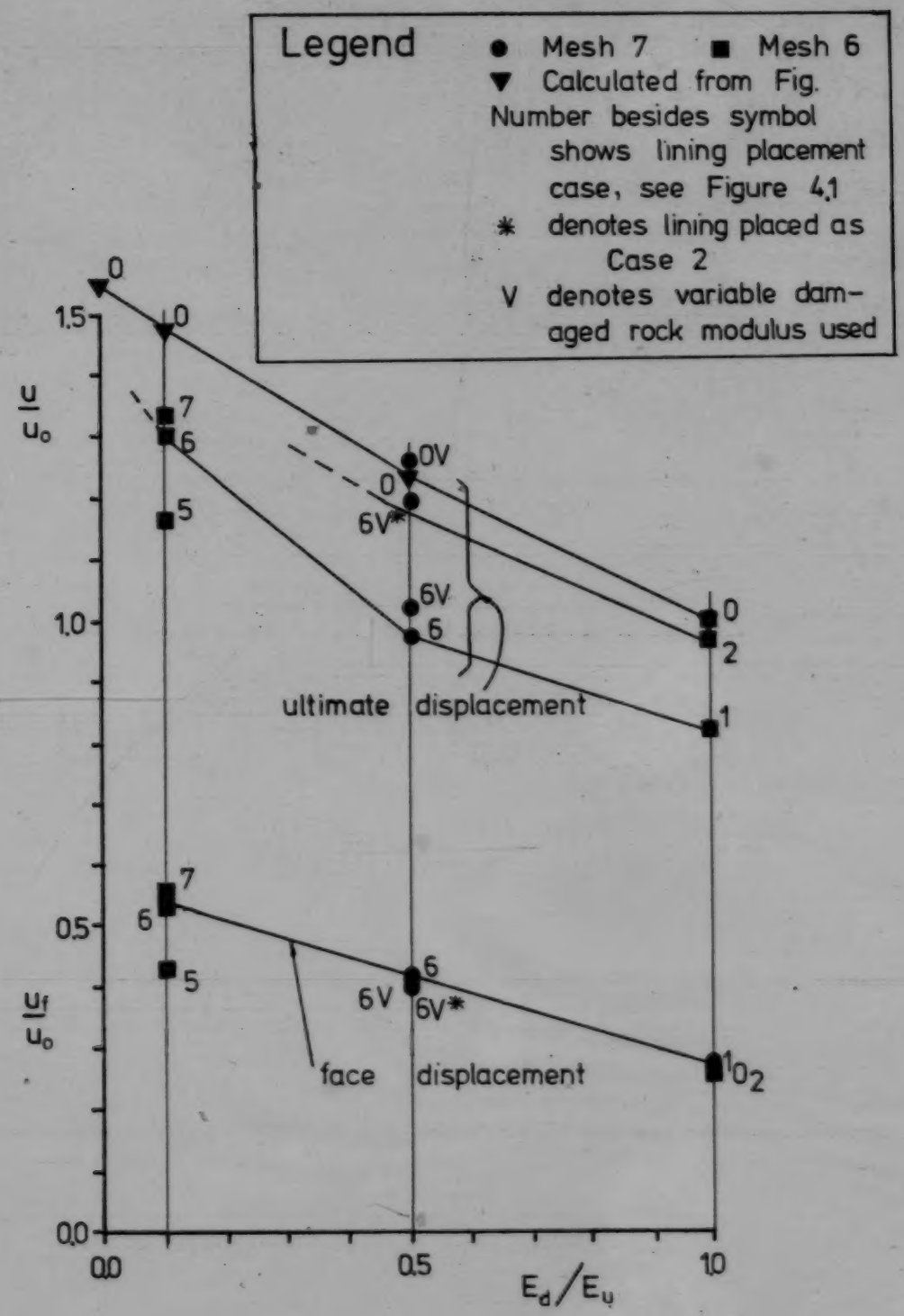

Figure 8.6 Variation of Displacement with Damage

extensometer or convergence measurements are to face damage and the location of the support installation, and that these factors must be considered during numerical modelling and evaluation of field measurements.

Figure 8.7 presents some results from the analyses of a tunnel with a varying extent of rock damage ahead of the face (Cases 5,6 and 7 shown in Figure 4.1) and shows that damage beyond one half of a tunnel radius ahead of the face does not influence the face displacements significantly in situations where the Eu/Ed ratio is 10. For the same extent of damage ahead of the face an increase in the ratio Eu/Ed would be expected to increase uf. However Figure 8.6 shows that there is a limit to this value (about 0.58 uo for the particular situation studied here).

Further study is required for a better assessment of the effects of the position, extent and degree of damage near the face on radial displacements at the face.

8.6 Variation of Stresses within a Liner

The periodic variations of stresses along a liner have already been discussed in Section 6.2 and are shown, for example, in Figures A5.22, A5.23 and A5.24. The non-dimensionalised liner thrusts and displacements have been replotted in Figure 8.8 along the length of the liner segment for construction Cases 1,2,5,6 and 7. It shows the significant longitudinal variation in liner thrust which is

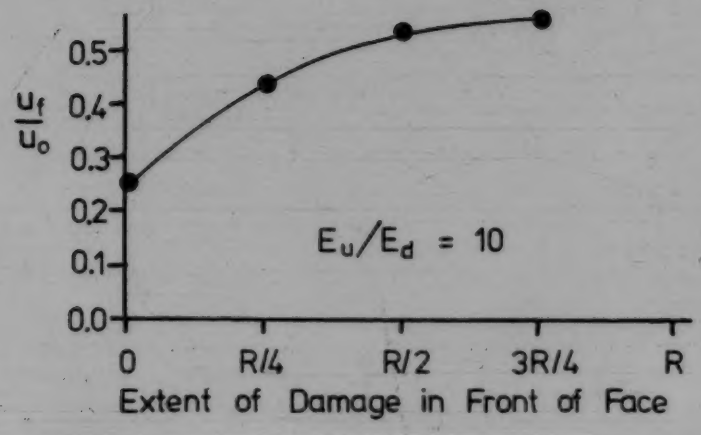

Figure 8.7 Face Convergence with Different Extents of Damage in Front of the Face

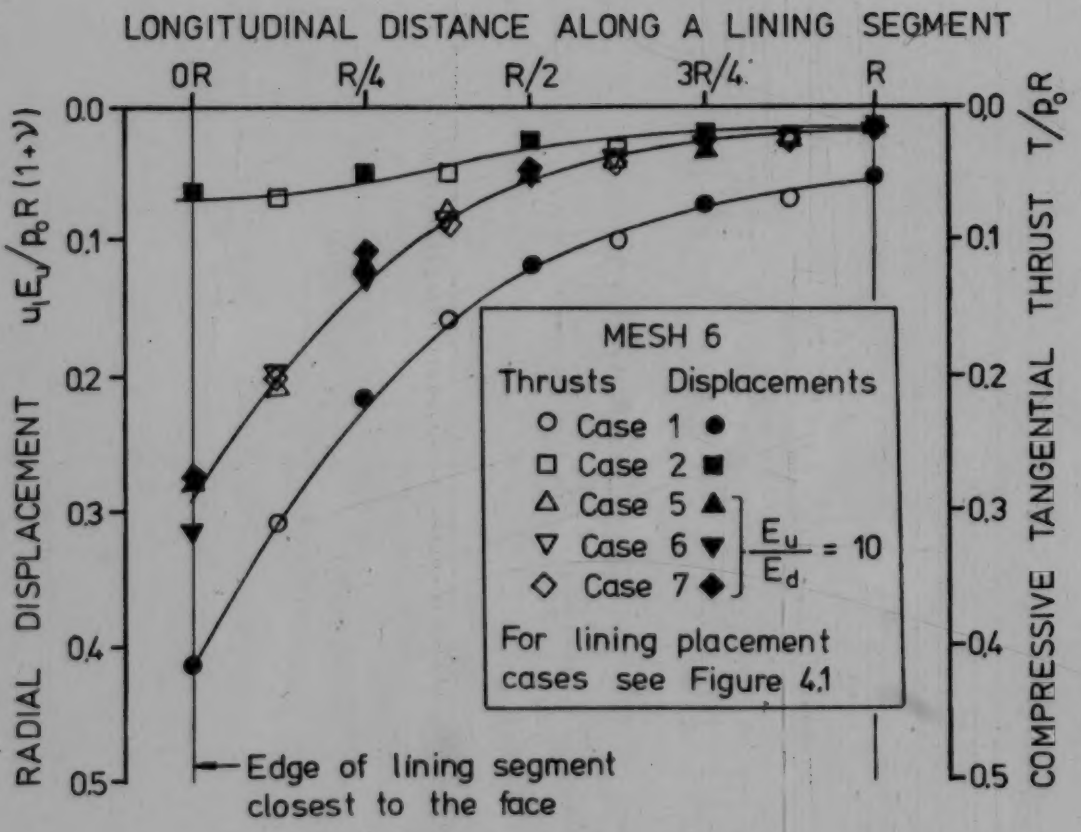

Figure 8.8 Longitudinal Variation of Radial Displacement and Tangential Thrust in the Liner

mainly influenced by the delay in liner placement, and the radial extent and degree of rock damage.

Damage in front of the face has previously been shown to have a similar effect as a delay in liner placement, for example compare Cases 1,2 and 3 shown in Figure 8.4 where Case 3, with face damage only, lies between Cases 1 and 2 (no damage) on the ground convergence curve. However in Figure 8.8 a variation in the extent of the damage ahead of the face (comparing Cases 5, 6 and 7) appears to have relatively little influence on the liner thrusts or displacements. Any effect is probably insignificant in comparison to the effects from excavating a round of length equal to one tunnel radius. The difference between the curves drawn for Cases 5, 6 and 7 and for Case 1 in Figure 8.8 can be explained instead by the influence of the ring of softened ground *around* the openings. The two curves are in fact very similar, but are transposed such that the softening of rock around the opening, before support is installed, is similar in this case to an additional delay in liner placement of about 0.1 R, and a reduction in the non-dimensional thrust by 0.04. A zone of rock damage right at the face may have some reducing effect on the thrust in the part of the liner closest to the face. This may occur because the stresses have been reduced in the zone of damaged rock and so less stress will be transfered to the leading edge of the liner in the next round of excavation than there would have been had the rock not been damaged.

Several interesting conclusions can be drawn from Figure 8.8. A liner placed right up to the face will have a large variation in tangential thrust along its length. This thrust will be "locked in" and hence leads to a stress variation repeated in each liner segment along the tunnel. Placing the liner one radius away dramatically reduces the liner thrust (comparing Cases 1 and 2), and the variation along the liner becomes less pronounced. If field measurements are made to determine the liner thrust the distance from the face to the point of installation is a very important factor. Softening the ground around the tunnel before support installation also reduces the liner thrusts by increasing the effective support delay. This makes the ground mass behave as if it were undamaged but had a lower stiffness than its original stiffness. Kaiser (1981) outlines the concept of analysing openings with surrounding damage by considering the ground to be undamaged, but with an equivalent (lower) stiffness.

The convergence-confinement diagram shown in Figure 8.4 contains only the average points for each excavation case considered. However as the stresses within the liner vary along the liner segment the support pressures will do so as well. In Figure 8.9 the points for individual liner elements are plotted in a convergence-confinement diagram, the support pressures being calculated by the two dimensional equations given in Appendix 3. It can be seen in the figure that individual points in the liner do not lie on the same

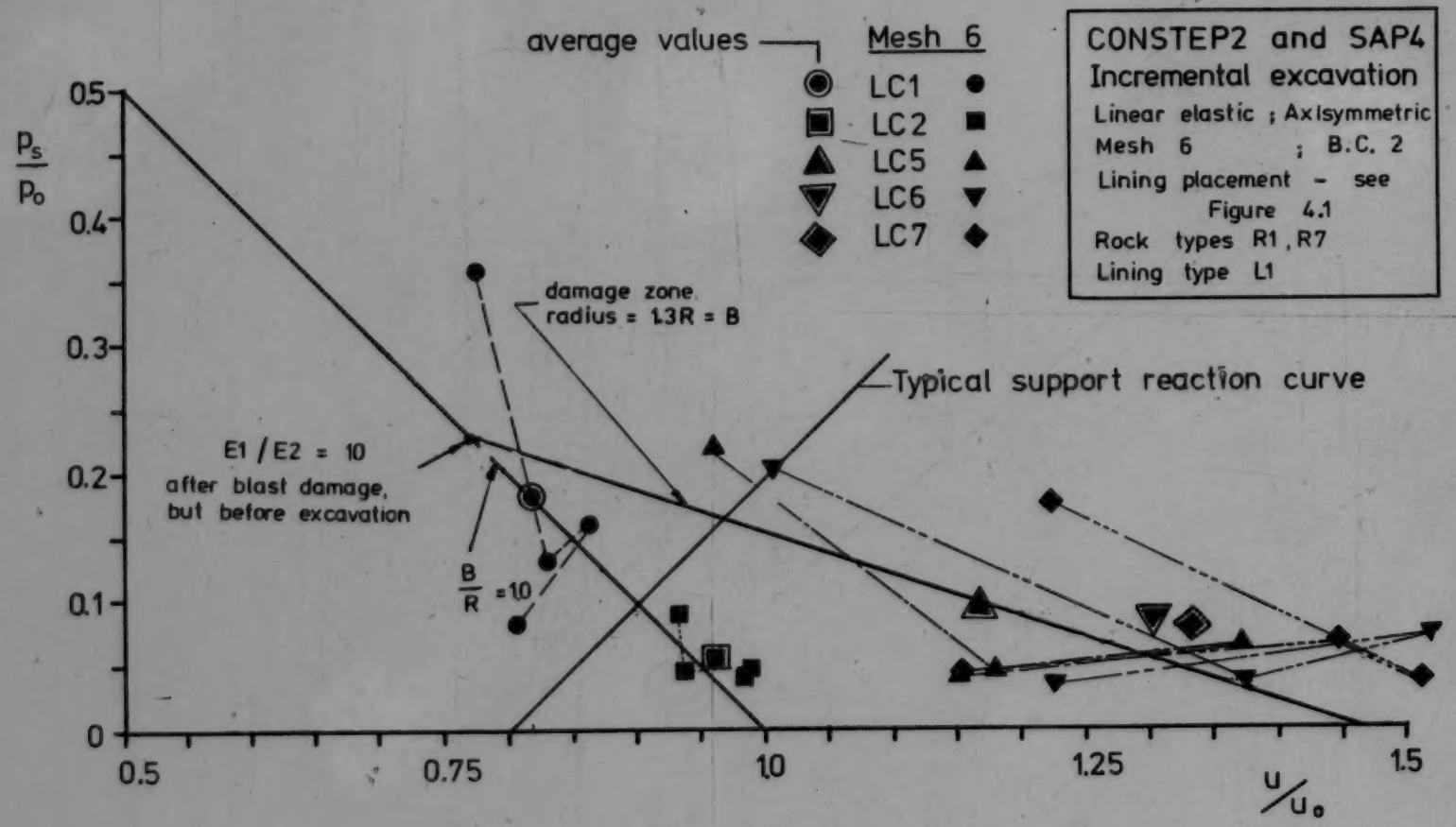

Figure 8.9 Ground Convergence Curves - Tunnels, Mesh 6

ground convergence curve, and are scattered around the curve on which the average points lie. Therefore individual parts of a liner segment cannot be accurately represented by a GCC calculated by two dimensional analysis, but that if the the average point plotted for a segment of liner (placed at one round of excavation) is used to represent the whole tunnel then the GCC is a reasonable model of the tunnel behaviour. The variation of support pressures shown in the figure indicates that within the same liner segment there will be a large range of factors of safety against liner failure. In Case 1 the factor of safety at the leading edge will be at least four times that at the trailing edge. This variation should be verified in the field by appropriate monitoring.

8.7 Changes in Ground Stresses

The rates of change in tangential and radial ground stresses at a point near the tunnel wall as the tunnel passes are not the same; the radial stress changes more rapidly as the face passes whereas the tangential stress change is more gradual over a distance from two radii ahead of the face to about two radii behind the face. This is shown in Figure 8.10 where the stresses at a point R/20 from the tunnel wall are plotted as the tunnel passes (for both lined and unlined cases with no rock damage). The ordinates of the tangential stress change data points are plotted for an increase in stress from the original insitu stress, and

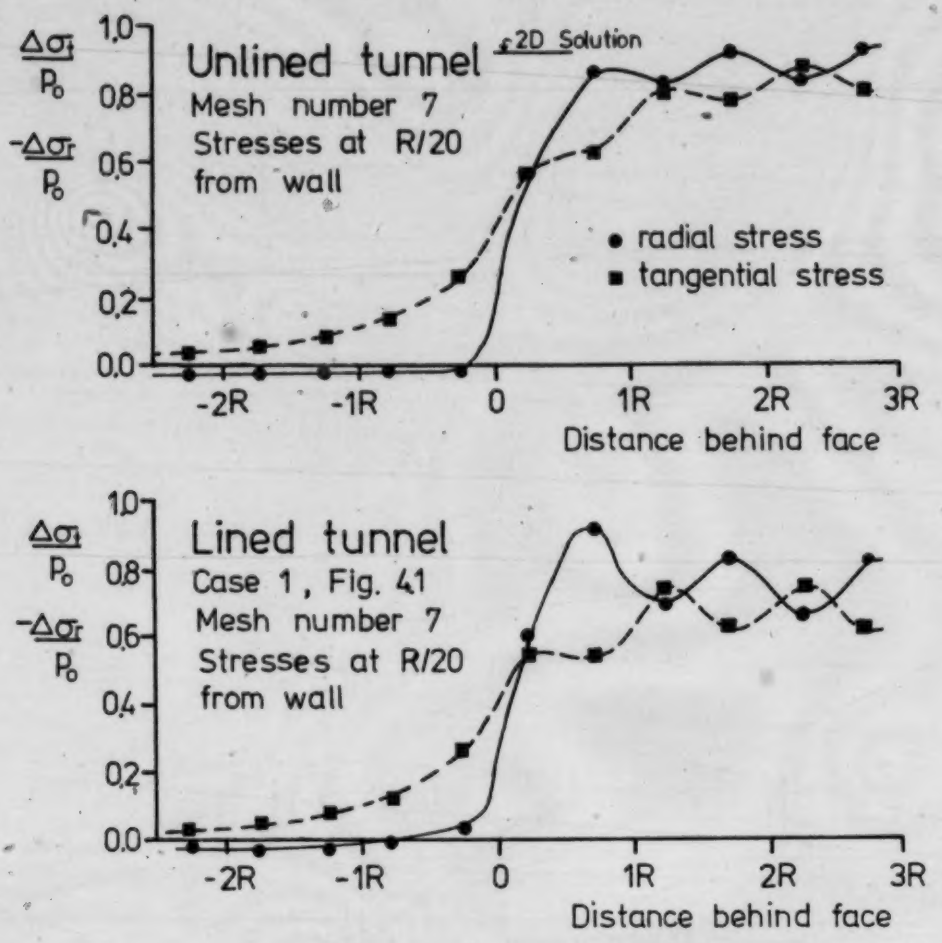

Figure 8.10 Longitudinal Variation of Radial and Tangential Stresses Close to the Tunnel Wall, Lined and Unlined Cases, No Rock Damage

the ordinates of radial stress change are for a decrease in stress. After the tunnel passes the measuring location the data points no longer lie on smooth curve, and show a periodic fluctuation, the reasons for which have been discussed earlier. This fluctuation is partly a function of the inaccuracy in the analytical method (particularly for the unlined case) and partly a function of the supporting (or "shielding") effect of the liner on the unsupported rock between the leading edge of the liner and the tunnel face.

The plots in Figure 8.10 show that the radial stress only begins to decrease just before the tunnel face passes, whereas the tangential stress builds up ahead of the face and varies with distance from it in a manner similar to the radial displacement distributions, shown for example in Figure 2.22c. In the unlined case the radial stress continues to decrease and the tangential stress continues to increase behind the face, tending toward the ultimate stresses of 0.8 po and 1.84 po repectively. (These stresses are from a two dimensional plane strain analysis for points at R/20 from the tunnel wall.) The stress values plotted in the figure have not been corrected and so trend towards slightly lower ultimate values. In the lined (undamaged) case the tangential stress also gradually increases behind the face, but the radial stress, instead of decreasing, begins to increase as the liner takes up load and applies a radial supporting pressure to the ground. For the lined case shown the ultimate stress changes are about 20% lower than

in the unlined case.

Similar diagrams for liner placement Case 6 are shown in Figure 8.11. The stress changes are however more complicated in the zone of damaged ground, as shown in the upper diagram where the stresses are plotted for points R/20 from the tunnel wall. In the lower diagram the points are in undamaged ground, at a distance of R/2.4 from the wall (the thickness of the zone of damage around the opening being R/3.3). The stresses in the damaged ground show a periodic fluctuation for the same reasons mentioned earlier, as well as because the damage ahead of the face was half the length of a round of excavation, which reduces the modulus and the stresses in that part of the ground, and hence reduces its capacity to take up further stresses in comparison with the ground undamaged before excavation.

Ahead of the zone of damage the tangential stresses increase in a similar manner to the increase observed in the undamaged case. Behind the face the tangential stresses continue to increase as they did in the undamaged case, but within the damaged zone they are reduced below the initial insitu field stress. However the radial stresses show a significant increase ahead of the zone of damage which was not observed ahead of the face in the unlined case or in Case 1. The radial stresses reduce very rapidly within the zone of damaged ground ahead of the face whereas if there had been no damage there would have been very little change in this region. Behind the face the radial stresses decrease

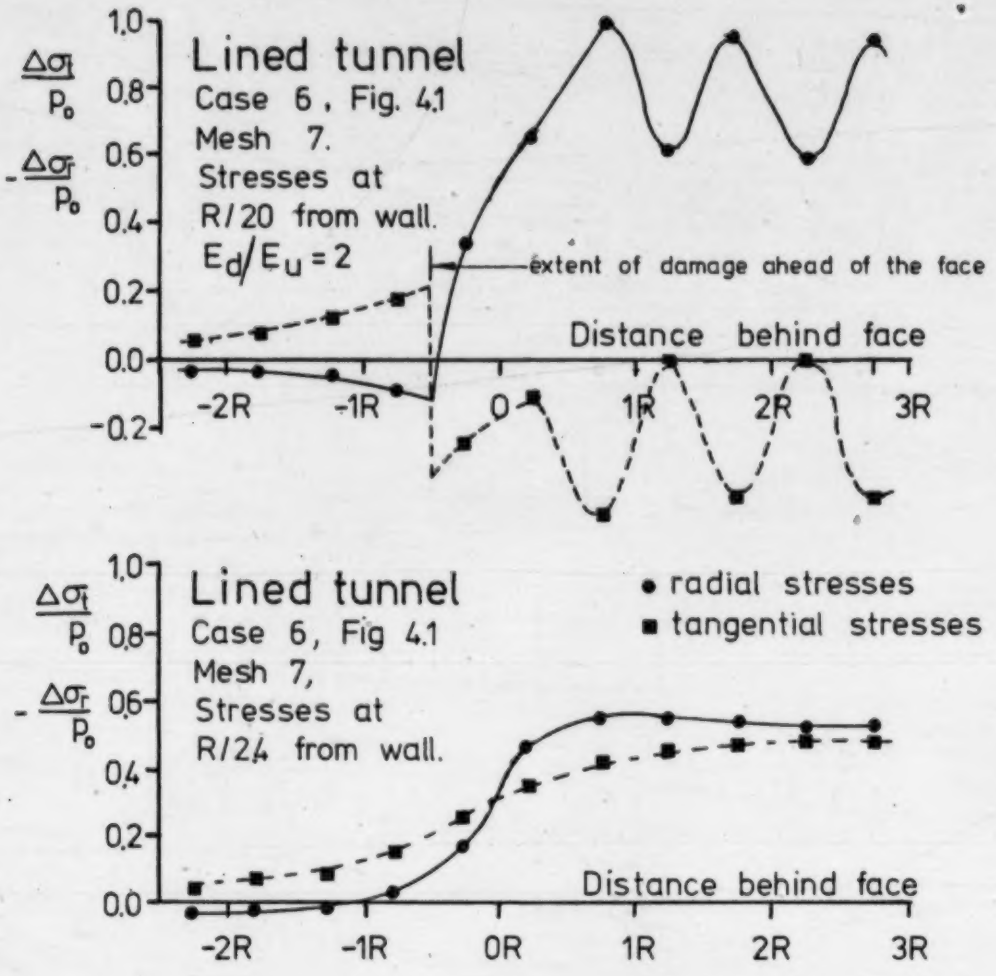

Figure 8.11 Longitudinal Variation of Radial and Tangential Stresses Close to the Tunnel Wall, Lined Case 6, with Rock Damage

in a manner similar to Case 1, having a slight increase after the liner is installed, due to the supporting effect.

Further details of the variation of stresses in the ground are shown in Figures A5.44, A5.45 and A5.46, from which Figures 8.10 and 8.11 were plotted. They show the variation of ground stresses in several planes perpendicular to the tunnel axis and at various distances in front of and behind the face.

These observations have recently been confirmed by insitu stress change measurements during the advance of a shaft, in Lethbridge, Alberta, Kaiser et al. (1982). Details of the case history taken from the paper are presented in Section 7.10. A plot of the stress changes measured at various points around the shaft at the 152 m level against distance behind the shaft base has been taken from MacKay (1982) and is shown in Figure 8.12. The stress changes have been normalised by dividing them by the estimated value of the maximum horizontal stress at the 152 m level. A better way of normalising the results might have been to divide them by the value of the original insitu stress in the direction of the measurement, but this was not done because of the difficulty in assessing accurately the original stress field.

On the same diagram results for the unlined case and lined Cases 1 and 6 from this study have been plotted. In addition the results for the unlined case have been advanced by one radius to simulate a highly damaged zone of one

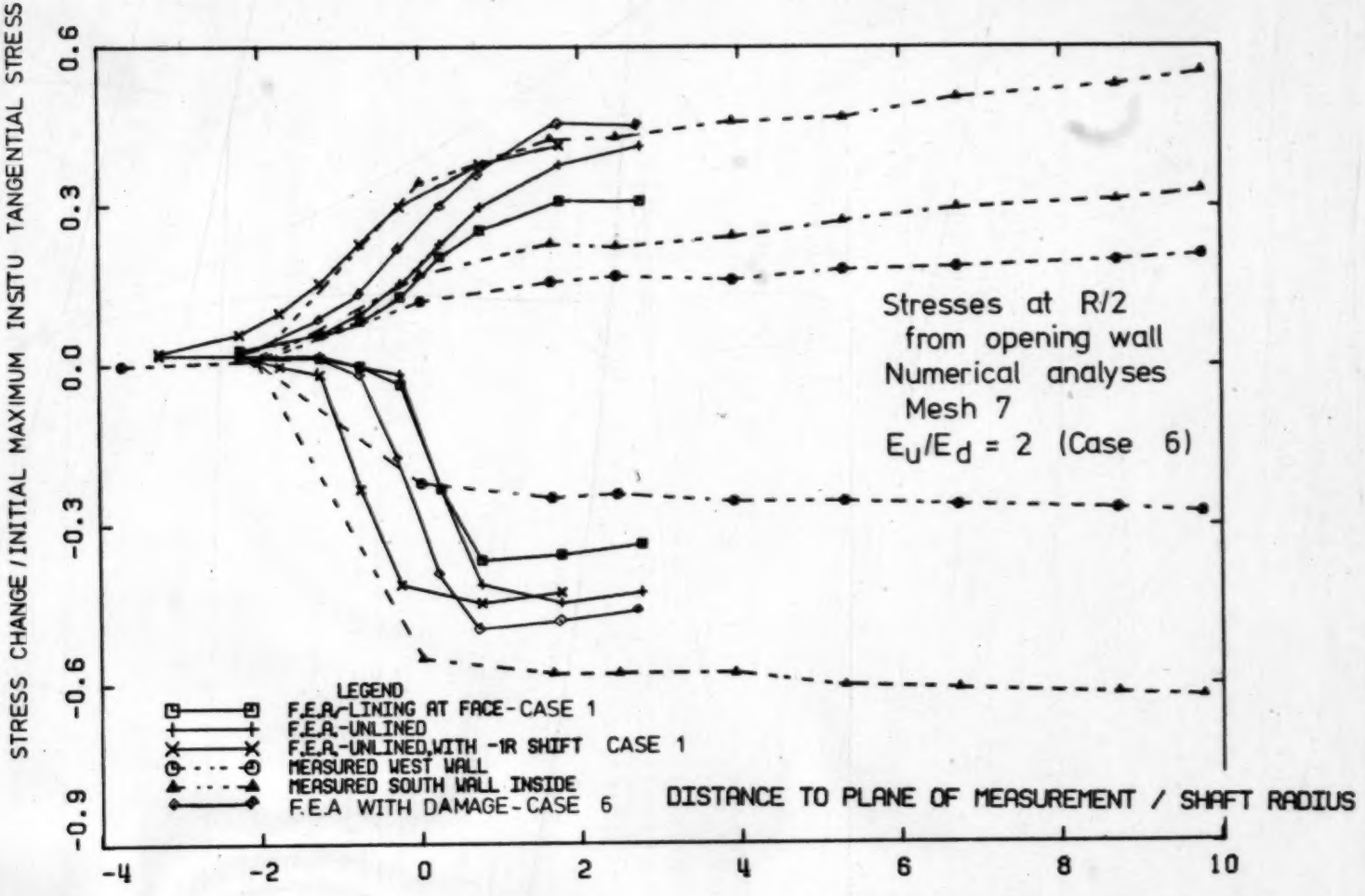

Figure 8.12 Comparison of Results of Radial and Tangential Stress Changes with the Lethbridge Shaft, MacKay (1982)

radius depth at the shaft base. This seems to be a reasonable assumption because of the high blast energies that were used in the excavation procedure, and on account of the muck that was left in the shaft, giving an inaccurate measurement of the base elevation. There is a good agreement between the curves of field observations and the Case 1 curve advanced by 1 R, particularly in their shapes and positions. The ultimate values (at a distance of 3R behind the face say) of the normalised stress changes do not agree so well, but this is due to the difficulty in measuring consistent stress changes and the anisotropic stress field.

These observations have important practical implications for the design of supports, for the evaluation of field observations, and for the use of rock bolts. For example rock bolts should be installed where the tangential stress increases and (ideally, but difficult practically) before the radial stress decreases. At this point the ground has not fully deformed and confinement by rock bolts will be most effective. This might only be achieved in practice by installing rock bolts at the face, angled so they protrude ahead of the face, called spiling or forepoling. Bolts installed close to the face, within about 2 to 4 radii, can rely on ground stress build up to provide a good bond between the rock and the bolt. Bolts installed further away cannot rely on elastic ground movements to provide a good bond to the rock. In such cases bolts that have other means of transferring their loads to the rock will have to be

used.

These stress variations are also very important factors where the ground stress change during tunnel advance is measured. It can be seen in Figure 8.10 that if measurements are not begun at least two radii ahead of the face a part of the tangential stress change may be missed, while the full radial stress change is measured. This is important if the field stress is to be assessed from radial and tangential stress changes. Also, if ground properties are to be determined from radial displacement measurements, which are usually only begun after the face has passed (e.g. in the Lethbridge shaft, Section 7.10) the fact that the tangential and radial stress changes will not be the same will affect the calculations.

8.8 Liner Placement Delay Factor

In Section 8.6 the variation of the liner stresses in a longitudinal direction were discussed, and were shown to vary considerably along a liner placed close to the face. This variation has important implications for the interpretation of stress measurements within a liner because it shows that varying the position of the instrumentation within the same segment can greatly affect the readings. Stress measurements may be made in a liner to determine its factor of safety against either complete failure, or against cracking and the loss of water tightness (important for

sewer tunnels for example). Stress measurements may also be taken in the liner to determine the support it applies to the surrounding ground, and this is one of the measurements required to determine the ground convergence curve. In order to obtain these factors measurements of radial or tangential stresses may be made and the thrusts and support pressures calculated from the elastic thick walled hollow cylinder equations. Measurements of tangential thrusts are usually preferable because of the large variation in radial stress across the thickness of the liner (from zero on the inside to the support pressure ps on the outside of the liner), and if radial stresses are measured at the wall they may be affected by any uneven contact between the liner and the ground. Therefore only the longitudinal variation of tangential thrusts is discussed below.

The variation of thrusts in the liner was shown in Figure 8.8, and a diagram showing a similar variations is given in Figure 8.13 in which the thrusts have been non-dimensionalised and then normalised by dividing them by the non-dimensionalised values of thrust given by the relative stiffness solution (see Section 7.2). The points shown are for the ultimate thrust in each individual liner element in the numerical analyses (except for Mesh 7 where pairs of liner elements at the same distance from the face were taken), or for each measurement of thrust taken in the case histories shown. They are plotted against the distance between the location of the measurement and the face just

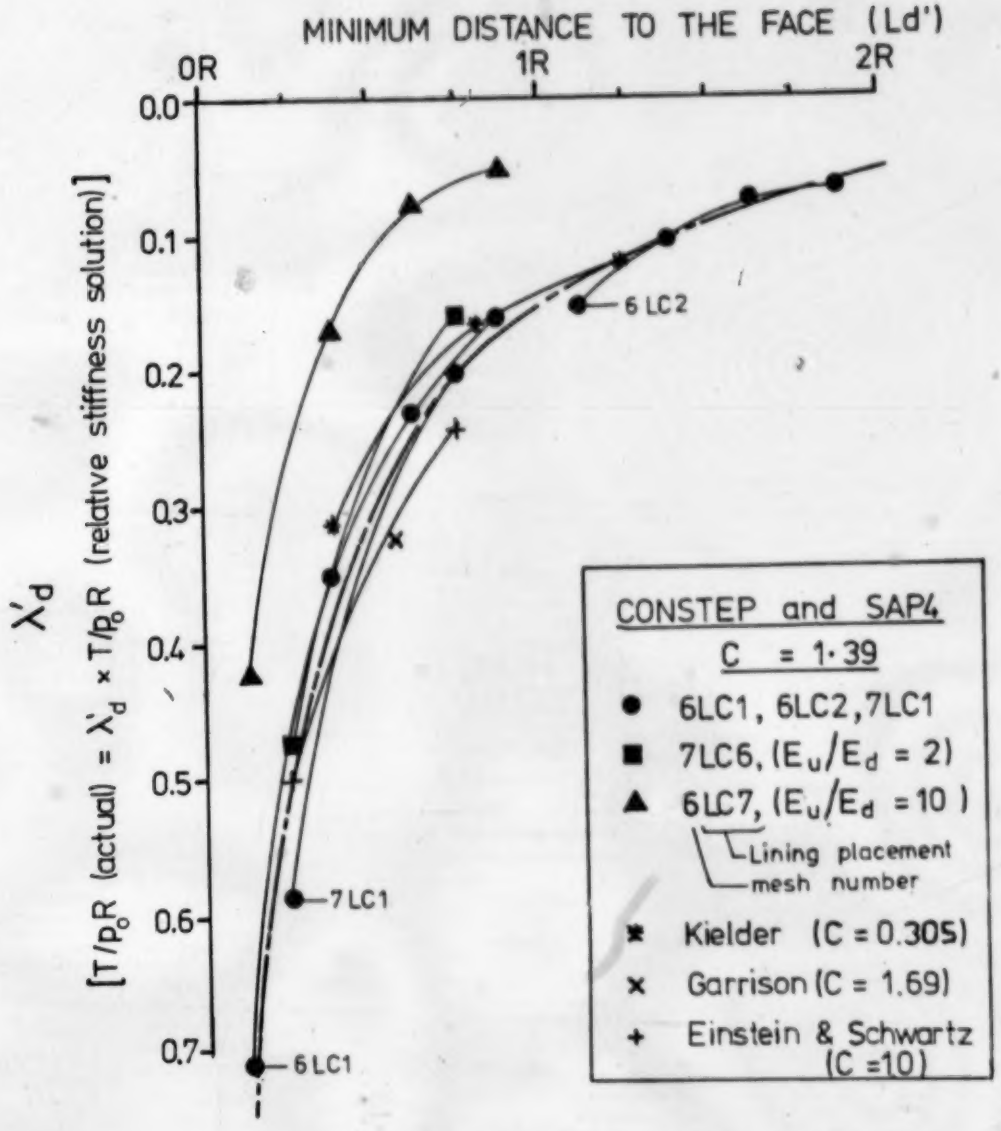

- For definition of C and T. see Section 7.1
- For liner placement cases see Figure 4.1

Figure 8.13 Support Delay Factor

before excavation is carried out.

In Figure 8.13 it can be seen that there is good agreement between the results of the two different numerical analyses and the two case histories. The distribution of liner thrusts in Cases 1 and 2 is almost continuous with distance from the face, although the thrust at the leading edge of the liner segment in Case 2 is only just less than the thrust at the trailing edge of the liner segment in Case 1. It is therefore possible from this graph to approximately determine the thrust at a point within a liner placed in undamaged ground given its compressibility ratio, initial insitu stress (assumed hydrostatic) and the tunnel radius in order to calculate T/po.R from the relative stiffness solution, and given the distance of the point from the tunnel face before excavation. If the point is close to the leading edge of the liner segment it will be at the higher end of the range of the points plotted, and if it is at the trailing edge it will be at the lower end of the range.

The graph in Figure 8.13 is similar in concept to that shown in Figure 8.1 taken from Einstein and Schwartz (1980). However Figure 8.13 uses a more flexible parameter to represent the support delay (Ld'), extends the range of the support delay, and can be used to give the variation of thrusts within the liner. (Note that one of Einstein and Schwartz's values has not been plotted because the liner was most likely installed ahead of the face.) Although only case histories with a value of C close to 1.0 have been plotted

on Figure 8.13, all Einstein and Schwartz's (1980) results for cases with very different values of C lie close together on the diagram in Figure 8.1. These would be also expected to lie close together in Figure 8.13, and so the curve may be valid for a large range of compressibility ratios.

Two curves on Figure 8.13 are for cases with ground damage. If damage is only slight (Eu/Ed = 2), and the radial and longitudinal extent of the damage is not too great, the average curve (or just below it) may be used. For greater damage, e.g. Case 7 (Eu/Ed = 10), the curve lies below the average curve. A further study is necessary to determine other curves for various values of degree and extent of rock damage. It should be noted that the damage occurs before the liner is placed. Any damage, softening, weakening or ground creep that occurs after the liner is placed will cause the thrusts to rise above the line shown.

8.9 Shaft Analyses

The analyses carried out on shaft construction were not as detailed and as accurate as those for tunnels, and so only preliminary interpretations and conclusions are presented here.

The results of the analyses carried out on shallow and deep shafts for values of Ko equal to 0.5, 1.0 and 2.0 have been corrected in the manner described in Appendix 3 and are plotted on a convergence-confinement diagram, Figure 8.14.

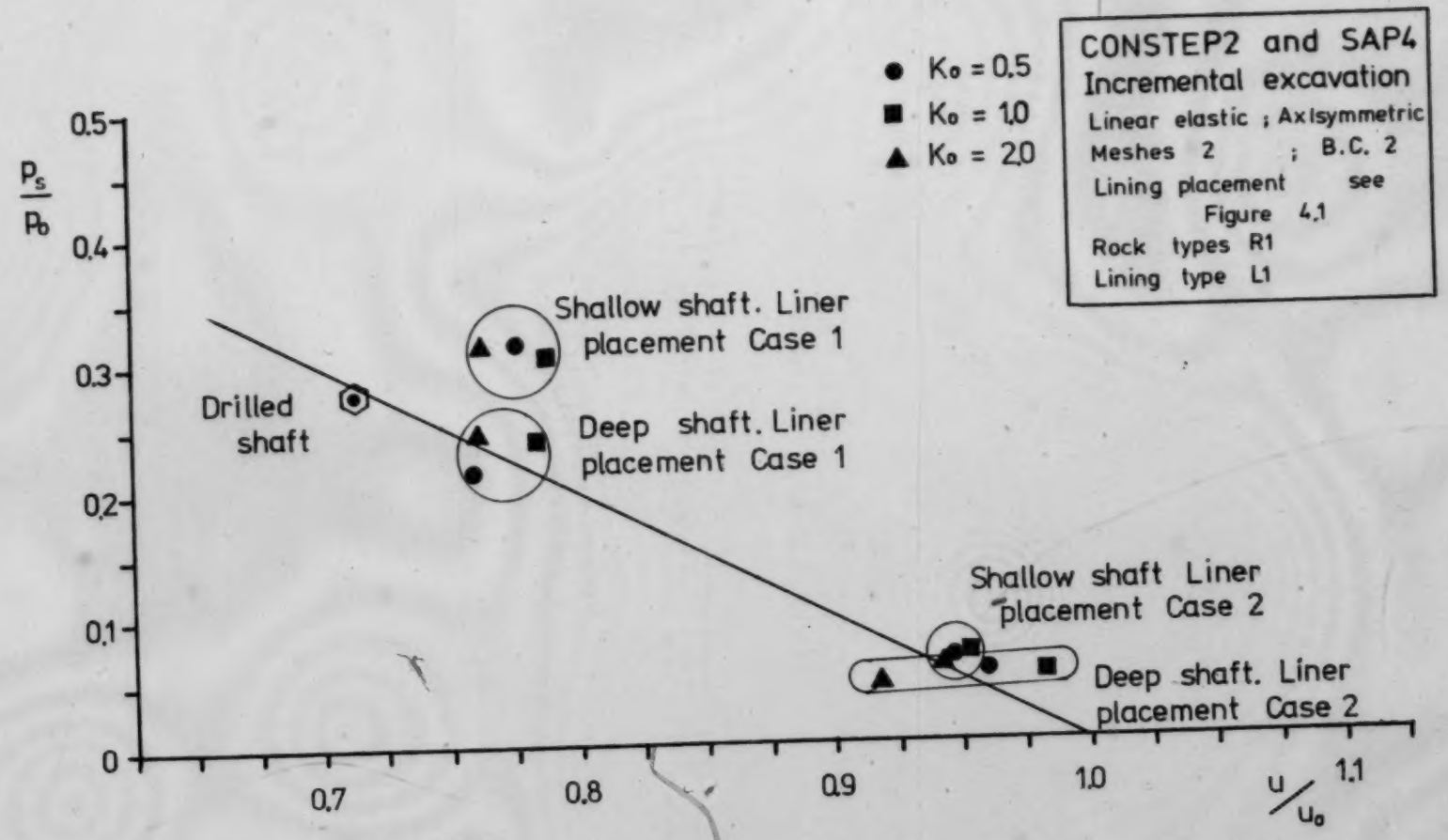

Figure 8.14 Ground Convergence Curve - Shafts

The depths of the shallow shafts are 7 R, and the level for which the points have been plotted is 3.5 R above the base of the shaft. Also plotted on the figure is the ground convergence curve calculated from the two dimensional plane strain closed form analysis presented in Appendix 1 and Figure 5.1b. The values of po and uo used to normalise the support pressures and wall convergence are the uniform horizontal stresses with the different values of Ko and the corresponding value of the ultimate convergence calculated from two dimensional plane strain analysis respectively.

The points plotted generally lie close to the calculated ground convergence curve, with the exception of those for the shallow shaft, Case 1, which lie above the line because of the influence of the unrestrained ground surface boundary. At the ground surface the ground is not restrained by any material above and so the radial displacements are not zero (which they would be in the symmetric case with material above having a continuation of the insitu stress field). These extra radial displacements can be seen in Figures A6.1 to A6.8. (It is of interest to note that where Ko = 0.5 there is outward radial movement at the ground surface in the first step or so of excavation because of the extra heave at the base of the shaft caused by the relatively larger vertical insitu stresses). In Case 2 these "extra" displacements have virtually ceased by the time the first liner segment is placed, but with Case 1 the first liner segment has to restrain a portion of them.

The liner radial and tangential stress distributions are shown in Figures A6.11 and A6.12, and it can be seen that extrapolations of the ultimate stresses show non-zero values at the ground surface for Case 1, but not for Case 2. The first segment of liner placed in Case 1 carries part of the extra load caused by the lack of restraint above ground level. The stresses in the next segment placed are relatively lower, more so for Ko = 0.5 and almost not at all for Ko = 2.0, because it only carries a very small part of this extra load. It would appear that at depth the distributions of liner stresses do not rejoin a line which passes through the origin. The reason is that the linearly increasing ground stress distribution will cause the effect of the ground surface to be felt at greater depths, but this is attenuated by the increasing depth of the excavation. As the shaft is sunk deeper these additional liner stresses will become a smaller portion of the total stress and become insignificant. The points on the convergence-confinement diagram will then fall on to the GCC shown in Figure 8.14. Another point shown on Figure 8.14 is that for any particular case the values of convergence are greatest for the case with Ko = 1.0 and least for the case with Ko = 2.0, and is most evident for the deep shaft Case 2. It is considered that this is an effect of the analysis and the method used to correct the results rather than any effect from a variation in Ko. The differences observed are generally quite small, particularly with respect to the

correction factors that were required, Mesh 2 (used here) giving the least accurate results of all the meshes used. For larger values of liner delay the values would be expected to converge to one point on the (normalised) GCC - that for the unsupported two dimensional case. This appears to occur with the shallow shaft Case 2 results, but is not so for the deep shaft Case 2 results. Further work with a finer mesh and shorter support delays is required to explore any effects on the liner and shaft behaviour due to a variation in Ko.

The result from the analysis of a drilled fluid supported shaft is also plotted on Figure 8.14. This lies on the GCC, and is at a higher level of support pressure than for a deep shaft, Case 1, excavated and supported in steps. An equivalent value of support delay, Ld', can be estimated from Figure 8.13 given the non-dimensional liner thrust (which will be constant except near the base of the shaft, Figure A6.17). This is found to be R/4. Comparing the non-dimensionalised thrust with the other cases on Figure 8.13 shows that it is at the upper end of the range, but is not the largest. The leading edge of the liner placed by Case 1 right up to the face is relatively more stressed. The drilled, fluid supported, method of shaft construction will therefore enable weaker liners to be installed in ground where by other methods the liner would have to be placed close to the base. Although the liner thrust will on average be larger in the drilled shaft case, it will be more

uniform, and the liner will not have to be designed for the peaks of high thrusts at the leading edges of the segments installed by other methods.

Figures 8.15 and 8.16 show the longitudinal variation of radial and tangential stresses at R/3.3 from the wall of shallow lined and unlined shafts. The stress changes shown are very similar to those presented in Figure 8.10, and the discussion in Section 8.7 on that figure in general applies here and is not repeated. These figures are slightly different in that the stress changes have been normalised by dividing them by the value of the initial insitu horizontal stress which varies with the depth of the measurement. There is also no "fluctuation" as the length of the elements in Mesh 2 were the same as the length of a round of excavation.

There is a slight variation in the radial and tangential stress distributions with different values of Ko, but generally the results lie in fairly tight bands. The relative stress change always appears to be greatest for Ko = 0.5 ahead of the base, but the order behind the face is reversed, with the relative stress change greatest for Ko = 2.0. The exception is in the tangential stresses for the lined case, where the liner installation appears to have "locked in" the order of stress change magnitudes that existed ahead of the base of the shaft.

Behind the base the radial stress increases again in both the lined and unlined cases. In the lined case this can be explained by the build up of support from the liner, but

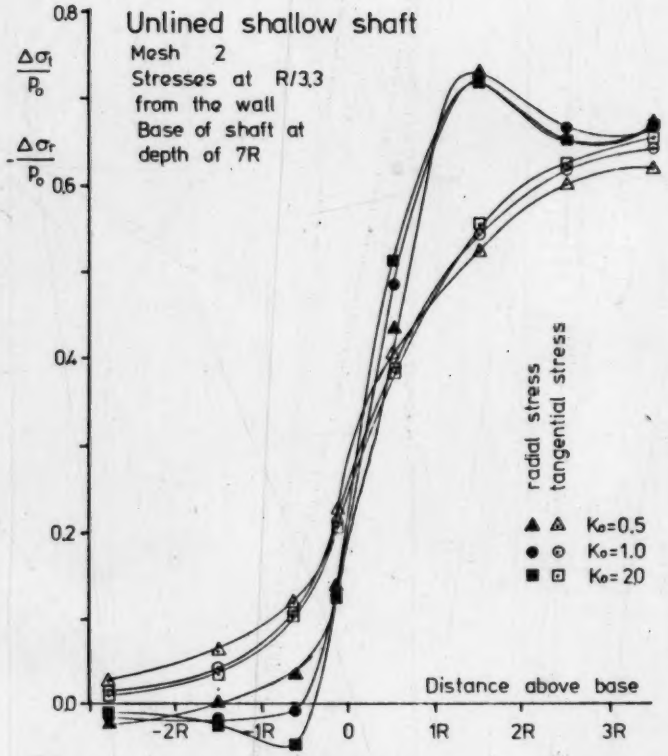

Figure 8.15 Longitudinal Variation of Radial and Tangential Stresses Close to the Wall, Unlined Shallow Shaft

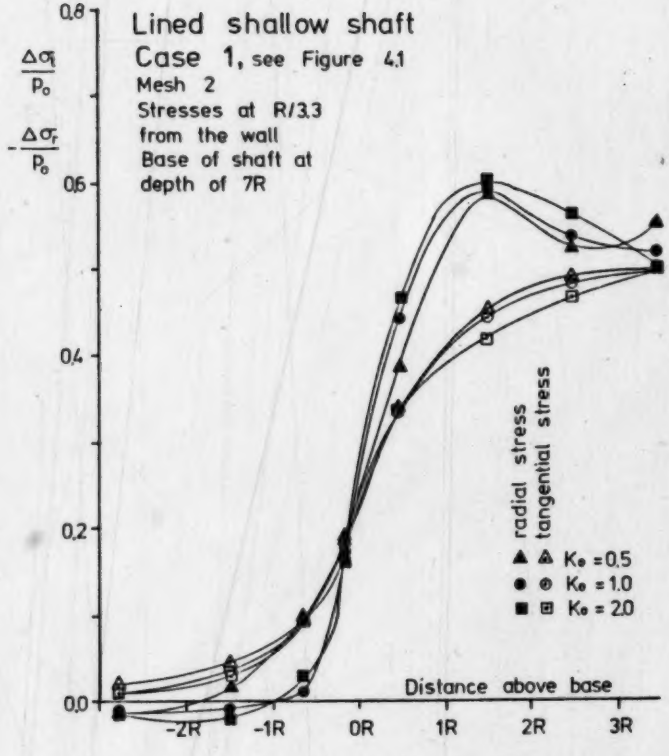

Figure 8.16 Longitudinal Variation of Radial and Tangential Stresses Close to the Wall, Lined Shallow Shaft

in the unlined case the reason is not so clear. The most likely explanation is that it is an effect from the ground surface. When a hollow cylinder has a linearly increasing stress applied along its outer or inner faces its deformations are not uniform, but assume a wavy distribution. This can also be seen in the distributions of radial stress in a liner shown, for example, in Figure A5.18. Because of the linearly increasing initial insitu stress distribution the same effect probably occurs here and the radial stress changes plotted against distance from the face will also vary in a wavy manner.

CHAPTER 9

CONCLUSIONS

9.1 Introduction

A finite element analysis has been developed to study the effects of construction on tunnel and shaft behaviour by modelling the excavation and support procedures incrementally. Ground behaviour was assumed to be linear elastic and the ground strength to be infinite. The effects of rock damage during construction, and of ground freezing and thawing, were simulated by a change in ground stiffness. Although this technique was straightforward, various practical implications follow from the results, and these are summarised in Section 9.3. Several important aspects for the numerical modelling of construction processes were also revealed by the study, and these are presented in the following section.

9.2 Numerical Technique

9.2.1 Introduction

The technique used here shows that the results from a numerical analysis have to be carefully assessed before conclusions can be made, and that the procedures used in the technique have a critical effect on the information obtained. The major factors that need to be considered are

discussed below.

9.2.2 Simulation of Excavation

The method adopted for simulating ground excavation is an important aspect of any analysis. In this study the "excavation unloading" technique was used whereby the ground is initially stressed before construction begins, and displacements and stress changes from the initial condition are calculated. Excavation is carried out by reducing the modulus of the excavated elements to a small value and applying nodal forces to reduce the stress across the boundaries of excavated elements to zero. The procedure used to calculate these nodal forces has a large influence on the displacements and stress changes obtained. The assumption of linear stress distributions between points within the mesh was shown to be inaccurate in areas of high stress gradients. This is most important across the wall of an opening where the stress gradient is extremely large. Some methods (e.g. Kulhawy, 1977) interpolate nodal stresses from the centres of surrounding elements. An improvement in this method was made by screening the elements so that any which had already been excavated were not used in the interpolation.

9.2.3 Size of Elements

The size of the elements in relation to the size of the opening within the mesh, and to the size of a round of excavation, is very important. (In fact it is the node spacing rather than the element size which should be considered, but in this study meshes were used which only had nodes at the element corners, and so the element sizes are equivalent to the node spacings.) Within the ground mass the assumption of linear stress distributions causes the actual stress distribution to be overpredicted where stresses are rapidly increasing, and to be underpredicted where they are rapidly decreasing. The smaller the elements are in relation to the stress gradients (and hence in relation to the size of the opening) the better the prediction. Near the wall and the face the stress gradients will be very large and so it is important that the elements are small in these regions. However it was shown that a small element close to the face, but surrounded by large elements, would lead to an overprediction of the stresses within the ground mass close to the face. Consequently the mesh should contain small elements in areas of large stress gradients, which become gradually larger in areas where the stress gradients are low. Although not possible in the present version of CONSTEP2, the use of elements with additional nodes other than those at the corners, and interpolation functions of a higher order than the one used here, would enable less elements to be used to achieve the

same accuracy.

9.2.4 Mesh Geometry in the Region of the Excavation

The design of the geometry of the mesh (i.e. pattern of elements in the mesh) in the region around the excavation, and in particular within the area that will eventually be excavated, is also important for another reason. If the geometry of the elements within the part of the mesh being excavated in one step is different from the geometry in another step then different radial displacements are calculated. This is a result of the inaccuracies in the stress interpolation which depend on the particular distribution and combination of element sizes that is used. It is therefore essential that within the region affected by the excavation the geometry of the elements in the mesh is exactly the same for each round of excavation.

It was shown that if the length of one round of excavation is equal to the length of an element in the direction of the tunnel axis, then a smooth displacement distribution curve would be obtained. This smooth curve would not necessarily indicate that the analysis was accurate, and because of the large size of the elements in relation to the size of the opening the analysis might in fact be quite inaccurate. However if more than one element (along the direction of face advance) is excavated at each step, an inaccurate analysis produces results that show a "kink" in the radial distribution curve, and this gives an

indication of the magnitude of the inaccuracy. (A kink can be obtained as a result of the construction procedure as well, and so an analysis of an unlined excavation in a homogeneous material should be carried out to give some idea of the performance of the numerical analysis, as in this situation there should be no kink.) This has important implications for assessing published results of finite element analyses, as most of these appear to excavate the ground in lengths of one element, and so will produce a smooth curve no matter how inaccurate they are.

9.2.5 Application of Nodal Excavation Forces

Inaccurate calculation of nodal excavation forces also causes another problem. This study shows that the places where nodal forces are applied have to be carefully considered. In the finite element meshes used here the elements remain connected throughout the analysis. This means that unless the mesh is either carefully designed, has special elements, or material strengths are specified, tensile stresses can develop across regions which usually have no tensile strength, e.g. between the leading edge of the liner and the face. Inaccurate nodal forces can exacerbate this situation, and initially in this study such forces were applied to the liner so that unreasonably large longitudinal liner tensile forces and longitudinal ground displacements were developed. This problem can be partly overcome by applying the forces to only those nodes which

are directly affected by the removal of ground and not to those where the stress in a direction normal to the boundary of excavated ground should be zero.

9.2.6 Additional Effects

There are various other minor effects which are more obvious, but of which a user of the results from an incremental finite element analysis should be aware. These include the effects of the mesh boundary condition, the depth to which excavation into the mesh occurs, and the effect from the first few excavation steps which may have an excavation sequence different from the remaining steps.

Choice of the boundary conditions should take into account the asymmetry of the analyses across planes perpendicular to the tunnel axis. This has been achieved in this study by using a mixture of rollered and free boundaries, and by excavation sufficiently far into the mesh for the boundary effects to be small. Use of more complex boundary conditions, such as spring restrained boundaries, may help to reduce the length of excavation within the mesh and consequently the size of the mesh. For smaller lengths of excavation each construction step may be identical, but where larger excavation lengths are required the first few construction steps may be longer than the final ones that are to be studied. In such cases a difference in the performance of the two sections will be observed.

9.3 Practical Aspects

9.3.1 Support Delay and Liner Stresses

This investigation has confirmed that in a material with linear elastic time independent properties the delay in placing a support has a dominant effect on support thrusts and ground movements. If support is placed close to the face of undamaged rock before the next round of excavation the thrust at the leading edge of the support, after excavation, will be relatively large, and will diminish with distance from the face. This variation in tangential thrust becomes less pronounced if the support is placed further away from the face. In addition there is a variation in stresses across the thickness of a liner, which also generally becomes less pronounced with distance from the face.

A method has been presented in Section 8.2 whereby the longitudinal distribution of thrust within a liner can be estimated from a knowledge of the initial insitu stress, the ground and liner moduli, the liner geometry, and a parameter which indicates the support delay. This parameter, Ld', is the distance from the point to the face immediately before the next round of excavation, and Figure 8.13 shows how the thrust is calculated.

The variation of stresses within a liner has important practical implications, particularly for the measurement of liner thrusts. The results from this study show that the location of any instrumentation, both within the liner, and

most importantly, its distance from the face, should be accurately determined during any monitoring programme. This important factor is often not reported in the published literature, even where otherwise a comprehensive monitoring programme has been carried out. In addition a high factor of safety on the liner is required to withstand the very high thrusts at its leading edge. Thus most of the liner segment, where the thrusts are much less, will be overdesigned. Special measures could be undertaken to locally strengthen the leading edge of the liner segments. Alternatively, the leading edge might be made more compressible so that in does not "shield" the part of the liner further from the face and allows it to carry more of the load.

9.3.2 Effect of Rock Damage

Damage to the rock around an opening was simulated by a reduction of its deformation modulus, i.e. a softening of the ground. This was shown to be a reasonable simplification of the effect on rock strength and deformation properties due to rock fracture caused by drill and blast excavation. Ground weakening was not considered in this study, although this process could also occur during excavation. The various excavation sequences carried out showed that alteration of the ground properties ahead of liner installation drastically affected the behaviour of the ground around the opening and the performance of the liner.

A softened zone around the opening will cause a transfer of stress to areas where the ground capacity is greater due to the higher radial confinement. The reduction in stress near the wall of the opening may prevent, or reduce, the propagation of a zone of strain-weakening rock, and increase the stability of the opening, particularly where brittle failure modes such as spalling may occur. The zone of softening will cause additional deformations at the wall of the opening, making the overall rock mass behave as if it were softer. This increase in convergence due to softening must be taken into account when analysing field meaurements and comparing them to the results from numerical analyses.

9.3.3 Identification of Zones of Softened Ground

Although the identification of zones of softened ground should be attempted whenever field measurements are available, this may often prove to be rather difficult or inconclusive. Ideally softened zones would be identifiable from the distribution of radial displacements or strains around an opening, particularly as displacement measurements are more common than stress measurements. However, where the modulus of the damaged rock increases from the wall to the contact between the undamaged and damaged zones because of increasing radial confinement and decreasing severity of the damage, the form of the radial strain distribution does not significantly differ from the distribution in the undamaged

case. Only where the damaged rock modulus is constant can a zone of softening be identified, but this could be masked by any dilation that might occur in the same zone due to yielding.

Determination of softened zones by radial displacement measurements in borehole extensometers will be made more difficult by the usually relatively wide spacing between anchoring points. Identification of soft zones would therefore appear to be much easier from measurements of stress changes. Changes in the tangential stress will be particularly easy to detect because within a softened zone there is a reduction of stress from that in the adjacent undamaged zone, and possibly even below the initial insitu stress. If only a few measurement positions are used, a reduction in the tangential stress will be easier to detect than an extra increase in the radial strain or displacement distribution. However rock stress measurements are usually more erratic than radial displacement measurements, and so care has to be taken in the installation of the gauges and in the interpretation of the readings.

There is also a stress reduction in zones of weakened rock, and it may be difficult to identify whether weakening or softening has taken place in any particular case. Indeed both processes may be occuring simultaneously. An attempt should be made to identify which process is occuring because although the correct stress and strain distributions can be obtained by using the wrong process model, the same model

may not be applicable to other situations and predict unrealistic zones of weakened or damaged rock as well as incorrect failure modes.

The processes of dilation during damage and of arching have not been considered in this study. Both of these will have an influence on the stress observations, and dilation can have a large effect on measurements of strain and displacement.

9.3.4 Effect of Softening on Liner Thrust

Softening a ring of ground around the opening and before support installation causes significant reductions in the liner thrusts. The effect on the longitudinal variation of thrust within a liner segment is equivalent to a delay in the support in addition to a uniform reduction in the thrust along the liner. Because of the equivalent delaying effect there is a reduction not only in the maximum thrust in the liner but also a reduction in the variation of the thrust along the liner. This implies that where damage occurs around an excavation, for instance when excavation is by drilling and blasting, there will be less variation in the thrusts in the liner than where there is no damage, for example in machine excavated tunnels supported by segmented linings.

9.3.5 Bilinear Ground Convergence Curves and Face Convergence

The average support pressures for liner segments and the ground convergence for the construction cases studied were plotted on a two dimensional convergence-confinement diagram. The results lay close to the bilinear ground convergence curves calculated from a two dimensional closed form solution that was developed to model the effect of a modulus reduction ahead of the face and around the tunnel.

In any design of tunnel supports using the convergence-confinement diagram the value of the radial displacement at the face is an important parameter because it defines the earliest point at which the liner can be installed. There appears to be no effect from the liner support on the face convergence when the distance from the liner to the face after the round of excavation is greater than one tunnel radius. Rock damage at distances of greater than about half a radius ahead of the face do not produce a change in convergence either. A knowledge of the value of the radial displacement at the face is important in order to be able to assess convergence measurements made at the face of a tunnel or at the base of a shaft, or the results from borehole extensometer installations. These measurements can usually only be started once the face has passed the measuring point, and so after the radial face displacement has occured.

9.3.6 Changes in Ground Stresses

The rates of change in tangential and radial ground stresses at a point near the tunnel wall as the tunnel passes are not the same. The radial stress remains relatively unchanged until the face is very close to the point (it may even increase slightly), and as it passes the change in radial stress is very rapid and it quickly reduces to its ultimate value. The tangential stress change is more gradual, with the stress starting to increase when the point is still about two tunnel radii ahead of the face, and only reaches its ultimate value at more than two radii behind the face. These observations have practical important implications for the design of supports, the evaluation of field observations and for the use of rock bolts. Where ground stress change measurements are made they must be started at least two radii ahead of the face or else the complete tangential stress change will not be recorded. The full radial stress change will be measured as long as the measurements are started just ahead of the face. If any damage is expected at the face the measurements must be commenced further ahead. Rock bolts which rely on the build up of ground stresses to provide a good bond between the rock and the bolt should be installed within 2 to 4 radii of the face. Bolts installed further from the face would need to be self bonding because the (elastic) stress changes will have virtually ceased.

9.3.7 Excavation in Frozen Ground, and Drilled Fluid Supported Shaft

Excavation within frozen ground which is subsequently softened by thawing, and construction of a shaft by drilling using fluid support which is later removed, are two ways by which a liner can be installed earlier, i.e. at lower values of radial convergence. In both these cases the liner thrusts are on average greater than those for a similar construction sequence without using ground freezing or fluid support. However the thrusts do not vary as much along the liner. For a drilled shaft the maximum thrust is in fact less than the maximum thrust in a similar situation, but where the liner is placed close to the face in steps as the shaft is advanced.

9.3.8 Shallow Shafts

It was found that for these analyses the performance of a shaft could be generally represented by a ground convergence curve normalised to the values of the initial insitu horizontal stress, and to the two dimensional plane strain radial displacement calculated by using that stress. For shallow shafts of depth 7 R, where the support was placed close to the base, higher support pressures were obtained than indicated by the ground convergence curve because of the influence of the unrestrained ground surface boundary.

9.4 Further Work

There are several aspects of this investigation where further analysis could be carried out, still using the numerical technique developed here. The extra analyses would use finer meshes than the ones used and described here, and would have to incorporate the comments made on the improvements in the mesh design required to increase the accuracy of the results.

More work is required to evaluate the variation of $\lambda d'$, the support delay factor, for a range of extents of damage ahead of the face and around the tunnel, and for a range of degrees of damage (rock softening). This would lead to the development of a "damage factor" which could be used in a similar manner as $\lambda d'$.

Further evaluation of the effects of the variation of confining pressure and severity of the damage on the distribution of the damaged rock modulus is required, and this should be related to field measurements where possible. This would be incorporated into an attempt to develop some method by which the extent of a softened zone could be identified from field measurements.

Evaluation of the effects of rock dilation during damage should be carried out. This will influence the radial displacements and the ground stresses, and will be required to analyse the convergence-confinement diagrams obtained from field measurements.

The variation of the face convergence should be explored for shorter excavation rounds, when there should be more influence of the support on the face displacements.

The effect of different values of Ko on the behaviour of shafts constructed by different methods should be considered further. This would initially be done by using a finer mesh, and also with shorter excavation rounds.

The numerical technique developed here is a relatively quick and inexpensive method of analysing the performance of shafts and tunnels constructed incrementally. It clearly illustrates the significant effect that the construction procedure has on the performance of an opening, particularly the influence of the support delay, and the process of ground softening.

REFERENCES

Andersland O.B. and D.M. Anderson, 1978. Geotechnical Engineering for Cold Regions. McGraw Hill, New York, 566 p.

Bieniawski Z.T., 1970. Time-dependent behaviour of fractured rock. Rock Mech., Vol. 2, pp. 123-137.

Bieniawski Z.T., 1978. Determining rock mass deformability; experience from case histories. Int. J. Rock Mech. and Min. Sci., Vol. 15, No. 5, pp. 237-247.

Burns J.Q. and R.M. Richard, 1964. Attenuation of stresses for buried cylinders. Proc. Symp. on Soil Structure Interaction, Tucson, Arizona, pp. 378-392.

Einstein H.H. and C.W. Schwartz, 1979. Simplified analysis for tunnel supports. ASCE JGED GT4, April, pp. 499-518.

Einstein H.H. and C.W. Schwartz, 1980. Improved design of tunnel supports - Volume 1 - Simplified analysis for ground structure interaction in tunnelling. Report UMTA-MA-06-0100-80-4, U.S. Dept. of Transportation, 427 p.

Flügge W., 1975. Viscoelasticity. Springer-Verlag, Berlin, 2nd ed., 194 p.

Franks F., 1972. Editor, Water: a comprehensive treatise. Plenum Press, New York, 596p.

Golder Associates and James F. MacLaren Limited, 1976. Tunnelling technology, an appraisal of the state of the art for application to transit systems. Published by the Ontario Ministry of Transportation and Communications, 166 p.

Gouch A.E. and J.B.Conway, 1976. Field measurements and corresponding finite element analysis of closure during shaft sinking at the Lucky Friday Mine. Report of

Investigation, RI 8193 U.S. Bureau of Mines, 19 p.

Gustafsson R. 1976. Smooth blasting. Tunnelling '76, Proc. Int. Symp. Inst. Min. and Metall. London, pp. 141-146.

Hanafy E.A. and J.J. Emery, 1980. Advancing face simulation of tunnel excavation and lining placement. 22nd Canadian Rock Mech. Symp., Vol. 22, CIM, pp. 119-125.

Hobbs D.W., 1970. The behaviour of broken rock under triaxial compression. Int. J. Rock Mech. and Min.Sci., Vol. 7, pp. 125-148.

Hoek E. and E.T. Brown, 1980. Underground excavations. Inst. of Min. and Metall., London, 527 p.

Jones J.S. and R.E. Brown, 1978. Temporary tunnel support by artificial ground freezing. ASCE JGED GT10, Oct. pp. 1257-1276.

Kaiser P.K., 1981. A new concept to evaluate tunnel performance - influence of excavation procedure. 22nd U.S. Symp. on Rock Mech., pp. 264-271.

Kaiser P.K. and D.E. Hutchinson, 1982. Effects of construction procedure on tunnel performance. 4th Int. Conf. on Numerical Methods in Geomechanics, Edmonton (to be published).

Kaiser P.K., C. MacKay and N.R.Morgenstern, 1982. Performance of a shaft in weak rock (Bearpaw Shale), Int. Symp. Rock Mech. on Caverns and Pressure Shafts (ISRM), Aachen (to be published).

Kulhawy F.H., 1977. Numerical methods in geotechnical engineering. Chapter 16, Embankments and excavations. Editors C.S. Desai and J.T. Christian McGraw Hill, New York, pp. 528-555.

Lombardi G., 1973. Dimensioning of tunnel linings with regard to constructional procedure. Tunnels and Tunnelling, Vol. 5, pp. 340-351.

MacKay C., 1982. Performance of a shaft in weak rock. MSc thesis, Department of Civil Engineering, University of Alberta, 250p.

Peck, R.B., A.J. Hendron Jr. and B. Mohraz, 1972. State of the art of soft ground tunnelling. Proc. American Conf. on Rapid Excavation and Tunnelling, Vol 1, pp. 259-286.

Peng S. and E.R. Podnieks, 1972. Relaxation and the behaviour of failed rock. Int. J. Rock Mech. and Min. Sci., Vol. 9, No. 6, pp. 699-712.

Ranken R.E. and J. Ghaboussi, 1975. Tunnel design considerations, analysis of stresses and deformations around advancing tunnels. Report No. FRA-OR&D 75-84, Federal Railroad Administration, U.S. Dept. of Transportation. 148 p.

Roesner E.K. and S.A. Poppen, 1978. Shaft sinking and tunnelling in the oil sands of Alberta. AOSTRA Seminar, Edmonton, Alberta.

Sharp, J.C., L. Richards and J. Byrne, 1977. Instrumentation considerations for large underground trial openings in civil engineering. Proc. Int. Symp. Field Measurements in Rock Mech., Zurich, Vol. 2, pp. 587-609.

Thyssen Mining Co. Canada Ltd., 1978. Shaft sinking and tunnelling study, oil sands deposit, Cold Lake, Alberta, Internal report, 27p.

Timoskenko S., 1941. Strength of Materials, Part II, Advanced Theory and Problems. 2nd Ed. Van Nostrand, New York. 510p.

University of California, 1972. Computer program for static and dynamic analyses of linear structural systems. 1) Computer program manual for SAP4, 2) Users guide for SAP4, Report EERC 72-10.

Walli J.R.O., 1964. The application of European shaft sinking techniques to the Blairmore Formation. Canadian Min. and Metall. Bull., Vol. 57, February, pp. 139-146.

Ward W.H., 1978. Ground supports for tunnels in weak rocks. Geotechnique, Vol. 28, 2, pp. 133-171.

Ward W.H., D.J. Coats and P. Tedd, 1976. Performance of tunnel supports systems in the Four Fathom Mudstone. Tunnelling '76, Proc. Int. Symp. Inst. Min. and Metall., London, pp. 329-340.

Wawersik W.R. and W.F. Brace, 1971. Post failure behaviour of a granite and a diabase. Rock Mech., Vol. 3, No. 2, pp. 61-85.

APPENDIX 1

GROUND REACTION CURVES AND MODULUS REDUCTION

Summary

In this appendix the closed form equations are derived for ground softening and subsequent excavation within a linear elastic material. The equations are developed in two stages for a two dimensional plane strain situation. In Stage 1 a core of ground is softened and equations for the radial stress and displacement within the softened material are presented. In Stage 2 the opening is excavated within the softened ground by the excavation unloading technique, in which the radial stress at the boundary of the opening is reduced to zero. The relationship between the radial stress (or support pressure) and the radial displacement at the wall of the opening is presented for a range of ratios of unsoftened to softened moduli for the two stages by means of a bilinear ground convergence curve.

Ground Reaction Curves and Modulus Reduction

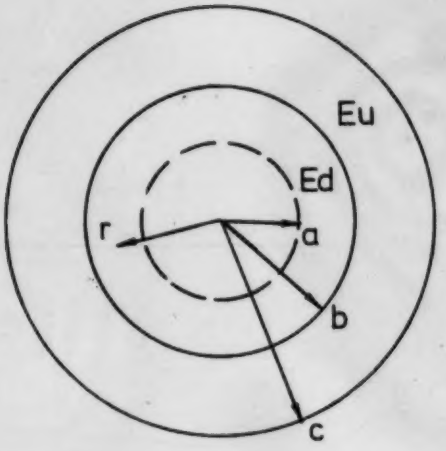

Eu	Undamaged Young's Modulus
Ed	Damaged Young's Modulus
a	Radius of tunnel wall
b	Radius of damaged zone
c	Radius of ground $\longrightarrow \infty$
ν	Poisson's ratio
P_o	Initial insitu stress

Stage 1

Assuming 2D plane strain, reduce the modulus of the core from Eu to Ed. This should be considered in two steps. Firstly the stresses in the damaged zone are uniformly reduced but with additional forces applied at r=b to give no displacements. (At this step the undamaged ground will not be affected.) The next step is when the forces are removed and the ground moves inwards to equilibrium and the stresses adjust accordingly as shown below.

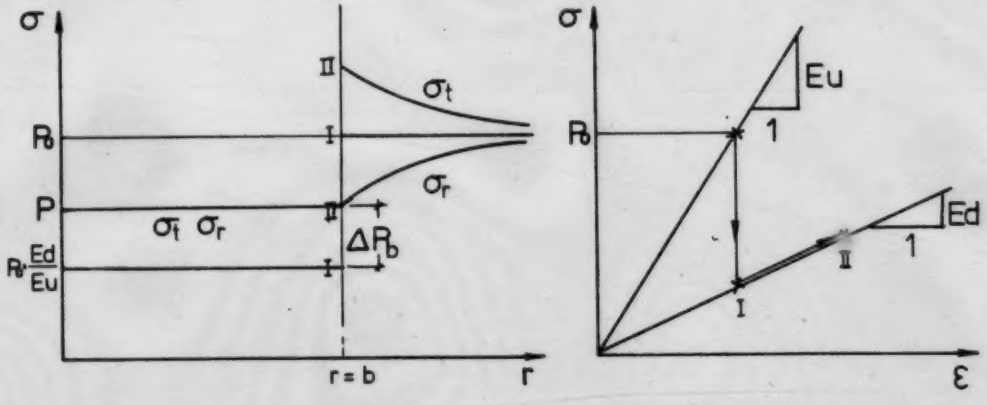

Plane strain deformations in a hollow cylinder

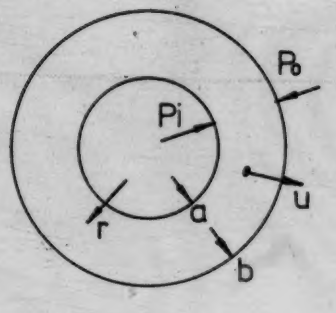

$$u = \frac{(1-\nu-2\nu^2)}{E}\cdot\frac{(a^2Pi - b^2Po)}{(b^2-a^2)}r + \frac{(1+\nu)}{E}\cdot\frac{(a^2b^2(Pi-Po))}{(b^2-a^2)r}$$

Consider the deformations within the cylinder of damaged ground.

$$u = \frac{(1-\nu-2\nu^2)}{Ed}\cdot\frac{(-\Delta Pb)}{1}r \qquad \ldots\ldots\ldots\ldots (1)$$

where ΔPb is the pressure imposed at $r=b$ as a result of the modulus reduction.

Consider the deformations within the hollow cylinder of undamaged ground.

$$u = \frac{(1-\nu-2\nu^2)}{Eu}\cdot\frac{(A.b^2)}{(\infty^2-b^2)}r + \frac{(1+\nu)}{Eu}\cdot\frac{(b^2\infty^2A)}{(\infty^2-b^2)}\cdot\frac{1}{r}$$

$$= \frac{(1+\nu)b^2A}{Eu.r} \qquad \ldots\ldots\ldots\ldots (2)$$

Where

$$A = -[Po(1-Ed/Eu) - \Delta Pb]$$

Solve equations 1 and 2 for ΔPb at $r=b$

$$\Delta Pb = \frac{(1-Ed/Eu).Po.Ed}{(Ed + (1-2\nu).Eu)}$$

So deformations within cylinder of damaged ground

$$u = -\frac{(1+\nu).(1-2\nu).(1-Ed/Eu).Po.r}{Ed + Eu(1-2\nu)}$$

or at $r=a$

$$\frac{u}{u_o} = \frac{(1-2\nu)(1-Ed/Eu)}{(Ed/Eu) + (1-2\nu)} \qquad \ldots\ldots (a)$$

where with $Ed = 0$

$$u_o = Po.a.(1-\nu)/Eu$$

Now

$$P = P_o.Ed/Eu + \Delta Pb$$

So

$$\frac{P}{P_o} = \frac{2(Ed/Eu)(1-\nu)}{(Ed/Eu) + (1-2\nu)}$$

For $\nu = 0.2$

Eu/Ed	u/u₀	P/Po
0.0	1.0	0.0
0.1	0.771	0.229
0.2	0.600	0.400
0.3	0.467	0.533
0.4	0.360	0.640
0.5	0.273	0.727
0.6	0.200	0.800
0.7	0.138	0.862
0.8	0.086	0.914
0.9	0.040	0.960
1.0	0.0	1.0

Stage 2

Excavate the tunnel by reducing the radial stress at the wall to zero.

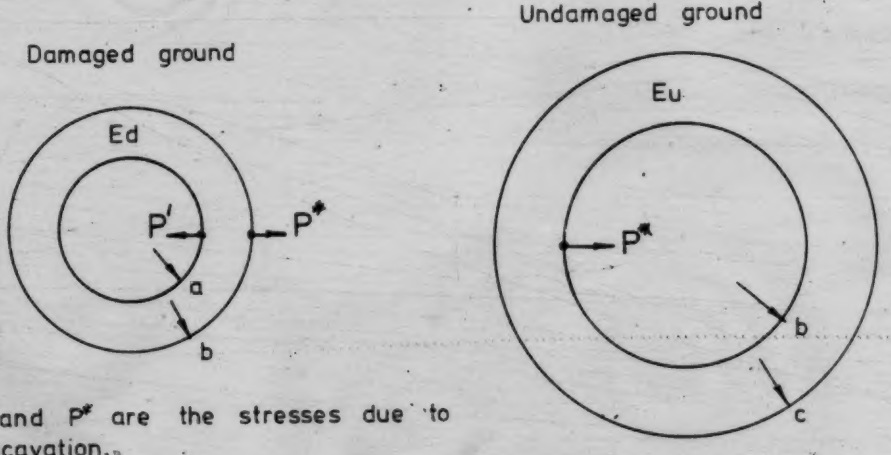

P' and P* are the stresses due to the excavation.

Consider deformation in the damaged ground at r = b

$$u = \frac{(1-\nu-2\nu^2).(a^2P' - b^2P^*).b}{Ed.(b^2-a^2)} + \frac{(1+\nu).(a^2b^2).(P'-P^*)}{Ed.(b^2-a^2)}.\frac{1}{b} \quad \text{.....(3)}$$

Consider deformation in the undamaged ground at r = b

$$u = \frac{(1+\nu)\,b.P^*}{Eu} \quad \text{.....(4)}$$

Eliminate u from equations 3 and 4

$$P^* = \frac{2.(1-\nu).a^2.P'}{(1-2\nu).b^2 + a^2 + (b^2-a^2).Ed/Eu}$$

Now $P' = P$ from stage 1, so

$$\frac{P^*}{P_o} = \frac{2.(1-\nu).a^2}{(1-2\nu).b^2 + a^2 + (b^2-a^2).Ed/Eu} \cdot \frac{2.Ed.(1-\nu)}{Ed + Eu.(1-2\nu)}$$

Now consider the displacement at the tunnel wall

$$\frac{u}{u_o} = \left[\frac{(1-\nu-2\nu).a.(P' - P^*b^2/a^2)}{Ed.((b^2/a^2)-1)} + \frac{(1+\nu)(b^2/a^2)(P'-P^*)a}{Ed((b^2/a^2)-1)}\right]\frac{Eu}{P_o a(1+\nu)}$$

Simplify and tabulate values for $\nu = 0.2$

$$\frac{u}{u_o} = \frac{P'}{P_o}.\frac{Eu}{Ed}.\frac{(1-2\nu).(Ed/Eu - 1) + (b/a)^2.(1-2\nu+Ed/Eu)}{(1-Ed/Eu) + (b/a)^2.(1-2\nu+Ed/Eu)} \quad \text{.....(b)}$$

Ed/Eu	b/a	u/u₀ (b)	u/u₀ (a)	u/u₀ (tot.)
0.0	1.0	0.0	1.0	1.000
	1.3	0.548	1.0	1.548
	1.8	1.217	1.0	2.217
0.1	1.0	0.229	0.771	1.000
	1.3	0.706	0.771	1.477
	1.8	1.247	0.771	2.018
0.5	1.0	0.727	0.273	1.000
	1.3	0.961	0.273	1.234
	1.8	1.168	0.273	1.441

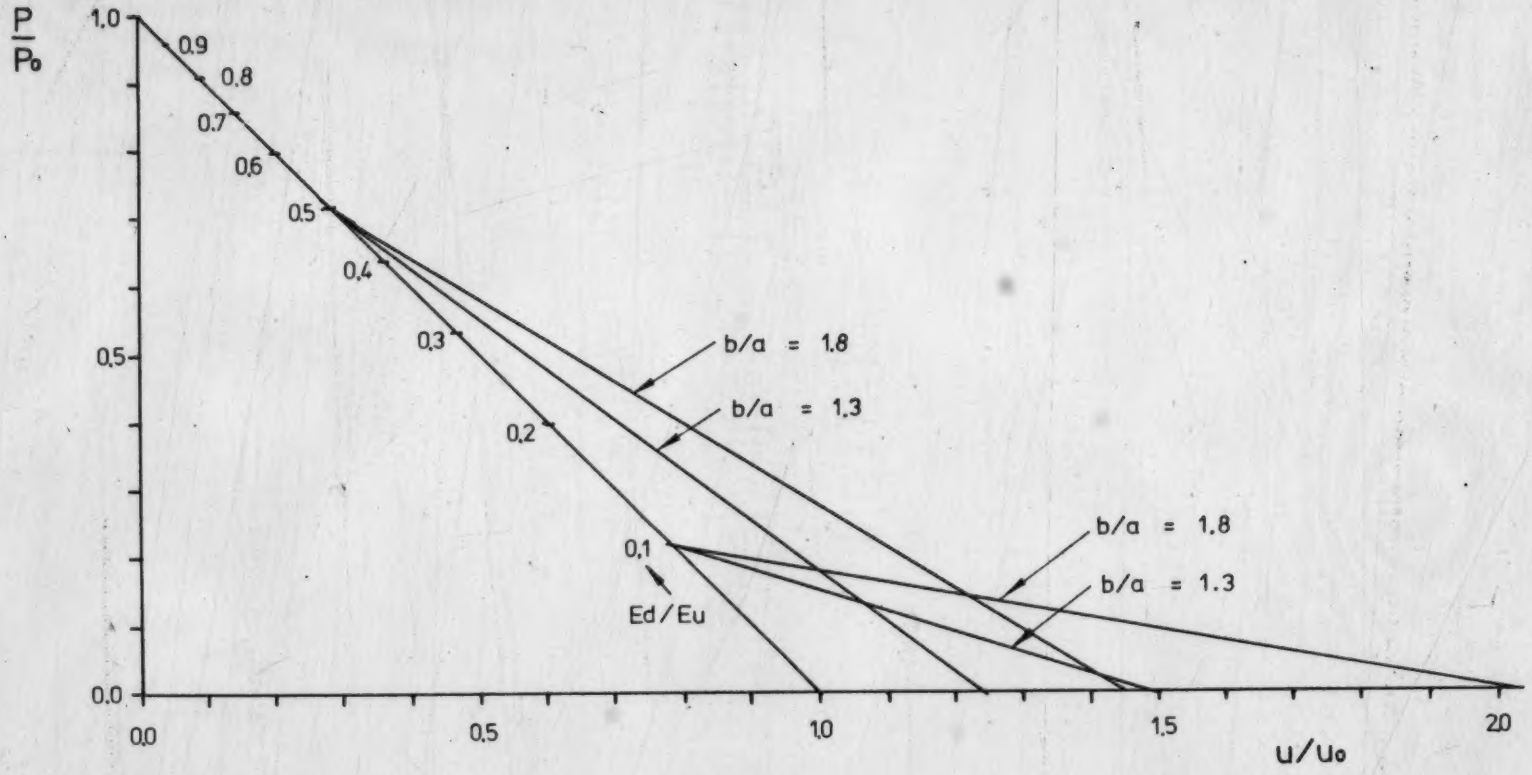
P/Po
1.0
0.5
0.0
0.9
0.8
0.7
0.6
0.5
0.4
0.3
0.2
0.1
Ed / Eu
b/a = 1.8
b/a = 1.3
b/a = 1.8
b/a = 1.3
0.0
0.5
1.0
1.5
2.0
u/uo

APPENDIX 2

GENERALISED PROCEDURE FOR FINDING NODAL POINT FORCES FROM ELEMENT CENTRE STRESSES

Summary

A procedure for calculating nodal forces equivalent to the stress distribution along the boundaries of an element is presented. The forces are determined from the stresses at the nodes which are interpolated from the stresses known at four points. The points are usually the centres of nearby elements. These nodal forces are used to reduce to zero the stresses across element boundaries to simulate ground excavation. This procedure is similar to the one presented by Kulhawy (1977), but has been adapted to the axisymmetric situation.

Generalised Procedure for Finding Nodal Point Forces from Element Centre Stresses

The following procedure was developed by Clough and Duncan and is described by Kulhawy in Numerical Methods in Geotechnical Engineering chapter 16 Embankments and Excavations edited by Desai and Christian.

The procedure has been developed for quadrilateral linear strain elements. The nodal point forces to be applied along the excavation surface are computed from the nodal point stresses which are interpolated from the centre stresses of the adjacent elements.

The basic interpolation formula is:

$$\sigma = a_1 + a_2 x + a_3 y + a_4 xy$$

where σ = (known) element stress
x, y = coordinates where stress is known
$a_{1,2,3,4}$ = interpolation coeffients

From the 4 elements surrounding a given nodal point the three stresses in each element become:

$$\{\sigma_e\} = [m]\{a\}$$

where $\{\sigma_e\}$ = known element stress vector
$[m]$ = known stress coordinate matrix.
$\{a\}$ = unknown interpolation coefficent vector

The nodal point stresses $\{\sigma_n\}$ of the element to be excavated are then:

$$\sigma_n = [n]\{a\} = [n][m]^{-1}\{\sigma_e\}$$

in which the matrix $[n]$ is the known coordinate matrix for the I, J, K, L nodal points shown in the figure overleaf.

Using the principle of virtual work and the linear boundary stress distribution shown overleaf the equivalent horizontal and vertical nodal point forces can be established at each nodal point.

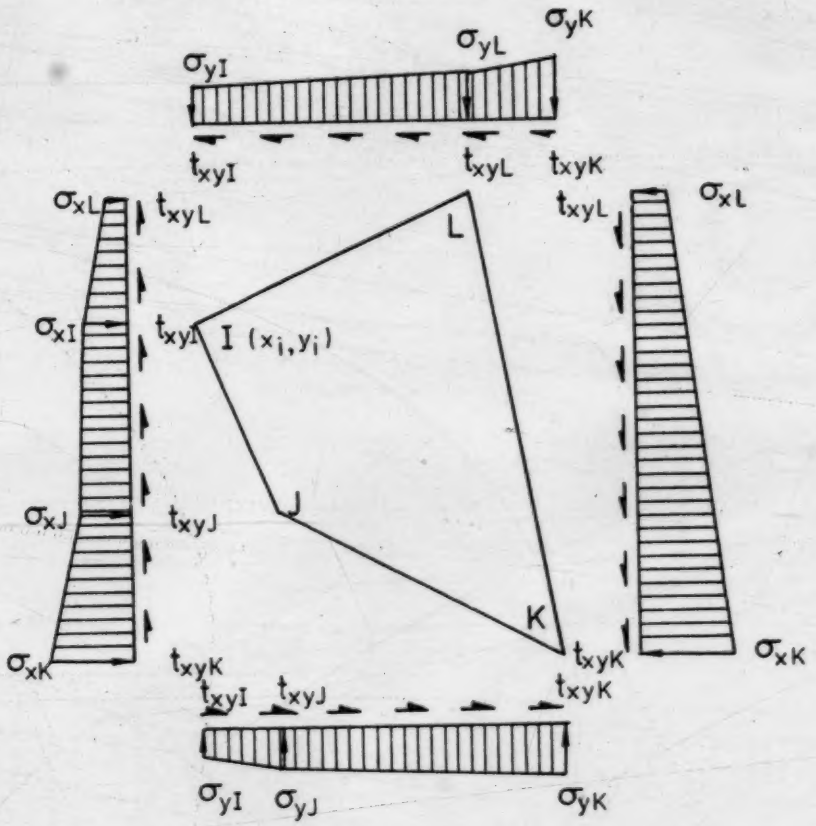

All stresses and gradients are shown positive.

For example, the force in the y direction at point J is:–

$$F_y^J = \frac{1}{6}\left[(X_{JI})\sigma_{yI} + 2(X_{JI} + X_{KJ})\sigma_{yJ} + (X_{KJ})\sigma_{yK} + (Y_{IJ})t_{xyI} + 2(Y_{IJ} + Y_{JK})t_{xyJ} + (Y_{JK})t_{xyK} \right] \quad \ldots\ldots 1$$

where

$$Y_{IJ} = y_i - y_j \qquad Y_{JK} = y_j - y_k$$

$$Y_{KL} = y_k - y_l \qquad Y_{LI} = y_l - y_i$$

and similarly for the X direction.

This operation is repeated for all 8 nodal point forces resulting in:–

$$\{F_n\} = [H]\{\sigma_n\} = [H][n][m]^{-1}\{\sigma_e\} = [Q]\{\sigma_e\}$$

where

$\{F_n\}$ = 8 × 1 nodal force vector

$[H]$ = 8 × 12 boundary geometry matrix

$\{\sigma_n\}$ = 8 × 1 nodal stress vector

$[Q]$ = 8 × 12 resultant matrix relating unknown nodal forces and known element centre stresses.

Equation 1 may be calculated in the following manner. Work done by nodal forces must be the same as the work done by the boundary stresses in order to give the same internal energy. Consider the forces and stresses in the y direction.

$$F_I^y d_I^y + F_J^y d_J^y + F_K^y d_K^y + F_L^y d_L^y =$$

$$\int_0^{X_{JI}} \left(d_I^y + \frac{x}{X_{JI}}(d_J^y - d_I^y)\right) \times \left(\sigma_I^y + \frac{x}{X_{JI}}(\sigma_J^y - \sigma_I^y)\right) dx$$

$$-\int_0^{Y_{JI}} \left(d_I^y + \frac{y}{Y_{JI}}(d_J^y - d_I^y)\right) \times \left(t_I^y + \frac{y}{Y_{JI}}(t_J^y - t_I^y)\right) dy$$

plus similar terms rotating I,J,K,L 2

where d_I^y is the y displacement applied to point I.

Equation 2 must hold for any combination of d's, thus collect terms with the same d in them on both sides and equate. This gives an equation for each F^y which can be integated and simplified to give equation 1.

Equation 1, and the similar equations, only apply to 2D cases. With an axisymmetric case the thickness of the element increases with increasing distance from the axis of symmetry.

Sum the total work done by the boundary stresses in the x (radial) direction.

$$\text{Work done} = \int_0^{Y_{JI}} \left(d_I^x + \frac{y}{Y_{IJ}}(d_J^x - d_I^x)\right).\left(\sigma_I^x + \frac{y}{Y_{IJ}}(\sigma_J^x - \sigma_I^x)\right).\left(x_i + \frac{y}{Y_{IJ}}X_{JI}\right)\theta\, dy$$

$$+\int_0^{X_{JI}} \left(d_I^x + \frac{x}{X_{JI}}(d_J^x - d_I^x)\right).\left(t_I^x + \frac{x}{X_{JI}}(t_J^x - t_I^x)\right).(x_i + x)\,\theta\, dx$$

. plus other terms rotating I,J,K,L. 3

This equation may then be integrated and simplied Collect terms containing the same d's and equate. For example sum up all terms with d_J^x.

$$F_J^x d_J^x = \theta\left[\sigma_I^x \frac{Y_{IJ}}{6} + \sigma_J^x \frac{Y_{IJ}}{3}\right] d_J^x x_i + \theta\left[\sigma_I^x \frac{Y_{IJ}}{12} + \sigma_J^x \frac{Y_{IJ}}{4}\right] d_J^x X_{JI}$$

$$+ \theta\left[t_I^x \frac{X_{JI}}{6} + t_J^x \frac{X_{JI}}{3}\right] d_J^x x_i + \theta\left[t_I^x \frac{X_{JI}}{12} + t_J^x \frac{X_{JI}}{4}\right] d_J^x X_{JI}$$

$$+ \theta\left[\frac{\sigma_J^x}{3} + \frac{\sigma_K^x}{6}\right] d_J^x Y_{JK} x_j + \theta\left[\frac{\sigma_J^x}{12} + \frac{\sigma_K^x}{12}\right] d_J^x X_{KJ} Y_{JK}$$

$$+ \theta\left[\frac{t_J^x}{3} + \frac{t_K^x}{6}\right] d_J^x X_{KJ} x_j + \theta\left[\frac{t_J^x}{12} + \frac{t_K^x}{12}\right] d_J X_{KJ} Y_{KJ} \quad \ldots\ldots 4$$

Similarly sum the total work done by the boundary stresses in the y (axial) direction.

$$\text{Work done} = \int_0^{X_{JI}} \left(d_I^y + \frac{x}{X_{JI}}(d_J^y - d_I^y)\right).\left(\sigma_I^y + \frac{x}{X_{JI}}(\sigma_J^y - \sigma_I^y)\right).(x_i + x)\,\theta\,dx$$

$$+ \int_0^{Y_{IJ}} \left(d_I^y + \frac{y}{Y_{IJ}}(d_J^y - d_I^y)\right).\left(t_I^y + \frac{y}{Y_{IJ}}(t_J^y - t_I^y)\right).\left(x_i + \frac{y}{Y_{IJ}} X_{JI}\right)\theta\,dy$$

plus other terms rotating I,J,K,L. 5

Now this equation is the same as equation 3 except that :-

t_I and t_J are replaced by σ_I and σ_J repectively,

σ_I and σ_J are replaced by t_I and t_J respectively,

and that all the stresses and displacements are in the y direction.

Thus from equation 4,

$$F_J^y d_J^y = \theta\left[\frac{\sigma_I^y}{6} + \frac{\sigma_J^y}{3}\right] d_J^y X_{JI} x_i + \theta\left[\frac{\sigma_I^y}{12} + \frac{\sigma_J^y}{4}\right] d_J^y X_{JI} X_{JI}$$

$$+ \theta\left[\frac{t_I^y}{6} + \frac{t_J^y}{3}\right] d_J^y Y_{IJ} x_i + \theta\left[\frac{t_I^y}{12} + \frac{t_J^y}{4}\right] d_J^y Y_{IJ} X_{JI}$$

$$+ \theta\left[\frac{\sigma_J^y}{3} + \frac{\sigma_K^y}{6}\right] d_J^y X_{KJ} x_j + \theta\left[\frac{\sigma_J^y}{12} + \frac{\sigma_K^y}{12}\right] d_J^y X_{KJ} X_{KJ}$$

$$+ \theta\left[\frac{t_J^y}{3} + \frac{t_K^y}{6}\right] d_J^y Y_{JK} x_j + \theta\left[\frac{t_J^y}{12} + \frac{t_K^y}{12}\right] d_J^y X_{KJ} Y_{JK} \quad \ldots\ldots 6$$

APPENDIX 3

CALCULATION OF VALUES FOR A CONVERGENCE CONFINEMENT DIAGRAM AND CORRECTION OF RESULTS

Summary

The procedure used to calculate the support pressure applied to the ground, given the radial stress at the centre of a liner, is presented. The two dimensional plane strain hollow cylinder equations are used.

A method for correcting the radial displacements and support pressures is outlined, in which the results from a numerical analysis of an unlined tunnel are compared to a closed form two dimensional plane strain solution. Factors are calculated which are applied to the results from the numerical analyses to give the closed form solution results. These factors are then used to correct the results from numerical analyses of lined excavations where the same mesh and excavation sequence have been used.

Calculation of Values for a Convergence - Confinement Diagram and Correction of Results

Calculation of Liner Support Pressure

With the analyses carried out using mesh number 6 (or number 2) the liner radial stress σ_r, is known at r = 4·7m (r = distance from tunnel centreline). So from the equation for plane strain:-

$$\sigma_r = \frac{p_s b^2 (1 - a^2/r^2)}{(b^2 - a^2)}$$

where

b = radius of outer edge of liner
a = radius of inner edge of liner
p_s = liner support pressure (ie the radial stress that the liner applies to the ground)

giving

$$p_s = \frac{\sigma_r (5^2 - 4.4^2)}{5^2 - (1 - (4.4/4.7)^2)}$$

$$\underline{p_s = 1.8255\ \sigma_r} \quad \ldots\ldots\ldots 1$$

With the analyses carried out using mesh number 7 the radial liner stress is known at r = 4·55m and r = 4·85m, From the equation for plane strain above:-

$$p_s = 3.479\ \sigma_{4.55}, \quad p_s = 1.275\ \sigma_{4.85}$$

These two values of p_s should be the same, so average the results giving:-

$$\underline{p_s = 1.740\ \sigma_{4.55} + 0.637\ \sigma_{4.85}} \quad \ldots\ldots\ldots 2$$

Correction of Radial Displacements

The ultimate radial displacement at each node in the unlined case must be factored to make it equal to the value of radial displacement given by closed form solutions. This factoring is necessary to reduce the inaccuracies arising from the calculation of the nodal excavation forces at the (old) face. In front of the face the radial displacements appear to agree with more accurate analyses. Therefore the factor has been calculated from the difference between the ultimate displacement and the displacement just in front of the face, see the figure below.

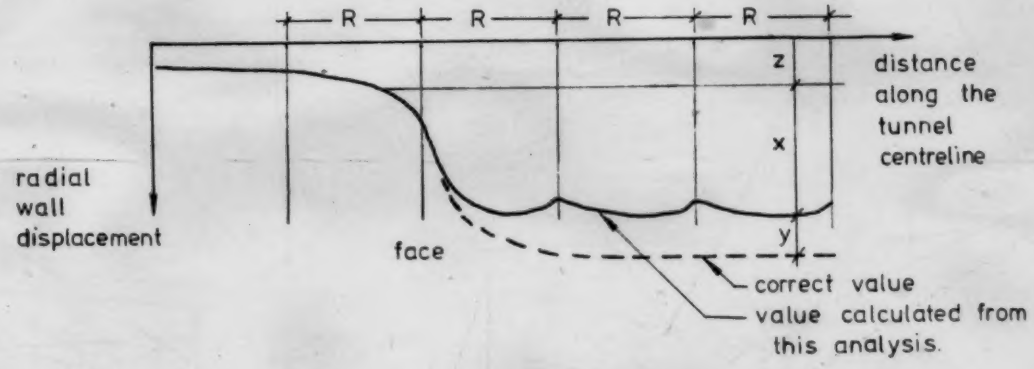

The factors A_1, A_2 etc. are applied to the values of x calculated for the corresponding nodes in the lined cases, giving the corrected ultimate radial wall displacements at the nodes when added to the z values.

Calculation of Corrected Values of p_s and u.

The notation for the nodes and elements is shown below.

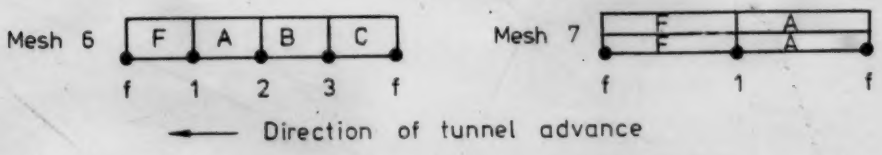

The average radial displacement of a liner segment is given by:-

$$u_{ave} = (u_f + 2u_1 + 2u_2 + 2u_3 + u_f) / 8 \qquad \text{(for mesh 6)}$$

where the values of u_f, u_1, u_2, u_3 are corrected values. Values of p_s are corrected by multiplying by the average of the A's from the surrounding nodes.

Examples of the correction calculations are shown on the next page.

Example of Correction Calculations

Mesh 6, Unlined case.

$\frac{z_1}{d_o} = 0.255$	$\frac{x_1}{d_o} = 0.635$	$\frac{y_2}{d_o} = 0.11$	$A_1 = 1.173$	$A_{1(\text{adj})} = 1.101$
$\frac{z_2}{d_o} = 0.185$	$\frac{x_2}{d_o} = 0.735$	$\frac{y_1}{d_o} = 0.08$	$A_2 = 1.109$	$A_{2(\text{adj})} = 1.053$
$\frac{z_3}{d_o} = 0.150$	$\frac{x_3}{d_o} = 0.790$	$\frac{y_3}{d_o} = 0.06$	$A_3 = 1.076$	$A_{3(\text{adj})} = 1.093$
$\frac{z_4}{d_o} = 0.110$	$\frac{x_4}{d_o} = 0.855$	$\frac{y_4}{d_o} = 0.025$	$A_4 = 1.029$	$A_{4(\text{adj})} = 1.141$

Mesh 6, Liner Case 1.		$\frac{R_1}{r_o}$ (corrected)		σ (MPa)	$\frac{P_1}{P_o}$	$\frac{P_1}{P_o}$ (corrected)
$\frac{z_1}{d_o} = 0.160$	$\frac{x_1}{d_o} = 0407$	0.737	$\frac{u_1}{d_o} = 0.774$	(F) 1.418	0.324	0.357
$\frac{z_2}{d_o} = 0.182$	$\frac{x_2}{d_o} = 0.625$	0.875	$\frac{u_2}{d_o} = 0.831$	(A) 0.541	0.123	0.130
$\frac{z_3}{d_o} = 0.156$	$\frac{x_3}{d_o} = 0.645$	0.850	$\frac{u_3}{d_o} = 0.863$	(B) 0.642	0.146	0.160
$\frac{z_4}{d_o} = 0.125$	$\frac{x_4}{d_o} = 0.667$	0.811	$\frac{u_4}{d_o} = 0.806$	(C) 0.318	0.073	0.083
			$\frac{u_{ave}}{d_o} = 0.818$			0.183 = ave $\frac{P_1}{P_o}$

Mesh 7, Unlined Case.

$\frac{z_1}{d_o} = 0.275$	$\frac{x_1}{d_o} = 0.605$	$\frac{y_2}{d_o} = 0.12$	$A_1 = 1.198$	$A_{1(\text{adj})} = 1.080$
$\frac{z_2}{d_o} = 0.150$	$\frac{x_2}{d_o} = 0.870$	$\frac{y_1}{d_o} = -0.02$	$A_2 = 0.977$	$A_{2(\text{adj})} = 1.058$

Mesh 7, Liner Case 1.		$\frac{u}{d_o}$ (corrected)		σ (MPa)	$\frac{P_2}{P_o}$	$\frac{P_2}{P_o}$ (corrected)
$\frac{z_1}{d_o} = 0.260$	$\frac{x_1}{d_o} = 0.407$	0.748	$\frac{u_1}{d_o} = 0.810$	(F) 1.07	0.244	0.266
$\frac{z_2}{d_o} = 0.156$	$\frac{x_2}{d_o} = 0.745$	0.884	$\frac{u_2}{d_o} = 0.816$	(A) 0.38	0.087	0.094
			$\frac{u_{ave}}{d_o} = 0.818$			0.180 = ave $\frac{P_2}{P_o}$

APPENDIX 4

VISCO-ELASTIC DEFORMATION OF A THICK WALLED TUBE

Summary

In order to check the ability of CONSTEP2 to simulate a modulus reduction an analysis was carried out which assumed the ground to be a visco-elastic material. The initial state at t = 0 was equivalent to the undamaged state, and the final state at t = infinity was equivalent to the damaged, softened, state. The situation used for the comparison was the softening, by thawing, of a ring of frozen ground in which an opening had been constructed.

Visco-Elastic Deformation of a Thick Walled Tube

In order to model the stiffening and softening processes by a closed form solution, consider the ground to be a visco-elastic material which changes from E_0 at time $t=0$, to E_∞ at time $t=\infty$.

The calculations presented below follow those by Flügge (1977). They consider a stiff frozen ring of ground (surrounded by a soft ring of unfrozen ground) which is subsequently softened by thawing.

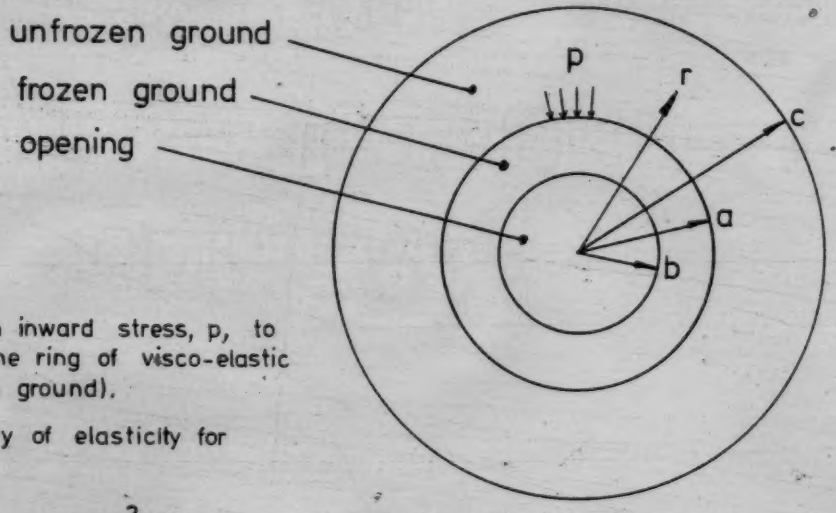

Apply an inward stress, p, to the outside of the ring of visco-elastic material (frozen ground).

By theory of elasticity for plane strain,

$$\sigma_r = A - B r^{-2}$$

$$\sigma_\theta = A + B r^{-2}$$

$$u = (1+\nu).[A(1-2\nu)r + Br^{-1}]/Eg$$

At $r=a$, $\sigma_r = p$; at $r=b$, $\sigma_r = 0$.

$\therefore\ 0 = A - Br^{-2}$, $\quad p = A - Br^{-2}$

$\therefore\ A = p a^2/(a^2 - b^2)$

$B = p a^2 b^2/(a^2 - b^2)$

$$\therefore \quad \sigma_r = \frac{p a^2}{(a^2 - b^2)} \left[1 - \frac{b^2}{r^2}\right] \qquad \ldots\ldots\ldots\ldots\ldots 1$$

$$u_r = \frac{(1+\nu)}{Eg} \cdot \frac{p a^2}{(a^2 - b^2)} \left[(1-2\nu)r + \frac{b^2}{r}\right]$$

Elastic constitutive relationships are,

$$s = 3Ke \quad , \quad S = 2GE$$

K = bulk modulus
G = shear modulus

where s, S and e, E stand for corresponding components of stress and strain deviators.

For visco-elastic materials, using the general correspondence principle, use the operator pairs P'', Q'' ; P', Q' which are independent of each other.

so

$$P''s = Q''e \quad , \qquad P'S = Q'E$$

For an elastic solid $P'' = 1$, $Q'' = 3K$; $P' = 1$, $Q' = 2G$.

Subject the equations to a Laplace transform by replacing the differential operators by the polynomials:-

$$p(\mathfrak{z}) \quad , \quad q(\mathfrak{z})$$

where $\mathfrak{z}$ is a function of the Laplace variable s.

so

$$p''(\mathfrak{z})\bar{s} = q''(\mathfrak{z})\bar{e}$$
$$p'(\mathfrak{z})\bar{S} = q'(\mathfrak{z})\bar{E}$$

These equations are identical with their elastic counterparts, giving

$$3K \rightarrow \frac{q''(\mathfrak{z})}{p''(\mathfrak{z})} \qquad 2G \rightarrow \frac{q'(\mathfrak{z})}{p'(\mathfrak{z})}$$

in terms of Eg and ν

$$Eg \rightarrow \frac{3q'q''}{2p'q'' + q'p''} \qquad \nu \rightarrow \frac{p'q'' - 2q'p''}{2p'q'' + q'p''} \qquad \ldots\ldots\ldots\ldots 2$$

For $E_o = 15$ GPa , $E_\infty = 5$ GPa and $\nu = 0.2$, using the relationships between the elastic constants,

$$G_o = 6.25 \text{ GPa} \qquad K_o = 8.33 \text{ GPa}$$
$$G_\infty = 2.08 \text{ GPa} \qquad K_\infty = 2.78 \text{ GPa}$$

Choose the visco-elastic material shown.

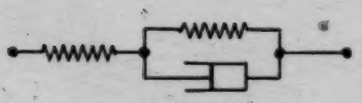

The differential operators for this material are,

Distortion $P' = 1 + p_2 s$, $Q' = q_2 + q_3 s$

Dilation $P'' = 1 + p_1 s$ $Q'' = q_0 + q_1 s$

now, $2G \longrightarrow Q'/P'$

$$\therefore \quad \bar{G} = \frac{1}{2} \cdot \frac{1}{s} \cdot \frac{(q_2 + q_3 s)}{(1 + p_2 s)}$$ (G has been transformed to $\bar{G}s$)

transform back to time t,

$$G = \frac{1}{2}\left[\frac{q_2}{p_2} \cdot \frac{p_2}{1}\left(1 - \exp\left(-\frac{1}{p_2} \cdot t\right)\right) + \frac{q_3}{p_2}\left(1 - \exp\left(-\frac{1}{p_2} \cdot t\right)\right)\right]$$

Similarly for K

Solve for p_1, p_2, q_0, q_1, q_2 and q_3 , given $G_0, G_\infty, K_0, K_\infty$. Choose $p_1 = p_2 = 1$.

$\therefore \quad q_0 = 8.33$, $q_1 = 25.0$, $q_2 = 4.17$, $q_3 = 12.5$

Substitute equations (2) for Eg and ν into equations (1).

Simplifying,

$$u = P'\left(\frac{p a^2}{a^2 - b^2}\right)\left(\frac{3 P'' r}{2P'Q'' + Q'P''} + \frac{b^2}{r Q'}\right)$$

$$u = \frac{p a^2}{a^2 - b^2}\left[\frac{3}{(2q_0 + q_2)} \cdot \frac{1(1 + s) r}{s(1 + 3s)} + \frac{1}{s q_2 r} \cdot \frac{b^2 (1 + s)}{(1 + 3s)}\right]$$

Transform back, but only consider times $t = 0$ and $t = \infty$,

$$u = p(1.4464)\left(0.144\, r \begin{bmatrix} t=0 \to 1/3 \\ t=\infty \to 1 \end{bmatrix} + \frac{6.0}{r} \begin{bmatrix} t=0 \to 1/3 \\ t=\infty \to 1 \end{bmatrix}\right) \quad \ldots 3$$

Thus we now have $u = p\, f(r)$

Now calculate the initial displacements in the frozen ground under the original insitu stress of 8 MPa (by elastic hollow cylinder equations).

u = 3.456 mm inwards, and occurs before the tunnel is constructed. It is not included in the finite element analyses, but is included in the displacements in the visco-elastic ground.

Consider the ring of unfrozen ground. Apply an inward stress p' to the inside edge of the unfrozen ground to give the changes from the initial state due to the excavation of the opening.

i.e. 8 MPa - p' = supporting pressure on the unfrozen ground from the frozen ground.

$u_{r=9}$ (unfrozen) = 2.4313 p' (from elastic hollow cylinder equations)..... 4

$u_{r=9}$ (frozen) = 0.94629 p (at t=0 equation 3)..... 5

but this includes the initial displacement of 3.456 mm, which must be subtracted to give changes from the initial state.

Now,

$$p = 8 - p'$$

So solving equations (4) and (5)

$$\left.\begin{aligned} p' &= 1.2181 \\ u &= 2.9616 \end{aligned}\right\} \text{ at } r=9$$

Similarly at $t=\infty$

Back substitute for p in equations (3) to give equations for σ_r, σ_θ and u, at t = 0 and $t=\infty$.

Similarly for the lined case.

See Figures 2.17 and 2.18 for the results.

APPENDIX 5

RESULTS FROM THE ANALYSES - TUNNELS

Summary

Presented in this appendix are the results of the analyses carried out on unlined and lined tunnels, with and without rock damage (simulated by rock softening). The results from cases where excavation was carried out in frozen ground, which was subsequently thawed, are also presented. Table A5.1 gives information on the different analyses carried out, and lists the figures (both in the appendix and in the main text) where the results for each analysis may be found.

Table A5.1
Analyses Carried Out - Tunnels

Run No.	Construction Case	Mesh Used	Ground Type	Damaged Ground Type	Liner Type	Excavation Steps	Relevant Figure Numbers for Data: Radial Displacements	Liner Stresses	Ground Stresses	Ground Displacements	Remarks
1	0	2	R1	-	-	6	2.20(A5.6)	-	A5.43*	A5.37*	*CONSTEP used
2	1	2	R1	-	L1	8	2.21(A5.7) 2.27,A5.1	A5.16-A5.21	A5.47,A5.51	2.28,2.29 A5.38	
3	2	2	R1	-	L1	8	A5.2	A5.16-A5.21	A5.48,A5.52	2.30,A5.40	
4	3	2	R1	R5	L1	8	A5.3	A5.16-A5.18 A5.20-A5.21	-	2.31	
5	4	2	R1	R5	L1	7	A5.4	A5.16-A5.18	A5.49,A5.53	A5.41	
6	4	2	R1	R7	L1	7	A5.5	A5.16-A5.18	-	-	
7	4*	2	R1	R7	L1	6	A5.5	A5.19	-	-	*Liner placed as Case 2
8	0	6	R1	-	-	4	2.20(A5.6)	-	-	-	
9	0	7	R1	-	-	4	2.20(A5.6)	-	8.2,8.10 A5.44	-	
10	1	6	R1	-	L1	5	2.21(A5.7) A5.8	A5.19-A5.24 A5.28-A5.30 8.8	A5.54	A5.39	
11	1	7	R1	-	L1	5	2.22,A5.8	A5.22-A5.24	8.2,8.10 A5.45	8.3	
12	2	6	R1	-	L1	4	A5.9	A5.28-A5.30 8.8	-	-	
13	5	6	R1	R7	L1	5	A5.10	A5.28-A5.30 8.8	-	-	
14	6	6	R1	R7	L1	4	A5.11	A5.25-A5.30 8.8	A5.50	A5.42	
15	7	6	R1	R7	L1	5	A5.12	A5.28-A5.30 8.8	-	-	
16	6	7	R1	R5	L1	4	A5.11	A5.25-A5.27	8.2,8.11 A5.46	8.3	
17	6V*	7	R1	R5,8,11	L1	4	A5.13	-	-	-	*Unlined
18	6V	7	R1	R5,8,11	L1	5	A5.13	A5.31-A5.33	8.2	8.3	
19	6V*	7	R1	R5,8,11	L1	5	A5.13	A5.31-A5.33	-	-	*Liner as Case 2
20	1*	7	R1	R4	L1	5	A5.14	A5.34-A5.36	-	-	*Frozen ground
21	2*	7	R1	R4	L1	5	A5.15	A5.34-A5.36	-	-	*Frozen ground

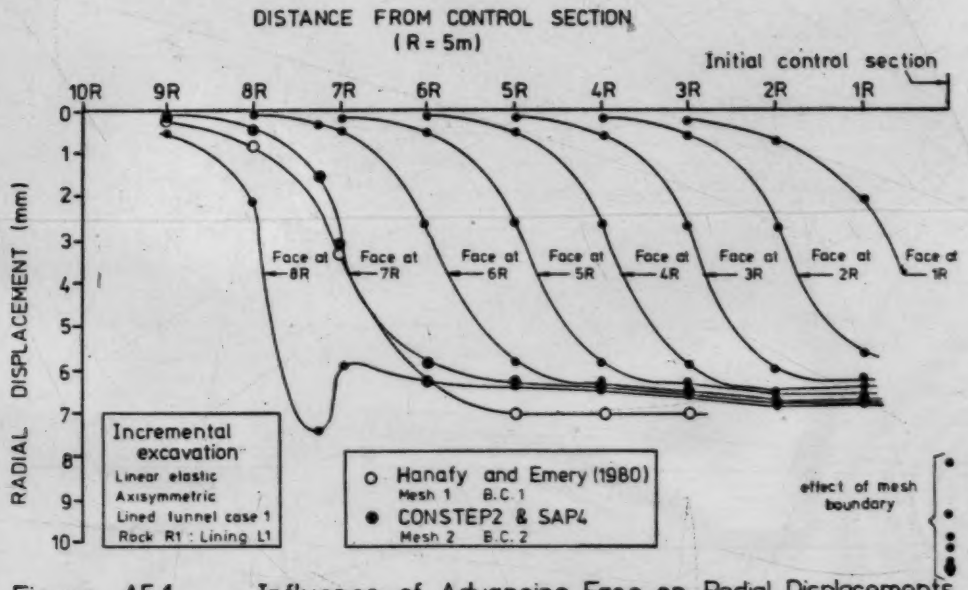

Figure A5.1 Influence of Advancing Face on Radial Displacements, Lined Tunnel Case 1, Mesh 2

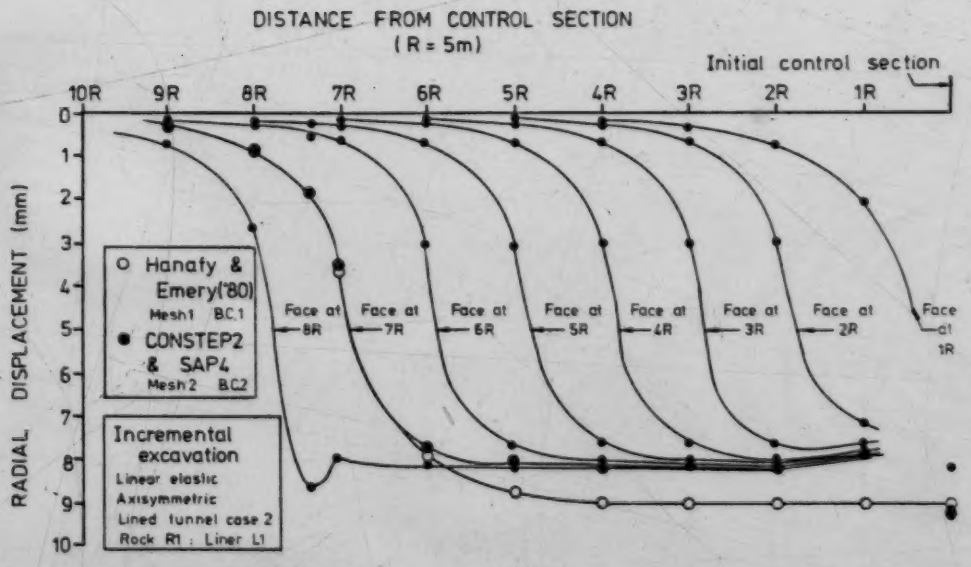

Figure A5.2 Influence of Advancing Face on Radial Displacements, Lined Tunnel Case 2, Mesh 2

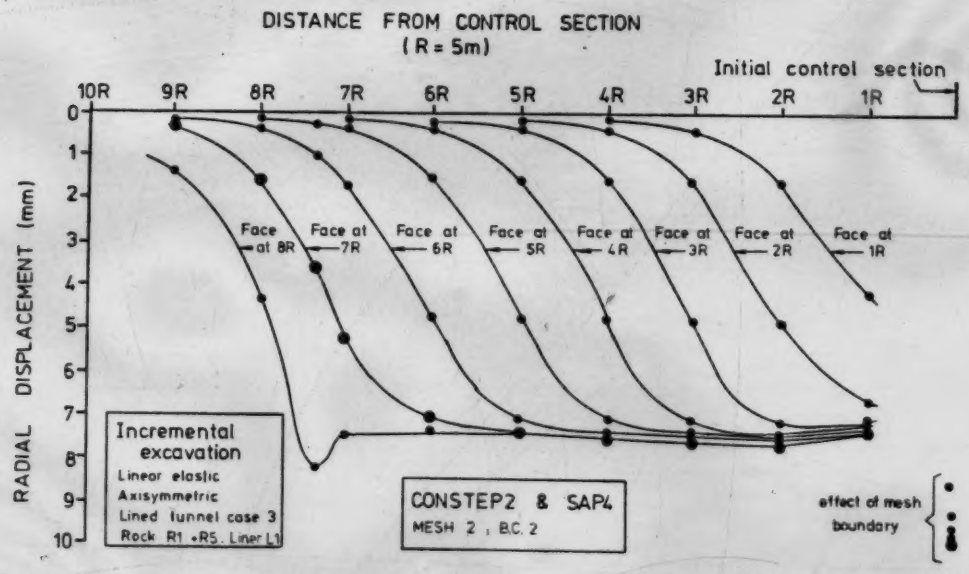

Figure A5.3 Influence of Advancing Face on Radial Displacements, Lined Tunnel Case 3, Mesh 2

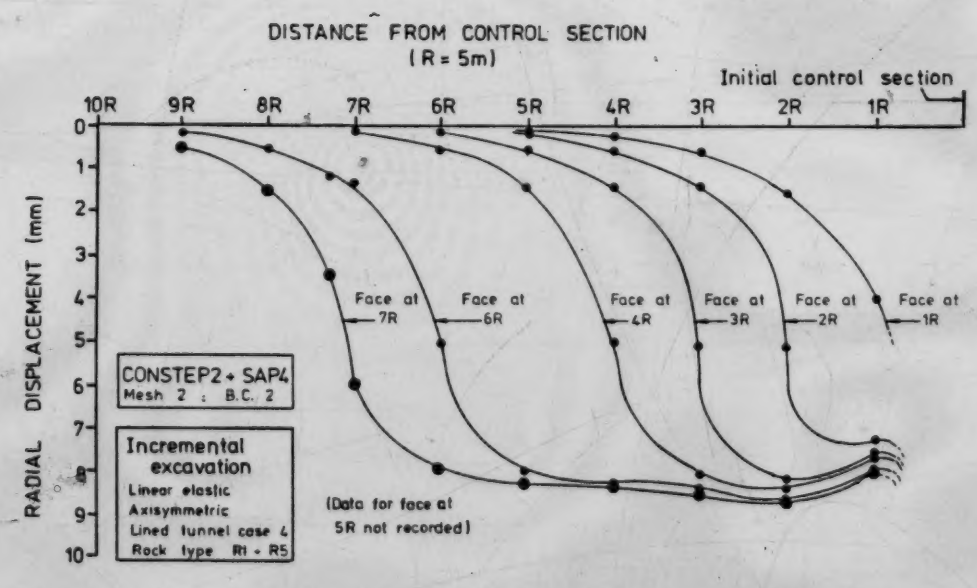

Figure A5.4 Influence of Advancing Face on Radial Displacements, Lined Tunnel Case 4 - a, Mesh 2

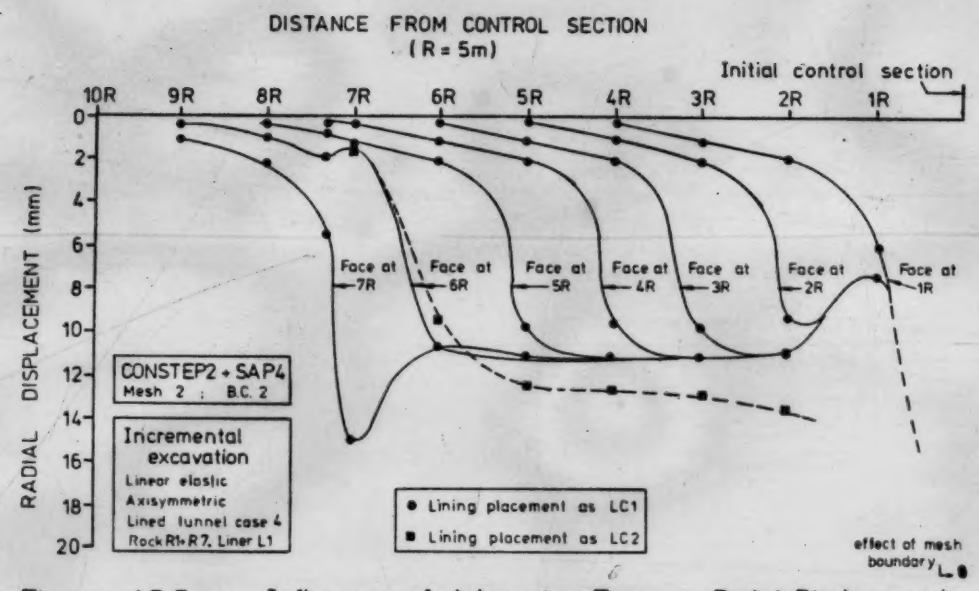

Figure A5.5 Influence of Advancing Face on Radial Displacements, Lined Tunnel Case 4 - b, Mesh 2

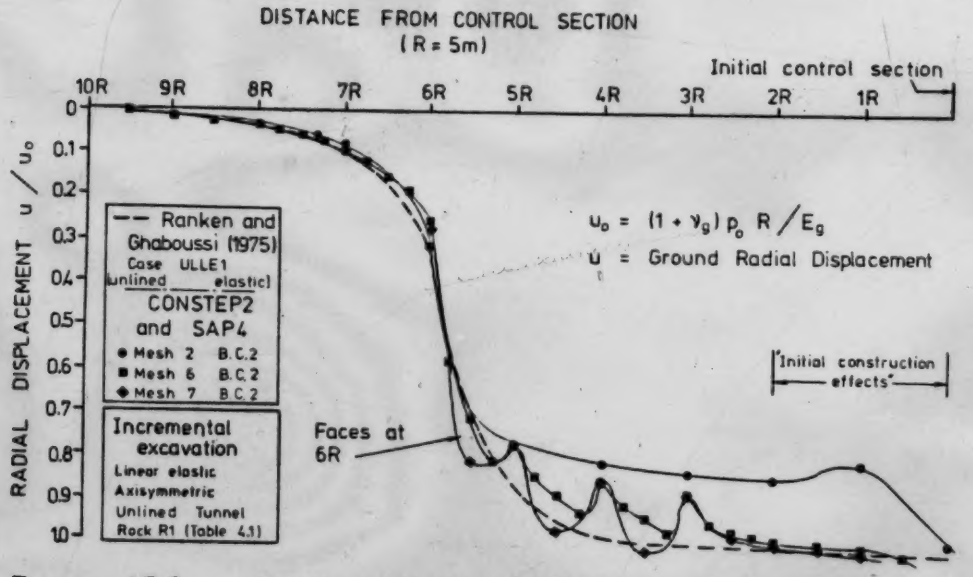

Figure A5.6 Influence of Advancing Face on Radial Displacements, Unlined Tunnel Case

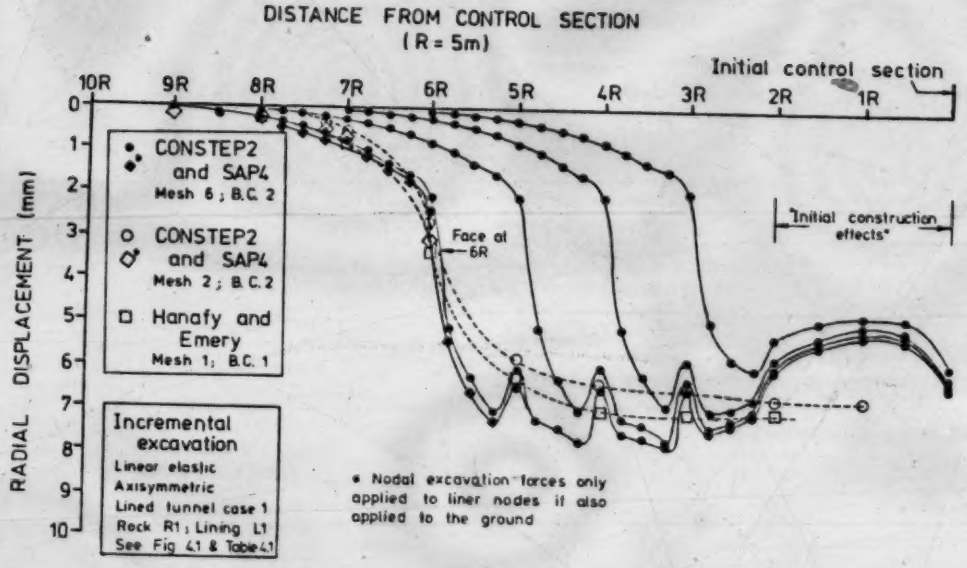

Figure A5.7 Influence of Advancing Face on Radial Displacements, Lined Tunnel Case 1, Meshes 2 and 6

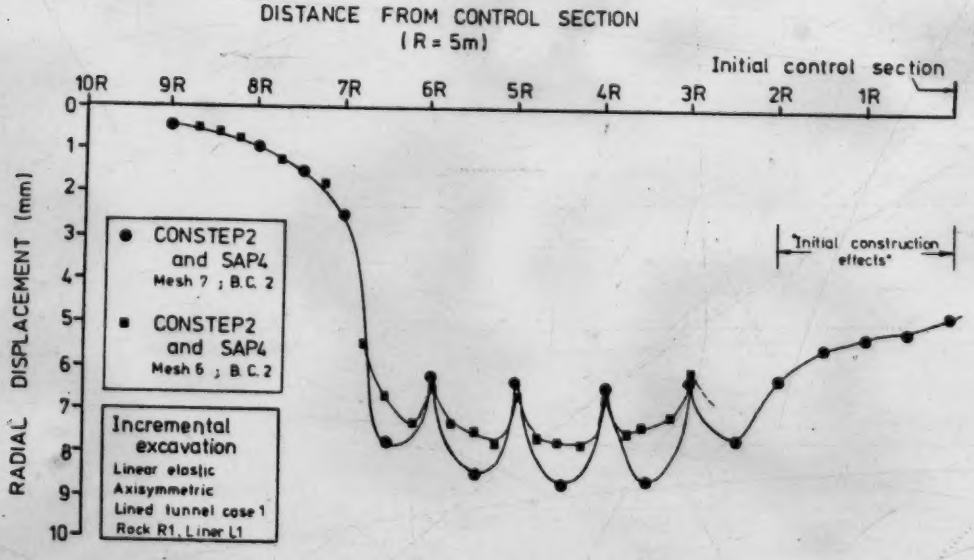

Figure A5.8 Influence of Advancing Face on Radial Displacements, Lined Tunnel Case 1, Meshes 6 and 7

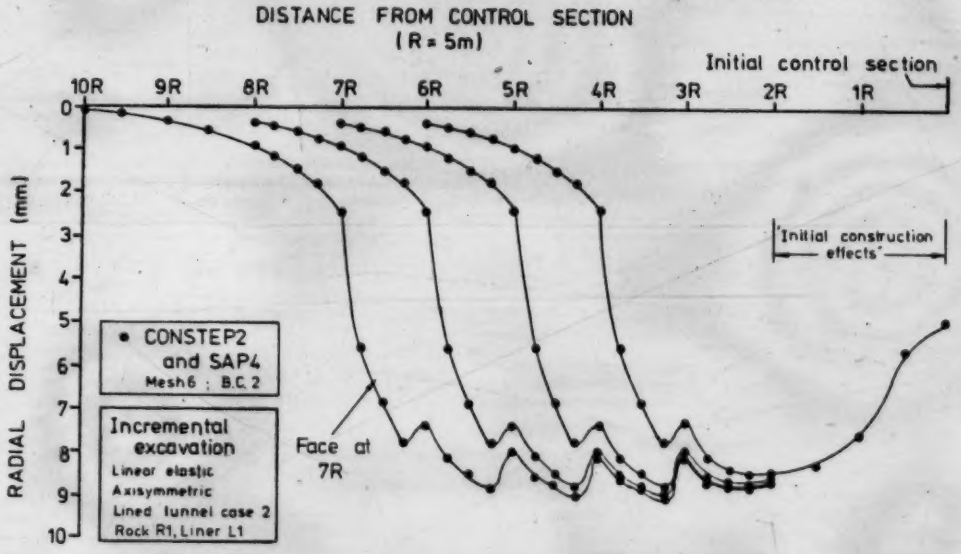
DISTANCE FROM CONTROL SECTION
(R = 5m)
Initial control section
10R 9R 8R 7R 6R 5R 4R 3R 2R 1R
RADIAL DISPLACEMENT (mm)
0 1 2 3 4 5 6 7 8 9 10
"Initial construction effects"
• CONSTEP2 and SAP4
Mesh 6 ; B.C. 2
Incremental excavation
Linear elastic
Axisymmetric
Lined tunnel case 2
Rock R1, Liner L1
Face at 7R

Figure A5.9 Influence of Advancing Face on Radial Displacements, Lined Tunnel Case 2, Mesh 6

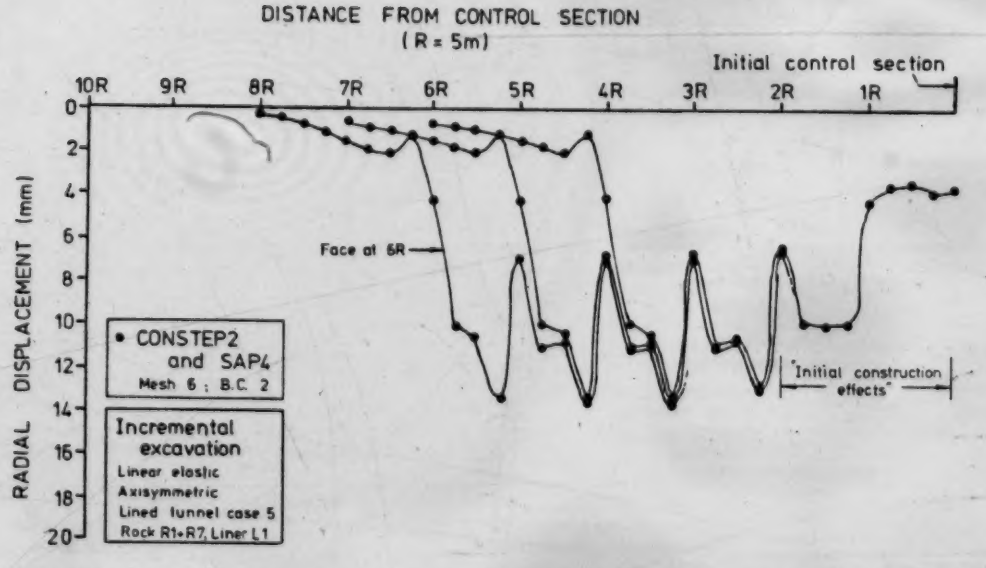
DISTANCE FROM CONTROL SECTION
(R = 5m)
Initial control section
10R 9R 8R 7R 6R 5R 4R 3R 2R 1R
RADIAL DISPLACEMENT (mm)
0 2 4 6 8 10 12 14 16 18 20
Face at 6R
"Initial construction effects"
• CONSTEP2 and SAP4
Mesh 6 ; B.C. 2
Incremental excavation
Linear elastic
Axisymmetric
Lined tunnel case 5
Rock R1+R7, Liner L1

Figure A5.10 Influence of Advancing Face on Radial Displacements, Lined Tunnel Case 5, Mesh 6

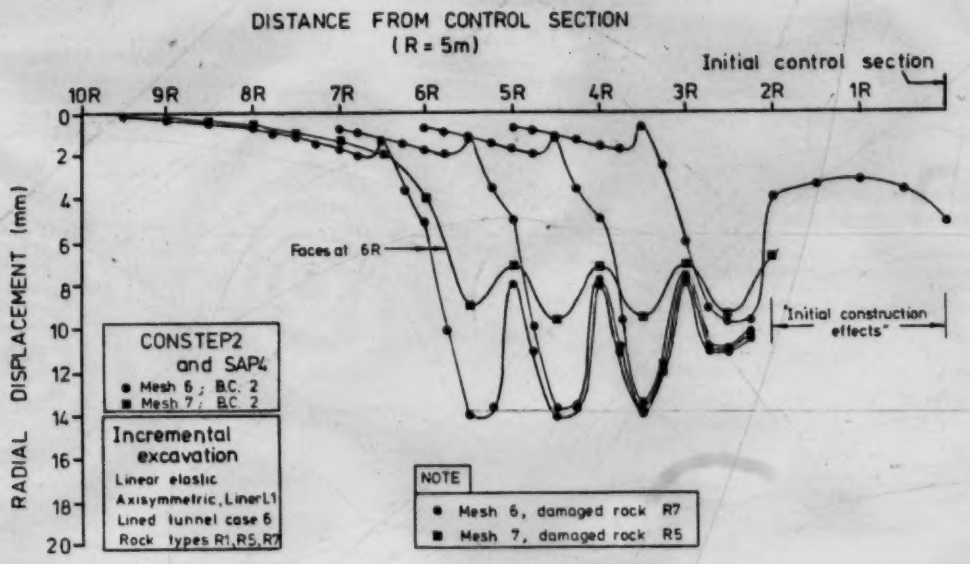
DISTANCE FROM CONTROL SECTION
(R = 5m)
Initial control section
10R 9R 8R 7R 6R 5R 4R 3R 2R 1R
RADIAL DISPLACEMENT (mm)
0 2 4 6 8 10 12 14 16 18 20
Faces at 6R
"Initial construction effects"
CONSTEP2 and SAP4
Mesh 6 ; B.C. 2
Mesh 7 ; B.C. 2
Incremental excavation
Linear elastic
Axisymmetric, Liner L1
Lined tunnel case 6
Rock types R1, R5, R7
NOTE
Mesh 6, damaged rock R7
Mesh 7, damaged rock R5

Figure A5.11 Influence of Advancing Face on Radial Displacements, Lined Tunnel Case 6, Meshes 6 and 7

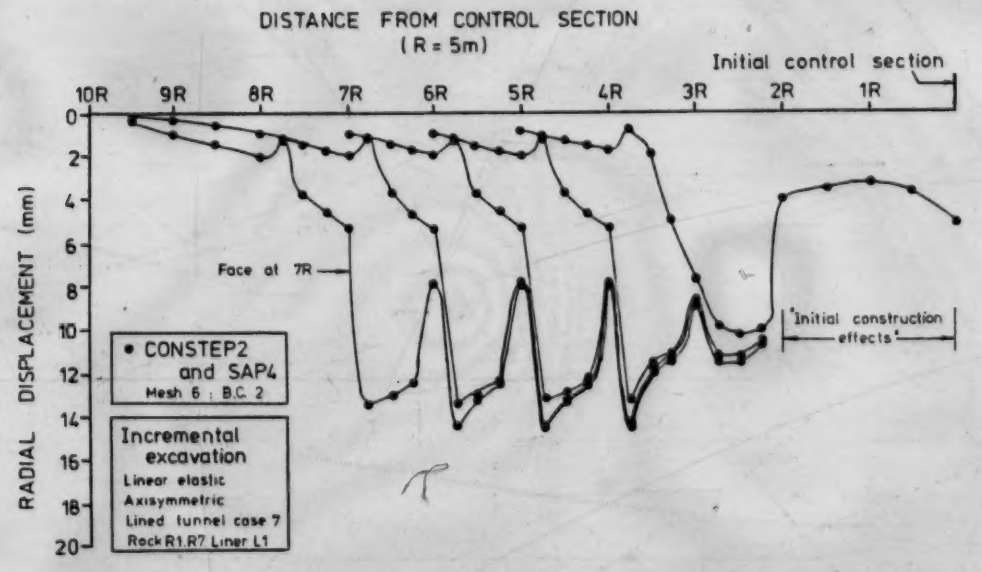
DISTANCE FROM CONTROL SECTION
(R = 5m)
Initial control section
10R 9R 8R 7R 6R 5R 4R 3R 2R 1R
RADIAL DISPLACEMENT (mm)
0 2 4 6 8 10 12 14 16 18 20
Face at 7R
"Initial construction effects"
CONSTEP2 and SAP4
Mesh 6 ; B.C. 2
Incremental excavation
Linear elastic
Axisymmetric
Lined tunnel case 7
Rock R1, R7 Liner L1

Figure A5.12 Influence of Advancing Face on Radial Displacements, Lined Tunnel Case 7, Mesh 6

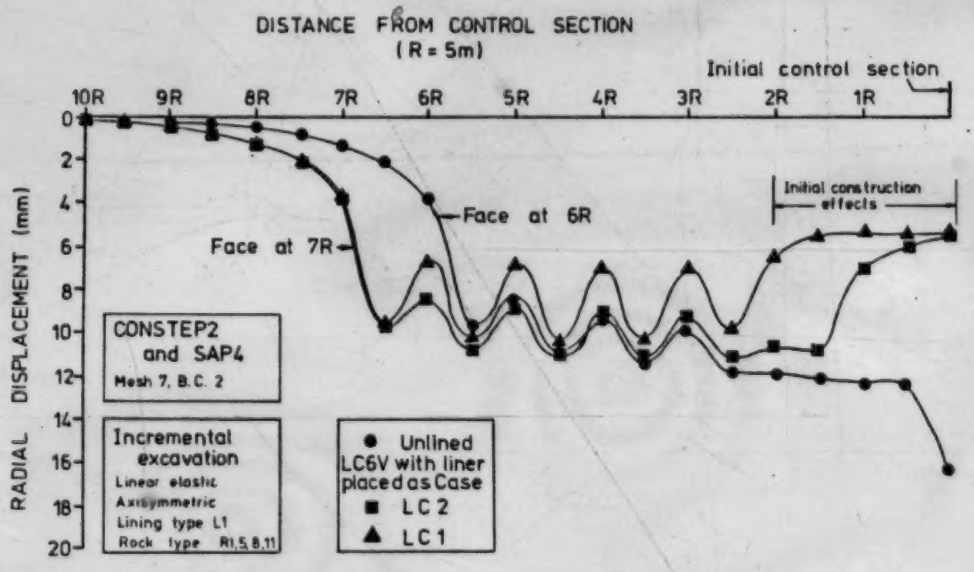

Figure A5.13 Influence of Advancing Face on Radial Displacements, Confining Pressure Effect Simulated.

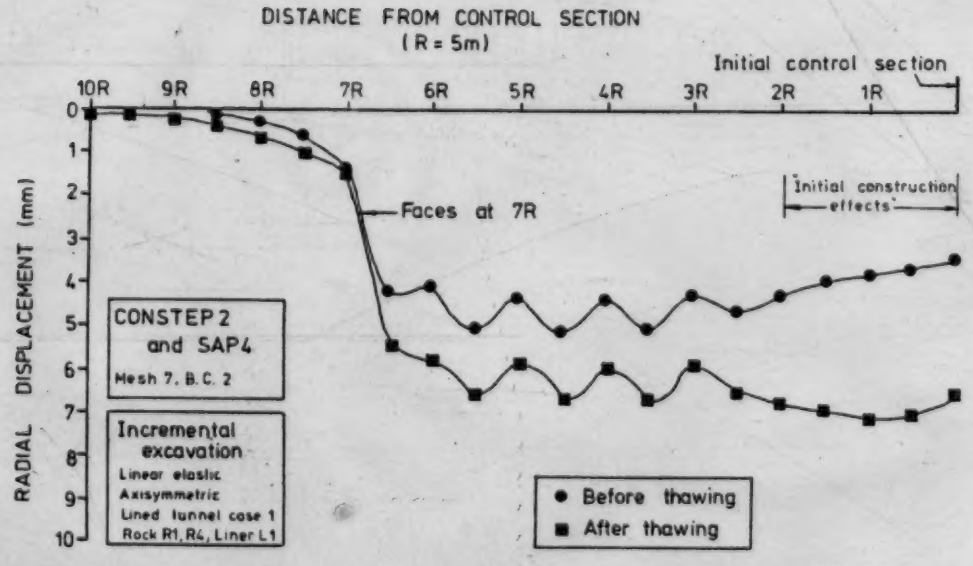

Figure A5.14 Influence of Advancing Face on Radial Displacements, Lined Tunnel Case 1 – Frozen Ground.

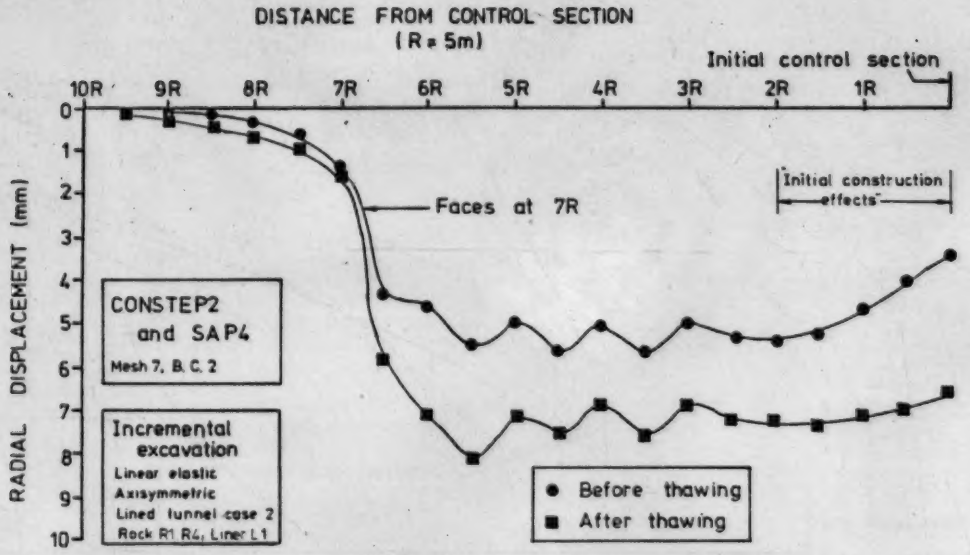

Figure A5.15 Influence of Advancing Face on Radial Displacements, Lined Tunnel Case 2 — Frozen Ground

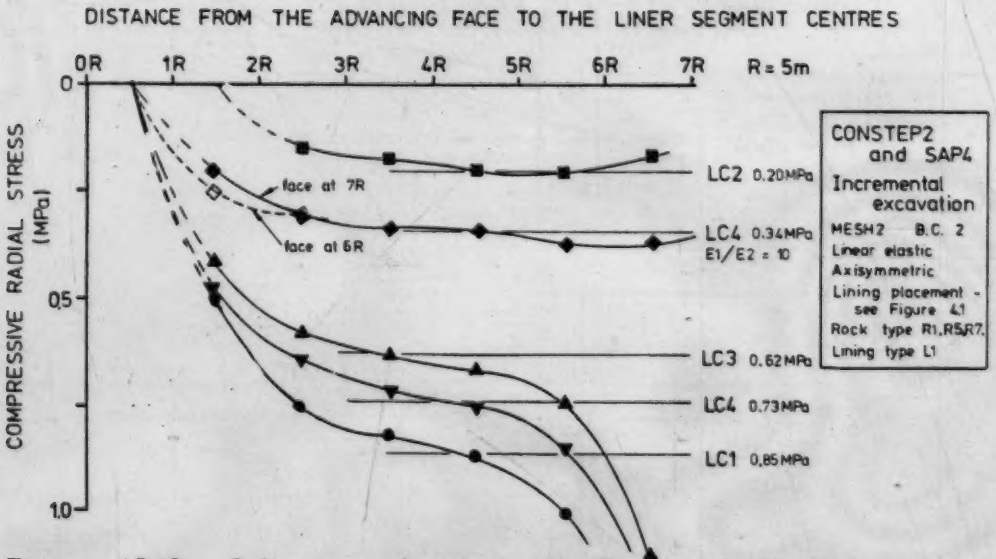

Figure A5.16 Influence of Advancing Face and Liner Placement on Liner Radial Stress, Mesh 2

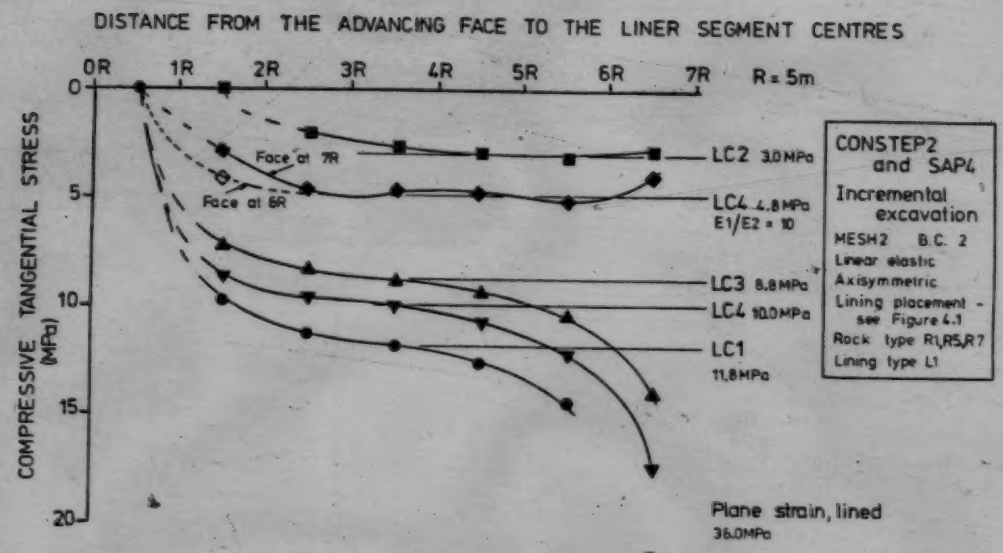

Figure A5.17 Influence of Advancing Face and Liner Placement on Liner Tangential Stress, Mesh 2

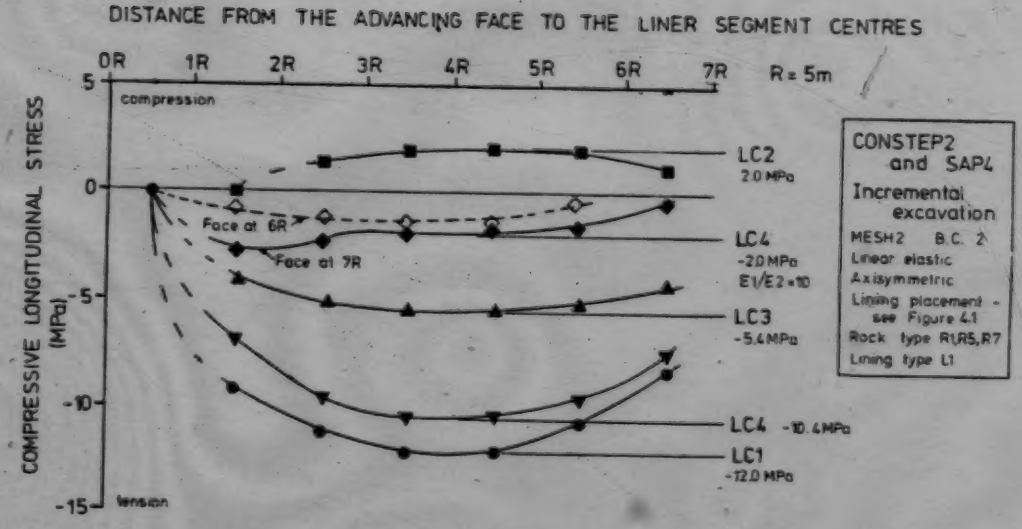

Figure A5.18 Influence of Advancing Face and Liner Placement on Liner Longitudinal Stress, Mesh 2

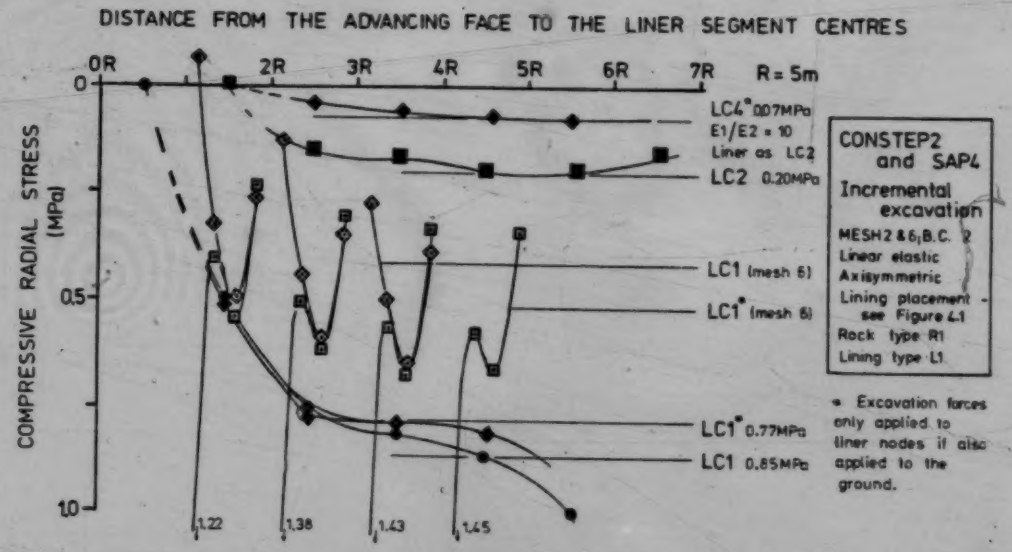

Figure A5.19 Influence of Advancing Face and Liner Placement on Liner Radial Stress, Meshes 2 and 6

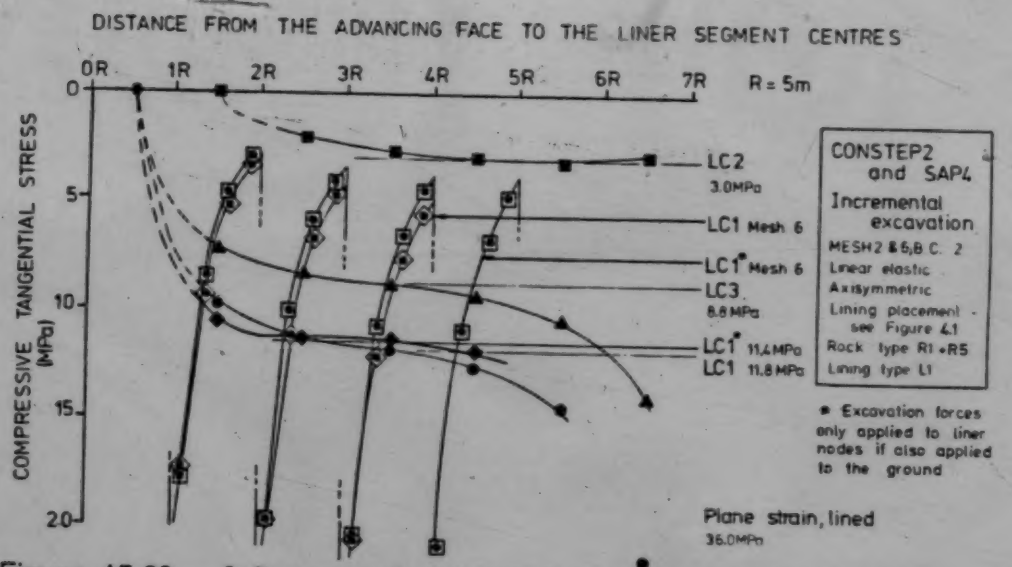

Figure A5.20 Influence of Advancing Face and Liner Placement on Liner Tangential Stress, Meshes 2 & 6

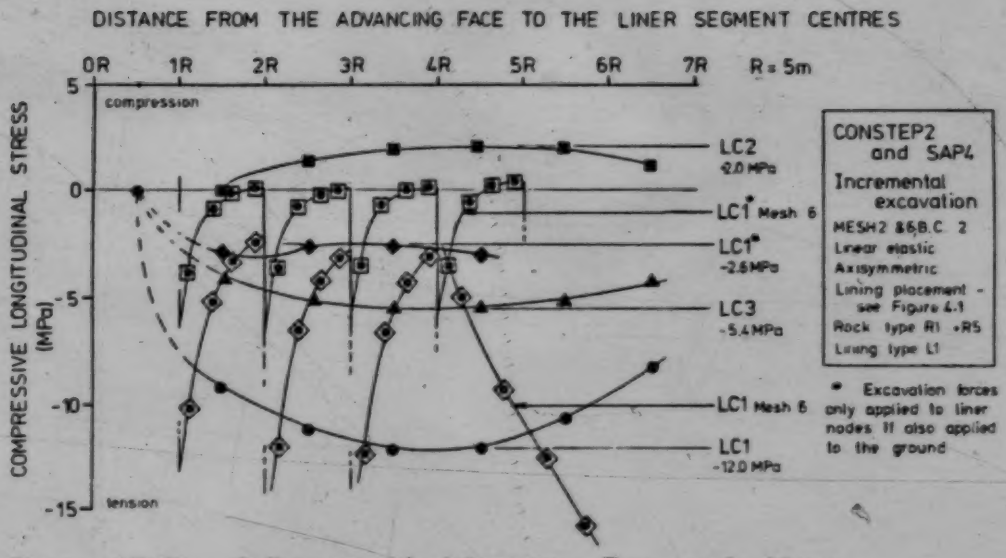

Figure A5.21 Influence of Advancing Face and Liner Placement on Liner Longitudinal Stress, Meshes 2&6

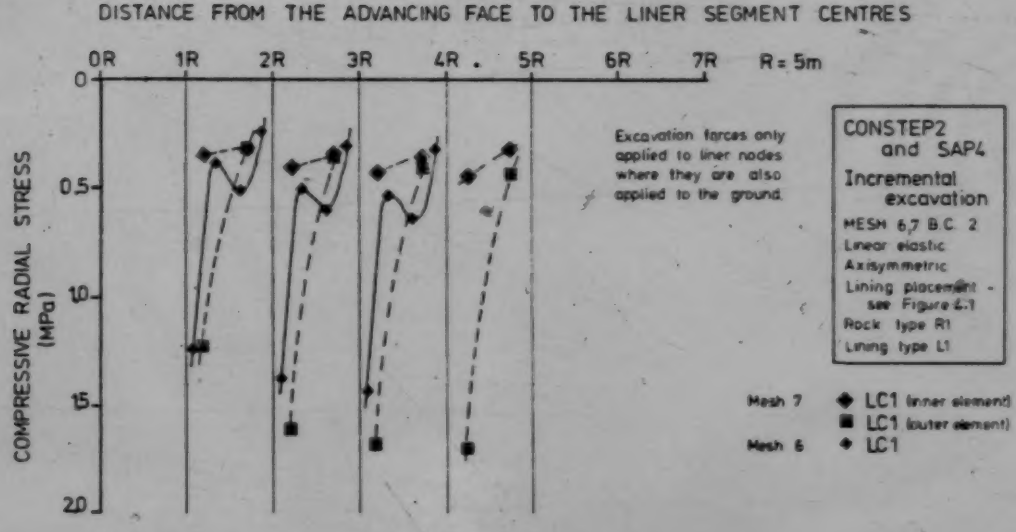
DISTANCE FROM THE ADVANCING FACE TO THE LINER SEGMENT CENTRES
0R 1R 2R 3R 4R 5R 6R 7R R = 5m
COMPRESSIVE RADIAL STRESS (MPa)
0
0.5
10
15
20
Excavation forces only applied to liner nodes where they are also applied to the ground
CONSTEP2 and SAP4
Incremental excavation
MESH 6,7 B.C 2
Linear elastic
Axisymmetric
Lining placement - see Figure 4.1
Rock type R1
Lining type L1
Mesh 7 LC1 (inner element)
LC1 (outer element)
Mesh 6 LC1

Figure A5.22 Influence of Advancing Face and Liner Placement on Liner Radial Stress, Meshes 6 and 7, Case 1

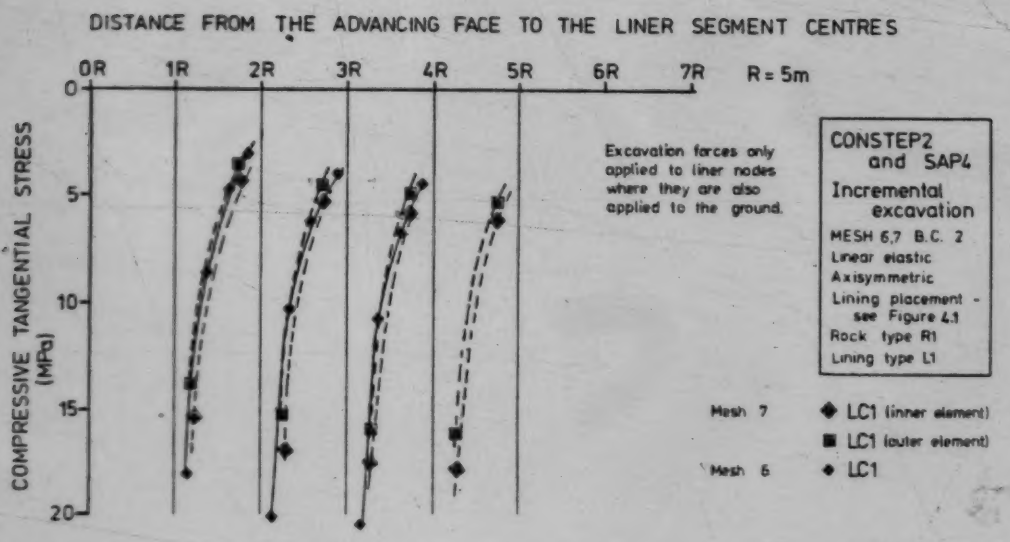

Figure A5.23 Influence of Advancing Face and Liner Placement on Liner Tangential Stress, Meshes 6 and 7, Case 1

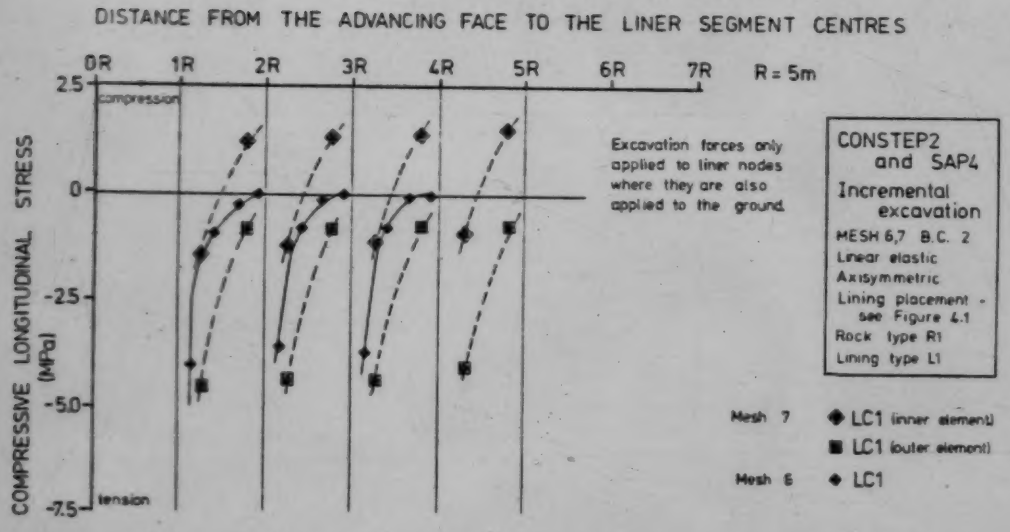

Figure A5.24 Influence of Advancing Face and Liner Placement on Liner Longitudinal Stresses, Meshes 6 and 7, Case 1

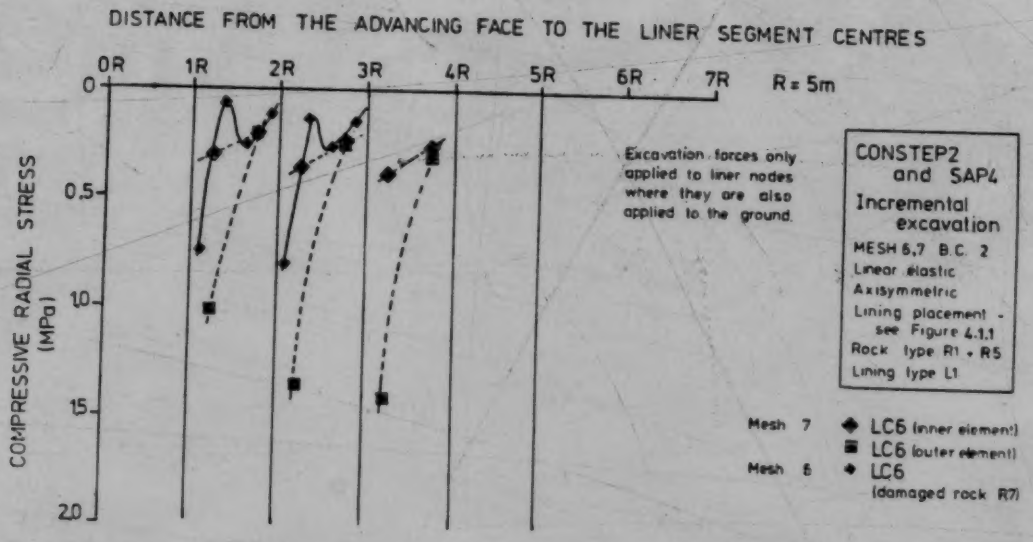

Figure A5.25 Influence of Advancing Face and Liner Placement on Liner Radial Stress, Meshes 6 and 7, Case 6

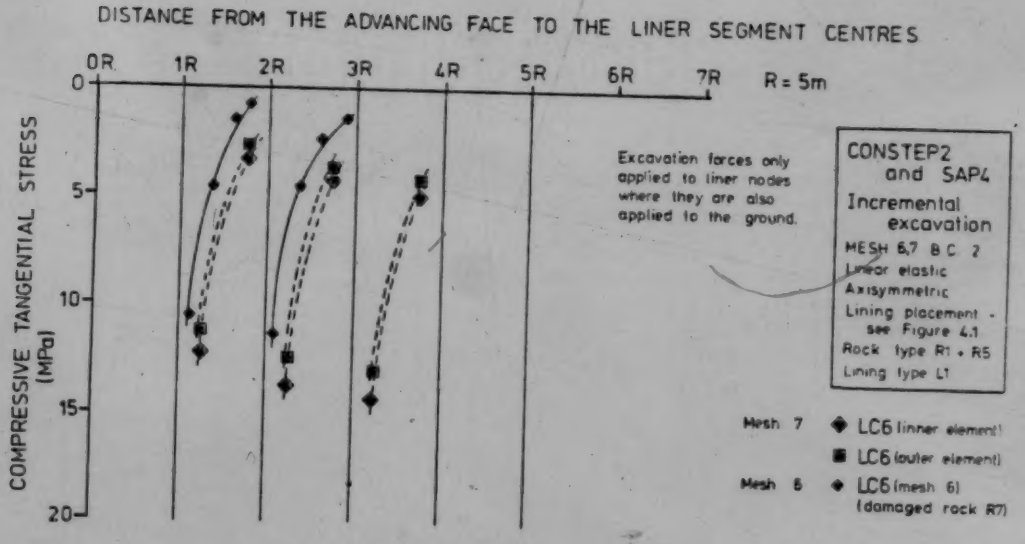

Figure A5.26 Influence of Advancing Face and Liner Placement on Liner Tangential Stress, Meshes 6 and 7, Case 6

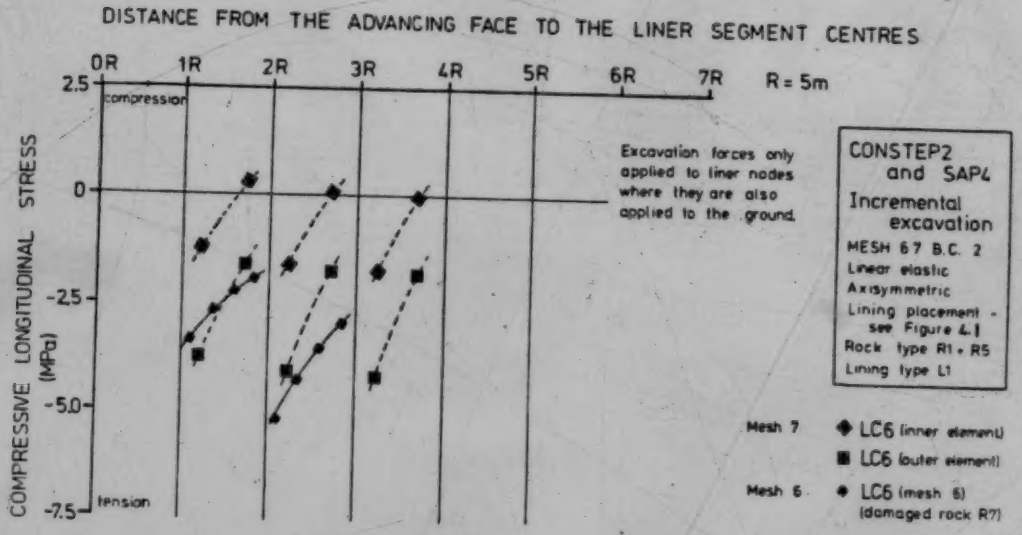

Figure A5.27 Influence of Advancing Face and Liner Placement on Liner Longitudinal Stress, Meshes 6 and 7, Case 6

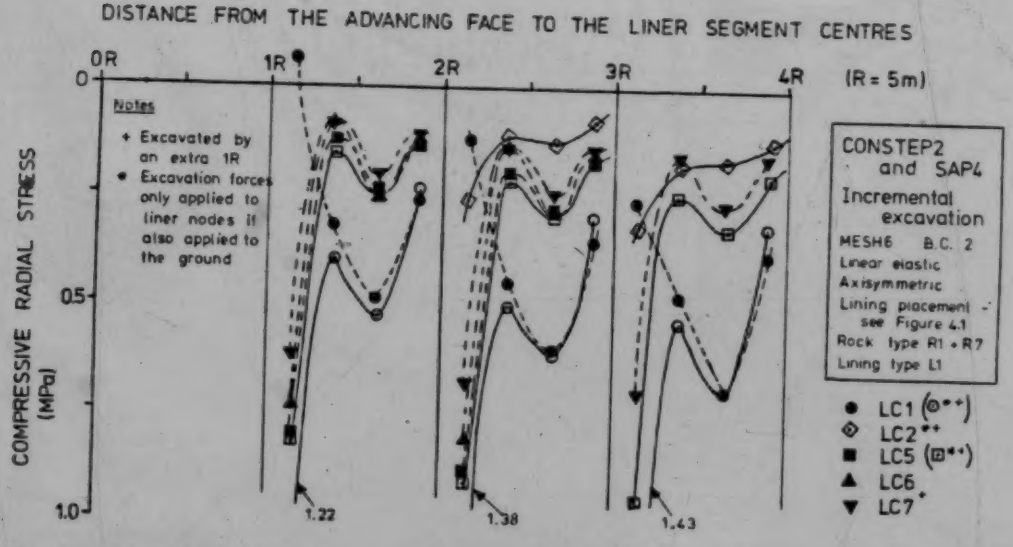

Figure A5.28 Influence of Advancing Face and Liner Placement on Liner Radial Stress, Mesh 6

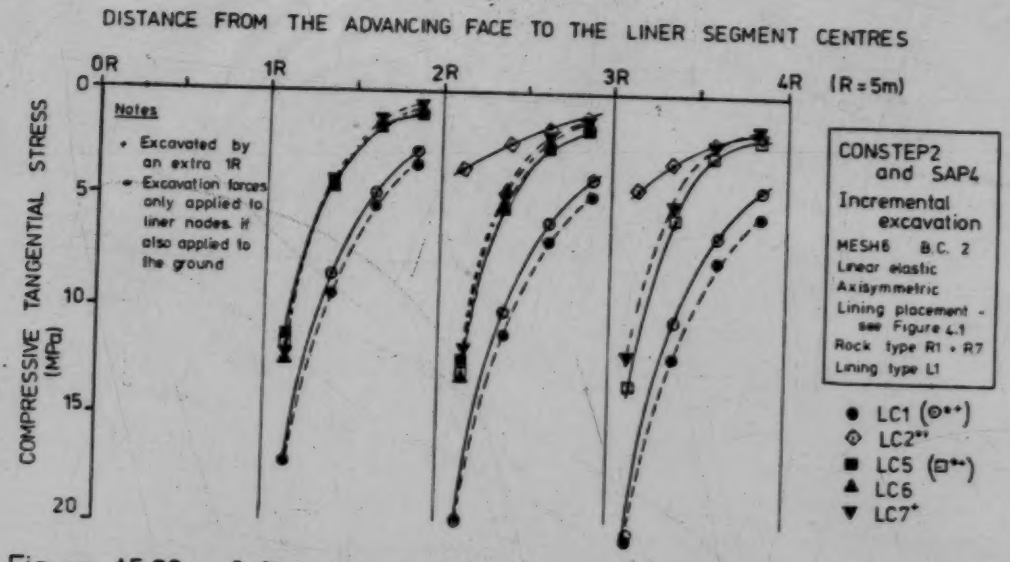

Figure A5.29 Influence of Advancing Face and Liner Placement on Liner Tangential Stress, Mesh 6

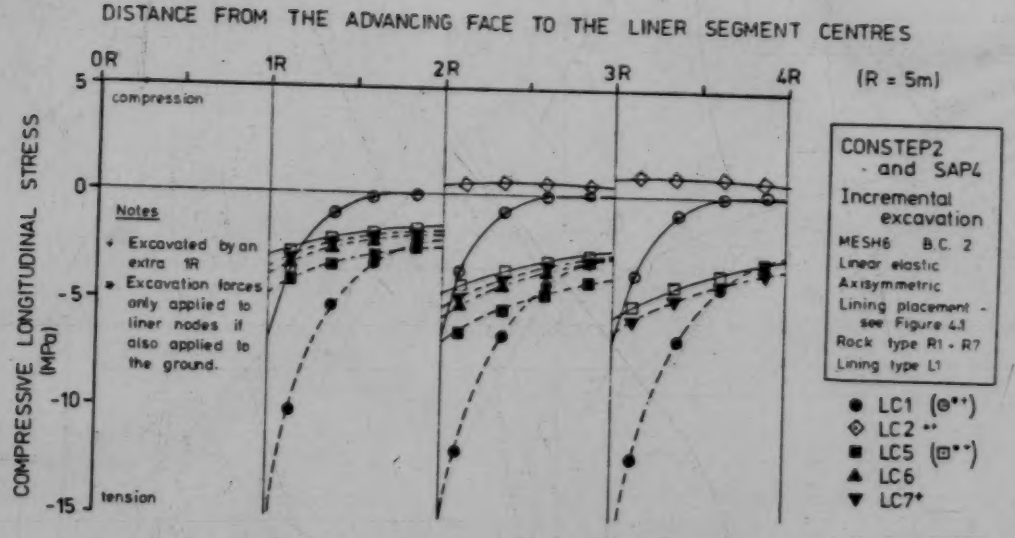

Figure A5.30 Influence of Advancing Face and Liner Placement on Liner Longitudinal Stress, Mesh 6

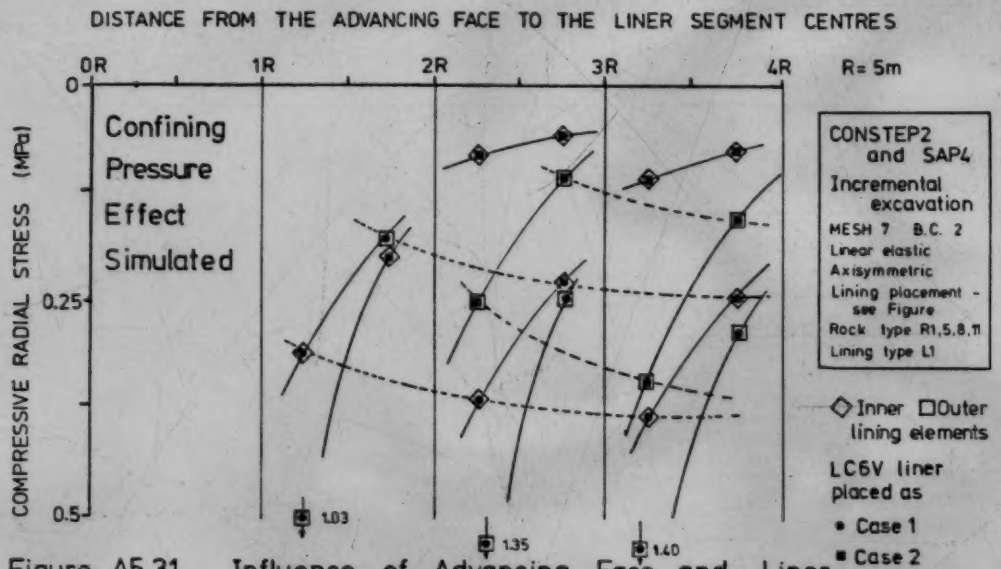

Figure A5.31 Influence of Advancing Face and Liner Placement on Liner Radial Stress

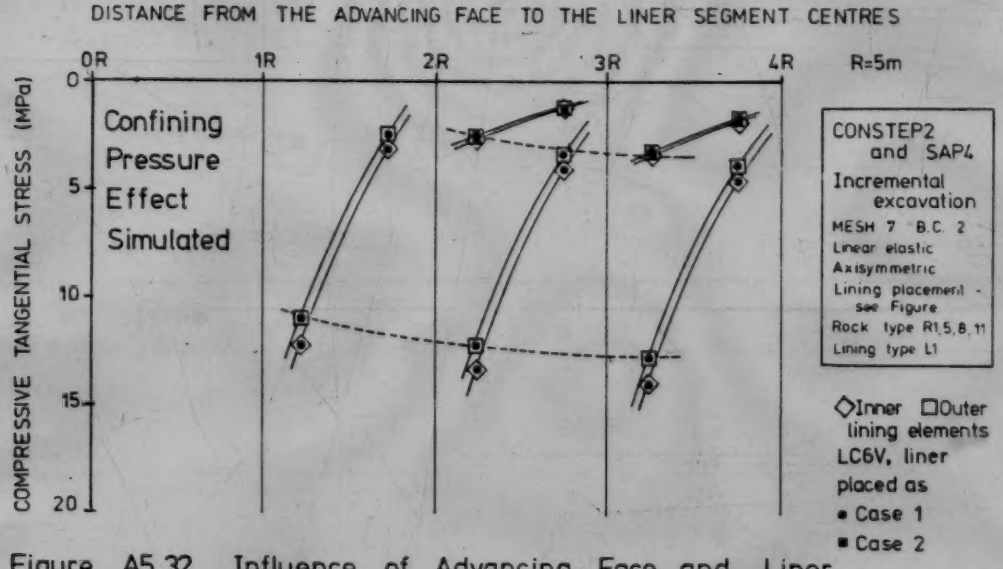

Figure A5.32 Influence of Advancing Face and Liner Placement on Liner Tangential Stress

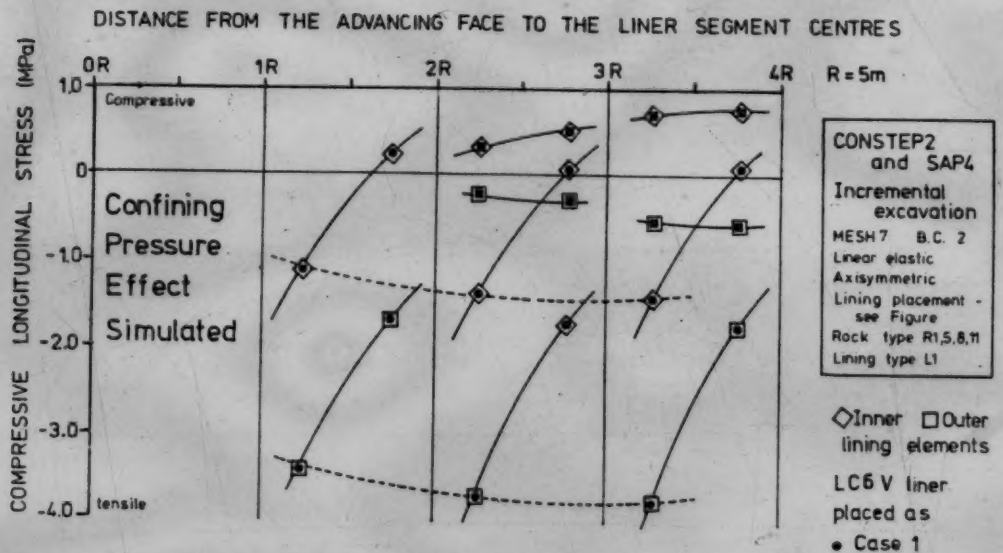

Figure A5.33 Influence of Advancing Face and Liner Placement on Liner Longitudinal Stress

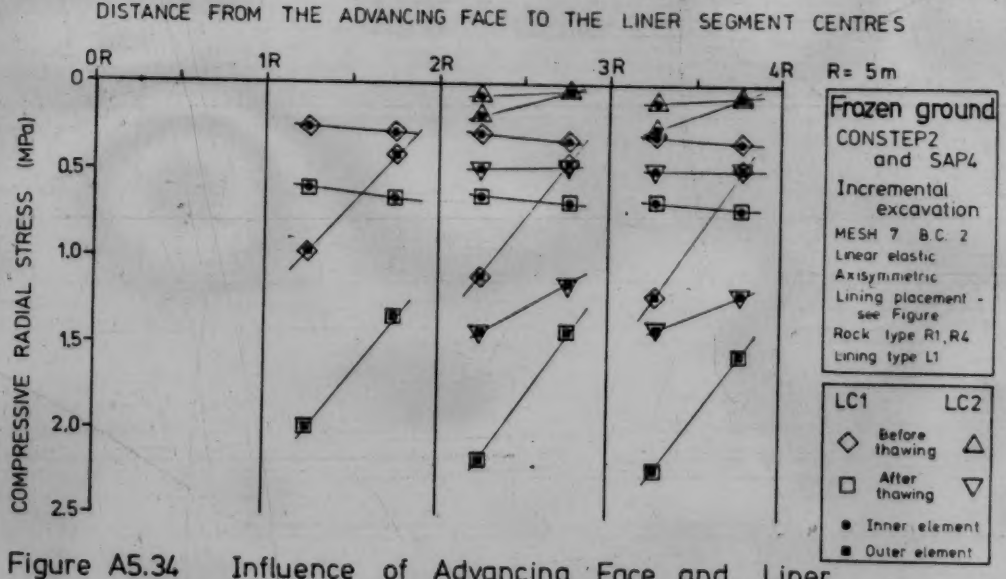

Figure A5.34 Influence of Advancing Face and Liner Placement on Liner Radial Stress

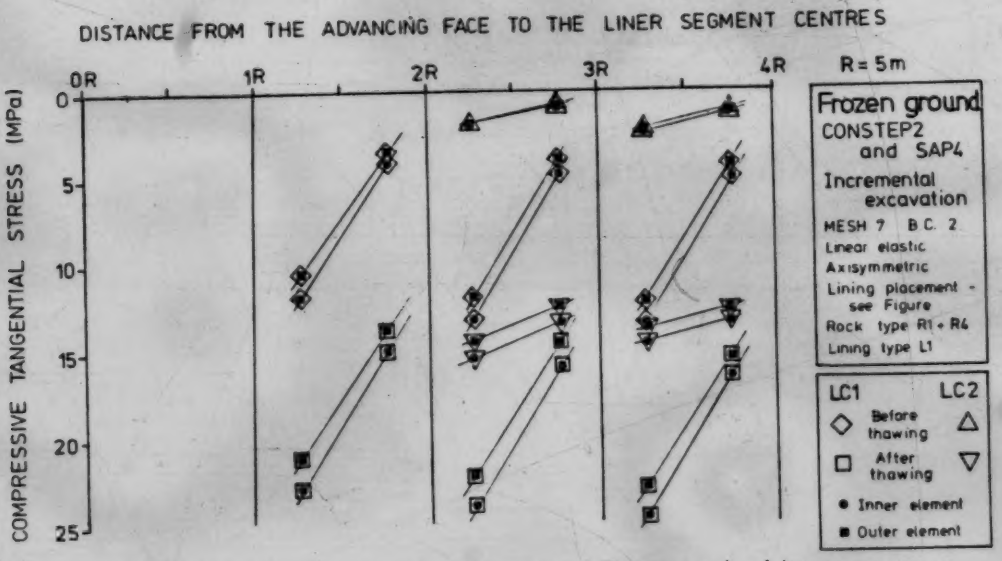

Figure A5.35 Influence of Advancing Face and Liner Placement on Liner Tangential Stress

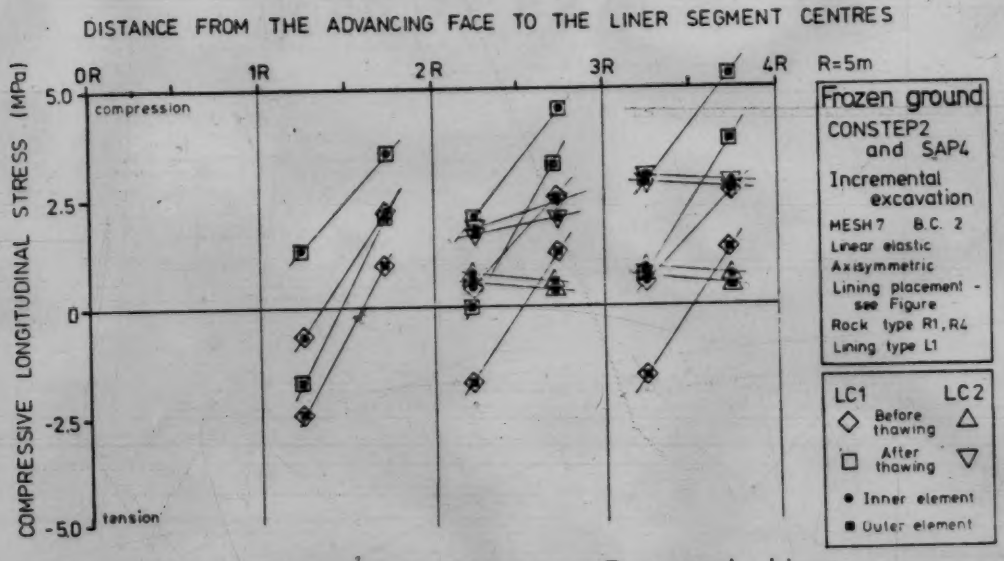

Figure A5.36 Influence of Advancing Face and Liner Placement on Liner Longitudinal Stress

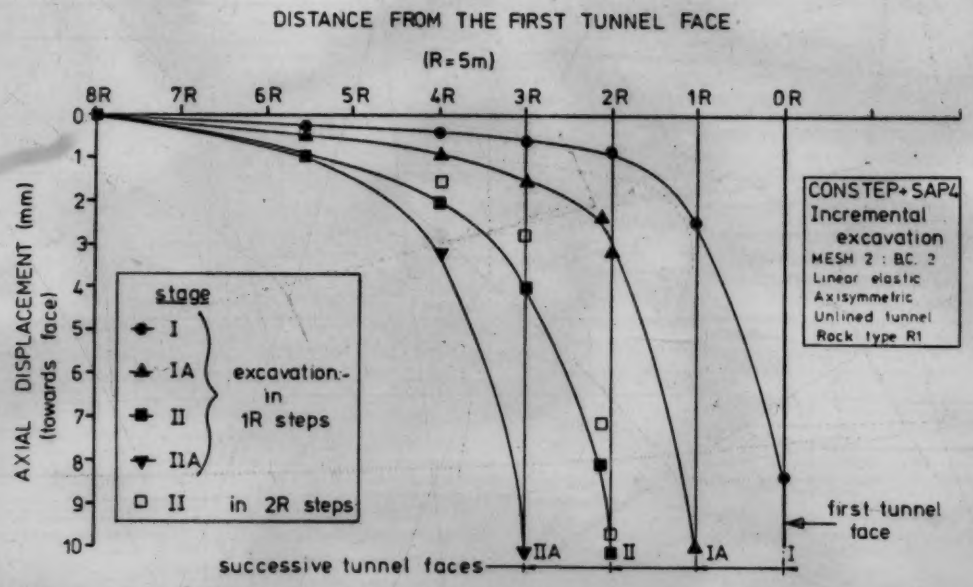

Figure A5.37 Influence of Advancing Face on Axial Displacements

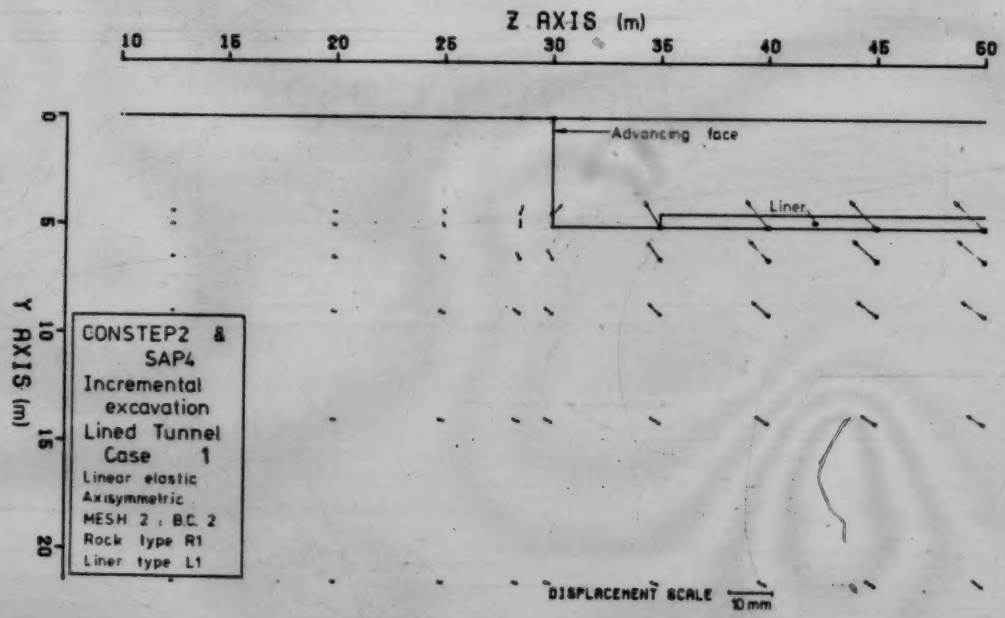

Figure A5.38 Advancing Face Effect on Radial Displacements
Mesh 2, Case 1

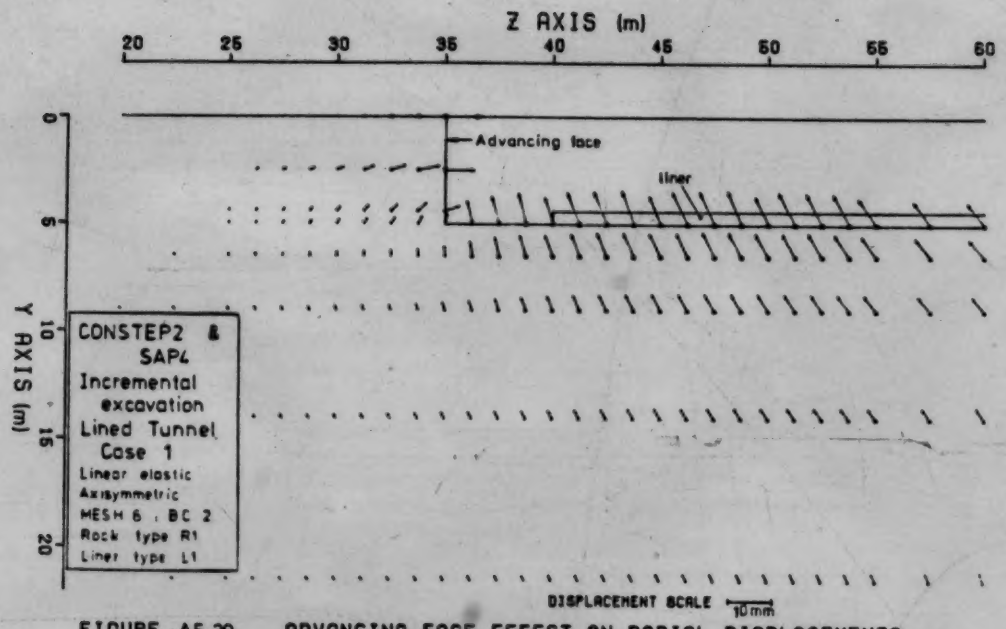

FIGURE A5.39 ADVANCING FACE EFFECT ON RADIAL DISPLACEMENTS, MESH 6, CASE 1

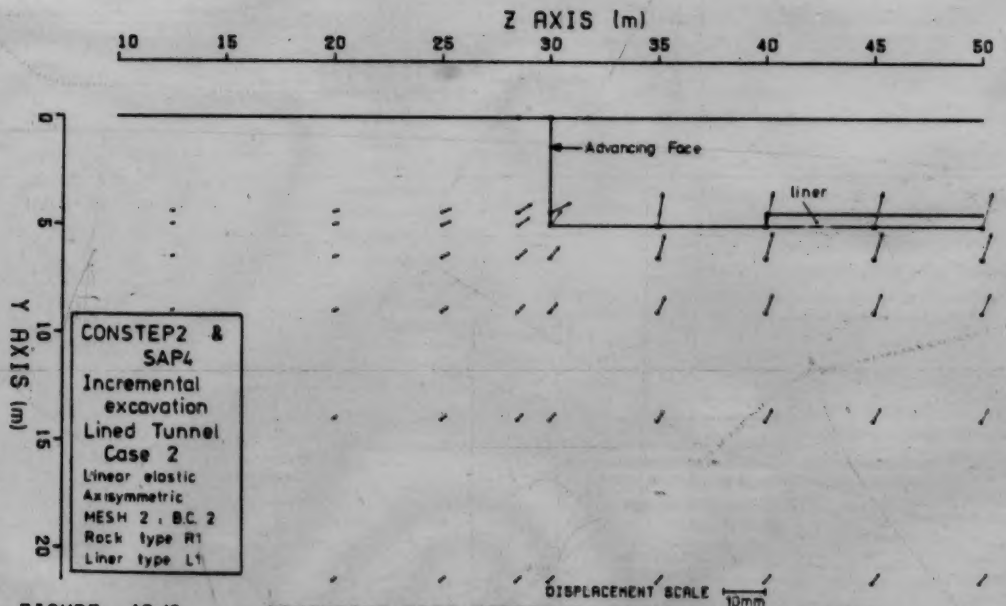

FIGURE A5.40 ADVANCING FACE EFFECT ON RADIAL DISPLACEMENTS, MESH 2, CASE 2

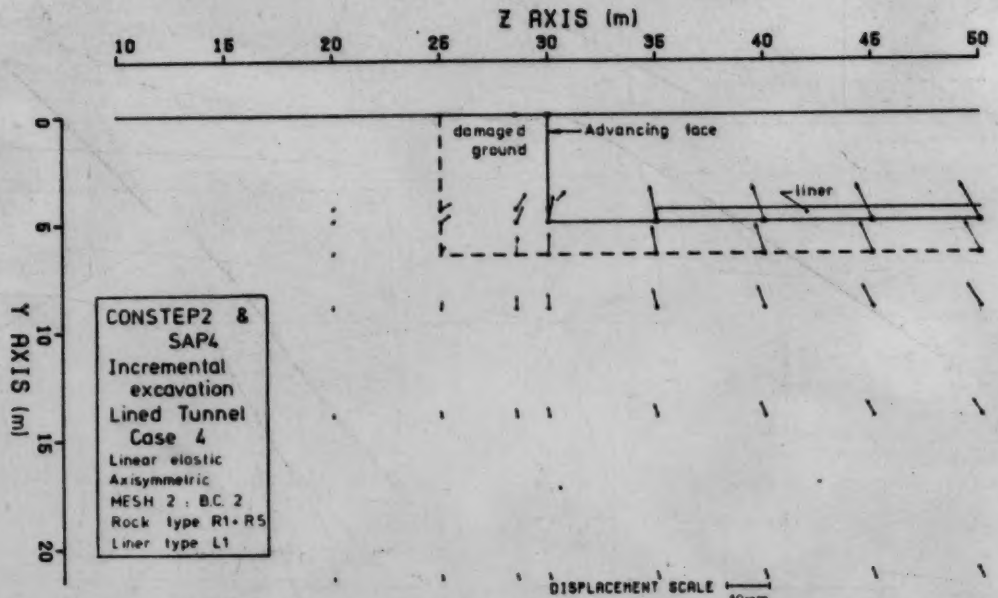

FIGURE A5.41 ADVANCING FACE EFFECT ON RADIAL DISPLACEMENTS, MESH 2, CASE 4

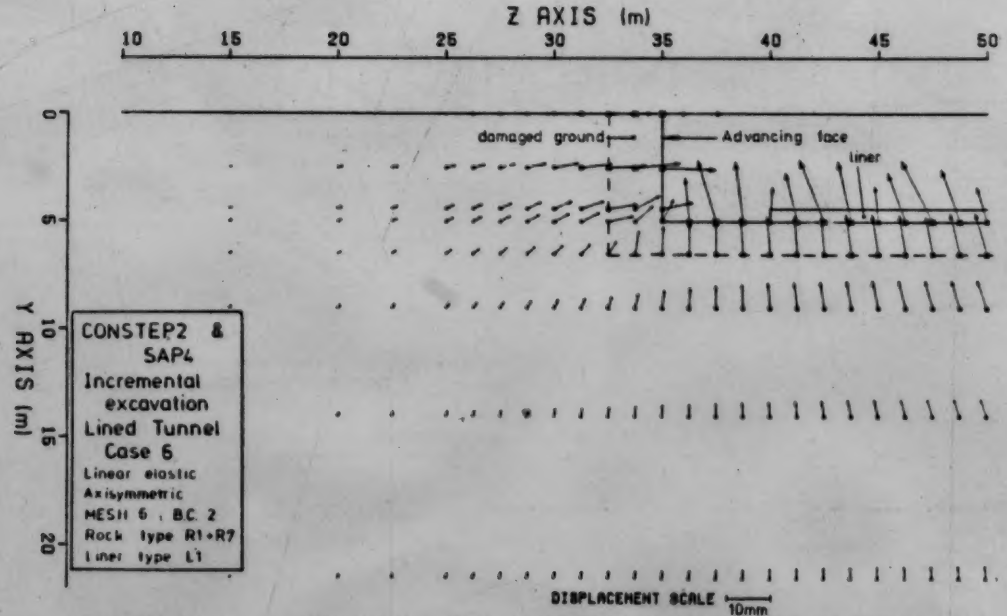

FIGURE A5.42 ADVANCING FACE EFFECT ON RADIAL DISPLACEMENTS, MESH 6, CASE 6

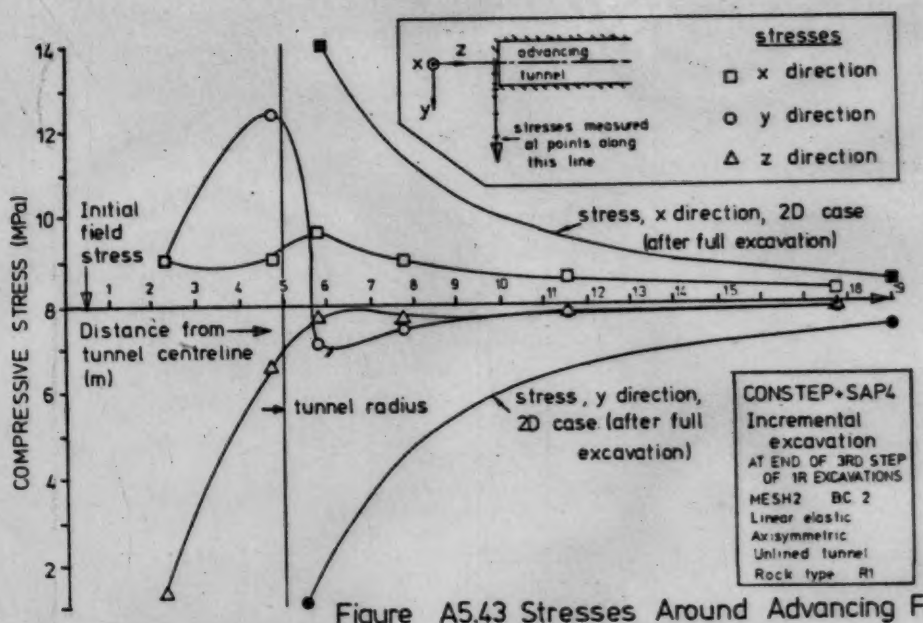

Figure A5.43 Stresses Around Advancing Face

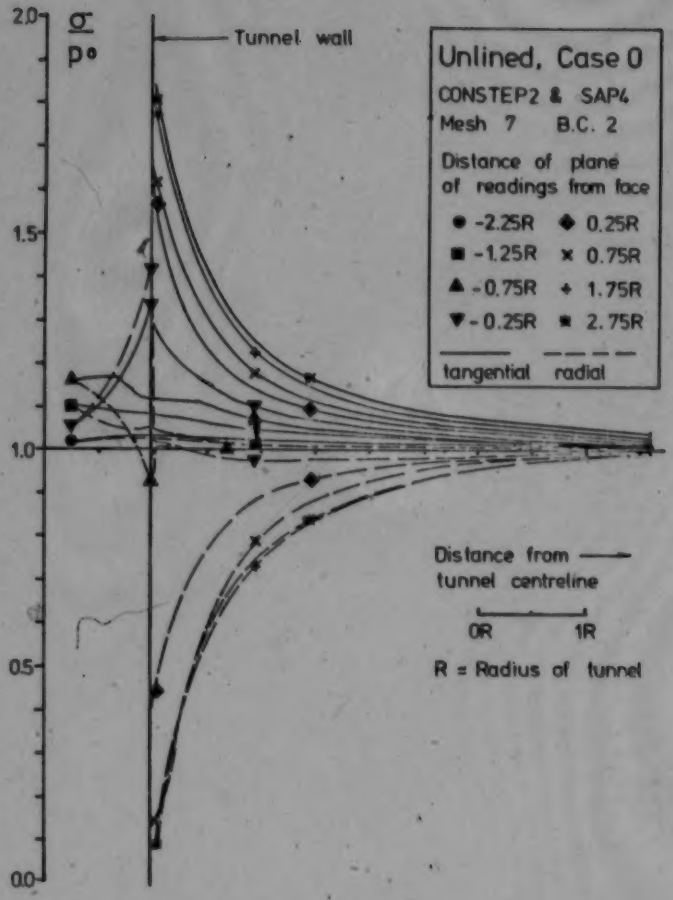

Figure A5.44 Variation of Ground Stresses, Unlined Case

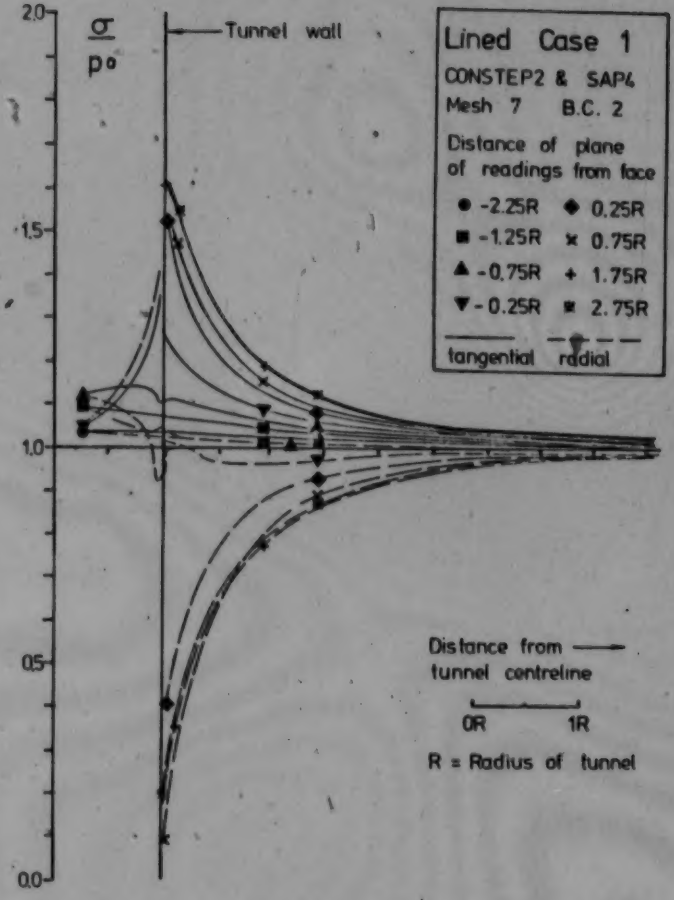

Figure A5.45 Variation of Ground Stresses, Case 1

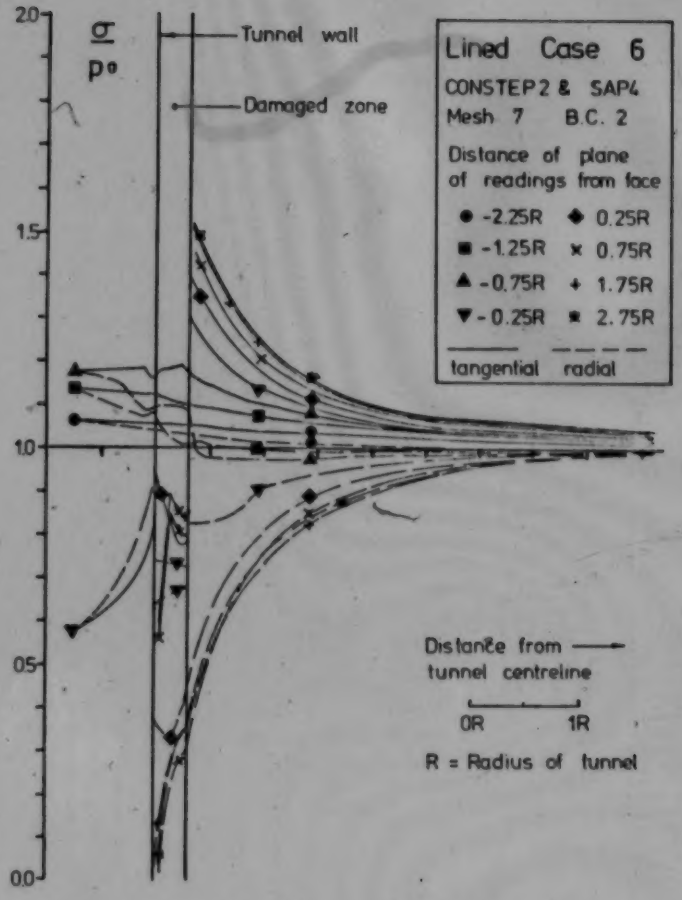

Figure A5.46 Variation of Ground Stresses, Case 6

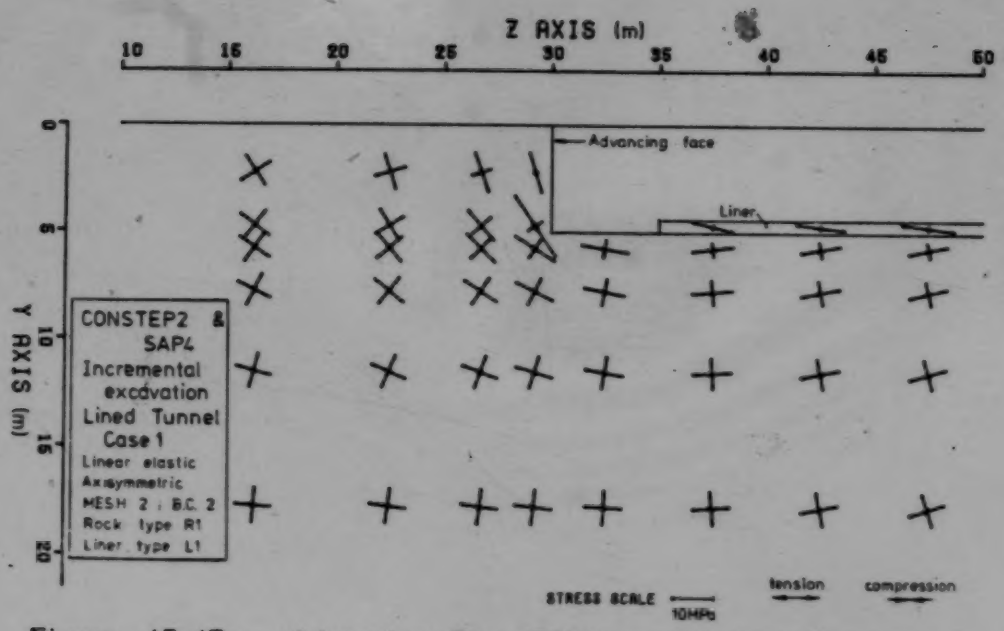

Figure A5.47 Advancing Face Effect on Principal Stresses, Mesh 2, Case 1

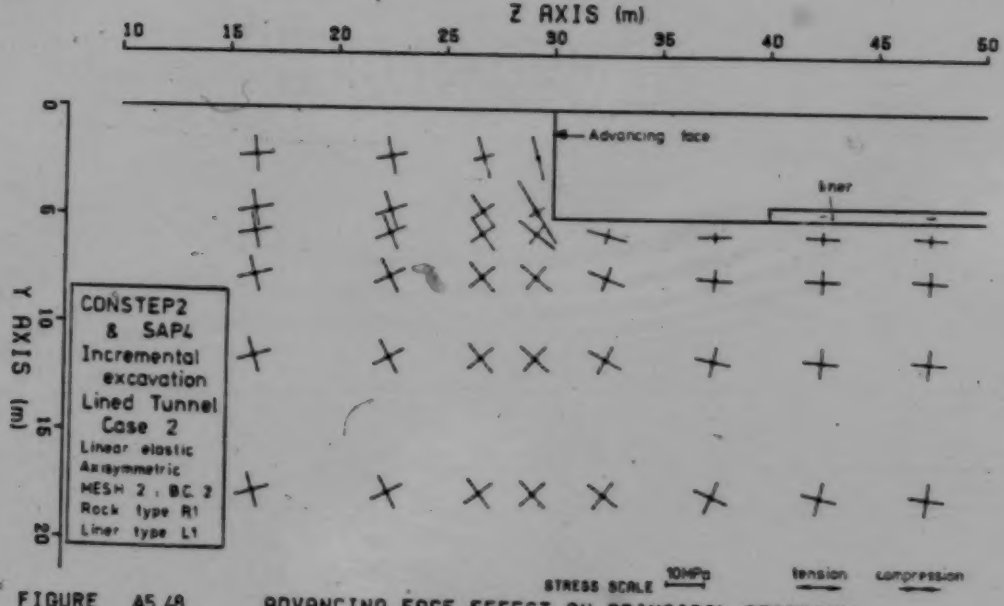

FIGURE A5.48 ADVANCING FACE EFFECT ON PRINCIPAL STRESSES, MESH 2, CASE 2

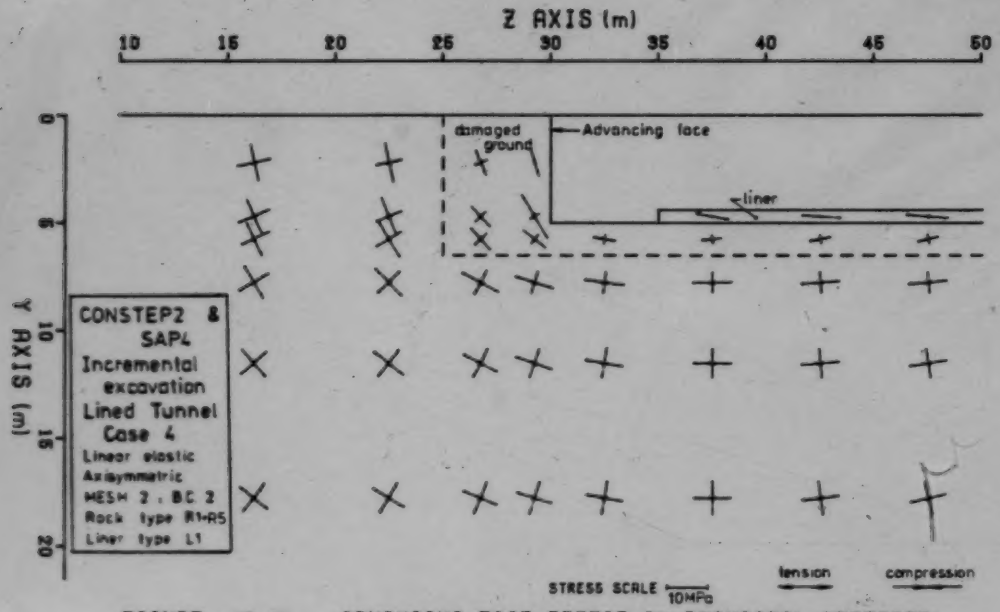

FIGURE A5.49 ADVANCING FACE EFFECT ON PRINCIPAL STRESSES, MESH 2, CASE 4

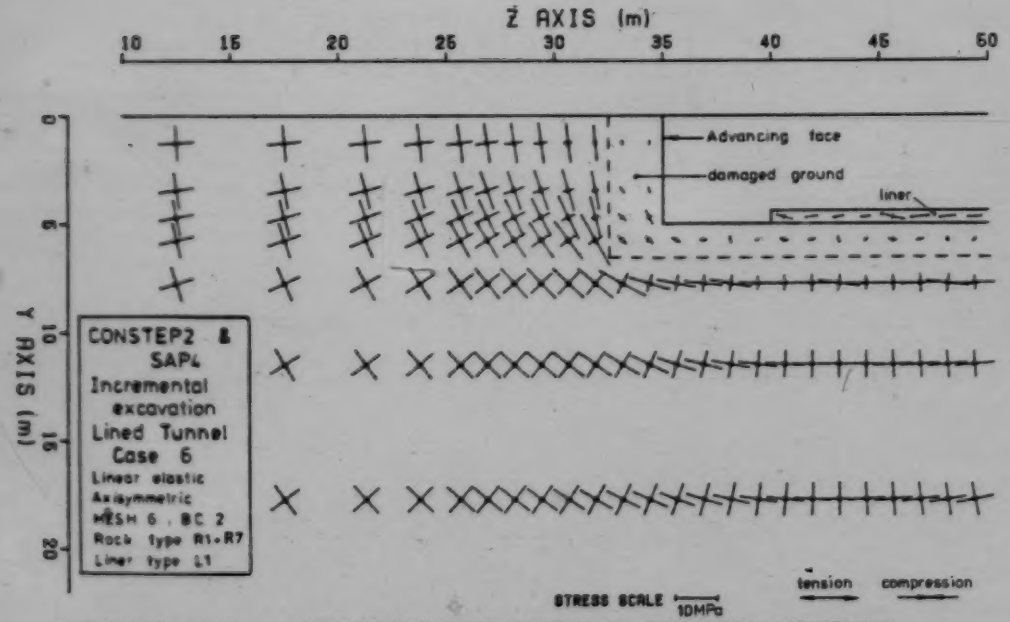

FIGURE A5.50 ADVANCING FACE EFFECT ON PRINCIPAL STRESSES, MESH 6, CASE 6

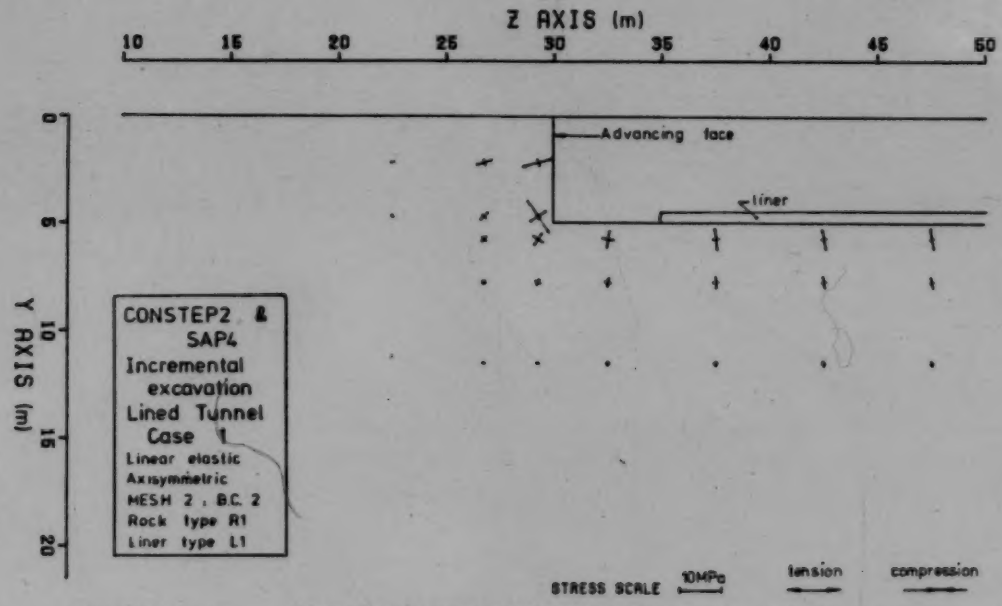

FIGURE A5.51 ADVANCING FACE EFFECT ON PRINCIPAL STRESS CHANGE, MESH 2, CASE 1

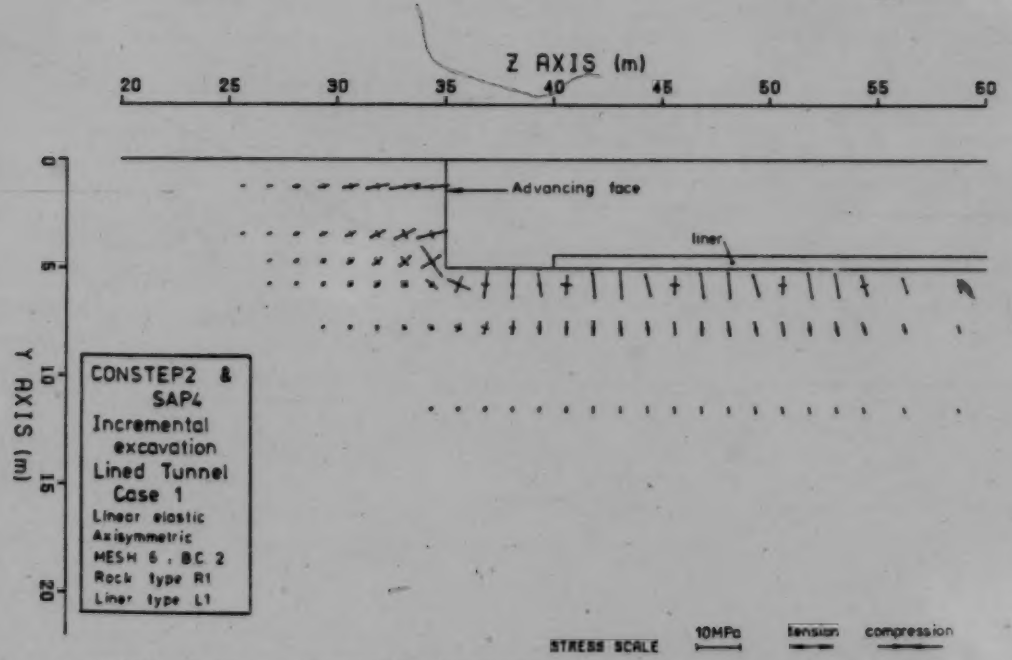

FIGURE A5.52 ADVANCING FACE EFFECT ON PRINCIPAL STRESS CHANGE MESH 6, CASE 1

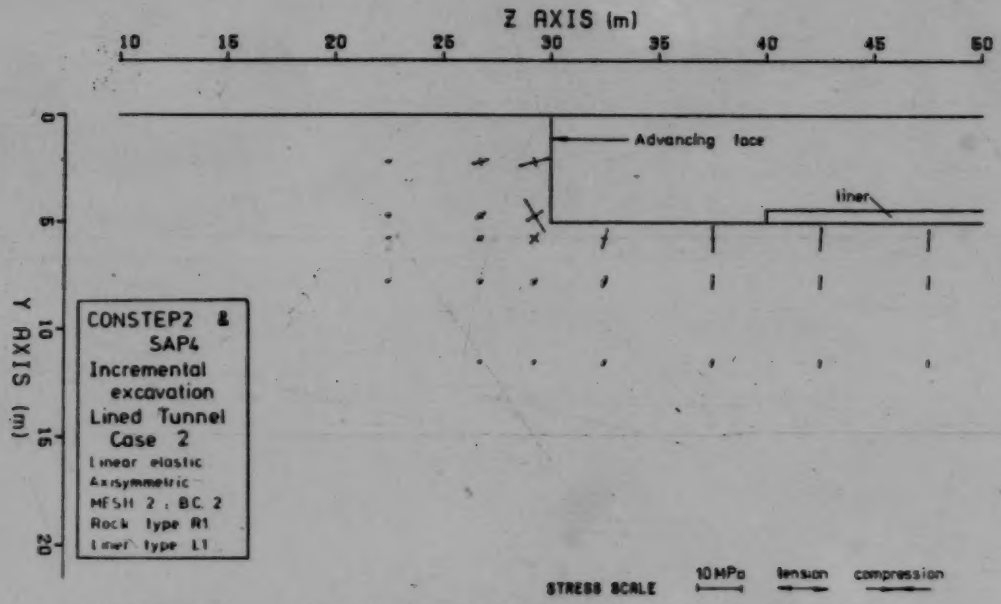

FIGURE A5.53 ADVANCING FACE EFFECT ON PRINCIPAL STRESS CHANGE, MESH 2, CASE 2

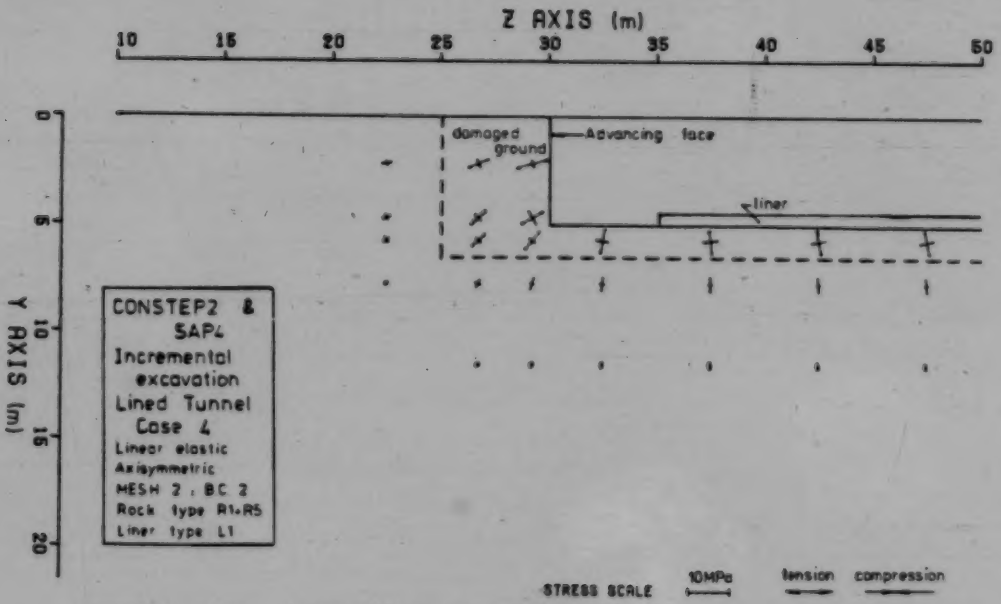

FIGURE A5.54 ADVANCING FACE EFFECT ON PRINCIPAL STRESS CHANGE, MESH 2, CASE 4

APPENDIX 6

RESULTS FROM THE ANALYSES - SHAFTS

Summary

Presented in this appendix are the results of the analyses carried out on unlined and lined, deep and shallow, shafts. Ko was varied, and was set to 0.5, 1.0 and 2.0. There was no rock damage. The results from a case where a drilled shaft was constructed with fluid support is also presented. Table A6.1 gives information on the different analyses carried out, and lists the figures (both in the appendix and the main text) where the results for each analysis may be found.

Table A6.1

Analyses Carried Out - Shafts

Run No.	Construction case	Shallow or deep	Ko	Mesh Used	Ground Type	Damaged Ground Type	Liner Type	Excavation Steps	Relevant Figure Numbers for Data: Radial Displacements	Liner Stresses	Ground Stresses
1	0	shallow	0.5	2	R1	-	-	7	A6.1,A6.2	-	8.15
2	0	shallow	1.0	2	R1	-	-	7	A6.1,A6.2	-	8.15
3	0	shallow	2.0	2	R1	-	-	7	A6.1,A6.2	-	8.15
4	1	shallow	0.5	2	R1	-	L1	7	A6.1,A6.3	A6.11-A6.13	8.16
5	1	shallow	1.0	2	R1	-	L1	7	A6.1,A6.4	A6.11-A6.13	8.16
6	1	shallow	2.0	2	R1	-	L1	7	A6.1,A6.5	A6.11-A6.13	8.16
7	2	shallow	0.5	2	R1	-	L1	7	A6.1,A6.6	A6.11-A6.13	-
8	2	shallow	1.0	2	R1	-	L1	7	A6.1,A6.7	A6.11-A6.13	-
9	2	shallow	2.0	2	R1	-	L1	7	A6.1,A6.8	A6.11-A6.13	-
10	1	deep	0.5	2	R1	-	L1	7	A6.9	A6.14	-
11	1	deep	1.0	2	R1	-	L1	7	A6.9	A6.14	-
12	1	deep	2.0	2	R1	-	L1	7	A6.9	A6.14	-
13	2	deep	0.5	2	R1	-	L1	7	A6.10	A6.14	-
14	2	deep	1.0	2	R1	-	L1	7	A6.10	A6.14	-
15	2	deep	2.0	2	R1	-	L1	7	A6.10	A6.14	-
16	Drilled	shallow	1.0	2	R1	-	L1	7	A6.15	A6.16-A6.18	-

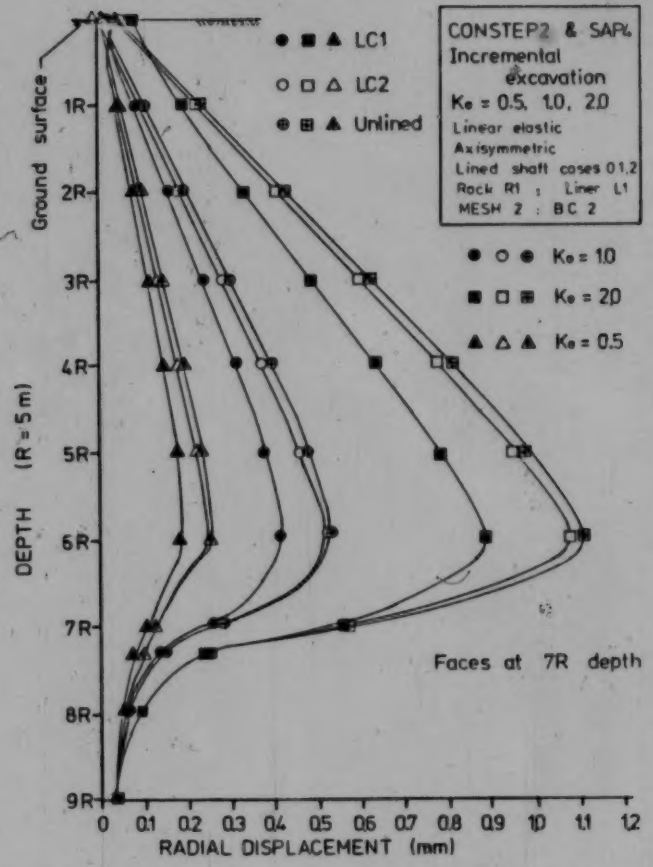

Figure A6.1 Influence of Advancing Face on Radial Displacements – Lined and Unlined Shafts

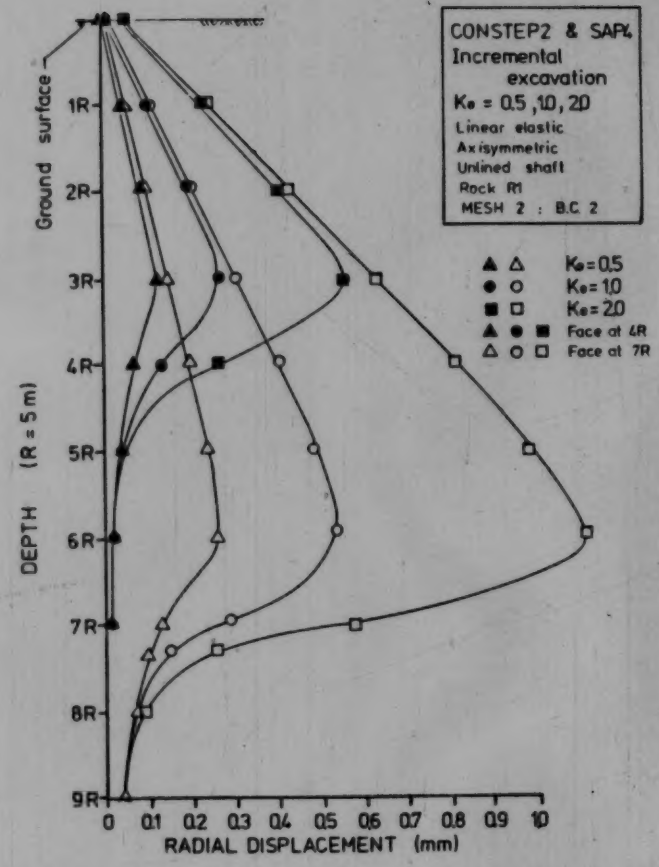

Figure A6.2 Influence of Advancing Face on Radial Displacements – Unlined Shaft

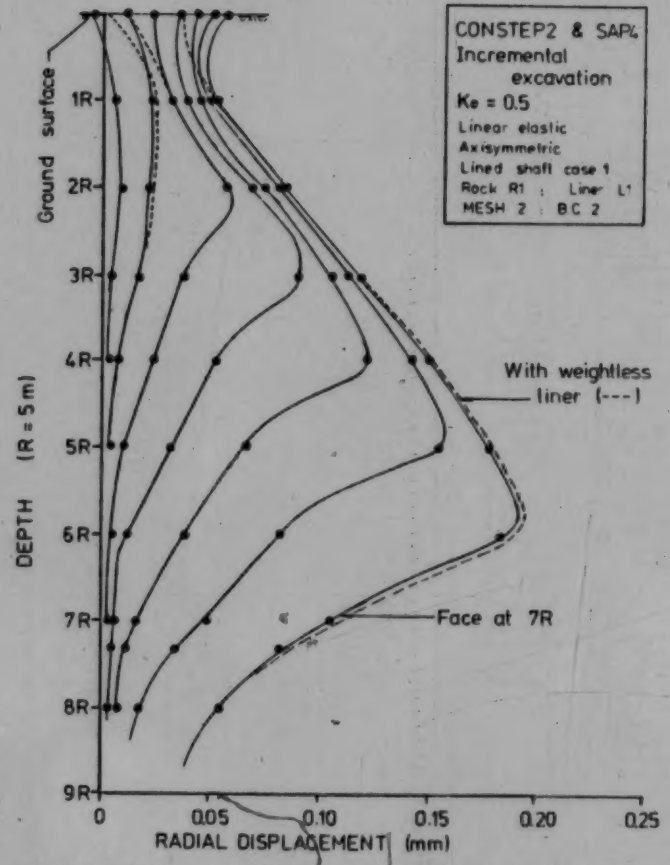

Figure A6.3 Influence of Advancing Face on Radial Displacements – Lined Shaft Case 1, K_o=0.5

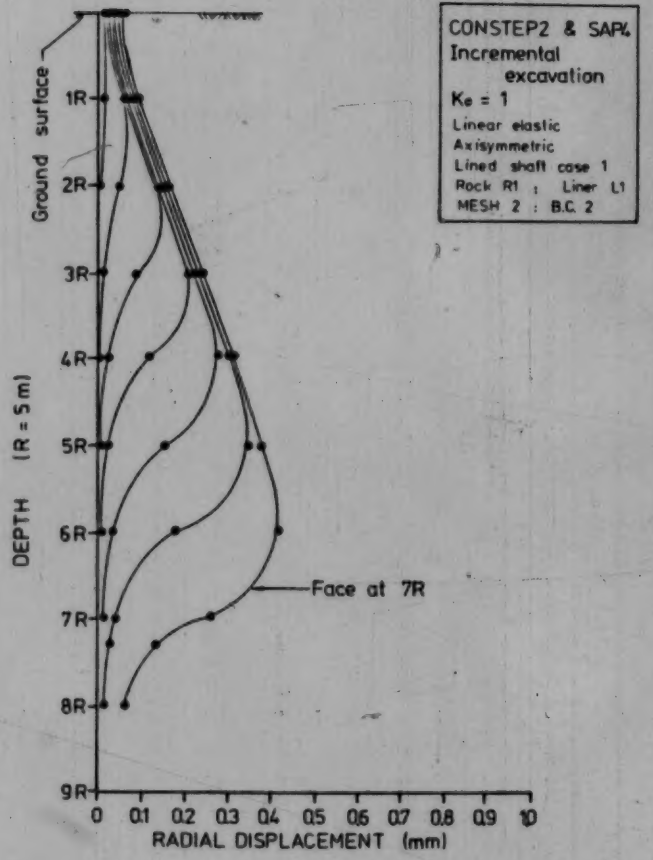

Figure A6.4 Influence of Advancing Face on Radial Displacements – Lined Shaft Case 1, K_o= 1.0

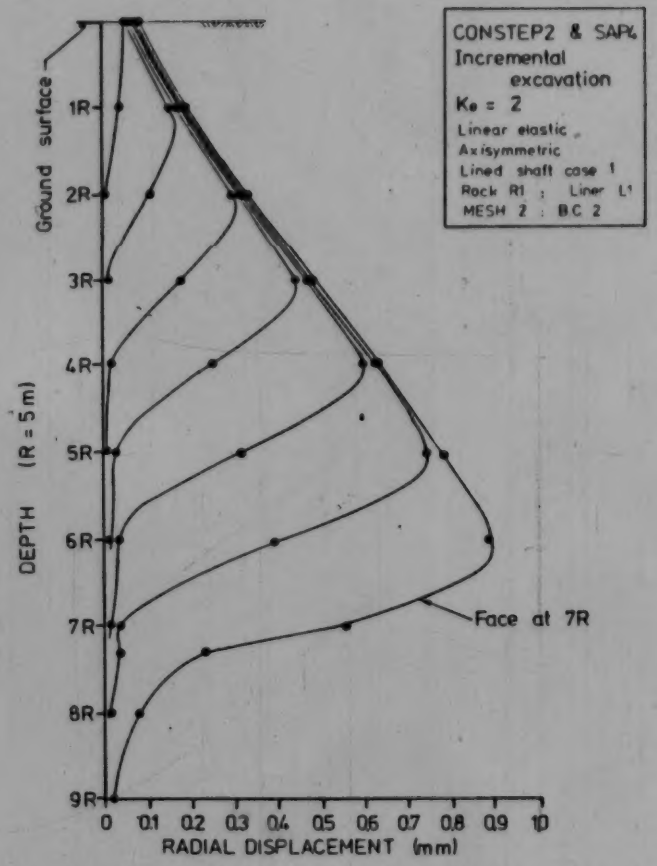

Figure A6.5 Influence of Advancing Face on Radial Displacements – Lined Shaft Case 1, $K_o = 2.0$

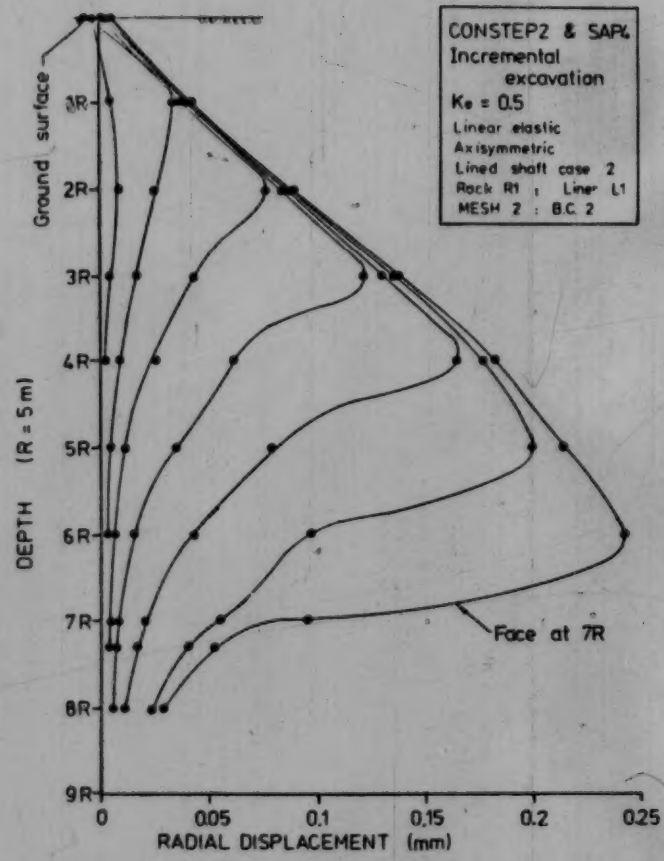

Figure A6.6 Influence of Advancing Face on Radial Displacements – Lined Shaft Case 2, $K_o = 0.5$

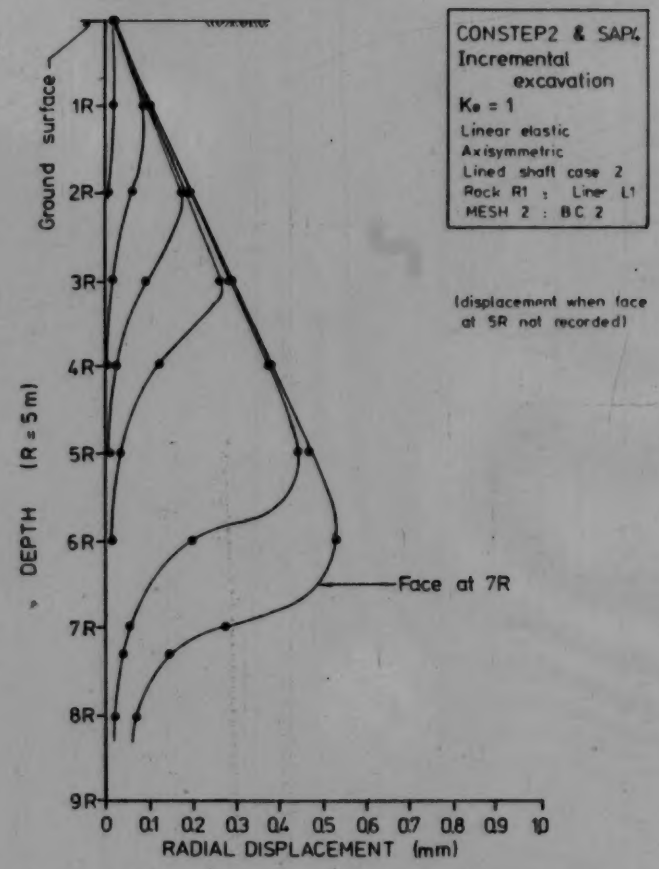

Figure A6.7 Influence of Advancing Face on Radial Displacements – Lined Shaft Case 2, $K_o = 1.0$

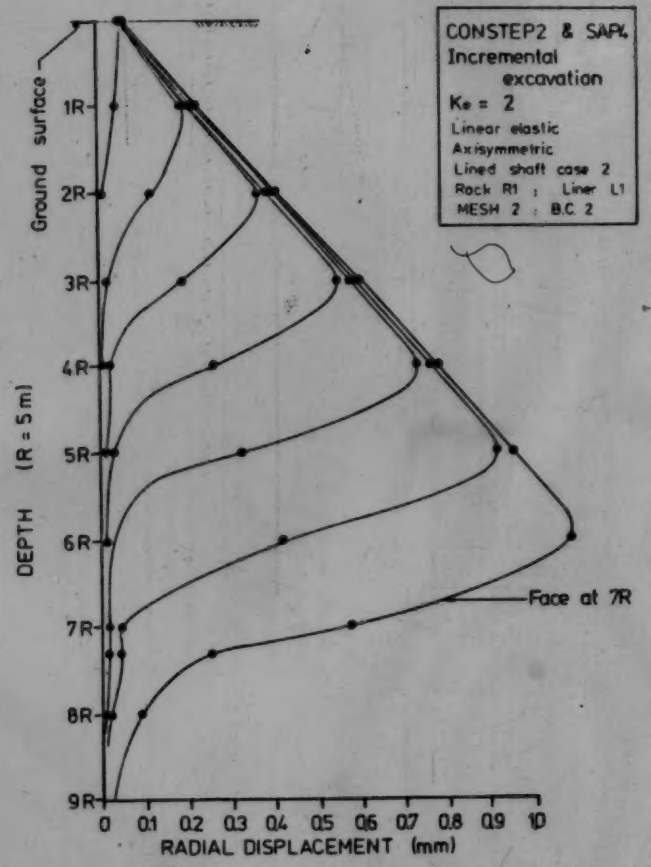

Figure A6.8 Influence of Advancing Face on Radial Displacements – Lined Shaft Case 2, $K_o = 2.0$

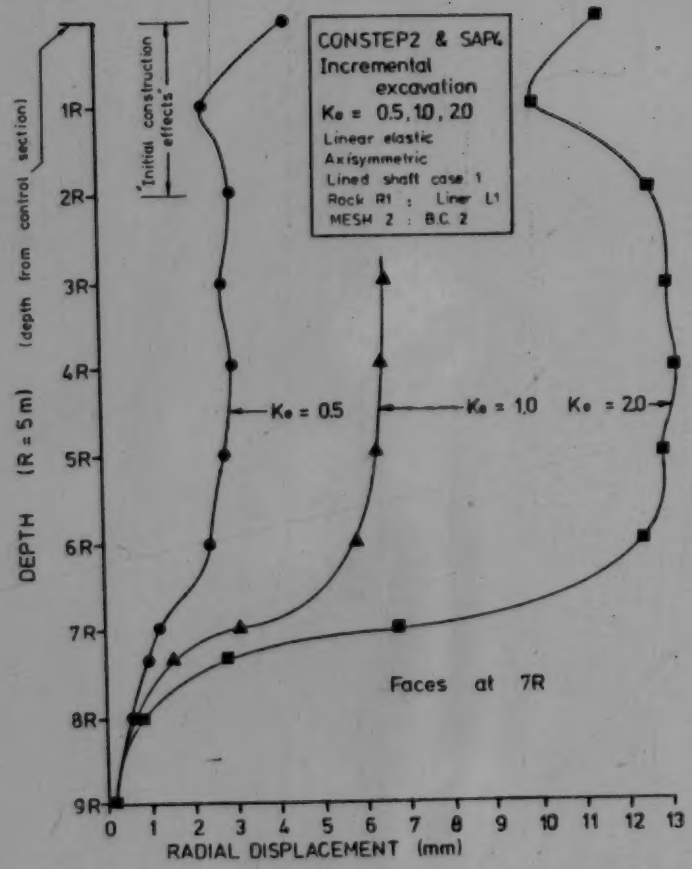

Figure A6.9 Influence of Advancing Face on Radial Displacements – Lined Shaft Case 1 (deep)

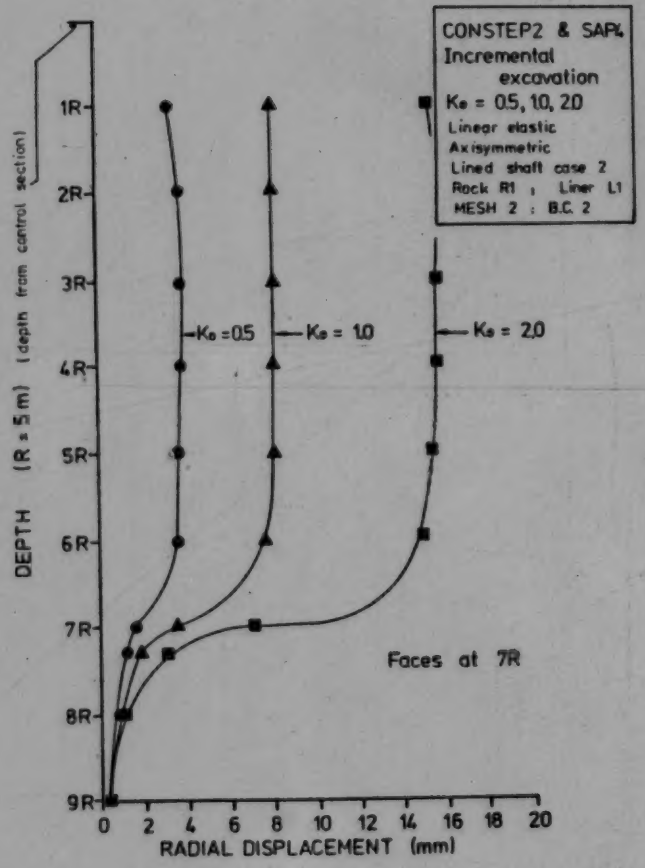

Figure A6.10 Influence of Advancing Face on Radial Displacements – Lined Shaft Case 2 (deep)

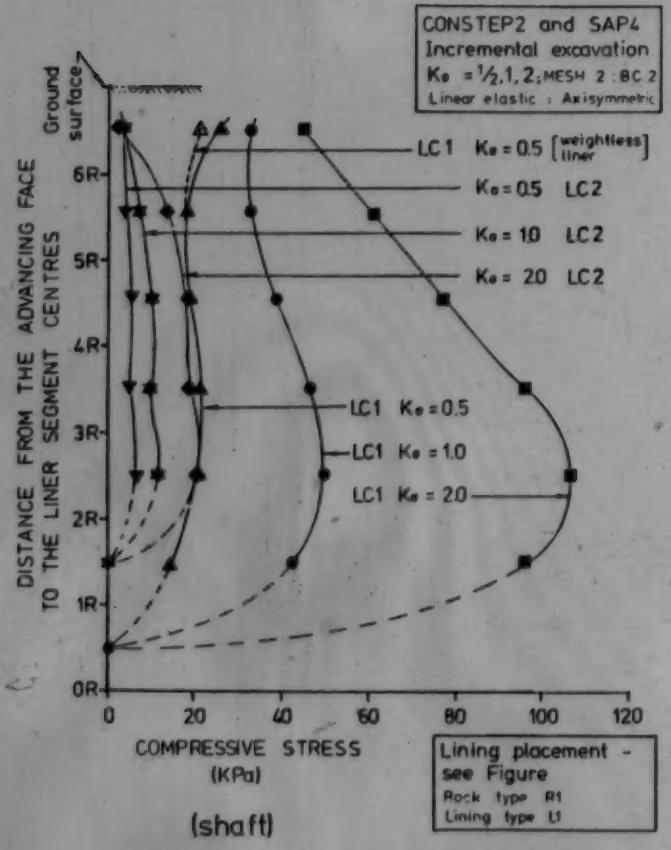

Figure A6.11 Influence of Advancing Face and Liner Placement on Liner Radial Stress

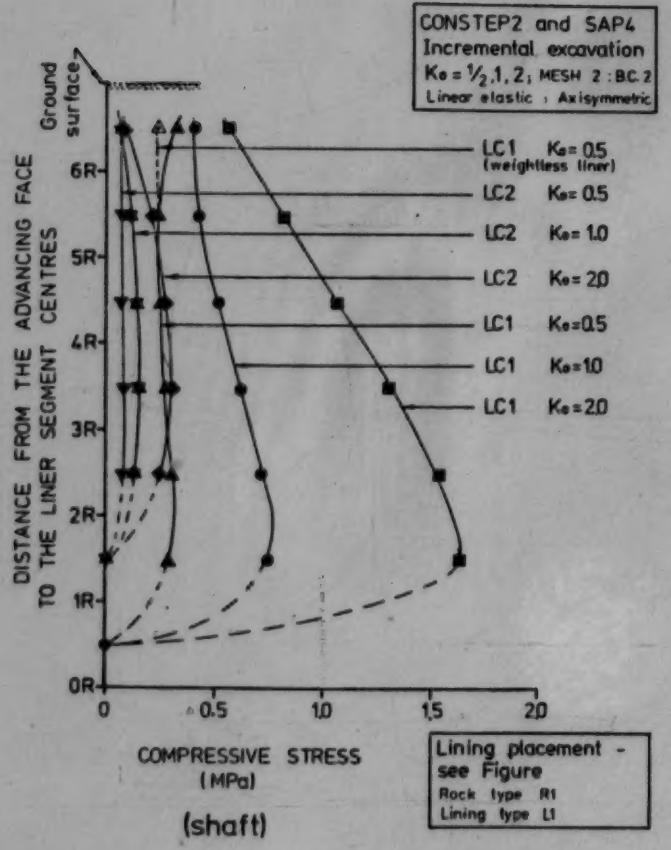

Figure A6.12 Influence of Advancing Face and Liner Placement on Liner Tangential Stress

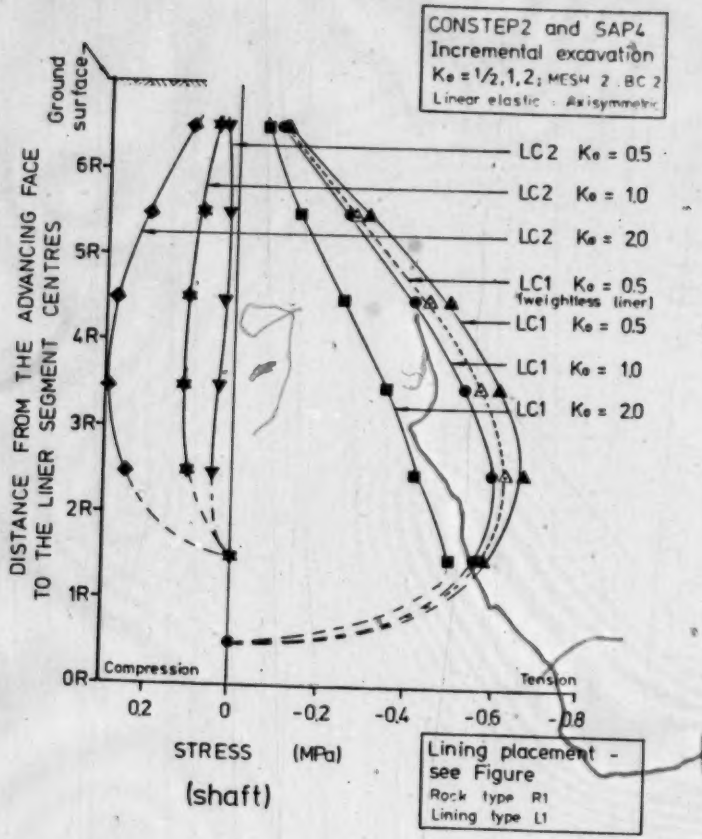

Figure A6.13 Influence of Advancing Face and Liner Placement on Liner Longitudinal Stress

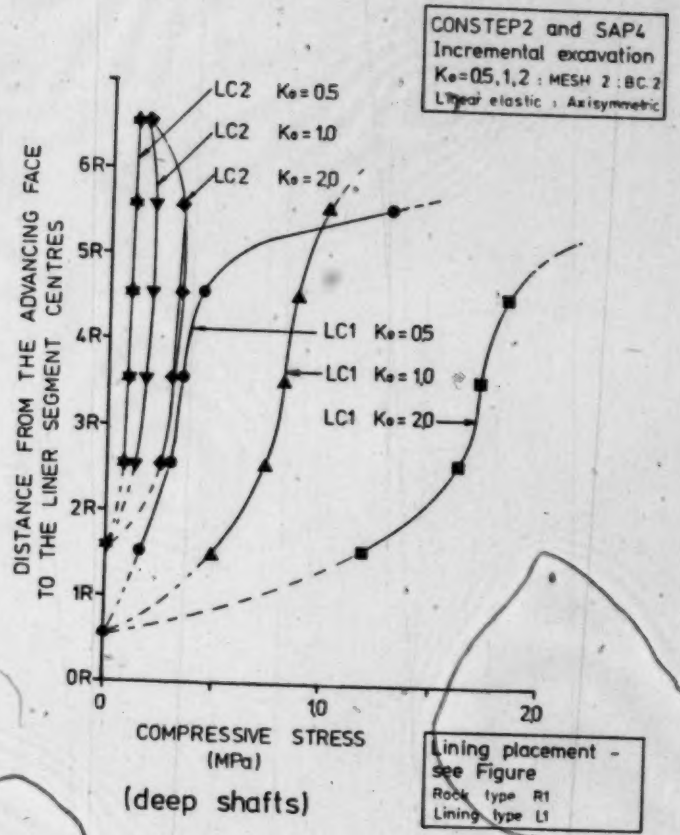

Figure A6.14 Influence of Advancing Face and Liner Placement on Liner Radial Stress

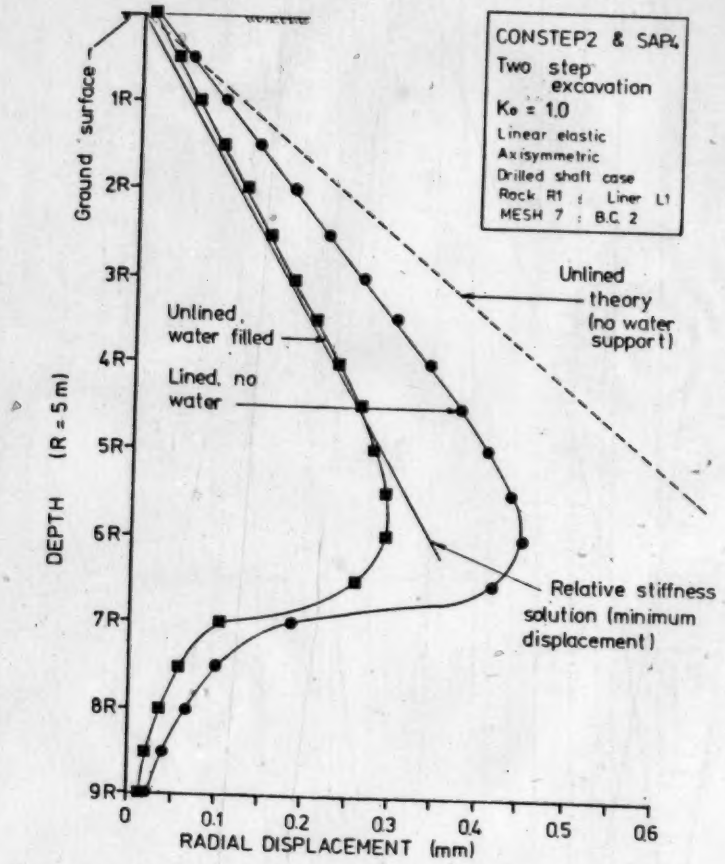

Figure A6.15 Influence of Advancing Face on Radial Displacements – Drilled Shaft Case

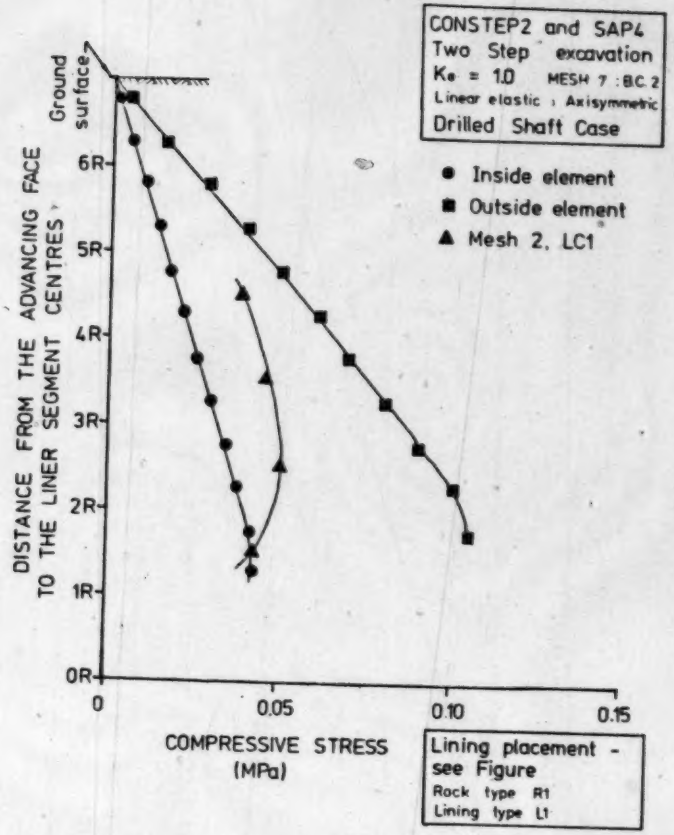

Figure A6.16 Influence of Advancing Face and Liner Placement on Liner Radial Stress

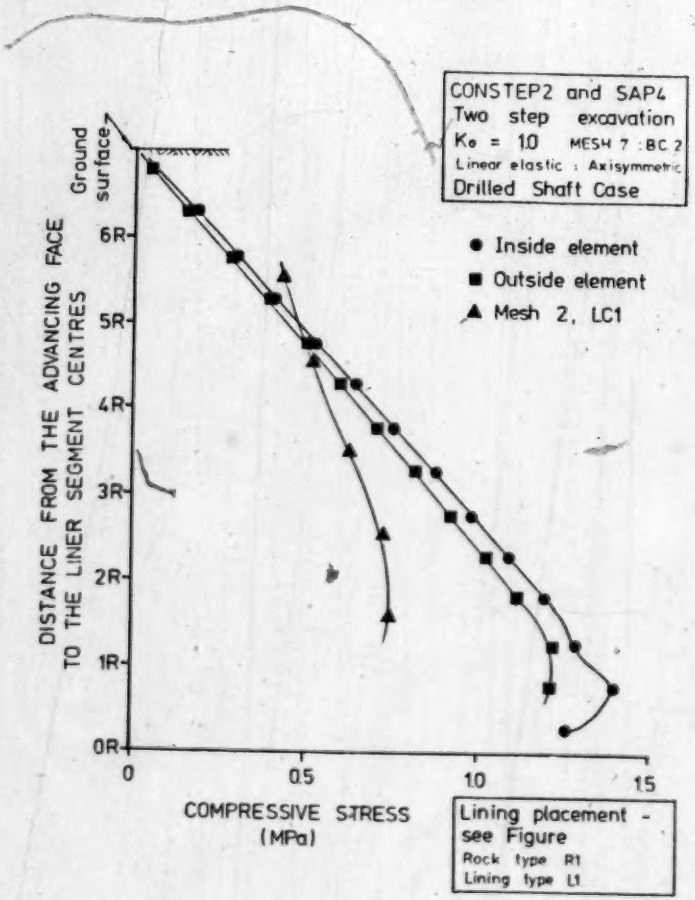

Figure A6.17 Influence of Advancing Face and Liner Placement on Liner Tangential Stress

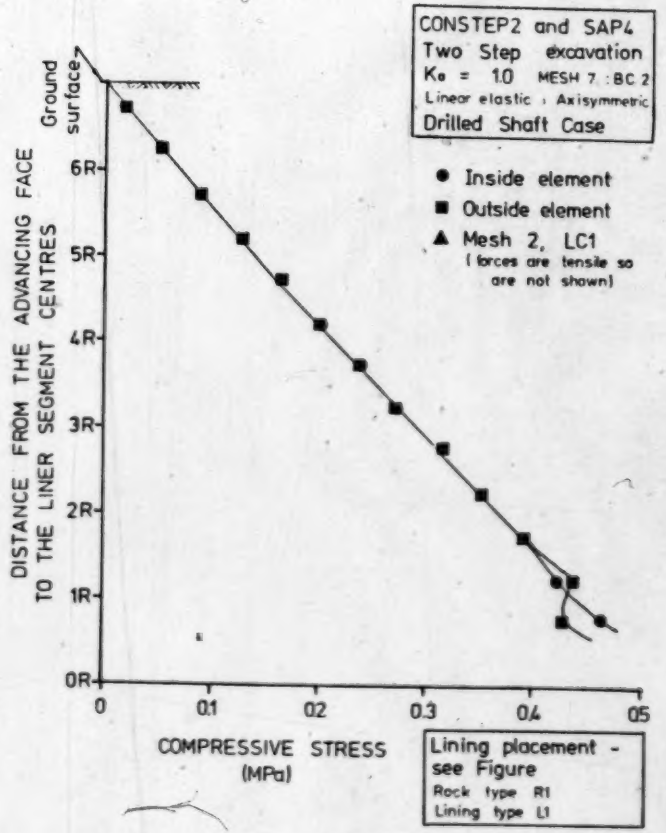

Figure A6.18 Influence of Advancing Face and Liner Placement on Liner Longitudinal Stress